

**A STUDY ON CHARACTERISATION, DETERIORATION
MECHANISMS AND PROTECTION OF BRICKS AND STONES IN
HISTORIC STRUCTURES**

A THESIS

Submitted by

SWATHY MANOHAR

for the award of the degree

of

DOCTOR OF PHILOSOPHY



**DEPARTMENT OF CIVIL ENGINEERING
INDIAN INSTITUTE OF TECHNOLOGY MADRAS
CHENNAI, INDIA**

MARCH 2020

THESIS CERTIFICATE

This is to certify that the thesis titled "**A STUDY ON CHARACTERISATION, DETERIORATION MECHANISMS AND PROTECTION OF BRICKS AND STONES IN HISTORIC STRUCTURES**", submitted by **Ms. SWATHY MANOHAR**, to the Department of Civil Engineering, Indian Institute of Technology Madras, Chennai, for the award of the degree of Doctor of Philosophy is a bona fide record of research work carried out by her under my supervision. The contents of this thesis, in full or in parts, have not been submitted and will not be submitted to any other Institute or University for the award of any degree or diploma.

Dr. Manu Santhanam

Research Guide

Professor

Department of Civil Engineering

Indian Institute of Technology Madras

Chennai - 600 036, India

Chennai, India

March 13, 2020

DEDICATION

To my family and teachers

ACKNOWLEDGEMENTS

A thesis will not happen to be possible with the unilateral efforts of an individual. I have a great bunch of people to whom I am thankful.

Foremost, I would like to offer the endeavour to God Almighty for the wisdom and sustenance he bestowed upon me and the peace of mind and strength in me throughout the entire duration of my research at Indian Institute of Technology Madras. I take extreme pride for the place, the people here and the opportunity I received to work here.

I convey my deepest sense of gratitude to my research guide, Prof. Manu Santhanam, Department of Civil Engineering, for his guidance and constant inspiration. This work would not get materialised in this form without his uncompromising standards for quality and intelligence combined with the incomparable patience. I appreciate his personal generosity which helped me to have an enjoyable time here. My sincere thanks to Dr. Arun Menon, Assistant Professor, Department of Civil Engineering for the support and the genuine kindness, which helped me tremendously to sustain a positive atmosphere around. His early insights in my research area launched a large part of this thesis work.

I am extremely grateful to Prof. Ravindra Gettu, Department of Civil Engineering, for his constructive criticisms and timely thoughtful suggestions he provided at various stages of my research. I would also like to thank Dr. Radhakrishna G. Pillai, whose mentoring and encouragement has been one of the constant driving forces that made me thrive for improvement. I extend my gratitude to Dr. Piyush Chaunsali, and my doctoral committee

members Dr. Sivakumar Palaniappan and Prof. Damodaran R., for reviewing my progress and the helpful suggestions they provided during my comprehensive viva exam and seminars.

My sincere thanks to Prof. K. Ramamurthy, former Head of the Department of Civil Engineering, for not only providing the excellent facilities of the department but also for mentoring and supporting me whenever in need, in professional as well as personal life.

I would also like to thank Prof. Mark Alexander, Professor, University of Cape Town, South Africa and Prof. Surendra P. Shah, Professor of Emeritus, North Western University, U.S.A and Visiting Professor, IIT Madras for their valuable inputs given during their stay at IIT Madras. With sincere gratitude, I thank Dr. R. Ramasamy for helping me by imparting the basic knowledge of geology and petrographic science.

Heartfelt thanks to Dr. Enrico Sassoni, Senior Assistant Professor, University Of Bologna, Italy for granting me an opportunity to work with him in his laboratory during my internship and to learn science and experimental hacks from him. His highly welcoming and friendly nature made me enjoy my stay and feel home in Italy. His ideas contributed a better shape and convergence to this dissertation.

My appreciation also extends to the National Centre for Safety of Heritage Structures (NCSHS), IIT Madras for providing me with the opportunity to explore the heritage structures in India and collect various historical samples. I am also thankful to all the supporting staffs in BTCM laboratories- especially Ms. A. Malarvizhi, Mr. G.Subrahmanian and Mr. Gasper.

I am indebted to my family for their prayers, sacrifice and love that kept me going. My husband, Espy, who is my champion, blessed each of my days with positivity. Espy, along with my son Ishaan made me feel ‘team’ while enjoying my Ph.D. tenure as the best years of our life so far. My mother Vijayakumary, siblings Dr. Shruthy and Shreyas have been continuously standing with me and provided all the support I needed throughout this journey. My father, Mr. Manoharan K., was the most excited person for all my endeavours in life, including my dream of doing Ph.D. Even though he is no more, I believe that, it is his blessings that keep my life at grace. I owe my finest gratitude to my in-laws Prof. G. Pushpaetha and Prof. G. Suresh, for their love and support they extended throughout the period.

My sincere gratitude to my friends and fellow researchers, whose presence and moral support redefined the BTCM research group as a second family to me. I cannot imagine a better work environment where such strong connection among faculties and scholars co-exists beautifully. I appreciate Sundar anna for being the ever-constant and caring friend in times of need. I thank Dyana Joseline for the many chats and the encouragement she showed, which gave me the strength to soldier on in good and bad times. I also thank Nithya, Anusha and Menaka to make my hostel memories evergreen. I would like to thank my dear friends Thangadurai, Yuvaraj D., Sachin Paul, Deepak Kamde, Vaishnav Kumar, Sanoop, Dr. Sripriya R., V. G. Ram, Dr. Prabha, Dr. Ramaswamy K. P., Fathima Suma, Anupama, Nila for the help they rendered during different stages of my life at IITM. May God bless you all.

SWATHY MANOHAR

ABSTRACT

KEYWORDS: Historic masonry, salt crystallisation, microstructure, pore structure

India possesses a rich stock of built heritage in masonry. A large number of these historical monuments are currently in different stages of deterioration and in need of repair. The deficiency of systematic understanding of historical materials and degradation mechanisms has led to deleterious repair methods using incompatible materials, which have resulted in frequent interventions. No studies have been reported on Indian masonry units on how the properties of some ancient materials provide them accentuated long life and durability. Moreover, an analysis of the deterioration they face over time is essential to provide imperative protection.

The crystallisation of soluble salts within the pores has been found to cause the greatest damage for heritage masonry units. For proper restoration works, understanding these ancient materials from an engineering perspective, and complementing that information with the durability criteria for salt crystallisation resistance is essential. This thesis addresses these issues through a comprehensive experimental program. Historic samples and fresh samples of fired clay bricks and stones such as granite and coral stone are studied for their characteristics. The process of salt crystallisation and its implications on the pore structure are understood through accelerated weathering studies. Factors that control the extent of damage on salt crystallisation are identified. Advanced micro-analytical techniques are used to link the microstructure of the material and its durability performance. Compatibility issues between protective treatments and substrate material and that between new and existing masonry units are also discussed.

The relationship between microstructure and durability performance in the first part of the study using brick samples confirmed that pore sizes and pore distribution in a material are the principal governing factors in determining the performance. Salt crystallisation was found to be favoured in pore sizes smaller than 1 μm and found limited to a minimum pore size of 0.2 μm for sodium sulphate. Differences in the solubility and precipitation mechanisms of sodium sulphate and sodium chloride salts were explained and experimentally illustrated in the study discussing the importance of ‘supersaturation’. The studies on stones also demonstrated how the grain strength of the material and interconnection of the pores act as additional factors which can sometimes over-rule the significance of pore-size.

The characterisation methodology proposed in the current study can be used to study and document the properties of the historic bricks of any conservation state (with no weathering traces to highly weathered) and from any environmental exposure to understand their performance. The results from the study can be used in the improvement of restoration procedures in the future. On parameterising the properties of bricks from different conservation states, the current study demonstrates how the systematic characterisation could help in understanding the behaviour of a material or to select a replacement material based on the required performance. A comprehensive understanding of the process of salt crystallisation, damage mechanisms of different salts and the requirement of various materials (based on their microstructure) in improving salt weathering resistance would help in predicting the behaviour of the material in the long run when exposed to salt-laden environments. The study also provides critical recommendations for the selection of water-repellent treatments for historic masonry.

TABLE OF CONTENTS

ACKNOWLEDGEMENTS	iv
ABSTRACT	vii
TABLE OF CONTENTS	ix
LIST OF FIGURES	xiv
LIST OF TABLES	xx
NOTATIONS AND ABBREVIATIONS	xxii
1 INTRODUCTION	1
1.1 PROBLEM STATEMENT	1
1.2 KEY RESEARCH QUESTIONS	3
1.3 RESEARCH OBJECTIVES AND SCOPE	4
1.3.1 Objectives	4
1.3.2 Scope.....	5
1.4 METHODOLOGY	5
1.5 THESIS LAYOUT.....	6
2 LITERATURE REVIEW	8
2.1 INTRODUCTION	8
2.2 CONSERVATION OF MASONRY STRUCTURES	9
2.2.1 Conservation of masonry structures- International status	9
2.2.2 Conservation of masonry structures- National status.....	11
2.3 Characterization and durability of masonry units	18
2.3.1 Mineralogical composition	21
2.3.2 Morphological characteristics	25
2.3.3 Pore structure and pore distribution	28
2.4 SALT CRYSTALLISATION	34
2.4.1 Significance of salt crystallisation in historic masonry structures	34

2.4.2	General mechanism of salt crystallisation.....	36
2.4.3	Mechanism of salt crystallisation with specific salts	40
2.4.4	Test methods for analysing salt weathering resistance	45
2.4.5	Application of microstructural analysis in analysing salt crystallisation weathering ..	49
2.5	PROTECTIVE TREATMENTS FOR HISTORIC MASONRY	55
2.5.1	History of use of protective treatments to masonry	55
2.5.2	Working of water repellent coatings	59
2.5.3	Advantages and disadvantages of water repellent coatings	60
2.5.4	Studies on efficiency of various protective coatings.....	60
2.5.5	Importance of compatibility between treatments and substrate	63
2.6	SUMMARY OF LITERATURE AND NEED FOR THE RESEARCH.....	64
3	MATERIALS AND METHODS.....	67
3.1	INTRODUCTION	67
3.2	MATERIALS USED IN THE STUDY	67
3.2.1	Samples collected.....	67
3.2.2	Water repellent coatings.....	71
3.3	EXPERIMENTAL PROGRAM	72
3.4	CHARACTERISATION OF SAMPLES	74
3.4.1	Physical and mechanical characterisation.....	74
3.4.2	Microstructural characterisation.....	79
3.4.3	Study of the impact of weathering in samples	86
3.4.4	Study of the suitability of protective treatments	87
3.5	WEATHERING TEST METHODS	90
3.5.1	Immersion test according to EN12370.....	90
3.5.2	Immersion test according to RILEM VI.b	91
3.5.3	Spraying test according to ASTM B117-11	92
3.6	DESALINATION	95
3.7	SUMMARY.....	97

4	CHARACTERISATION OF MASONRY BRICKS	98
4.1	INTRODUCTION	98
4.2	CHARACTERISTICS OF THE BRICK SAMPLES	99
4.2.1	Visual observations	99
4.2.2	Physical-mechanical characterisation	101
4.2.3	X-ray diffraction	104
4.2.4	Scanning Electron Microscopy	109
4.2.5	Mercury Intrusion Porosimetry (MIP)	115
4.3	EFFECT OF NATURAL SALT WEATHERING ON BRICKS	117
4.3.1	Visual observations	118
4.3.2	Physical and mechanical characterisation	119
4.3.3	Mineralogical characterisation	120
4.3.4	Pore structure and pore size distribution	123
4.4	EFFECT OF ARTIFICIAL SALT WEATHERING ON THE BRICKS	125
4.4.1	Accelerated salt weathering cycles as per EN12370.....	125
4.4.2	Porosity evaluation after weathering test	129
4.5	SUMMARY	131
5	CHARACTERISATION OF MASONRY STONES	134
5.1	INTRODUCTION	134
5.2	CHARACTERISTICS OF THE STONE SAMPLES.....	135
5.2.1	Introduction to the nature of stones.....	135
5.2.2	Visual observations	136
5.2.3	Physical-mechanical characterisation	140
5.2.4	X-ray diffraction	146
5.2.5	Scanning Electron Microscopy	150
5.2.6	Thin section petrography	156
5.2.7	Mercury Intrusion Porosimetry (MIP)	160

5.3	EFFECT OF ARTIFICIAL SALT WEATHERING ON THE STONES.....	166
5.3.1	Performance of granite in salt exposure.....	166
5.3.2	Performance of coral stones in salt exposure.....	169
5.4	SUMMARY.....	175
6	SELECTION AND EVALUATION OF PROTECTIVE TREATMENTS.....	177
6.1	INTRODUCTION.....	177
6.2	BASIC PROPERTIES OF PROTECTIVE TREATMENTS.....	179
6.2.1	Application of water repellent treatments.....	179
6.2.2	Waterdrop absorption test.....	180
6.2.3	Water Sorptivity test.....	181
6.2.4	Karsten tube test.....	182
6.2.5	Breathability test.....	185
6.2.6	The penetration depth of treatments.....	187
6.3	ACCELERATED SALT WEATHERING TESTS.....	189
6.3.1	Mass changes on accelerated weathering.....	191
6.3.2	Visual observations of damages.....	195
6.3.3	UPV measurements.....	206
6.3.4	Modification of pore structure on accelerated weathering.....	208
6.4	DESALINATION OF WEATHERED SPECIMENS.....	216
6.4.1	Scanning Electron Microscopy.....	216
6.4.2	Porosity measurements.....	221
6.5	SODIUM CHLORIDE SPRAY TEST.....	223
6.5.1	Mass changes and visual damages.....	223
6.5.2	UPV measurements.....	226
6.5.3	Microstructure modification.....	227
6.6	SUMMARY.....	236

7	GENERAL DISCUSSIONS.....	239
7.1	INTRODUCTION	239
7.2	DEVELOPMENT OF A FRAMEWORK FOR CHARACTERISING HISTORIC MASONRY MATERIALS	239
7.3	FACTORS CONTROLLING THE SALT CRYSTALLISATION PROCESS.....	244
7.3.1	Size of the pores.....	244
7.3.2	Pore-interconnection	246
7.3.3	Nature of salt.....	248
7.3.4	Strength of the material.....	249
7.3.5	Temperature and rate of evaporation	250
7.4	PRESERVATION STRATEGIES.....	250
7.5	SUMMARY	254
8	CONCLUSIONS.....	256
8.1	INTRODUCTION	256
8.2	CHARACTERISATION OF HISTORIC MASONRY UNITS	257
8.2.1	Characteristics of bricks.....	257
8.2.2	Characteristics of stones.....	259
8.3	SALT CRYSTALLISATION IN POROUS MASONRY UNITS	260
8.4	MAJOR CONTRIBUTIONS.....	264
8.4.1	Scientific contributions	264
8.4.2	Engineering contributions	265
8.5	RECOMMENDATIONS FOR FURTHER RESEARCH	266
	REFERENCES.....	268
	LIST OF PUBLICATIONS BASED ON THIS THESIS	289
	DOCTORAL COMMITTEE.....	291
	CURRICULUM VITAE.....	292

LIST OF FIGURES

Figure 2.1. Map showing World heritage Sites in India (courtesy: mapsofindia.com)	14
Figure 2.2. Main tools of stone testing in the quarries, at the laboratory and the monuments and the use of techniques at different levels (Torok and Prikryl (2010)	20
Figure 2.3. SEM images of calcareous (left column) and non-calcareous (right column) bricks fired at 800 °C (a and b), 900 °C (c and d), 1000 °C (e and f) and 1100 °C (g and h) (Elert et al., 2003)	26
Figure 2.4. Comparison of total porosity for different images taken for a single sample	31
Figure 2.5. Sketch showing overlapping ranges of pores investigated with different techniques (Coletti et al. 2016)	31
Figure 2.6. Examples of the devastating action exerted by salts on heritage masonry structures (Flatt et al. 2014)	35
Figure 2.7. Representation of crystal formation inside a small pore	36
Figure 2.8. Phase diagram of sodium sulphate (Robert J. Flatt 2002).....	42
Figure 2.9. Phase diagram of sodium sulfate showing the equilibrium solubilities of various phases (h, t, m for heptahydrate, thenardite and mirabilite respectively) (Saidov et al. 2017)	42
Figure 2.10. Micrograph of precipitated thenardite crystals (a) at 20 °C, RH > 40%- needles are phase III of sodium sulphate and prisms are phase V (b) Phase V bipyramidal prisms at 20 °C, 13% RH, with minor amounts of phase III needles (Rodriguez-Navarro et al. 2000)..	53
Figure 2.11. Protective coating damaging the stone substrate upon peeling (Mack and Grimmer 2000).....	57
Figure 3.1. Locations from which the samples are collected.....	71
Figure 3.2. Methodology of the study.....	73
Figure 3.3. Helium gas pycnometer	76
Figure 3.4. (a) Illustration of water-sorptivity test (b) Desiccator used for vacuum saturation	78
Figure 3.5. Illustration of UPV test on a brick sample	79
Figure 3.6. X-ray diffractometer.....	81

Figure 3.7. Steps in the process of sample preparation for XRD (a) brick chunks (b) powdering the bricks chunks (c) sieving the powder through 75-micron sieve	81
Figure 3.8. Emcrafts SEM equipment.....	83
Figure 3.9. A typical example of MIP cumulative and derivative curves for Portland Cement, showing the pore parameters (Scrivener, Snellings 2016).....	85
Figure 3.10. Thermo Scientific Mercury Intrusion Porosimeter.....	86
Figure 3.11. Illustration of Karstens’ pipe test	89
Figure 3.12. Test setup of vapour permeability test showing the measure cells	90
Figure 3.13. Schematic diagram of the salt spray chamber used for the study.....	93
Figure 3.14. Working of atomised nozzle.....	94
Figure 3.15. Salt-spray chamber	95
Figure 3.16. Steps followed in the process of poulticing (a) cellulose powder in the dry form (b) mixing of cellulose powder with water to prepare the poultice (c) samples covered with the cellulose poultice left for drying	97
Figure 4.1 (a) Compressive strength (b) Bulk density (c) water absorption (d) UPV	103
Figure 4.2. X-ray diffractograms of the brick samples (a) historic bricks V1, V2, V3 fired at high temperature (b) historic bricks K, T1, T2 fired at low temperature (c) new bricks VN, C1, C2	108
Figure 4.3. SEM images of the samples: (a) C1, fired at just above 900 °C showed vitrified matrix but with larger pores; (b) C2 fired at temperature much higher than 900 °C showed a denser matrix with smaller pores; (c) V1 (d) V2, both are less weathered historic brick samples, with the pores filled with deformed feldspar particles; (e) V3, well vitrified historical sample with macropores; (f) VN, the replacement brick made for ancient brick V2 and V1 showing a similarly dense matrix with diffusing feldspar into pores; (g) K, the poorly baked brick sample with heavy fissuring and poor interconnectivity; (h) T2 with recrystallized precipitates of carbonates filling in the large fissures due to poor baking; (i) T1 with gypsum nodules; (j) A gypsum nodule in T1	114
Figure 4.4 (a) Cumulative intrusion curves; (b) Differential intrusion curves from MIP data	116
Figure 4.5. (a) Brick wall showing T1 bricks (b) T2 sample bricks which were partially immersed in seawater.....	119
Figure 4.6. Diffractograms showing the peaks of major mineral phases of T1 and T2 samples	122

Figure 4.7. (a) Cumulative intrusion curves from MIP (b) Differential intrusion curves showing the critical pore diameter	124
Figure 4.8. Mass changes for the samples during accelerated salt weathering (for 15 cycles)	126
Figure 4.9. Visual changes of the specimens during salt weathering test.....	128
Figure 4.10. Comparison of porosities calculated for brick before and after weathering test	130
Figure 5.1. (a) Granite column showing flaking and delamination as weathering signs (b) An unweathered granite column from the same structure	137
Figure 5.2. Coral stone columns showing damages of different degree (a) no damage (b) minor (spalling of plaster) (c) major (usage of improper incompatible brickbats leading to deterioration).....	139
Figure 5.3. Examples of extreme damages in the columns (a) heavy ridging (b) deep cracking (c) fissures and loss of section	140
Figure 5.4. Failure of a coral stone cube under compression	142
Figure 5.5. X-ray diffractogram of granite stone used for the study	147
Figure 5.6. X-ray diffractogram of coral stone showing the major peaks	149
Figure 5.7. SE image of weathered granite.....	151
Figure 5.8. SE image of weathered granite depicting atmospheric depositions	151
Figure 5.9. Biotite and hornblende in an unweathered granite sample.....	152
Figure 5.10. SEM images of coral stone (a) Quartz grains (Q) lined by magnesian calcite (M) along with calcite (C) (b) less dense distribution of magnesian calcite around quartz grains	153
Figure 5.11. Petal-like lining of magnesian calcite around the quartz grains.....	154
Figure 5.12. Distribution of prismatic crystals of calcite in the coral stone microstructure.	155
Figure 5.13. (a) Prismatic calcite crystals (b) A magnified view elucidating the habit of calcite crystals showing corrosion pits	156
Figure 5.14. Petrographic images: (a&b) Unweathered granite (c & d) Weathered granite	157
Figure 5.15. Plane polarized petrographic images of coral stones (a) least weathered sample (b) calcite grains lined by magnesian calcite (c) sample from a weathered column surface	160
Figure 5.16. Cumulative intrusion curves for granite samples	161

Figure 5.17. Differential intrusion curves for granite samples	162
Figure 5.18. Cumulative and differential intrusion curves for a typical coral stone sample	164
Figure 5.19. Images of granite specimens (a) before salt weathering (b) after sulphate exposure (c) after chloride exposure.....	167
Figure 5.20. Mass change for granite samples under sodium sulphate salt weathering cycles	168
Figure 5.21. Mass change for granite samples under sodium chloride salt weathering cycles	168
Figure 5.22. Coral stone specimens a) before subjecting to artificial weathering cycles b) after subjecting to Na ₂ SO ₄ exposure c) after subjecting to NaCl exposure	169
Figure 5.23. Mass change for the specimens (a) with Na ₂ SO ₄ exposure (b) with NaCl exposure	170
Figure 5.24. Curves from MIP data for natural undamaged coral stone and accelerated weathered coral stone.....	172
Figure 5.25. SEM image depicting preferential deposition of NaCl crystals over magnesian calcite	174
Figure 6.1. Illustration of water drop absorption test.....	181
Figure 6.2. Variation of capillary porosity for specimens with different coatings	182
Figure 6.3. Water absorption by Karsten tube test.....	184
Figure 6.4. Mass variation of the measure-cell with time.....	186
Figure 6.5. Illustration of cut specimen wetting with water to find penetration depth.....	188
Figure 6.6. Cut-surfaces of specimens wetted in water, showing the penetration depth of treatments	189
Figure 6.7. Mass changes with increasing wet-dry cycles with Na ₂ SO ₄ solution	192
Figure 6.8. Mass changes with increasing wet-dry cycles with NaCl solution	194
Figure 6.9. Damage state of specimens C1, C1-SC and C1-AS respectively after 20 weathering cycles.....	196
Figure 6.10. Damage state of specimens C2, C2-SC and C2-AS respectively after 20 weathering cycles.....	196
Figure 6.11. Comparison of damage patterns with silicone-based (SC) and acrylic-based (AS) coatings	199

Figure 6.12. Surface of C2-AS specimen showing cracking of the acrylic-siloxane based coating.....	200
Figure 6.13. Sudden rupture of VN- specimen after 7th, 8th and 9th cycle respectively.....	200
Figure 6.14. Different morphologies of salt crystals seen in efflorescence.....	202
Figure 6.15. C1, C1-SC and C1-AS specimens respectively before and after weathering...	203
Figure 6.16. C2, C2-SC and C2-AS specimens respectively before and after weathering...	204
Figure 6.17. UPV variation for the specimens during weathering	207
Figure 6.18. (a) Cumulative intrusion curves (b) Differential intrusion curves	209
Figure 6.19. Comparison of differential intrusion curves for unweathered and weathered specimens with coatings wit Na_2SO_4 (a) for C1, (b) for C2	212
Figure 6.20. Relative volume fraction of pores of various size ranges for unweathered and weathered samples	214
Figure 6.21. Comparison of differential intrusion curves for unweathered and weathered specimens with coatings with NaCl (a) for C1, (b) for C2	216
Figure 6.22. Interior of weathered (with Na_2SO_4) C2-SC sample after desalination	217
Figure 6.23. Surface of weathered (with NaCl) uncoated C1 sample before and after desalination	219
Figure 6.24. Interior of weathered (with NaCl) uncoated C2 sample after desalination.....	220
Figure 6.25. Comparison of total porosity values before and after desalination on (a) Samples weathered with sodium sulphate (b) Samples weathered with sodium chloride	222
Figure 6.26. Mass changes with increasing exposure with NaCl spray.....	224
Figure 6.27. Images of specimens after 450 days of NaCl spray test.....	225
Figure 6.28. Ultrasonic pulse velocity values for the specimens during NaCl spray test.....	226
Figure 6.29. SEM image of C1 specimen after being subjected to NaCl spray test.....	228
Figure 6.30. SEM image showing the larger unfilled pores in C1 samples after salt spray test	229
Figure 6.31. NaCl efflorescence in the exterior surface of a specimen subjected to salt spray test	230
Figure 6.32. Desalinated pores in sample C1 weathered with NaCl spray test	231
Figure 6.33. Differential intrusion curves for specimens subjected to NaCl spray test	233

Figure 6.34. Relative volume fraction of pores in different size ranges	235
Figure 7.1. Framework for characterising historic masonry materials	243
Figure 7.2. The relative volume fraction of pores of different sizes in various brick samples	246
Figure 7.3. Representation of crystal formation in an interconnected pore-network	247
Figure 7.4. Conceptualisation of the bonding of an ideal water-repellent to the substrate...	252

LIST OF TABLES

Table 2.1 Summary showing estimated firing temperature from mineral identification.....	24
Table 2.2. Pore sizes and corresponding water transport mechanisms.....	29
Table 2.3. Various expressions for crystallization pressure in a pore	39
Table 2.4. Factors in the test conditions of accelerated weathering tests	48
Table 2.5. Results of the performance analysis of various protective treatments for masonry (Kronlund et al., 2016).....	61
Table 3.1. Particulars of water repellent treatments selected for the study	72
Table 4.1. Visual evaluation of brick samples.....	100
Table 4.2. Mineralogical quantification from XRD data.....	106
Table 4.3. Physical and mechanical properties of the natural salt-attacked samples	120
Table 4.4. Quantification of mineral phases in bricks T1 and T2.....	123
Table 4.5. Relative proportions (as % volume) of various pore sizes	125
Table 4.6. Pore parameters obtained from MIP	125
Table 5.1. Compressive strength of granite cubes collected from the site	141
Table 5.2. Compressive strength of granite cubes collected from the nearby quarry (fresh granite)	141
Table 5.3. Compressive strength of dry coral stone cubes	143
Table 5.4. Compressive strength of dry coral stone cubes	143
Table 5.5. Water absorption values for granite and coral stones	144
Table 5.6. Capillary porosity for granite and coral stone specimens.....	145
Table 5.7. Ultrasonic pulse velocity (m/s) for granite and coral stone specimens	146
Table 5.8. Quantified data for the composition of minerals in granite	147
Table 5.9. Quantified data for composition of minerals in coral stone.....	149
Table 5.10. Pore parameters of the granite samples	163
Table 5.11. Relative volume fractions of different pore size ranges	163

Table 5.12. Relative volume fractions of pores of various size range for coral stone sample	165
Table 5.13. Pore size ranges for coral stone samples before and after accelerated weathering tests (with sodium sulphate).....	173
Table 6.1. Equivalent air layer thickness values (S_d).....	187

NOTATIONS AND ABBREVIATIONS

η	porosity
A	Cross-sectional area of the specimen (mm ²)
ASI	Archaeological Survey of India
d	Average specimen thickness (mm)
EDS	Energy Dispersive Spectroscopy
ESEM	Environmental Scanning Electron Microscope
FESEM	Field Emission Scanning Electron Microscope
HCC	Heritage Conservation Committee
ICP	Induced Coupled Plasma
INTACH	Indian National Trust for Art and Cultural Heritage
MIP	Mercury Intrusion Porosimetry
M _{s0}	Mass of the dry specimen (g)
M _{sv}	Vacuum saturated mass of the specimen (g)
S	Supersaturation degree
SEM	Scanning Electron Microscope

TGA	Thermo-Gravimetric Analysis
XRD	X-ray Diffraction
XRF	X-ray Fluorescence
γ_{cl}	Interfacial free energy
Δp	Crystallization pressure in a pore
ρ_w	Density of water (g/mm^3)

1 INTRODUCTION

1.1 PROBLEM STATEMENT

India possesses a rich built heritage that includes several monuments of international and national importance. Among these, around 3691 monuments are well documented and protected by the government (by Archaeological Survey of India), which also includes the 38 UNESCO identified world heritage sites as of 2019. However, thousands of heritage buildings remain unidentified and unprotected, and some are not even listed under the control of state governments or any local departments. Heritage structures constitute the identity of a civilisation, which is passed on from one generation to the other. Thus, their preservation is of utmost importance.

Most of the historic buildings in India are of either brick or stone masonry. The importance of masonry structures lies in the fact that they consume the least energy while providing the greatest natural comfort, in addition to their longevity if well preserved. Many of the protected, and mostly all of the unprotected heritage masonry structures in India are on the verge of damage and demand repair. In most cases, the repair methodologies used have been from a reactive approach, without the support of a proper background scientific study. This often results in further frequent interventions. To avoid this, detailed documentation of the current state of the structure, a study on the properties of the original units used in it and the deterioration processes that the system has undergone in the past is essential. This

information will provide the solution for the most suitable repair methods, with the compatible repair units. However, no studies so far have attempted a scientific investigation on the characteristics of any of these Indian historic masonry units. Also, a general methodology to characterise the historic bricks of any conservation state to understand their performance has not been established. India needs to develop a formal system of conservation with knowledge of material properties from different ages, and selection of repair strategies based on the previous history of restorations, if any.

A major difficulty is the lack of a formal methodology for characterising the materials, and the challenges could be entirely different for building stones and bricks. In the case of stone masonry, identifying the type of rock using microscopic techniques, and analysing the petrophysical properties and the decaying state are critical for suggesting compatible materials (De Kock et al. 2015). The unknown origin and the uncontrolled degree of variability in environmental effects on the stones create high ambiguity in the study. Regarding bricks, uncertainties about the raw materials used in the past, the firing temperature and the manufacturing processes in the ancient times are the challenges. Compatibility of repair materials needs to be determined based on the porosity and moisture transport characteristics, which mainly depend on the factors mentioned above.

Salt crystallisation is reported as the major deterioration mechanism affecting historic masonry structures. The extent of damage depends on the material properties as well as the environmental condition. The pore structure of the material determines the durability to salt attack and freeze-thaw weathering. Hence, micro-analytical studies on the pore structure evolution with weathering also need to be performed to understand the process better.

The protection of masonry structures by applying coatings is another important aspect of conservation. Conventional methods being employed include the usage of either silicone-based or acrylic-based coatings for stone masonry irrespective of the type of stone and kind of damage and plastering for brick masonry structures, which even ruins the aesthetic value. Various water repellent coatings, which vary in their performance, can have different actions with varying substrates. There is a need to analyse the efficiency of different water repellent coatings for different masonry units for a durable restoration and maintenance. Also, it is essential to look for the compatibility features between the protective treatment and the substrate material to ensure effective conservation practices.

1.2 KEY RESEARCH QUESTIONS

The following are the key research questions that the current study intends to address:

- i. Why are some of the historical masonry structures still sturdy and in excellent conservation state, while some are heavily weathered, irrespective of their age?
- ii. What are the fundamental properties in a brick or stone unit that determines the durability of the material in salt exposure?
- iii. What are the important properties to be investigated for new masonry units that are intended as replacement for historic masonry units?
- iv. How does the process of salt crystallisation and subsequent damage differ in materials of different microstructure, when they are exposed to the same extent of weathering?
- v. Na_2SO_4 is established as the most deleterious salt for masonry, and its damaging effects are studied extensively, whereas NaCl is reported as a less damaging salt.

However, since NaCl is an omnipresent salt, how is the effect of NaCl different from that of Na₂SO₄ for materials of different microstructures when subjected to long-term exposure?

- vi. Is there any possible relationship between the properties of a water-repellent treatment and the microstructure of the substrate material on which it is coated, in determining the durability of the new treated system?

1.3 RESEARCH OBJECTIVES AND SCOPE

1.3.1 Objectives

The principal objective of this study is to create a better understanding of the science of salt crystallisation - which is the most common deterioration mechanism concerned with porous masonry units. More profound knowledge of the phenomenon would help in improving the efficiency of conservation practices by choosing the right replacement materials and right protective methods for a historic structure in a particular environment. The overall study is divided into different phases so that the following sub-objectives are achieved:

- i. To characterise historic masonry units from India and identify the parameters determining the durability of the materials, on considering specific environmental exposure conditions.
- ii. To study the effect of pore structure and pore size in masonry materials on the degradation mechanism of salt attack by conducting artificial accelerated weathering tests.

- iii. To evaluate the efficiency and compatibility of water-repellent protective treatments for masonry units and identify the role of the pore structure of the material in improving the performance of the treatment in resisting salt attack.

1.3.2 Scope

This study was limited to:

- i. Samples of fired clay bricks, granite and coral stones, all collected from within the state of Tamil Nadu in India.
- ii. Salt crystallisation mechanisms with respect to only two salts - Na_2SO_4 and NaCl .
- iii. Action of two types of water-repellent treatments - a silicone-based treatment and an acrylic-siloxane based treatment.

1.4 METHODOLOGY

The research methodology adopted for this thesis is mainly divided into three phases.

Phase 1: Sample collection and characterisation of materials: This phase constituted the process of sample collection - both historic and commercial fresh samples, and evaluating their properties. The mineral composition, physical properties, and microstructural features were understood by basic and advanced analytical techniques.

Phase 2: Salt weathering resistance of materials and the role of microstructure: Naturally and artificially weathered samples were subjected to micro-analytical characterisation techniques to understand the phenomenon of salt crystallisation and subsequent modifications in microstructure.

Phase 3: Evaluation of efficiency and compatibility of protective treatments: This phase pertains to the study on various water-repellent treatments, their properties and their compatibility with masonry units of different microstructure in resisting salt weathering.

The detailed methodology followed for the study is presented in Chapter 3.

1.5 THESIS LAYOUT

The thesis comprises eight chapters including the current chapter. A brief summary of the contents in each of the subsequent chapters is given here.

Chapter 2 provides the background information to the research problem by a critical review of the available literature on the characterisation of the microstructure of historic masonry materials, and salt crystallisation - which is identified as the most significant deterioration mechanism. This chapter also discusses the role of the microstructure of the material in determining the durability, and the variation with respect to the action of different salts. The chapter ends with discussions on the studies reported so far in the area of protection of the masonry constructions with treatments.

Chapter 3 provides information pertaining to the experimental program. The testing philosophy, the overall methodology of the thesis, which is divided into different phases, various types of samples used in the study and the test methods adopted are presented.

The characteristics of brick and stone samples collected from various heritage sites, as well as from commercially available stock, are covered in Chapters 4 and 5. In Chapter 4, the experimental results that pertain to the characterisation of brick units, including the

physical-chemical-mechanical and microstructural properties of each type of brick, are explored. The chapter presents the evaluation of salt weathering resistance of each material. Chapter 5 presents the characteristics of stone samples - a low porosity stone (granite) and a high porosity stone (coral stone). On conceiving the significance of pore structure of a material from the results of Chapter 4 with respect to bricks, the contents of Chapter 5 reconfirm the role of pore size and pore distribution of a material in determining its durability performance by conducting similar studies with stones of different pore structures.

Chapter 6 presents the experimental results on evaluating the performance and suitability of water-repellent treatments for a historical masonry unit. This chapter also investigates the compatibility between the water-repellent and the substrate-microstructure.

A general discussion of the complete experimental program is attempted in Chapter 7. This chapter helps in consolidating all the major learnings from the study and discusses them with the aim of improving the scientific knowledge on the topic of salt crystallisation through the results observed. Chapter 8 presents the conclusions from the study, along with recommendations for future work.

2 LITERATURE REVIEW

2.1 INTRODUCTION

India possesses a diverse stock of masonry heritage buildings, among which many are in need of conservation. There is a lack of adequate documentation on the properties of ancient building materials and construction technology, which is necessary to understand the process of conservation. In this chapter, several studies on Indian built heritage from various domains have been reviewed and presented systematically. Aspects such as history and status of historic masonry conservation, the major deterioration problems associated with masonry units like bricks and stones with the different mechanisms and the methods of protecting the historic masonry are presented. This would provide a background for studying and reporting the required properties of heritage masonry units which can be linked to the deterioration mechanisms to assess or alter the performance. Salt weathering was identified as the most crucial deterioration mechanism affecting these porous masonry structures. The importance of this phenomenon and the causes and variations that can occur in the mechanisms are well studied. The action of various protective treatments and the methods to identify their effectiveness are presented and critically reviewed.

2.2 CONSERVATION OF MASONRY STRUCTURES

2.2.1 Conservation of masonry structures - International status

The UNESCO (United Nations Educational, Scientific and Cultural Organization) supports and encourages identification and protection of heritage sites of cultural importance around the world, which includes monuments of historical, archaeological, aesthetic and scientific value. Following this, UNESCO had laid the foundation of an international agreement called World Heritage Convention that was acknowledged in UNESCO General Conference Meeting in 1972, which emphasized the importance of national-level team works with the aim of addressing issues with World Heritage (UNESCO World Heritage Centre, 2005 a).

The World Heritage Convention (WHC) is one of the best known and foremost international tools of conservation. As of 2019, there are a total of 1121 World Heritage properties registered on behalf of 167 countries. The context of heritage preservation from a global perspective has changed over the past four decades with increasing complexity in the operations. When the number of world heritage sites grows to more than 1000, commitments for sustainable development, enhanced capacity requirements etc. intensifies. UNESCO's fiscal crisis was exacerbated by the United States' recent financial withdrawal after the controversy over recognition of Palestine as a signatory, and issues with expert opinions and decision making etc. acted as mounting challenges. On the 30th anniversary of the World Heritage Convention, UNESCO developed a new strategy with Five Cs: Credibility, Capacity Building, Conservation, Communication and Communities. But the five issues still continue as unresolved as per the report by Meskell (2013).

Jones and Munday (2001) stated that a unique trade-off between maintaining cultural value and promoting tourism over local communities happens in most international built heritage protection projects. The article demonstrates this by examining the case of Blaenavon Industrial Landscape in South Wales, which was then a recently recognized UNESCO World Heritage Site.

Harrison and Hitchcock (2005) compiled different papers in the book “The Politics of World Heritage” which provided priceless insights into the negotiation between tourism and conservation in a variety of different contexts. Somuncu and Yigit (2010) have analyzed all the World Heritage sites in Turkey and identified the site-specific and general issues in conservation and management of heritage sites. The need for appropriate management plans with efficient implementation to deal with issues faced by heritage sites, implementing efficient visitor management plan framework and efforts to spread awareness to the local population about the significance of heritage sites and preventing vandalism etc. were suggested. They observed that the issues in heritage conservation on an international perspective are more in the managerial domain. The new doctrines of heritage protection which are being applied internationally, like the Venice Charter, ICOMOS Charter etc. play significant roles in the process of managing conservation (Menon, 2014). There are many studies taken up on various historic materials abundantly in European countries, which have helped in establishing the characteristics and behaviour of such materials. Also, the protection and maintenance of historic buildings usually are practised periodically in most European heritage cities through different organizations because they are well established as historic places (Hitchcock 2005). Constant financial sources, awareness on the significance

of heritage protection, and obviously the lesser population which could be easily trained and made aware of conservation must have acted as supporting agents.

To summarize, transparency and efficiency in the management plans of responsible authorities and financial crisis are the two major challenges reported in the field of international heritage conservation. The significance of protection and preservation of heritage is mostly well addressed. And thus, the most necessary work is ensuring efficient and optimized protective protocols. Research has been carried out and is continuing on heritage materials and effective conservation - this will be reviewed in the subsequent sections.

2.2.2 Conservation of masonry structures- National status

2.2.2.1 History

India is very well known for its indigenous wealth of built heritage with the richest and most diverse stock of masonry structures, being the birthplace of Indus valley and Harappan civilizations. The first instance of conserving structures in India was recorded in the 14th century AD when Firuz Tughlaq gave the order to protect ancient structures. Further instances of conservation ideas documented were the “Bengal Regulation (XIX)” and “Madras Regulation (VII)” passed in 1810 and 1870 respectively, which vested the power to the government to intervene when public buildings possess any threat of damage. Again in 1863, Act XX gave the authority to the government for preventing any threat of injury and ensure the conservation of buildings with historical value. But in the course of time, with changing rulers and kingdoms, many buildings were destroyed by the prevalent government

itself. In 1861, the Archaeological Survey of India (ASI) was established for initiating legal provisions in preserving/protecting the heritage structures all over India, which is active and influential at present also. The State Department of Archaeology was established in 1978 and Indian National Trust for Art and Cultural Heritage (INTACH) in 1984, which works for stimulating awareness in the area of conservation of heritage in the country. Currently, there are several agencies which are concerned with the conservation of built heritage, and they are listed as: Heritage Conservation Committee (HCC) under Ministry of Urban Development, Archaeological Survey of India (ASI), State Archaeological Department, Govt. of NCT of Delhi, Delhi Development Authority (DDA), INTACH, Aga Khan Trust, etc.

2.2.2.2 Current status

According to the current status, out of the extensive count of historic buildings in India, 36 edifices are declared as World Heritage sites by UNESCO - the sixth most of any country in the world (UNESCO World Heritage Convention 2020, Ministry of Culture - Government of India 2020). Figure 2.1 shows the location of the World Heritage Sites in India. Around 3650 historic monuments in India come under Archaeological Survey of India (ASI), and are officially declared to be known as monuments of national importance, thousands of structures are under the control of Archaeology Departments under state governments and other religious endowments, and many thousands that are not even listed or documented under any formal system. Non-Governmental Organizations like INTACH now take charge of protecting these formerly unprotected heritage structures. Even though the traditional materials and manufacturing techniques are mostly undocumented, the renovation process of heritage buildings still sometimes employs the involvement of conventional masons and

artisans. The history of heritage monuments and the conservation practices followed in past are to be known and practised in future also with acceptable robustness. So, it is vital to follow systematic, documented procedures of scientific value in the process. Heritage conservation is primarily an interdisciplinary field which demands to protect the history of civilization and spirit of place. The efficiency of the process simultaneously should be optimized by inculcating science and engineering in it (Menon, 2017).

The action of incorporating advanced science and engineering into effective conservation practices is at a nascent stage in India. The available knowledge on materials and their behaviour from heritage monuments in India is minimal. There are only very few numbers of studies reported in the area of historic conservation in India.

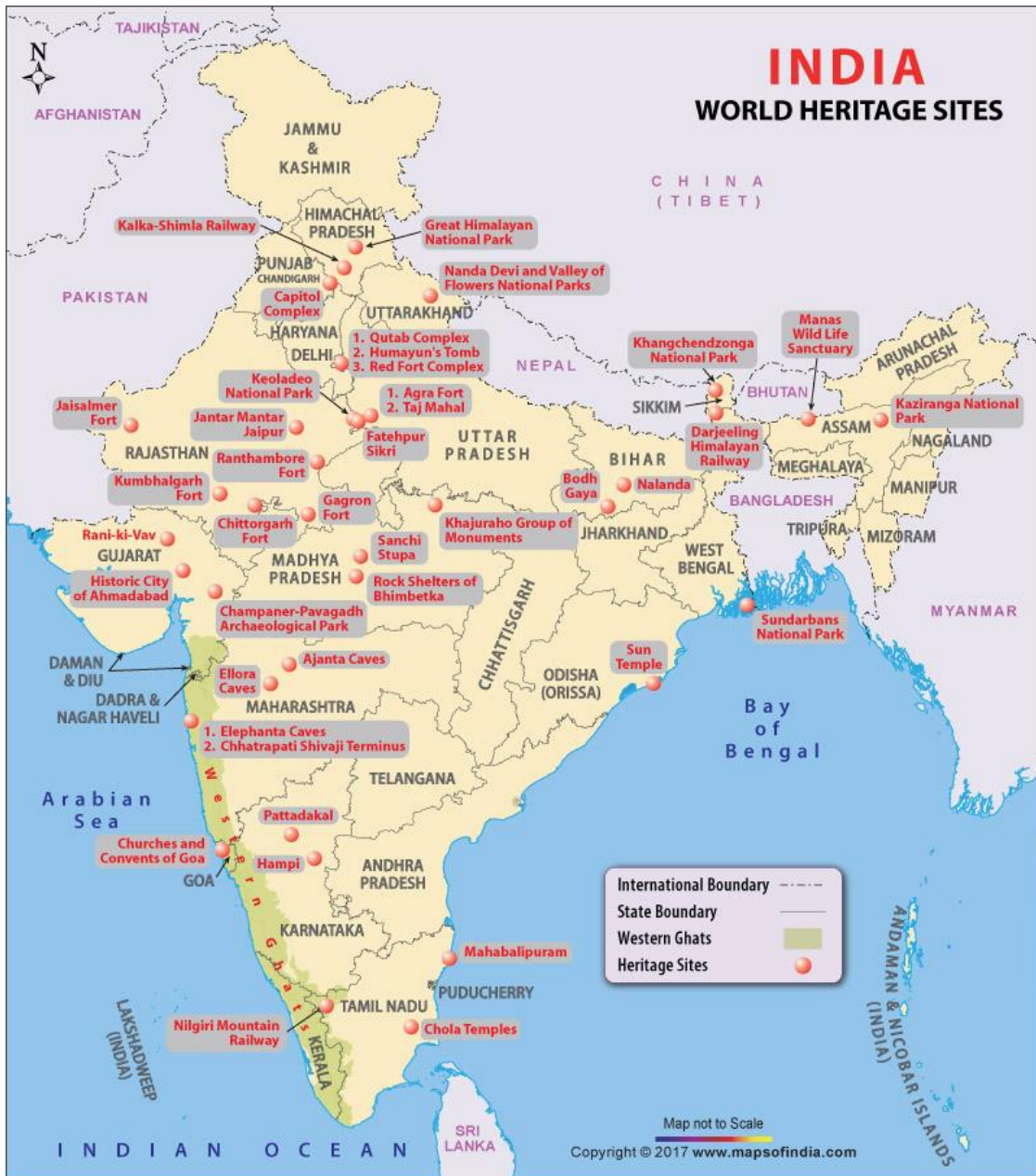


Figure 2.1. Map showing World heritage Sites in India (courtesy: mapsofindia.com)

2.2.2.3 Heritage studies based on archaeological motives

Excavation studies from historic locations in Eastern India by Smith and Mohanty (2016) showed archaeological evidence of 1000 years old construction in Sisupalgarh, Odisha with remnants of laterite blocks, bricks, tiles and terracotta. The study acted as a surface survey on the culture but did not look into the ancient construction materials or properties. Similar historical survey studies were reported by Lal (1949), Mate (1969), Chakrabarti and Dilip (2000) and Mohanti et al. (2013). Kennet and Rao (2010) presented a well-described excavation study on a historic brick temple from Goa, India, probably of 6th century AD. The different phases of construction were identified from the different layered bricks and stones of varying quality. Bricks were found with different grade of weathering at various locations. Other than laterite, no other stones or bricks were identified or mentioned for its properties. Most of the construction materials in all these studies were in severely weathered condition, and lack of literature on the performance and properties of these historic masonry units blocked the detailed understanding of probable causes of damage. A lack of correlation existed between the conditions of materials observed with history and exposure.

2.2.2.4 Indian studies on heritage material characterization

Studies from India on heritage structures that had an engineering perspective include some initial investigations on mud (Mathews and Somayaji, 1993) and traditional timber from ancient structures (Shaji et al., 1992; Somayaji et al., 1994). The studies demonstrated renovation strategies for heritage structures made with these materials, focusing on diagnostic intervention. Attempts to study the deterioration processes of heritage materials from India were carried out on laterite stones from Kerala in South-West India (Kasthurba et

al., 2007; Kasthurba et al., 2008). Properties and performance of the laterite as a building stone was studied in detail. The attempt to establish a correlation of the microstructural and chemical properties of laterites with their engineering aspects was supported by tests such as XRD, thin section studies, SEM and chemical analysis. The results showed that laterite is a particular type of indurated soil with unique pore parameters and physical-mechanical-chemical properties. However, the science behind the process of deterioration and thus protection based on the microstructural studies were not covered in this study – such reviews are equally crucial in conservation as about knowing the material properties.

A similar study was conducted by Anupadma (2009) in which methodological characterization of sandstone and granite samples from ancient sites of Tamil Nadu was presented. This study analysed the weathering process in stones using chemical and petrographic analysis, microstructural characterization and included the application of artificial dry-wet cycles. Rainwater ingress was identified as the major cause of deterioration in the studies conducted, and the possibility to use protective treatments was evaluated. But the altered behaviour of stones in the presence of protective treatments was not analysed in a sense to express the efficiency of a particular coating. Another study on heritage masonry unit was presented by Sharma et al. (2007) on Kota stones (a special type of limestone seen in the Kota district of Rajasthan, India) regarding their physio-mechanical properties in different environments. In India, the presence of Kota stone can be seen in many historic buildings from time immemorial for ornamental and decorative functions. The major physio-mechanical properties like uniaxial compressive strength, shear strength, tensile load, triaxial strength, bulk density, elastic modulus, Poisson's ratio, point load strength index and P-wave

velocity were measured at various pH values (by submerging the stone specimens in different pH solutions till they get saturated) in the laboratory. The properties were found to be adversely affected by highly acidic and alkaline environment, where the effect was worse with acidic environment.

2.2.2.5 Heritage studies based on structural stability

Research studies from the point of structural stability were carried out in different historical monuments where the properties of stones were tested with more emphasis on the physical-mechanical properties. Bagde (2016) had done a study on The Ajanta caves, located on the northern edge of the Maharashtra Plateau in Aurangabad District, India, which comes under the classification of UNESCO World Heritage Monument where ancient Buddhist rock-cut caves are present. The author characterized the failure modes in the caves and reported planned stabilization methods for the same. Weathering and deterioration of rocks were found to be critical, which led to boulder dislocations, water seepage, distressing and delamination of the material. The protective measures like spot bolting, grouting, wire mesh etc. were put forward based on factors like stress distribution, safety and preservation of heritage. A combined approach of geological and microstructural studies on the rocks would have enhanced the understanding of the reason behind the cracks, and thus in suggesting the action of efficient conservation practices in preventing the identified distresses.

Other significant studies from India on the structural stability of historic monuments based on seismic properties were reported by Menon (2002), Mathews et al., (2003) and Santhakumar et al. (2010). Studies based on seismic case studies and damage assessment

from ancient structures were also discussed by Menon et al. (2012) and Menon and Murthy (2013). Analytical and modelling studies on the same topic were presented by Varatharajan et al. (2012), Kollerathu et al. (2016) and Ronald et al. (2008). The structural responses of historical buildings from various materials are well discussed, but considering the importance of cultural heritage in India, sufficient knowledge of the material behaviour and properties is lacking. A combined understanding helps in correlating the material properties and performance to the structural behaviour and stability, thus resulting in better conservation methods.

2.3 Characterisation and durability of masonry units

Characterisation of masonry units can be broadly done in two stages – in-situ and laboratory analyses. In-situ testing deals with the identification of stone or brick types in the field by visual and simple surface tests and also, some semi-destructive or non-destructive testing of stones/bricks at monument scale. On the other hand, laboratory analyses include different destructive testing methods which can be physical, chemical, mineralogical or petrographical (Török and Píkryl, 2010). The division of broad stages of characterization is represented in Figure 2.2. These analyses aim at identifying the type and nature of the masonry units and to study their long-term behaviour and future preservation after understanding the current state. The detailed documentation and mapping of lithotypes, condition assessment and graphical demonstration of decay features are broadly accepted methods applied at monument scale (Fitzner et al. 1995). Schmidt hammer test, portable ultrasonic pulse velocity test, electrical resistivity etc. are common non-destructive tests carried out in

heritage sites for the in-situ evaluation of mechanical and physical properties of masonry (Griffin et al. 1991).

Laboratory analyses include a wide range of tests, in most cases with destructive methods. Laboratory tests provide an understanding of the long-term behaviour of natural stones. The selection of replacement stones satisfying the compatibility characteristics and aesthetic criteria is another important aspect of lab studies. The recommendations given by European standards, International Society of Rock Mechanics suggested methods, ASTM and RILEM guidelines are more often followed in the laboratory test procedures. Laboratory simulation of extrinsic factors such as thermal behaviour, salt weathering and artificial ageing is often used to assess the durability of natural stones (Luque et al., 2010; Vicente & Rives 2000). Advanced and standard analytical techniques such as portable XRF (X-ray Fluorescence) and portable XRD/XRF (X-ray Diffraction), X-ray tomography, SEM-EDS (Scanning Electron Microscopy/ Energy Dispersive Spectroscopy), TGA (Thermo-Gravimetric Analysis) etc. are used for advanced and more profound studies on the deterioration of masonry on weathering. ICP (Induced Coupled Plasma) along with infra-red spectroscopy was shown effective in determining the average chemical composition and mineralogical composition of materials too (Rozenbaum et al. 2008). The results demonstrated the importance of these techniques in discovering a potential incompatibility because of the difference of transfer properties.

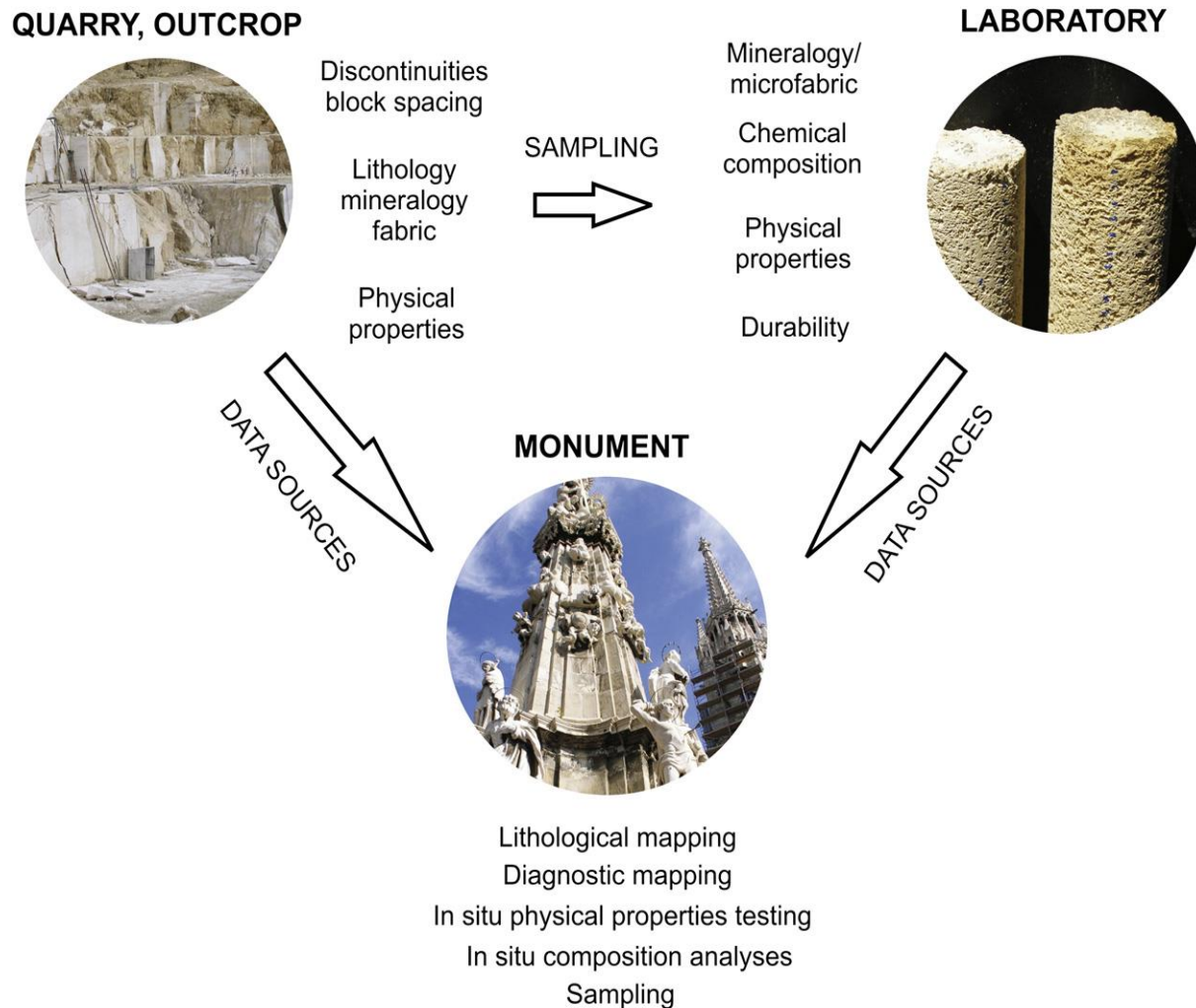


Figure 2.2. Main tools of stone testing in the quarries, at the laboratory and the monuments and the use of techniques at different levels (Torok and Prikryl (2010))

Microstructural characterization plays a pivotal role in understanding the durability of the material in different exposures with time. The following section explains the role of various microstructural characterisation techniques in determining specific properties of bricks that are directly linked to their durability.

2.3.1 Mineralogical composition

X-ray diffraction (XRD) is the most common technique in use to identify and quantify the mineralogical composition of heritage bricks. X-ray fluorescence (XRF) is another primary method used to analyse the elemental compositions. Scanning Electron Microscopy (SEM) with Energy Dispersive Spectroscopy (EDS) also helps in identifying phase compositions and sometimes the presence of rare inclusions in the brick matrix. Understanding the mineralogy of bricks is the key for two critical data regarding the ancient bricks - the raw materials and the firing temperature. Knowing the raw materials and firing temperature of ancient bricks is important in understanding the properties, the reason for the weathering behaviour and in manufacturing compatible replacement bricks wherever necessary.

2.3.1.1 Mineralogy and raw materials

Among the raw materials, clay can be either calcium-rich or low-calcium clay, which affects the properties of bricks significantly. This is due to the changes in vitrification and hence pore structure, which occurs in correspondence to the mineralogical transformations during heating (firing) of the brick (Cultrone et al. 2004; Elert et al. 2003). At a firing temperature of 800 °C, calcium compounds from Ca-rich clays decompose and form CaO, which turns to Ca(OH)₂ on combining with water. This Ca(OH)₂ (Portlandite) converts back to calcite when it reacts with CO₂. These reactions will finally result in a highly fissured system because of the increase in the volume called “lime blowing” (Cultrone et al. 2004; Elert et al. 2003). Correspondingly, bricks made with low-Ca clays show a slightly lesser porosity (Sağın and Böke, 2013a). In a study conducted by Elert et al. (2003), the total porosity of calcareous

samples was found to be 10 % greater than that of non-calcareous ones, when they were both fired at 1000 °C, which was similar to the results by Tite and Maniatis (1975).

2.3.1.2 Mineralogy and firing temperature

The process of firing is the key step in the manufacturing of brick units. During firing, chemical changes of mineral phases occur, and a bond is generated and strengthened by particle fusion and sintering of amorphous phases. Hence, the quality and degree of firing regulate the significant characteristics of the brick (Robinson, 1982). Firing temperature is the unknown factor in historic bricks, and is popular in research studies because it determines the physical and durability properties of clay bricks. Past studies have reported that smaller pores of size $< 1 \mu\text{m}$ predominate when the bricks are fired at temperatures less than 900 °C (Jin et al. 2017; Lopez-Arce and Garcia-Guinea 2005; Shu et al. 2017). At temperatures above 900 °C, bricks with low-Ca clays exhibited an increase in the number of pores $> 7 \mu\text{m}$ size, whereas no significant changes were seen for Ca-rich clays (Cultrone et al. 2004). The size of pores in the system is closely related to the durability of the bricks.

Salt crystallisation damage is the most crucial and common deterioration mechanism observed in porous masonry units and is caused due to the crystallisation pressure of the salt. This pressure is a function of supersaturation of the salt solution (exposure condition) and pore geometry (size and shape of pores) (Flatt et al. 2017). Past studies have shown that materials with most micropores have a high susceptibility to salt crystallisation damage (Maage 1980; Tsui et al. 2003; Russell 1927). Hence, knowing the combination of firing temperature and raw materials helps in assessing the salt weathering resistance of the

material. In heritage bricks, the firing temperature can be traced back from analysing the mineral composition using techniques like XRD and re-firing of bricks at different temperatures (Jordan et al. 2008; López-Arce et al. 2003; Peters and Iberg 1978). Many studies have reported that the primary minerals like calcite and dolomite decompose at temperatures around 750 and 800 °C. So, the presence of calcite and dolomite suggests that the bricks were fired at lower temperatures, of less than 800 °C. The calcite and dolomite react with silicates as the temperature rises to transform into neo-formed phases like gehlenite and diopside. Similarly, a significant contribution to the amount of hematite found in historic bricks was shown to come from the iron content in the phyllosilicates of raw clay material (De Bonis et al. 2017). Table 2.1 shows a summary from various papers reporting the identification of firing temperature from the presence of particular mineral phases.

Besides the high susceptibility to salt damage, poor physical-mechanical properties of bricks fired at low temperature (temperature less than 700°C) have been reported by Elert et al. (2003). Fracturing, weight loss, sanding, edge rounding etc. were the common damages reported. Shu et al. (2017) explained the reason for the inverse relationship between firing temperature and porosity as the molten phase formation, which occludes the pores at larger temperatures. Again, the authors suggested the conditional probability that the relationship may not stay consistent when the firing temperature is well below the onset of the melting process.

Table 2.1 Summary showing estimated firing temperature from mineral identification

Sl. No	Reference	Title of paper	Mineral phases	Suggested temperature(°C)
1	Peters and Iberg (1978)	Mineralogical Changes During Firing of Calcium-Rich Brick Clays	Kaolinite	< 500
			Dolomite	< 650
			Calcite	< 700
			Calcium oxide	700 to 900
			Illite, montmorillonite	< 950
			Gehlenite	860 to 1050
			Wollastonite, anorthite, diopside	> 860
			Sanidine	> 950
2	Cultrone et al. (2001)	Carbonate and silicate phase reactions during ceramic firing	Dolomite	< 700
			Muscovite	< 800
			Calcite	< 830
			Potassium feldspar	800 to 1000
			Gehlenite, wollastonite	> 800
			Diopside, anorthite	> 900
			Samidine, mullite	1000 to 1100
3	Cultrone et al. (2004)	Influence of mineralogy and firing temperature on the porosity of bricks.	Smectite, paragonite	< 450
			Dehydroxylated illite/ muscovite	< 900
			Gehlenite	> 800
			Mullite	> 900
			Wollastonite, diopside	> 1000
4	Lopez-Arce, Garcia-Guinea (2005)	Weathering traces in ancient bricks from historic buildings	Calcite, dolomite	< 800
			Gehlenite	> 800
			Diopside	> 900
5	Jordan et al. (2008)	Influence of firing temperature and mineralogical composition on bending strength and porosity of ceramic tile bodies	Illite	< 900
			Enstatite	1000 to 1150
			Gehlenite	950 to 1050
			Anorthite	> 1050
			Abundant mullite, amorphous phases	> 1100

2.3.2 Morphological characteristics

Scanning electron microscopy and optical microscopy are mostly used to observe textural and microstructural morphological features in the bricks which are then correlated with vitrification evolution, raw materials and pore distribution (Elert et al. 2003). Lopez-Arce and Garcia-Guinea (2005) showed interesting morphological observation in the ancient bricks through SEM images, which explained their surface chemistry. They demonstrated that SEM could be used for choosing preservation treatments and cleaning agents. Elert et al. (2003) presented SEM images of calcareous and non-calcareous brick fired at different temperatures starting from 800 to 1100 °C, which is the crucial range of firing temperatures. The authors clearly illustrated from the images that the degree of vitrification tremendously improves with increasing temperatures, as shown in Figure 2.3. Also, the difference between vitrification morphology and the change in cellular structure was shown between calcareous and non-calcareous bricks too, which were theoretically suggested in the past (Coletti 2016; Cultrone et al. 2005).

SEM imaging also helps in identifying the extent of weathering, the damage patterns and the reasons for the weathering in the ancient samples. Lopez-Arce and Garcia-Guinea (2005) showed fissures and corrosion pits in the calcite crystals within the brick and showed shreds of evidence of dissolution-corrosion-reprecipitation of calcite crystals in pores which finally end up bridging weathering cracks inside.

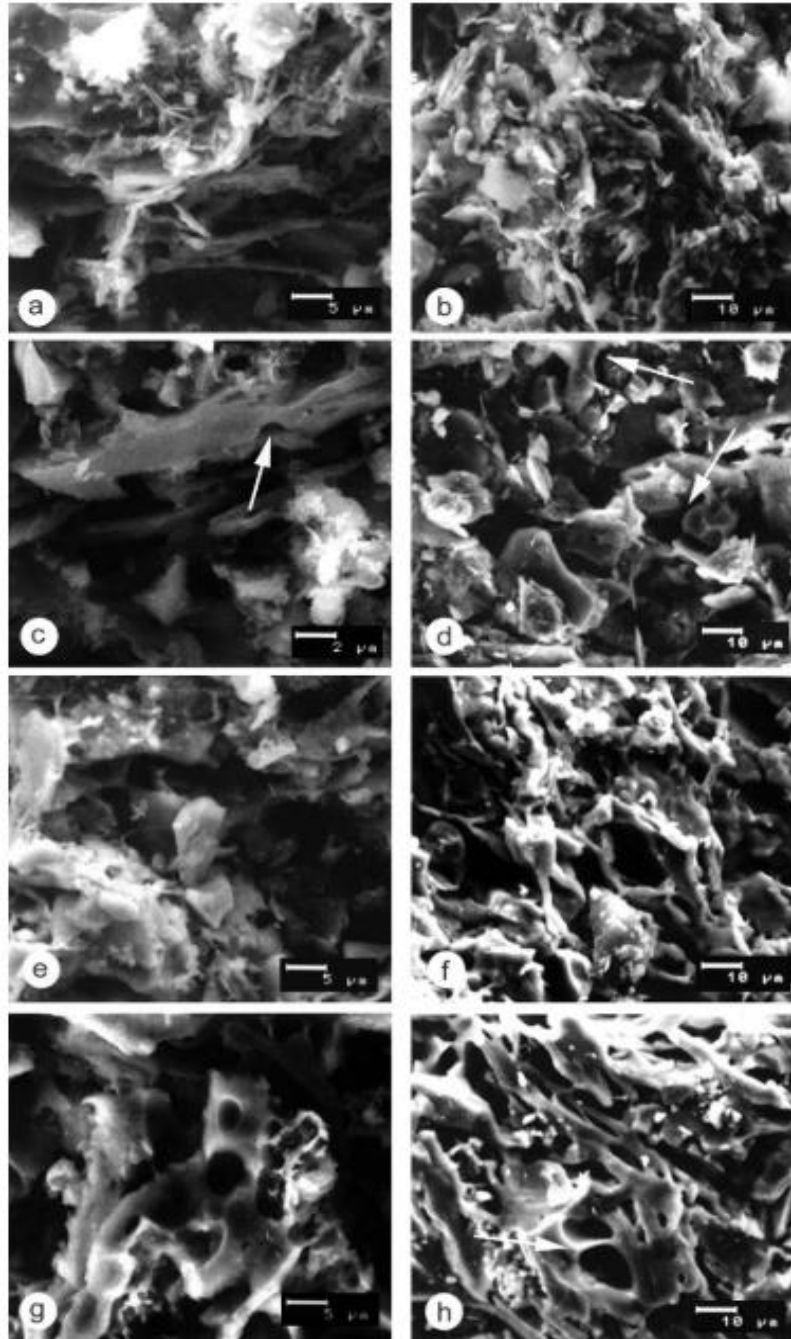


Figure 2.3. SEM images of calcareous (left column) and non-calcareous (right column) bricks fired at 800 °C (a and b), 900 °C (c and d), 1000 °C (e and f) and 1100 °C (g and h) (Elert et al., 2003)

It is also found that sometimes weathering decreases the water absorption and suction of bricks through cementing, dissolution and recrystallization processes that increase the compressive strength. In the study by Cultrone et al. (2005), this was found to be more common in bricks of calcareous clays and exposed to burial environments (under the soil) in which the pore system could get filled with secondary calcite by re-crystallization. SEM images were used in identifying the textural differences among various brick samples and connecting them to the presence of rounded and angular quartz fragments in different bricks, occurrence and distribution of crystals of hematite in one of the samples, lack of orientation of macropores and also presence of black stains which could result from burning of organic matter. The results were separately supported by other techniques like XRD, MIP etc.

The size, shape and distribution of pores in the brick matrix are highly significant with respect to durability. Larger and more rounded pores offer more salt crystallization resistance (Cultrone et al. 2004, 2005b). Sağın and Böke (2013) presented SEM images from which pore sizes were measured using image analysis and showed that the smaller pore sizes make the brick system more susceptible to salt weathering.

In the case of stones, SEM imaging was proved as an excellent tool in finding compatible replacement units for existing ancient rocks. De Kock et al. (2015) reported the problems in identifying different types of limestones through macroscopic observations and tests and hence used SEM imaging. From the weathering patterns and presence and distribution of pyrite particles observed through SEM images, the specific variety of limestone was identified. Palmer (2008) has similarly identified limestone varieties through petrographical images.

2.3.3 Pore structure and pore distribution

This section conveys the paramount significance of porosity and pore structure of a material in deciding its durability. The susceptibility of a brick to any deterioration mechanism is governed by its pore structure and composition (Robinson 1982). Pores or fissures are the in-built natural pathways in a material through which water or other fluids enter and flow through, thus facilitating physical, chemical and biological weathering (Dunning and Huf 1983; Franzen 2004). The pore structure is formed in case of bricks during the manufacturing process itself, which depends on a complex interaction of various factors like raw materials, firing temperature, manufacturing methodology (soaking time, weather conditions) etc. (Cultrone and Madkour 2013; Benavente et al. 2006). Parameters like the size of pores, their distribution and volume proportion, the shape of pores and the interconnections are all factors affecting the physical properties of bricks and stones. They are considered as the most important details to be studied for predicting durability of the material (Di Benedetto et al. 2015). Many researchers investigated the importance of porosity of different building units to understand how to reduce/prevent damage to the material (Molina et al. 2011). Theoretically, the total porosity in a material is the ratio of the total volume of pores to the bulk volume, as the sum of both closed and open porosity (Cueto et al., 2009). The open porosity is of more interest with respect to durability criteria because open pores are those involved in the hygric characteristics of materials (Vos 1978; Whiteley et al. 1977), which is the effective porosity (Anovitz 2015). Meanwhile, closed pores do influence the physical-mechanical characteristics of the materials as they are very much related to the strength, density, hardness and modulus of any material (Cultrone et al. 2004;

Lu and Zhou 2000; Dorey and Yeomans 2002; Seuba et al. 2016). Wendler and Charola (2008) had studied the role of different sized pores in water transport and corresponding processes during the interaction of liquids in these pores in porous inorganic building units. Table 2.2 shows the categorisation of the water transport mechanisms done by the authors at different pore sizes, which influences the durability of materials.

Table 2.2. Pore sizes and corresponding water transport mechanisms (Wendler and Charola 2008)

Macropores	Micropores		Nanopores	
> 1 mm	1 mm – 10 µm	10 µm – 0.1 µm	100 nm – 10 nm	< 10 nm
Liquid water flow				
	Capillary absorption			
		Water vapour adsorption and surface diffusion		
			Capillary condensation	
Water vapour diffusion				

There are a series of techniques available to study the pore size distribution in a material. Molina et al. (2011) found a remarkable difference between the porosity values measured by mercury porosimetry and microscopic images but also reported that the porosity obtained by the hygric test was more similar to that of mercury porosimetry. Digital image analysis measured the total porosity, but porosimetry and hygric test focused on only open porosity. The reason behind the difference in open porosity values with different techniques was suggested as the difference in the focused ranges of pores (macro, meso or micropores)

detected by various techniques. However, Zdravkov et al. (2007) reported that, on considering the properties of different sized pores, a unanimous classification of pores into specified ranges was difficult despite these various pore categories. Rodriguez-Navarro (1997) classified the pores as micropores for those with a diameter smaller than 60 μm , mesopores with diameter between 60 μm and 4 mm and macropores for those with a diameter greater than 4 mm. Coletti et al. (2016) presented a multi-analytical approach combining the direct and indirect methods for investigating pore structure in a brick system and evaluated these differences with different methods. Direct methods are the ones which use 2D and 3D images of the material microstructure like Computerized X-ray microtomography (micro-CT) and Scanning Electron Microscopy (SEM). The authors showed the unreliability of using image analysis as the only tool for measuring porosity by calculating porosities from three different images from the same sample and then by stitching them together as a single panoramic image (Figure 2.4). Indirect methods included Mercury Intrusion Porosimetry (MIP), hygric tests and nitrogen adsorption. Overlapping zones between each technique were identified by the author and a more realistic representation was obtained for the system combining the results from various methods judiciously as shown in Figure 2.5.

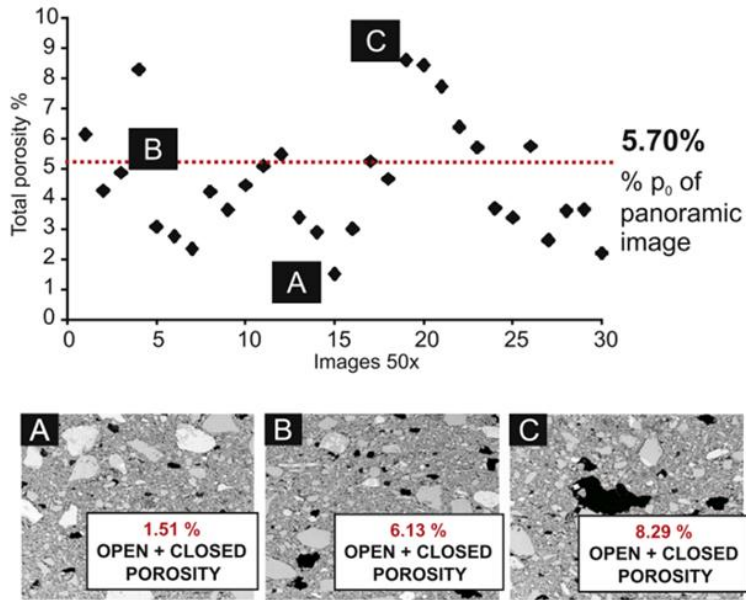


Figure 2.4. Comparison of total porosity for different images taken for a single sample (Coletti et al. 2016)

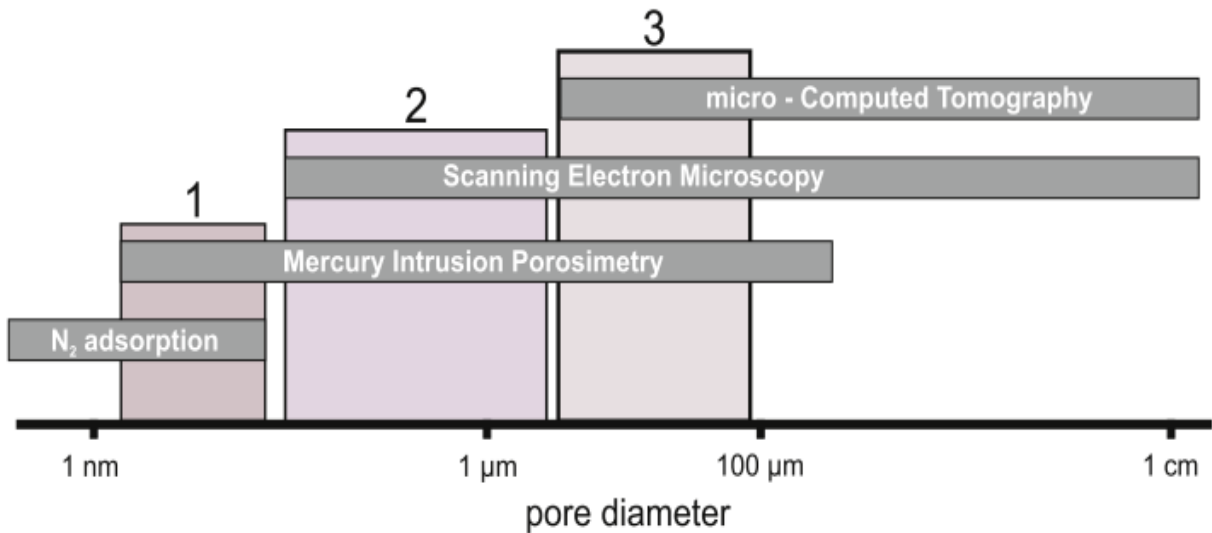


Figure 2.5. Sketch showing overlapping ranges of pores investigated with different techniques (Coletti et al. 2016)

For the common applicable range of pore sizes for a brick or stone system, Mercury Intrusion Porosimetry (MIP) was considered as an efficient tool by the research community. MIP permits a reasonable and reliable estimate of the open porosity. But there are certain limitations for the technique. The “ink-bottle effect” is a strong issue which can affect the determination of pore sizes of less than 1 μm . Another concern with MIP is the use of very small samples, whose selection needs utmost care to make it representative of the large unit (Abell and Willis 1999; Diamond, 2000; Coletti, 2016; Scrivener, 2016). Pore size distribution curves from mercury intrusion porosimetry data were used in many durability studies to analyze and quantify the weathering damage, and its causes. Ordonez et al. (1997) proposed a durability dimensional estimator to study the effect of pore system on limestones, using the porosimetry data. Similarly, Benavente et al. (2004) defined a new petrophysical durability estimator to correlate with the salt crystallization weathering, which was based on both grain strength and pore structure.

The study of pore system is significant in terms of durability in building units because of phenomena like freeze-thaw cycles being common in countries where temperatures near to zero are often reached, and salt crystallization where structures have easy access to soluble salts. Damages varying from minor external non-structural visual patches to extreme structural deteriorations have been reported due to both freeze-thaw and salt crystallization processes (Laycock 2002; Grossi et al. 2007; Steiger 2005; Espinosa et al. 2008). Fluid storage and circulation potential, salt crystallization and freeze-thaw cycles in the building materials are directly related to the open pores. Hence, these properties and their interconnection were found to have a direct influence on the deterioration rates in the

masonry units (Hall 2009; Aligizaki 2006; Cnudde 2013). The relation between pores and salt damage will be discussed in detail in the next section on ‘salt crystallization’.

Vazquez et al. (2015) did a comparative study of the microstructural properties of different stones and linked them with durability. The study included petrographical imaging, chemical analyses, and measurement of physical properties and porosity. The results demonstrated that it was the difference in the pore networks that created the high contrast in hydric characteristics and damage pattern in the different materials. Kasthurba et al. (2007) suggested pore structure as a major reason behind the unique behaviour of the laterite stones, which are common building stones in Kerala, India. It was the complex pore structure with micro-cracks around quartz grains, which contributed to high capillary rise that directly affected its durability. Similar studies emphasizing the importance of pore structure in deciding durability were carried out on other materials like basalt (Aldeeky and Al Hattamleh 2018), dolostone (Varas-Muriel et al. 2015), limestone, sandstone, biocalcarenes (Benavente et al. 2001) and bricks (Coletti et al. 2016a; Flatt et al. 2017; López-Arce et al. 2003; Noor-E-Khuda and Albermani 2019; Shu et al. 2017).

Investigation on porosity or pore structure after deterioration is also of high interest because that can give insights into the processes that have occurred, and performance of the material. Any anthropogenic or natural degradation process can disturb the microstructural characteristics, out of which the modification in pore structure is highly informative to capture. Weathered bricks or stones typically show increased porosity and water absorption but decreased mechanical properties like strength, density etc. (Amoroso 1983; Franzoni et al. 2013). Sassoni and Franzoni (2014) investigated the role of porosity on the artificial

deterioration of stones by heating. The authors heated marbles and limestones to deteriorate them and then studied the effect of using consolidants in them. But the mechanism of alteration of grain structure on heating was not closely examined or explained. The authors found that the impact of heating changed significantly with respect to the initial porosity of the material. In a highly porous stone, the changes in the properties were less pronounced because of the larger available space in the form of voids for the calcite crystals to occupy on deforming without causing extra stress. The decisive role of the initial porosity was also investigated and confirmed by other similar studies (Ferrero and Migliazza, 2009; Nicholson 2001; Franzoni 2011). It is thus evident that the initial porosity can alter the effect of processes and also the action of consolidants in masonry units. The exact relationship between the initial porosity and pore structure and properties of protective treatments needs to be investigated in detail.

2.4 SALT CRYSTALLISATION

2.4.1 Significance of salt crystallisation in historic masonry structures

One of the most important issues faced by the world's architectural heritage is the deterioration of building units in heritage structures. Deterioration occurs due to various reasons, including but not limited to biological growth, chemical attack, freeze and thaw cycles and salt crystallization. Among these mechanisms, crystallisation of soluble salts within the pores of the building units has been found to cause the most considerable damage (Kronlund et al. 2016). This is very clearly visible in buildings that are exposed to saline

solutions in their built environment. Every building unit consists of minerals and empty space. Empty space exists as a network of pores which may be open to the exterior at the surface of the masonry unit (Molina et al. 2011). Salt solutions enter the brick or stone through these openings and occupy the pores inside. Eventually, salt crystallisation may occur with the onset of precipitation and growth of those crystals subjected to various factors (Flatt et al. 2017; Flatt 2002). From the last 25 years, a large amount of research has been done on the process of salt crystallization based on theoretical understandings and field-laboratory experiments. Many of the world's significant heritage structures are affected by salt weathering severely, like Harappan remains at Mohenjo-Daro in Pakistan, the Nabatean rock-hewn temples at Petra in Jordan, the Sphinx in Egypt etc. (Flatt et al. 2014). Figure 2.6 shows some examples of the devastating action of salts in ancient structures.



Figure 2.6. Examples of the devastating action exerted by salts on heritage masonry structures (Flatt et al. 2014)

2.4.2 General mechanism of salt crystallisation

Salt crystallisation and/or generation of a high supersaturation may occur due to evaporation of water, a sudden drop in temperature, or due to dissolution mediated phase transformation (Flatt et al. 2017; Flatt 2002). When a crystal in contact with a highly supersaturated solution grows in a pore, such that its growth is restrained by the pore walls, tensile hoop stresses are induced in the material supporting the pore. If the stress is high enough to exceed the tensile strength of the material, the building unit undergoes damage (Flatt et al. 2014). Figure 2.7 shows the representation of the growth of a crystal in a small pore, where the growth is restrained in one direction, which will result in the development of hoop stress at the loading face.

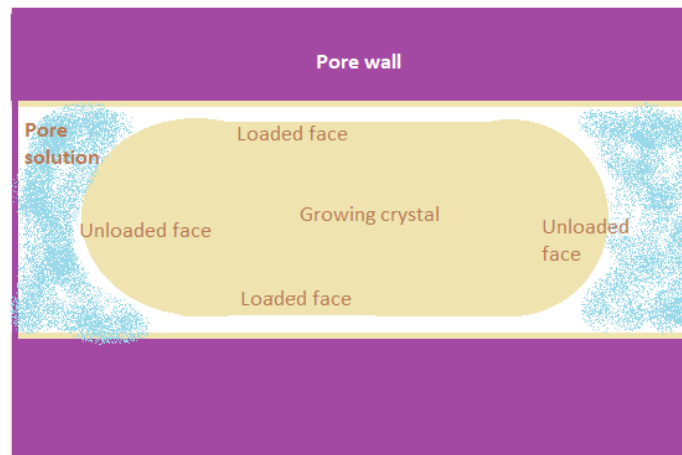


Figure 2.7. Representation of crystal formation inside a small pore

At this stage, it is worth mentioning a few interesting aspects of salt crystallization in pores for a deeper understanding. First, there should always be a film of pore solution sandwiched between the crystal face and the pore wall (Steiger 2005b; Steiger 2005a). This

is because, due to the enormous difference in free energies, directly establishing an interface between the crystal and the pore wall is not favourable (Scherer 2004a). It is thermodynamically easier to sustain two interfaces, namely, crystal - solution and solution - pore wall interfaces than to sustain the single crystal - pore wall interface. Another reason is that crystal growth cannot occur if there is no film of solution around it to supply ions for its growth (Flatt et al. 2017).

From the viewpoint of thermodynamics of crystal growth, the free energy of a growing crystal has two components viz., the pressure component and the interfacial free energy component. These two components, together, should balance the free energy of the same salt in the solution phase (Steiger 2005b; a). Otherwise, the phase of the salt at lower free energy will be favoured, and thermodynamics does not allow both the crystal phase and the aqueous phase of the salt to coexist in equilibrium. Thus, the crystallisation pressure, or the ‘disjoining pressure’ as described by Flatt (Flatt et al., 2017) is a result of thermodynamic balance of free energies. Secondly, the crystallization pressure (defined as the pressure that should be exerted on a growing crystal to arrest its growth) is a function of the degree of supersaturation of the pore solution and the geometry of the pore (Flatt et al. 2017). Many researchers have derived multiple expressions for the crystallisation pressure in a pore. Crystallisation pressure on a crystal face arises to balance the free energy associated with the supersaturation of the pore solution in excess to what is required to sustain the curvature of the concerned crystal face. Table 2.3 summarises the observations from the literature on this subject.

In addition to the expressions listed in the table, the derivation presented by Flatt expressed crystallisation pressure as a function of mole fractions, which is usually a known parameter (Flatt, 2002). The derivation does not assume the ideal behaviour of the aqueous solution either. Having calculated the crystallisation pressure in a pore using any of these expressions, the average hoop stress in the bulk of the porous material can be determined, applying suitable corrections. If the tensile strength of the material is known, damage can be predicted (Flatt et al. 2017, 2014).

One exciting feature is that the crystallisation pressure is more substantial in smaller pores. This happens due to the difference in geometry of the crystal in a small and sufficiently big pore. In a small pore, the crystal is restrained from growing in some directions by the pressure from the pore and grows in the unrestrained directions to a depth, where it attains a curvature not higher than what is allowed by the existing supersaturation. On the other hand, if the pore is big enough to accommodate the growing crystal, the free energy due to supersaturation is balanced by the curvature alone, without generating harmful stresses (Scherer 2004). Russell (1927) first suggested that materials with most micropores are more susceptible to salt damage, which was later supported by many studies (Tsui et al. 2003).

Table 2.3. Various expressions for crystallisation pressure in a pore

Author(s)	Equation proposed	Advantages	Drawbacks
Correns and Steinborn (1939)	$\Delta p = (RT/V_m) \cdot \ln(S)$ S = supersaturation degree = ratio of present concentration to the concentration at saturation, R = gas constant, T = Temperature, V_m = molar volume of solid.	First ever expression to be derived, relating supersaturation to the crystallization pressure.	'S' was erroneously defined as a concentration ratio. This led to inconsistent results
Neugebauer (1973)	$\Delta p = (RT/\Delta V_m) \cdot \ln(S)$ S = supersaturation degree = ratio of present activity to the activity at saturation, R = gas constant, T = Temperature, ΔV_m = molar volume change of solid during dissolution	Using activities instead of concentrations reduced the errors.	Does not account for shape (curvature) of crystal and interfacial energy.
Xie and Beaudoin (1992)	$\Delta p = (RT/\Delta V_m) \cdot \ln(K/K_0)$ K and K_0 are ion activity products in supersaturated and saturated states respectively	Reduction of errors	Does not account for shape (curvature) of crystal and interfacial energy.
Everett (1961)	$\Delta p = \gamma_{cl}(dA/dV)$ Δp is the pressure difference between two crystals of different sizes. γ_{cl} is the interfacial free energy.	Easier to use, based on pore size distribution, not on supersaturation. It considers surface energy, curvature.	Does not relate supersaturation to the crystallization pressure

Steiger (Steiger 2005a)	$P_i = -\gamma_{cl,i} \left(\frac{dA_i}{dV} \right) + \left(\frac{RT}{V_m} \right) \ln(S)$ $P_i = \text{Pressure on 'i' }^{th} \text{ crystal face, } S$ $= \text{ratio of present activity to the activity required to sustain an infinitely large crystal under the same conditions}$	It includes both Correns and Everett's terms	Assumes ideal behaviour of aqueous phase and does not consider salt mixtures.
-------------------------------	---	--	---

Another factor affecting crystallisation pressure in a pore is the ease of ion transport in the pore network (Flatt 2002). Several experiments have confirmed that as a stressed crystal is at a higher chemical potential than an unstressed one, the former dissolves spontaneously to supply ions for the growth of the latter when both are in contact with the same pore solution. Therefore, crystallisation stress is a transient phenomenon that is experienced only until a crystal has nucleated in an adjacent connected bigger pore. Thus, the crystallisation pressure in a pore is smaller if the pore is closer to a bigger pore or the free surface, provided that the pore solution offers a continuous matrix for ion transport. High rates of evaporation lead to discontinuities in the pore solution, thereby increasing the duration and intensity of transient crystallisation pressure in the bulk of the material (Scherer 2004).

2.4.3 Mechanism of salt crystallisation with specific salts

Sodium sulphate has been prescribed to be used as the deteriorating agent by various laboratory salt degradation tests. This is due to its highly damaging nature (Alves et al. 2017; Rodriguez-Navarro et al. 2000). Even though at a given supersaturation, the crystallization

pressure due to sodium chloride is much higher than that due to sodium sulphate, the damage due to sodium sulphate is very high as compared to sodium chloride (Rodriguez-Navarro and Doehne 1999; Steiger 2005a). This can be attributed to the temperature-dependent solubility of sodium sulphate, and the dissolution mediated phase transformations undergone by the salt.

2.4.3.1 Mechanism with sodium sulphate salt

Sodium sulphate can crystallize in at least eight different crystalline phases. The two stable phases are mirabilite (or Glauber's salt) and thenardite (phase V). The metastable phases are a heptahydrate, $\text{Na}_2\text{SO}_4 \cdot 7\text{H}_2\text{O}$, and two other anhydrous ones (phases III and IV), Na_2SO_4 . Anhydrous phases I and II exist only at higher temperatures (4270 and 4225 °C, respectively), whereas the octahydrate, $\text{Na}_2\text{SO}_4 \cdot 8\text{H}_2\text{O}$, is formed under high-pressure conditions. The phase diagram is shown in Figure 2.8, which illustrates the conditions for different crystallization states. According to Saidov et al. (2017), the instantaneous transformation of thenardite-to-decahydrate by rewetting is the major reason for damage by sodium sulphate weathering within the temperature range between 22 and 25 °C. The authors presented the equilibrium solubilities of various phases in a phase diagram, as shown in Figure 2.9.

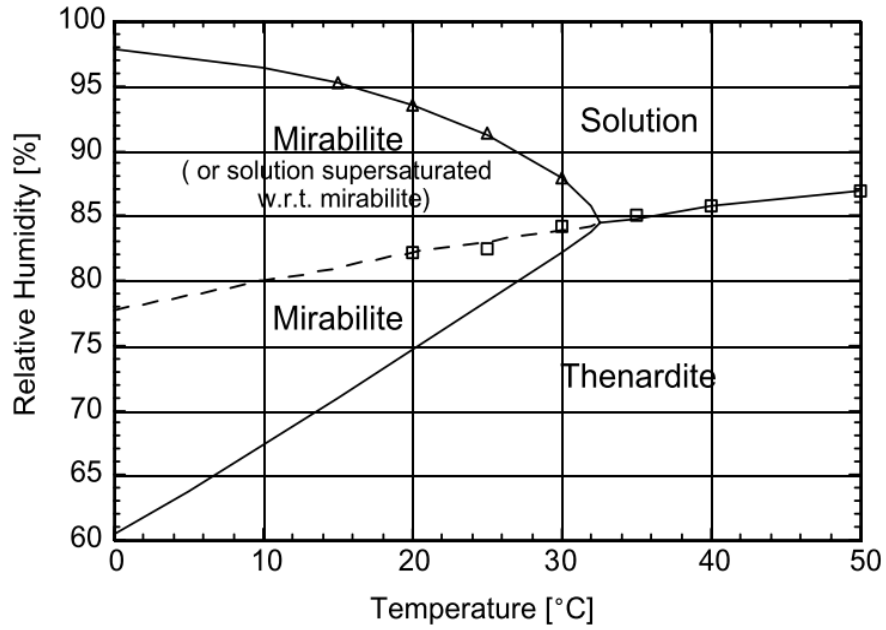


Figure 2.8. Phase diagram of sodium sulphate (Robert J. Flatt 2002)

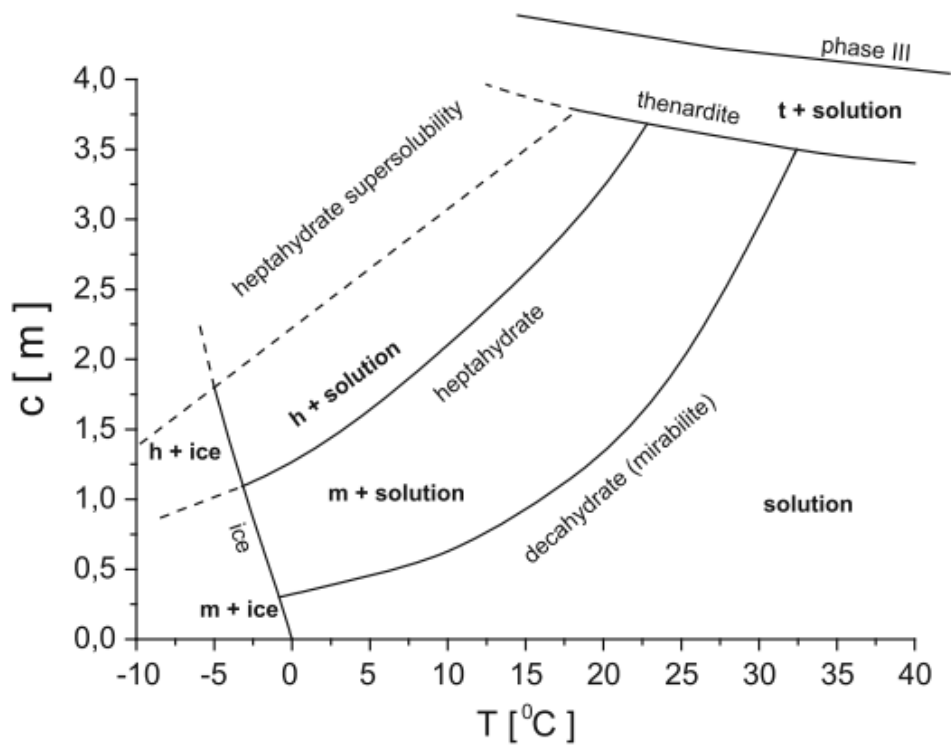


Figure 2.9. Phase diagram of sodium sulfate showing the equilibrium solubilities of various phases (h, t, m for heptahydrate, thenardite and mirabilite respectively) (Saidov et al. 2017)

The data seen in the figures for phase diagrams of sodium sulphate state the existence of two stable phases of sodium sulphate, which are more significant: thenardite (Na_2SO_4) and mirabilite ($\text{Na}_2\text{SO}_4 \cdot 10\text{H}_2\text{O}$). Previously, it was suggested that the damage to building materials was due to the hydration pressure when thenardite converts into mirabilite. The most common hypothesis for the heavy deteriorative nature of sodium sulphate salt was considered as the difference between molar volumes of mirabilite and thenardite, which is as high as 314%. It was believed that this could cause large stresses when high relative humidity allows conversion of thenardite into mirabilite (Winkler 1997). The theory was rejected, realizing the infeasibility of hydration by continuous water absorption into the crystal lattice (Rodriguez-Navarro et al., 2000). Thenardite to mirabilite conversion occurs by process of dissolution and recrystallization. The authors experimented and proved that both thenardite and mirabilite crystallize directly from the supersaturated solution, and the amount of each varies according to the environment condition. As the relative humidity decreases and evaporation rate increases, an increase in the relative proportion of thenardite is observed. At equilibrium, thenardite is not expected to crystallize at temperatures less than 32.4 °C, but it occurs only at non equilibrium condition in most porous materials. Below 32.4 °C, mirabilite ($\text{Na}_2\text{SO}_4 \cdot 10\text{H}_2\text{O}$) is the stable phase. Mirabilite rapidly dehydrates at relative humidity (RH) below 71% (20 °C) to form thenardite. Thenardite will rehydrate to mirabilite when the humidity exceeds 71%. Thus, the authors suggested a heterogeneous nucleation mechanism. Even though the phase relations explained only homogeneous nucleation from a saturated solution of the salt, heterogeneous nucleation is found more common in nature - around fractures, surface roughness, dirt and crystal defects. Therefore, the study concluded that the

heterogeneous, non-equilibrium crystallization of thenardite under normal conditions caused more damage to building materials than the crystallization of mirabilite or the hydration pressure. The concepts were supported by another study by Benavente et al. (2004), where the pattern of crystal growth was found differing for the different forms of sodium sulphate. The study showed that mirabilite crystallizes more homogeneously inducing a high disjoining pressure and creating more damage, whereas thenardite nucleates heterogeneously at edges, corners and defect points (Benavente et al. 2004).

The difference in the solubilities of thenardite and mirabilite increases with a decrease in temperatures (Flatt et al. 2014). So, a solution that is unsaturated with respect to thenardite may already be highly supersaturated with respect to mirabilite. This is how high supersaturations are generated in sodium sulphate by dissolution-mediated phase transformation.

2.4.3.2 Mechanism with sodium chloride and gypsum salts

NaCl is the ubiquitous salt in the masonry units. The commonly seen damages due to sodium chloride are powdering, which is due to the growth of cubic crystals of halite that moves the brick matrix powder away from each other, and flaking in which columnar crystal growth occurs (Cultrone and Sebastián 2008).

Sodium chloride tends to crystallise at the solution – vapour interface, unlike sodium sulphate that crystallizes rapidly in the bulk of its solution. In building materials, this interface is at the surface. That is why massive efflorescence is observed in many cases (Charola et al. 2017; Flatt et al. 2017). Sodium chloride cannot sustain high supersaturations

before crystal nucleation, unlike sodium sulphate that can generate very high supersaturations due to dissolution mediated phase transformation. As a result, the crystallisation pressure exerted by sodium chloride is much lower than by sodium sulphate (Rodriguez-Navarro and Doehne 1999). Also, it was seen from macroscopic experiments that supersaturations higher than 10% by mass are generally not reached in case of sodium chloride salt (Chaterji et al. 1989). But the variations incurred for the same kind of specimens exposed to sodium sulphate and sodium chloride damages are needed to be examined closely to have more insights into the sequence of processes and net damage.

Gypsum is comparatively a less damaging salt, because of its lower solubility, which improves in the presence of NaCl. Normally, gypsum gets poorly crystallized inside the substrate where moisture is less. But when the salts reach the surface and get exposed to enough moisture, large crystals are formed that can increase the damage to the system with time (Charola et al. 2017).

2.4.4 Test methods for analysing salt weathering resistance

The durability of any building unit in an environment prone to salt crystallization is normally tested by implementing artificial accelerated salt weathering tests in the laboratory. There are several procedures to simulate salt weathering of rocks and bricks in the laboratory, as prescribed by many national and international standard codes, guidelines and recommendations. Despite the availability of several of these reference test methods, there are no commonly accepted protocols (Lubelli et al. 2018). The European standard EN 12370 (EN-12370: 1999) is the most commonly used test that uses full immersion wet cycles in

14% sodium sulphate decahydrate solution following a drying phase at 105 °C, with subsequent cooling at room temperature before the onset of next cycle; this is a very aggressive test (RILEM TC 127-MS 1998). Another common test procedure is the one given by RILEM V.1 a- 1980 (RILEM 1980) which is similar but uses 60 °C as the drying temperature and uses 10% sodium sulphate anhydrite as the salt solution. The RILEM test also gives a provision for testing the efficiency of protective treatments in resisting salt weathering by applying the same tests on treated samples. The outcome was mostly found unrepresentative of real conditions, but rather dependent on the test conditions that are compiled and categorized in Table 2.4. RILEM TC 127-MS 1998 suggested a more reliable test procedure with capillary absorption as the contamination method, but it was exclusively for testing wallets and also was very time consuming (RILEM TC 127 MS A.1 1998).

Another major drawback found with all the existing methods is the lack of a quantitative measurement or representation of the salt weathering resistance of a material. Some studies have reported compressive, flexural or tensile strength before and after salt weathering cycles as a quantitative estimate. Despite the fact that they are destructive tests, there is a limitation for strength tests when dealing with salt contaminated specimens (Nunes 2013, Akin 2011, Aly 2016, Luodovica 2012, Foraboschi and Vanin 2014). Uniaxial compressive strength results on travertine stones before and after salt weathering cycles showed a significant reduction of strength on weathering (Akin and Ozsan 2011). Similar procedure followed on sandstone blocks (Ludovico-Marques and Chastre 2012) reported the same trend. The salt deposition inside the pores was found to help increase the strength of the material in a few studies (Stefanidou, 2009). The combined effect of salt deposition inside

pores and cracks due to damage can thus result in misinterpretation of the results. The results of these analyses depend much not only on the lithology of the rock but also on the experimental procedure and conditions (Alves et al. 2017).

The test methods that are currently available do not consider the effect of salt mixtures. When more than one salt is present in a solution (which always happens in nature), the crystallisation of double salts is highly probable (Flatt et al. 2017). Lubelli et al. (2018) presented the work of RILEM Technical Committee 271 ASC, which emphasizes the lack and requirement of a commonly accepted testing protocol for accelerated salt weathering tests. The paper also critically evaluates the different test protocols with identification of their advantages and disadvantages. The work also aimed at proposing new ideas for an improved test procedure considering the facts like reliable results in a reasonable time, proper quantification of results, and procedures which do not alter the deterioration mechanism on accelerating the process. The paper focused on five areas - specimens, salt, contamination procedure, method of drying and damage assessment, and on reviewing the past studies in the area. The authors also suggested the importance of providing a criterion for classifying the durability of materials which can confer an additional value to the whole salt crystallization test procedure. Assessment methods should be economically affordable and easily accessible in most laboratories and should be preferably non-destructive. The studies and reports in this field lack a comparison of crystallization mechanisms that could happen in specimens on following various procedures. The reasons behind the possible difference in mechanisms with a focus on the supersaturations developed in each test procedure are not reported or calculated in the literature.

Table 2.4. Factors in the test conditions of accelerated weathering tests

Factor	Dependence
Specimen geometry	Salt crystallization is concentrated near the surface, and the rate of weathering is proportional to the surface area/volume ratio. This ratio is dependent on the specimen geometry and size. Smaller specimens have a larger ratio of surface area/volume. So the weathering rate is faster in smaller specimens.
Salt contamination conditions	Immersion: Immersion tests produce results in a smaller number of cycles and the dispersion of results due to heterogeneities is minimized.
	Capillary directional imbibition is commonly found in a built environment. But heterogeneity affects the results badly. This simulates the fractionation of solute in upward movement also (Flatt et al., 2017).
	Surface deposition is similar to sea spray falling on rocks. It is useful in studying the surface but gives no information about the effects of bulk rock features.
Drying conditions	<p>High-temperature drying is required for obtaining results in a short period of time. But some rocks may show effects of wet-dry cycles rather than the effects of crystallization.</p> <p>Most of the test methods do not assess the effect of recrystallisation (Flatt et al., 2017).</p>
Test stopping criterion	Fixed number of cycles: The variations of a parameter are studied until a certain number of cycles, fixed at the beginning of the experiment, is completed.
	Carrying out any number of cycles until a particular result is achieved: While the previous criterion may cut off the information after the fixed number of cycles, this criterion will not.

Flatt et al. (2017) suggested focusing on the rate of salt accumulation which happens at the initial stage during a salt crystallisation weathering test, especially for considering replacement bricks, mortars or stones. This is because, in field conditions where crystallisation pressures are more often not too high, a particular amount of salt accumulation should happen before the onset of damage. This new concept of focusing on the “accumulation stage” in the test procedure seems logical, but experimental studies incorporating this idea are not reported.

2.4.5 Application of microstructural analysis in analysing salt crystallisation weathering

Any material being subjected to artificial weathering tests should be tested for its characteristics before and after weathering. Physical, mechanical, chemical and microstructural characteristics can give an idea of the alterations to the material. Since the samples undergo significant disintegration, microstructural investigations are more useful than physical or mechanical characterization to establish the modifications. Physical-mechanical tests like measuring strength, density, UPV etc. gives scope for comparative study, but microanalytical features are required to obtain insights into the process within the material (Antonelli et al. 2002, Jin et al. 2017, De Kock et al. 2015, Coletti et al. 2016, Anovitz 2015).

Salt crystallisation is mostly an in-pore phenomenon. It happens inside the pores of the material (sometimes outside in the form of efflorescence, but which again depends on the pore system), and directly depends on the pore parameters. Size of the pores, number of pores of a particular size and the pore connectivity determines the susceptibility of a material

to salt crystallization. Mercury Intrusion Porosimetry (MIP) is the most used tool to observe the changed pore structure on salt crystallisation - both pore occlusion and pore widening/new fissures. Fitzner (1988) studied the porous network in sandstones exposed to salt using MIP and concluded that pores smaller than 100 nm are not affected by the entry of salt solutions. Benavente et al. (1999) analyzed the salt-weathered and desalinated samples of Bateig stones and quartzarenite (a variant of sandstone with more than 90% detrital quartz) using MIP. The authors reported that stones with high mesoporosity (pores of size range 0.1 to 2500 μm) have high accessibility and pore interconnectivity, that increase the susceptibility of salt crystallisation. The reason quoted was the governing capillary flow pattern in that particular pore range. The detailed analysis of pore redistribution in stones after salt weathering, performed by Rodriguez-Navarro and Doehne (1999), showed the slight shrink in the peak of pore entry around 1 μm and a shift to lesser values indicating mild occlusion or obstruction in a large portion of pores due to crystals of sodium sulphate. It was also found that when exposed to sodium chloride, all the pores less than 0.2 μm were filled by sodium chloride crystals which reduced porosity to half. Theories of lower supersaturation ratios and thus lesser crystallization pressures supported this observation of crystal deposition in small pores reducing porosity. Angeli et al. (2008) also used MIP and digital imaging (SEM) to conclude that no noticeable changes occurred in the porosity of samples on weathering. MIP data analysis showed that only 8% porosity was filled with sodium sulphate crystals. Additionally, the authors investigated the most affected range of pores on salt crystallization tests in stones. It was found that pores between 10 nm and 20 μm

were most affected with accelerated ageing tests, which was concluded from SEM observations and data from MIP.

Another study of accelerated salt weathering on calcarenite stones showed a substantial increase in the pores of size ranging from 0.01 to 0.1 μm after weathering. The reasons for the observed initial increase in mass for calcarenite and decrease in mass for a particular limestone were investigated and connected to the crystallization mechanisms on determining the alterations at pore structure level through MIP tests (La Russa et al., 2013). However, the study did not analyze the salt depositions and crystallisation damages in pores of different sizes, so that the pore sizes stimulating crystallisation could be captured. The concept of crystallisation pressure was addressed in the paper for the stones, aimed at a deeper understanding of the correlation between the crystallisation process and weight loss. But weight loss can be a damage indicator only when it is very prominent (at a stage where damages are visual), else it will account for both deposition of salt and damage. Hence, the model for the process could have been more telling if the real microscopic-porosimetry data was used instead of weight loss - which was captured well in the study.

Digital imaging techniques (Scanning electron Microscopy - SEM, ESEM, FESEM, X-ray tomography) etc. have been used extensively in visualizing the salt distribution inside the pores, pore distribution and redistribution after salt weathering, and the damage patterns. One of the most significant contributions to the knowledge on sodium sulphate crystallization damage - which was the conversion of thenardite to mirabilite through dissolution and precipitation - was observed with ESEM (Rodriguez-Navarro and Doehne, 1999). This observation indicated the difficulty of mirabilite nucleation and hence the possibility of

thenardite saturation to occur first. Navarro et al. (2000) illustrated the morphology of thenardite crystals at different test conditions which are still considered as a useful reference for identifying the phases in microscopic imaging (Figure 2.10). The study also showed SEM images depicting the different morphology which the thenardite crystals adopt on precipitating over glass slides, when formed on dehydration of mirabilite and when they were precipitated directly from solution. Benavente et al. (2004) also used SEM and stereomicroscopy to interpret the salt localization within pores in stones with both NaCl and Na₂SO₄ salts at different zones in the stone samples. Stereomicroscopic images showed the mirabilite crystal growth occurring far from the solution-air interface, which indicated the homogeneous nucleation of mirabilite. It was visualized in the SEM images that halite (NaCl) crystallizes on the surface as efflorescence and grows heterogeneously on the pore walls, facilitating a functional interaction between the stone surface and halite crystals. Also, the heterogeneous nucleation of thenardite and the mirabilite habit with scarcer interaction with pore wall were visualized through SEM. Yu and Oguchi (2010) investigated the effect of salt crystallization on different sandstones, with different salts. The study used the morphological features observed in SEM images to identify the location and distribution of various crystal forms with different salts. From samples which underwent accelerated salt weathering tests, magnesium sulphate was identified as the radiating needle-shaped crystals and sodium carbonate as massive prismatic precipitation within the pore network of sandstone. Those dehydrated crystal forms indicated the attaining of higher supersaturation before the occurrence of nucleation, which was a significant lead to further understanding of the mechanisms. However, a demarcation between different crystal forms of sodium sulphate

was not attempted to be observed by the authors. Other studies have revealed the morphological differences between different forms of thenardite, which act mostly as evidences for the actual damage mechanisms in the case of sodium sulphate exposures.

Studies on historic lime mortar subjected to long natural adverse environmental exposures showed SEM images where gypsum nucleation and encrustation of carbonate phases were identified as remnants of salt attack, and they were visualized with prismatic and long needle-shaped formation (Haneefa et al. 2019). Even though crystal habits were illustrated clearly through the images in many such studies with SEM, lack of EDS data (on chemical composition) made the information incomplete. Also, the depth at which the formation of particular crystals would give realistic ideas of the process of crystallization in specific materials related to their pore structure is not studied in most cases.

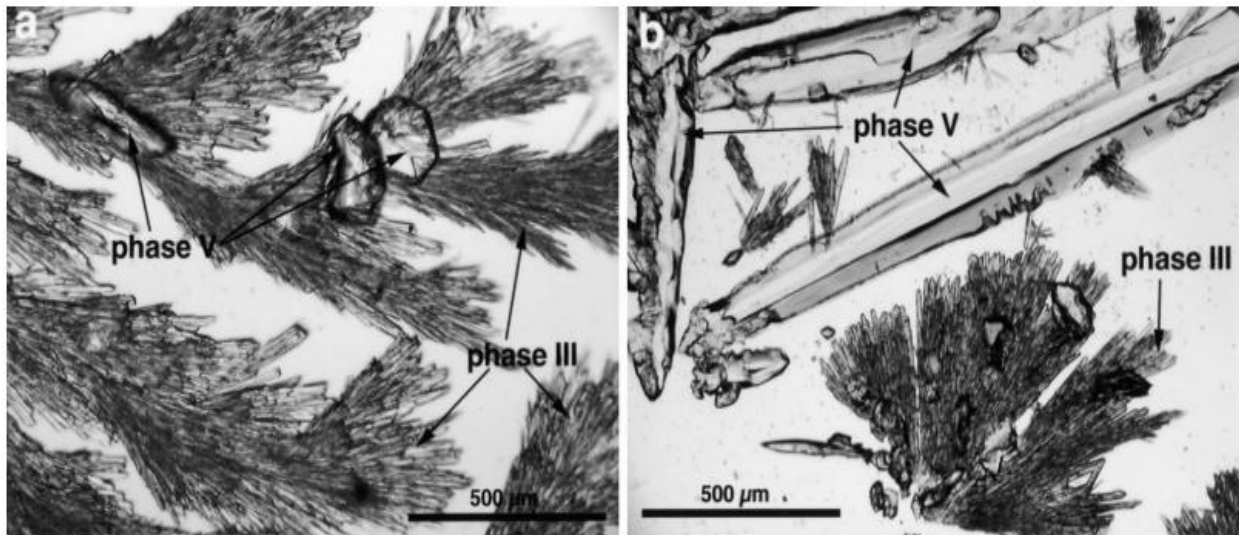


Figure 2.10. Micrograph of precipitated thenardite crystals (a) at 20°C, RH > 40%- needles are phase III of sodium sulphate and prisms are phase V (b) Phase V bipyramidal prisms at 20°C, 13% RH, with minor amounts of phase III needles (Rodriguez-Navarro et al. 2000)

Shu et al. (2017) used FT-IR technique to identify crystalline gypsum in ancient brick samples from a Chinese church and found that the crystallization of gypsum was the underlying cause for the deterioration observed in the bricks. Thin section petrographic images also provide data regarding the deteriorating agents or any inclusions in historical material which are affected by crystallization damages (Sanjurjo-Sánchez et al. 2016; Shu et al. 2017, Zhang et al. 2018).

Increase in percentage of coarser and finer pores of masonry materials on exposing to salt crystallization was determined, which helped in understanding durability issues with the application of the treatments concerned (Correns 1949). The action of consolidants on bricks during accelerated salt crystallization was studied by Graziani et al. (2016) where the pore distribution curves from MIP were used to quantify the reduced porosity and pore occlusion.

Having had a detailed discussion of the mechanism of brick damage by salt crystallization, it is now clear that the ingress of salt solution into building materials poses a major threat to their durability in the form of crystallization within the pores. To prevent damage, either the porosity should be reduced, or the surface should be made impervious. Reducing the porosity involves the risk of increasing the fraction of micropores, which is very dangerous as the crystallization pressure is higher in smaller pores (Emery and Charola 2007). Rendering the surface impervious is facilitated by the application of protective treatments over the surface, which will be discussed in the next section in detail.

2.5 PROTECTIVE TREATMENTS FOR HISTORIC MASONRY

Salts enter a porous masonry material in their aqueous states, through the pores on the surface. Therefore, by restricting the entry of water into the pores of the masonry, degradation due to salt crystallization can be controlled. This calls for the need to use water repellents. This section briefly describes the working of a water repellent coating and reviews the past studies based on testing several water repellent coatings for their efficiency.

2.5.1 History of use of protective treatments to masonry

Coatings are provided for the masonry surface to slow down further deterioration. To begin with, the difference between water-repellent coatings and waterproof coatings should be understood. Waterproof coatings are those materials which will completely seal-up the surface, and will not allow movement of liquids or water vapour to and from the substrate. On the other hand, water repellent coatings are intended to keep away the liquid water from penetrating through the surface but permit the passage of water vapour to through the masonry surface (Mack and Grimmer 2000). Masonry of heritage monuments, being highly porous, needs breathability. So only water repellent coatings can be used which will prevent the stress build-up inside because of the water vapour, thus preventing cracks. In early ages, in special structures that retained or transported water, waterproofing was a necessity. This was traditionally achieved through various techniques, such as heavy compaction or by the application of organic wax/ oil on the surfaces. Linseed oil was widely used due to its hydrophobic properties. But such treatments were found to undergo biological degradation (Stefanidou and Karozou 2016). Even clay was used in order to protect constructions from water. But clay is not at all a water repellent coating. Clay, being highly hydrophilic, absorbs

large amounts of water and retains the saltwater from entering the stones. This is a method of ‘sacrificial’ protection. The first water repellent coatings developed were acrylic or silicone-based resins in organic solvents. However, now water-based products are available which are formulated from silanes, siloxanes and other alkoxy silanes. The modern coatings, instead of forming a film over the substrate like the older formulations, penetrate below the surface a little and adhere well (Tsakalof et al. 2007).

The treatments to historic structures are often applied without proper scientific study, and without identifying the actual requirement and the properties of the chemicals being applied. If not selected and appropriately applied, the coatings can cause deleterious actions, and it is difficult to remove them from the surface properly if they fail. Figure 2.11 shows a case where a clear coating has failed and has pulled off some of the stone substrates upon peeling (Mack and Grimmer 2000). Cleopatra’s Needle, the Egyptian obelisk in New York City, was once treated with wax as a protective sealant, but the process sealed in saline moisture. The treatment provoked an already deleterious action of moving the monument from an arid to a humid environment (Winkler 1997). Binders derived from mortars or cements may exert new pressure on masonry when they solidify or crystallize, such that the substances used to repair the stone end up actually causing greater destruction (Pope et al. 2002).



Figure 2.11. Protective coating damaging the stone substrate upon peeling (Mack and Grimmer 2000)

An ideal surface coating for stone/brick historic masonry should be oil repellent, transparent, inert with respect to the substrate, durable, chemically and photochemically stable, easy and safe to handle and removable. It should also be optically stable to preserve the original stone colour. The coating should be non-hydrophilic and waterproof (Tsakalof et al. 2007). Nevertheless, the coating layer should allow breathability or water vapour transmission to prevent stress cracking from inside due to the water from rain or capillary rise. Commonly used water repellent coatings are fluoropolymer-based, alkoxsiloxane (silicone)-based and acrylic siloxane-based ones. These may be modified by silica

nanoparticles to increase surface roughness and hence, the hydrophobicity. Fluoropolymer based coatings were reported to be the least effective ones in resisting damage due to salt crystallization. Also, they were found to be vulnerable to degradation by ageing factors like UV (Kronlund et al. 2016). Epoxy-based and anti-graffiti coatings are being used recently.

The epoxy resins were not considered as an efficient coating for masonry in the past because of the stiffness and yellowing property (Eric and Clifford 2010). But interesting studies were later conducted for using epoxy resins for coatings (Cardiano et al. 2005; Tulliani et al. 2014). The yellowing was found to be avoided by use of a cycloaliphatic monomer with it. Tulliani et al. (2014) specifically developed and tested a visible and long-wavelength photoinitiated polymerized epoxy and its potential use as a coating for masonic stones. Through the thorough characterization of the coating chemical and the analysis of the coated sample, it was found that the particular epoxy is suitable for stone protection.

The low surface energies of the anti-graffiti coatings limit the graffiti adhesion, thus facilitating easy cleaning while ensuring waterproofing of the masonry surface. The two types of anti-graffiti coatings are temporary (sacrificial) and permanent. The temporary coatings which are made of waxes and silicones are removed while cleaning, and hence having low durability under intense environments. The permanent coatings which are polyurethanes, fluorocarbon, alkyl alkoxysilanes etc. can resist many cleaning cycles without removal. Gomes et al. (2017) observed that anti-graffiti coatings improved the removal efficiency of graffiti paints, but the efficiency was found compromised in more porous substrates like limestone. Hence further research is necessary before promoting its use for more porous materials like bricks.

The surface protective coatings need to be tested in aged substrates rather than in freshly baked substrates without any ageing. It is crucial to understand the cohesive action of the coatings on the substrate in holding the decayed surfaces. This ensures reliable data on the behaviour of the coatings (Lubelli et al. 2014).

2.5.2 Working of water repellent coatings

Application of protective coatings aids in making the material surface impervious to salt solution/liquid. Impregnating the surface of bricks with protective coatings makes them hydrophobic and reduces the capillary absorption of water (Stefanidou and Karozou 2016). In addition to rendering hydrophobicity, they are found to provide ‘sacrificial’ protection. As liquid water cannot migrate across the coating, salts crystallize just beneath the coating, causing the coating to blister and peel off (Emery and Charola 2007). In case any water enters the material through the discontinuities in the coating, they reduce the vapour transmission rate across the surface, thereby pulling the evaporation front (and crystallisation front) closer to the surface. Closer the crystallization front to the surface, lesser is the damage due to efflorescence, in contrast to the sub-florescence that occurs during a high rate of evaporation. However, this property of water repellent coatings involves a potential risk of moisture entrapment in the porous network (Stefanidou and Karozou 2016).

The crystallization of soluble salts occurs where the water in the salt solution evaporates. Water repellent coatings are impermeable to liquid water but permeable to vapour. However, the water vapour permeability of coated bricks is slightly less than that of

uncoated bricks. This decreases the evaporation rate and brings the evaporation front closer to the surface.

2.5.3 Advantages and disadvantages of water repellent coatings

Water repellent coatings reduce water infiltration due to their hydrophobic nature. In case water infiltration does occur due to any reason, like due to a discontinuity in the coating or prolonged exposure to water, the evaporation front and therefore, the crystallization front is pulled to the surface, due to low rate of vapour transmission across the coating. Thus, the damage to the masonry is reduced, in case it is not prevented (Emery and Charola 2007).

Coated masonry units give a more visible warning than uncoated ones. The blistering and spalling that occurs in the first stage of deterioration along with efflorescence in coated bricks can be easily noticed. But in uncoated bricks, the evaporation front lies somewhere in its bulk, and the damage is visualized only when the brick cracks due to crystallization pressure. This may lead to the failure of the structure itself (Emery and Charola 2007).

The biggest disadvantage of water repellent coatings is humidity entrapment in a porous network. When the coatings are impregnated to a profound depth in the bricks, they completely block the pore water inside from reaching the surface for evaporation. Thus, the evaporation front will be at a depth of impregnation, resulting in spalling due to crystallization (Stefanidou and Karozou 2016).

2.5.4 Studies on efficiency of various protective coatings

Several studies have been conducted for evaluating the performance of different coatings on different materials. Kronlund et al. (2016) studied the effect of a water-based commercial

coating and a polydimethylsiloxane coating on granite, under various conditions. In the same year, Stefanidou and Karozou (2016) studied the effect of various coatings on traditional bricks. Some more work has been carried out by Emery and Charola (2007) in relating the vapour permeability of coatings to their performance.

Kronlund et al. (2016) investigated the effect of accelerated ageing, acid degradation, salt weathering and freeze and thaw cycles on the mass loss, contact angle, capillary absorption and colour alterations of uncoated samples of granite and those coated with different coatings. Table 2.5 shows the overall results of that study.

Table 2.5. Results of the performance analysis of various protective treatments for masonry (Kronlund et al. 2016)

Degradation mechanism	Performance of uncoated granite	Performance of granite coated with Faceal Oleo HD (fluorinated acrylic copolymer)	Performance of granite coated with Polydimethylsiloxane (PDMS)
Accelerated ageing tests	Moderate	Very poor	Very good
Acid degradation	Moderate	Moderate	Poor
Salt crystallization	Poor	Poor	Very Good
Freeze and thaw cycles	Good	Poor	Poor

A few conclusions that can be drawn from these tests are as follows: (i) Ageing factors (like UV) degrade the commercial organic coating, and cause more damage to granite, (ii) PDMS (Polydimethylsiloxane) coatings are significantly affected by acid degradation, (iii) Salt weathering has the greatest influence on granite as compared to any other degradation mechanism; the commercial coating agents are ineffective in resisting salt

degradation, and (iv) Freeze and thaw cycles cause more damage to the coating than to the granite itself.

Stefanidou and Karozou (2016) did a number of tests, including capillary absorption test, porosity, water drop test by measuring contact angle, Karsten tube test, penetration depth, change in colour as per Munsell system, freeze and thaw deterioration cycles, salt deterioration cycles, and SEM observation of surfaces after deterioration. They tested the effectiveness of linseed oil, siloxane coatings, alkosiloxane coatings modified with silica nanoparticles. A review of a large number of such studies being reported in analysing the performance of conventional treatments like these converged in some general points, which are as follows:

- Alkosiloxanes are the most effective coatings. Linseed oil is vulnerable to biological alterations. Siloxanes perform the poorest among these due to their cracking tendency.
- Relatively high values of water absorption and porosity in siloxane coated samples were observed. This suggests that they do not cover the pores on the brick surface. From SEM images, it was hypothesised to be due to the cracking of the coating on the surface.
- Modification of the ordinary coatings by silica nanoparticles increased the roughness and the hydrophobicity of the surface.

Emery and Charola (2007) examined silicate and acrylic coatings over high-quality brick and found their efficiency with respect to reduction in infiltration, reducing the depth of the salt damage zone and extending the lifetime of material. However, the performance of the coatings on different types of materials was not evaluated. The authors cite the experiments

conducted by Franke and Reimann-Oenel (2001). Their research compared the deterioration of painted and unpainted stones. They also discovered that the effectiveness of the paint in preventing deterioration depends upon the substrate. Furthermore, Emery and Charola (2007) established that lesser the water vapour permeability, better is the performance of the coating (which was not necessarily water repellent). However, even they did not evaluate the performance of water repellents in particular, with different substrates. So, there is a need to study the effect of different water repellent coatings on different materials commonly used in historic and contemporary masonry.

Most studies and industrial use show that silicone-based and acrylic-based are the two most common and significant water-repellant coatings which are adopted for masonry structures. Silicone-based coatings have been reported to be better than acrylic siloxane-based (Anupadma 2009, Kronlund et al. 2016; Stefanidou and Karozou 2016). The values of capillary absorption and surface porosity were relatively higher for acrylic-siloxane coated samples (Stefanidou and Karozou 2016). Their poor behaviour may be attributed to the cracking tendency of acrylic-siloxane coating with salt exposure as discussed (Kronlund et al. 2016; Stefanidou and Karozou 2016).

2.5.5 Importance of compatibility between treatments and substrate

In all the studies assessing the performance of water repellent coatings, multiple tests were carried out on the same types of specimens. Although the application of water repellents has several advantages (hydrophobicity, reduced capillary absorption, etc.), the ultimate aim of the treatment is to improve the durability of the brick. As pointed out earlier, degradation by

salt crystallization is the most damaging mechanism. From the previous discussions, it is clear that the mechanism and the extent of damage by salt crystallization depend, to a great extent, on the pore size and the environmental conditions. Therefore, water repellent treatments aimed at improving the durability of the bricks should be studied for their compatibility with different types of substrates, because the prominent deterioration mechanism itself depends on the characteristic microstructural properties (pore size distribution, pore connectivity, etc.) of the substrate.

2.6 SUMMARY OF LITERATURE AND NEED FOR RESEARCH

The current status of conservation of masonry structures is examined in a global and national perspective in this chapter. It is evident that India needs to take strategic conservative measures based on an interdisciplinary combination of geological and engineering science to protect its vast built heritage. It is thus important that the ancient masonry units be understood for their properties so that performance can be understood and predicted and suitable replacement materials can be designed.

Salt crystallisation was identified as the most critical deteriorating mechanism for the masonry. A proper understanding of the mechanisms, the factors affecting the crystallization process as well as the role of the microstructure of material help in understanding the durability issues caused in heritage masonry and the measures for preventing the crystallisation damage. The crystallisation/nucleation of salts occurs inside the pores when high supersaturations are reached, and this primarily occurs in smaller pores (lesser than 1

μm). The pressure (crystallisation pressure) acting on the pore walls due to this restrained crystal growth in smaller pores initiates the damage. Hence, damage does not occur when the tensile strength of grains is higher than the crystallization pressure applied, or high supersaturations are not reached when the pores are much larger, or the entry of salt solution into the material is prevented. Studies on all these aspects were critically reviewed in this chapter.

Water repellent coatings are the most adaptable protective treatments for historic brick masonry structures, as they provide breathability (vapour permeability), do not change the aesthetics and prevent the entry of salt solution. This is relevant in protecting the structure from exposure cases like marine aerosol, rain water seepage, acid rain etc. In cases of complexities like rising damp or complete immersion of structure in sea water, application of water-repellent treatment can be challenging. In such cases, customised approach of repair and retrofitting shall be preferred over providing protective treatment. Past studies have examined a broad range of water repellents for their properties and reported their disadvantages too. The features of the treatments and their effectiveness were dependent on their chemical composition. One issue which was not addressed in the studies was the evaluation of the compatibility of water repellents with different masonry units when they have different microstructure. There is a definite need to study the possible relationship between microstructure (pore structure) of the material and behaviour of the water repellent treatment in determining the durability of the material in a salt exposed environment.

The research gaps observed from the assessment of available literature can be summarised as follows:

- No studies have been reported on the characteristics of historic Indian masonry units in detail so far, even though efforts are being taken towards conservation of the heritage structures.
- A better understanding of the mechanism of salt crystallization, emphasizing the maximum and minimum pore sizes that affect the process is needed.
- There seems to be a general disagreement about the effect of sodium chloride on masonry units, because of the lack of long-term experimental data and insufficient information about the mechanism of decay.
- A possible relationship between the microstructure of the substrate material and action of water-repellents needs to be studied further.

3 MATERIALS AND METHODS

3.1 INTRODUCTION

This chapter provides details pertaining to the materials used in the study, type and quantity of samples used in the study and their nomenclature, the testing philosophy, experimental procedures and experimental variables. The standards that were used in the study are also discussed.

3.2 MATERIALS USED IN THE STUDY

3.2.1 Samples collected

Historic and fresh samples of bricks of different conservation state and properties, and two different types of stones were used in the study. The list of samples, along with their nomenclature used in the thesis (given in brackets), are as follows:

Brick samples

- (i) Three types of historic brick samples which differ in size, colour and texture, from Sri Veetrirundha Perumal Temple in Vepathur, Tamil Nadu, which is approximately 2000 years old (Rani et al. 2016) (V1, V2, V3)
- (ii) Heritage brick samples from Sri Pundarikaaksha Perumal Temple in Thiruvellarai, Kumbakonam, Tamil Nadu, which is around 1000 years old (Rani et al. 2016) (K)

(iii) Historic brick samples from Fort Dansberg, a Danish coastal fort in Tranqebur, Tamil Nadu, which is 400 years old and heavily salt weathered (T1, T2)

(iv) Hand-moulded normal commercial brick sample (C1) from a kiln in Chennai

(v) Wire-cut commercial brick sample from a modern kiln (C2) located at Chennai

(vi) Newly baked replacement bricks for a heritage temple (VN) manufactured for refurbishment works in the temple of Vepathur

Stone samples

(i) Weathered pink granite from Meenakshi Sundareswar Temple in Madurai, Tamil Nadu (GW)

(ii) Unweathered fresh granite from Meenakshi Sundareswar Temple in Madurai, Tamil Nadu (G)

(iii) Coral stone samples from Sri Ramanathaswamy Temple at Rameswaram, Tamil Nadu (CS)

The locations of the heritage sites from which various historical samples are collected and the kilns from which fresh commercial samples are collected are shown in Figure 3.1. Three different kinds of historic brick samples, which varied in colour, density and dimensions, from three different locations were collected from Sri Veetrirundha Perumal Temple during its refurbishment work at Vepathur village near Thanjavur in Tamil Nadu, India; the temple is reported to be approximately 2000 years old (Rani et al. 2016), and the

brick samples are denoted as V1, V2 and V3 in the study. V3 was collected from the foundation part of the temple and was thus older than the bricks V1 and V2, which were from the outer walls. Brick samples denoted as K were collected from another historic temple approximately 1000 years old in Kumbakonam in Tamil Nadu (Rani et al. 2016). These samples (K) could have been poorly baked, as they were seen with a pale reddish matrix and found with degraded surfaces. The sample collection from both these sites was conducted during refurbishment works. Both temples are located far away from coastal regions, by more than 60 km. The prevailing site conditions were similar for both of these locations as they were located in the same district of Tamilnadu, with the average annual temperature as 30.4 °C, average annual relative humidity 67.3% and average annual wind speed of 14.6 km/h (World weather online 2020).

Brick samples T1 and T2 were collected from a Danish fort in Tranquebar, Tamil Nadu, which is around 400 years old (Ahmed 2011). The average annual temperature at the site was 29.5 °C, average annual relative humidity 72% and average annual wind speed 18.4 km/h. The fort is on the sea coast (less than 0.5 km from sea) and is in a heavily deteriorated state. T1 samples were collected from the external walls of the fort, from a lower level. These bricks were in an exposed condition, but not in direct contact with the sea. Samples T2 were collected from the part of a wall that was partially in contact with the sea; hence, they were wet bricks, subjected to erosive forces as well.

To compare with the different historic bricks, three types of new bricks were considered for the study - VN, C1 and C2, which were having various sources of origin and manufacturing methods. VN was the freshly manufactured brick designated to replace the

damaged bricks in the historic temple of Veppathur, while C1 and C2 were commercially available bricks from modern kilns in and around Chennai. C1 was hand-moulded brick whereas C2 was a wire-cut, machine-made brick fired in a modern kiln. VN, C1 and C2 were manufactured in Chennai, Tamil Nadu.

Granite samples were collected from Meenakshi Sundareswar Temple, Madurai, Tamil Nadu, which is a historic stone temple from the 14th century (Ahmed 2011). The distance from sea to the temple is more than 110 km. Prevailing climatic conditions at the site includes average annual temperature of 29.8 °C, average annual relative humidity of 62% and average annual wind speed of 8.7 km/h (World weather online 2020). A few columns of the structure showed heavily weathered surfaces towards their lower portion, and samples were collected from there during refurbishing works (GW). Unweathered fresh granite samples were collected from the same temple, which were from the new columns constructed during recent repair works (GF). Coral stone samples were collected from Sri Ramanathaswamy temple, a prominent Hindu temple, built before 16th century, and located in Rameshwaram Island, Tamil Nadu which is separated from mainland India by the Pamban channel (Cole and Hardy 1885). This temple is on the coast of Bay of Bengal and is partially constructed with coral stone, which was sourced from the coast of Tamil Nadu at Rameswaram. The structure showcases the remarkable creative achievements of a momentous period in the history and has immense architectural significance because of the construction with coral stone, which is rare in India; additionally, it is difficult to source fresh material for replacement/restoration. Currently, the structure is in a partly deteriorating stage

at some locations. The coral stone samples were collected during the refurbishing works (CR).

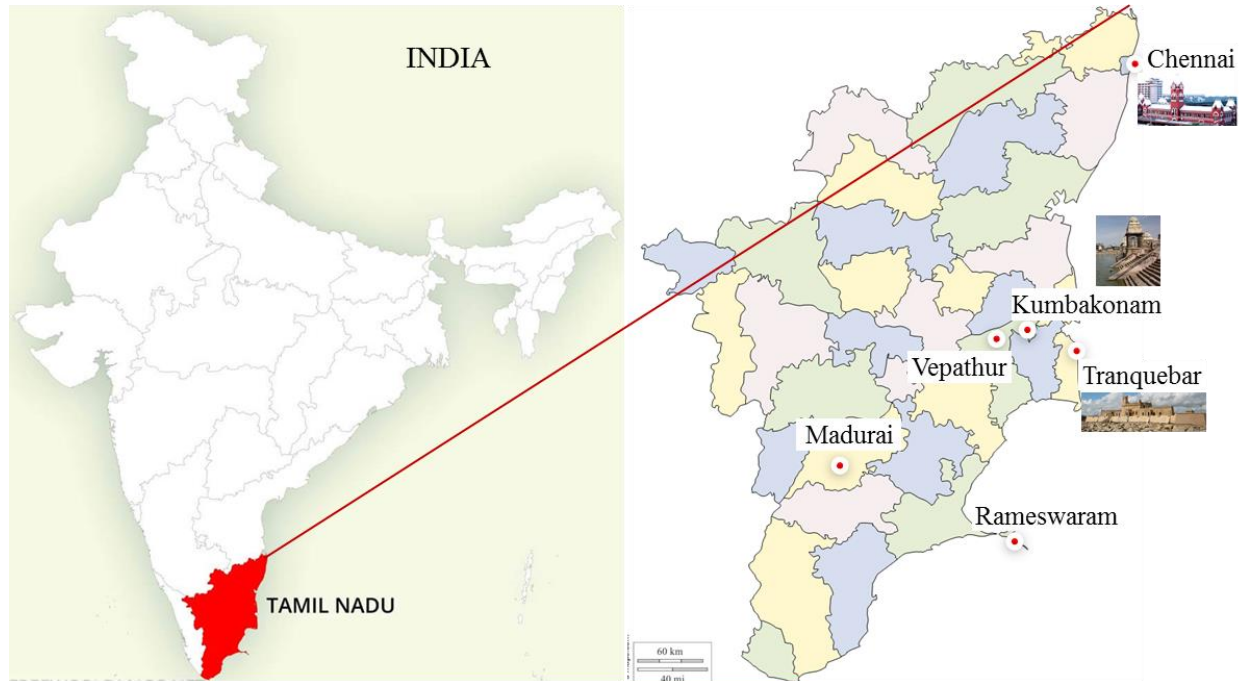


Figure 3.1. Locations from which the samples are collected

3.2.2 Water repellent coatings

Two commonly used and commercially available water repellent coatings were used in the study, which are:

- (i) Silicone-based water repellent
- (ii) Acrylic-siloxane based water repellent

The details of the two chemicals are given in Table 3.1.

Table 3.1. Particulars of water repellent treatments selected for the study

Water repellent	Silicone-based treatment	Acrylic-siloxane based treatment
Notation	SC	AS
Company name	MAPEI	MAPEI
Composition	Oligomeric organosiloxane	Methacrylate modified siloxane
Chemical formula	$\text{R}-\text{Si}\begin{matrix} \text{R} \\ \\ \text{R} \end{matrix}-\text{O}-\left[\text{Si}\begin{matrix} \text{R} \\ \\ \text{R} \end{matrix}-\text{O}-\text{Si}\begin{matrix} \text{R} \\ \\ \text{R} \end{matrix}-\text{O} \right]_n$	$\text{R}^1-\left(\text{Si}\begin{matrix} \text{R}^1 \\ \\ \text{R}^1 \end{matrix}-\text{O} \right)_i-\text{Si}\begin{matrix} \text{R}^1 \\ \\ \text{R}^1 \end{matrix}-\text{C}_3\text{H}_6\text{O}-\text{CH}_2\text{C}\begin{matrix} \text{CH}_2\text{O}-\text{C}(=\text{O})-\text{C}(\text{R}^d)=\text{CH}_2 \\ \\ \text{CH}_2\text{CH}_3 \end{matrix}$
Solvent	Solvent-free silicone-concentrate, dilutable with organic solvents	Organic solvents (aliphatic hydrocarbons)
Appearance	Colourless, hazy	Colourless, hazy
Proportion used	As available	As available
Application method	Brushing	Brushing

3.3 EXPERIMENTAL PROGRAM

The overall methodology of the study is divided into 3 phases, which are illustrated in Figure 3.2.

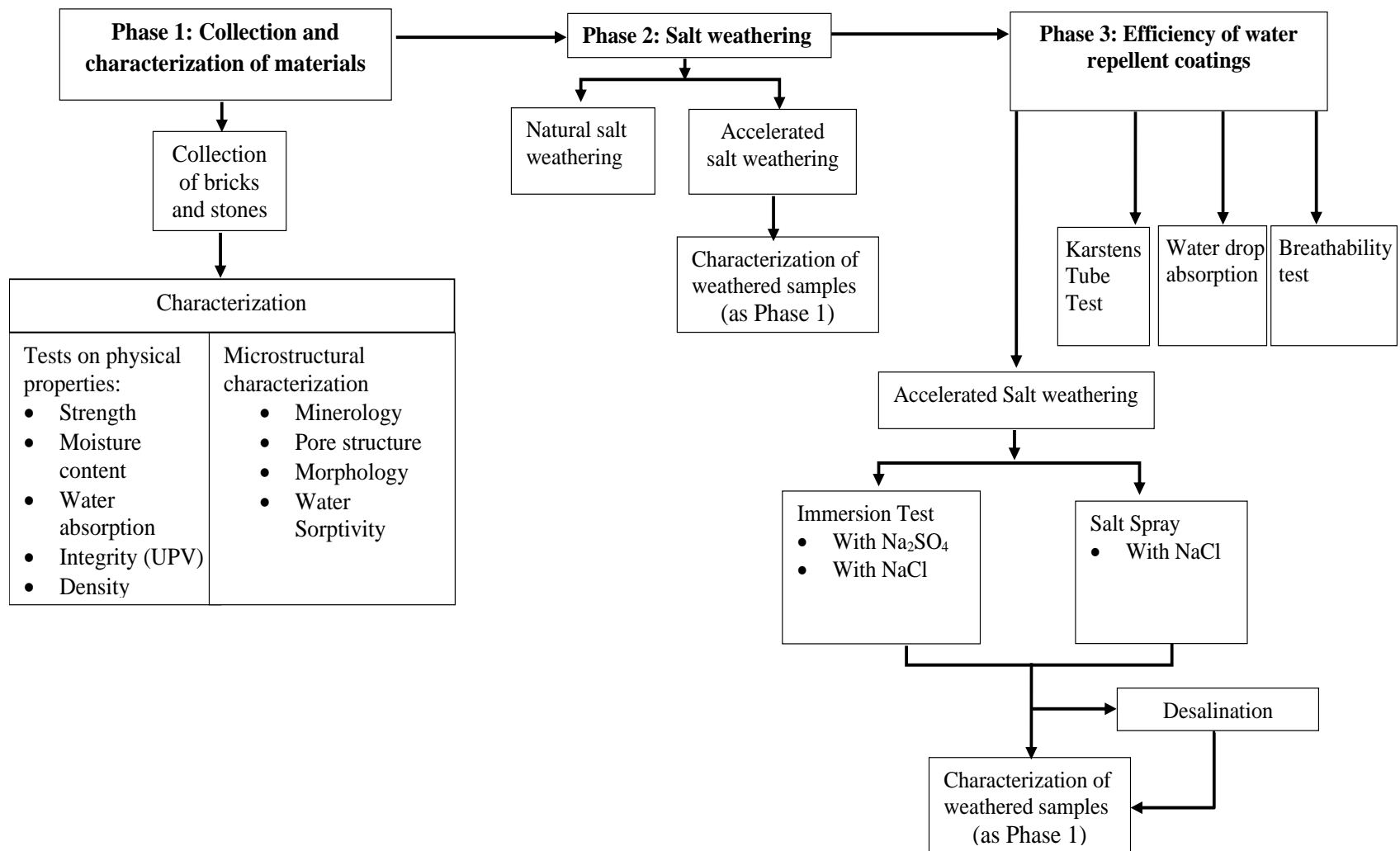


Figure 3.2. Methodology of the study

Among the 3 phases, phase 1 involved collection of samples from historical and commercial sources and characterizing them to understand their physical, chemical, mechanical and microstructural properties. In phase 2, the behaviour of these materials with salt exposure was studied. Both naturally weathered samples and samples on subjected to artificial accelerated weathering were analyzed to see the microscopical alterations. The mechanism of salt crystallization was addressed based on the results. The 3rd phase of the study constituted the evaluation of efficiency of protective treatments. In phase 3, the performance of water-repellent treatments in salt exposure was analysed for different materials to identify the compatibility between the efficiency of treatment and microstructure of material.

3.4 CHARACTERIZATION OF SAMPLES

3.4.1 Physical and mechanical characterization

3.4.1.1 Compressive strength

Compressive strength of the samples was determined on whole bricks, as per IS 1077:1997 (Indian Standard IS 1077: 1997) at a loading rate of 140 kg/cm²/minute. Three numbers of specimens were tested for each sample type, and the average value is reported as the strength. The standard compression test as per IS 1121:2017 (Indian Standard IS 1121- Part 1 2017) was carried out in the laboratory on coral stone cubes and granite cubes of size 100 mm to evaluate the mechanical strength of the stone.

3.4.1.2 Bulk density

Bulk densities were obtained using Helium gas pycnometer using small chunks of samples weighing approximately 1 g. An UltraPyc 1200e Automatic Gas Pycnometer was used for the measurements, as shown in Figure 3.3. The equipment works by detecting the difference in pressure resulting out of gas displacement by a solid sample. The quantity of gas at a known pressure is allowed to expand into an empty chamber, and the pressure is measured. Then, once the sample is placed in the sealed chamber, the same quantity of gas is again allowed to expand, and the pressure is measured. The difference in pressure combined with the known volume of the chamber provides the volume of the sample, using the gas law. The equation representing the principle is as follows:

$$V_s = V_c + \frac{V_r}{1 - \frac{P_1}{P_2}} \quad (3.1)$$

Where V_s is the volume of sample, V_c is the empty chamber volume, V_r is the known reference volume, P_1 is the pressure measured first in the sample chamber and P_2 is the second measured pressure. Reported results from the system include density and volume of samples with statistics.



Figure 3.3. Helium gas pycnometer

3.4.1.3 Water absorption

The water absorption was measured as per the standard IS 1124-2017 (Indian Standard IS 1124 2017) on cube specimens of 50 mm size. Cubes were oven-dried at 60 ± 2 °C for 48 hours and subsequently cooled at room temperature. Dry mass (M_d) of the specimens was measured, and the specimens were then immersed in water for 48 hours. After this immersion period, the specimens were removed from the water, wiped with a damp cloth and weighed to record the surface dry mass (M_a). The change in weight in percentage was calculated and represented as percentage of water absorption by the following equation:

$$\text{Water absorption (\%)} = \frac{M_a - M_d}{M_d} * 100 \quad (3.2)$$

3.4.1.4 Water Sorptivity

Water sorptivity test was carried out on cubical specimens (40 mm size for brick and 50 mm size for stone) as per the South African Durability Index testing procedure manual - Part 3 (“Durability Index Testing Procedure Manual” 2018). The oven-dried specimens were allowed to cool in room temperature for 2 hours. Dry weights of the specimens were recorded before the test. For the test, the specimens were placed on top of the knife edges kept in a tray with water, as illustrated in Figure 3.4 (a). The stopwatch was started immediately after placing the first specimen in solution, and weights were measured at 3, 5, 7, 9, 12, 16, 20 and 25 minutes as per the procedure. Just before measuring each time, the wet surface of specimens was patted with a wet cotton cloth to remove extra water. The stopwatch was stopped after the reading at 25 minutes. Then, the tested specimens were kept inside a desiccator for vacuum saturation, which is shown in Figure 3.4 (b). After a day, the fully saturated weights were measured for the specimens. From the tests, porosity values were calculated as per equation 3.3, which gives the capillary porosity.

$$\eta = \frac{M_{sv} - M_{so}}{A d \rho_w} X 100 \quad (3.3)$$

Where

η porosity

M_{sv} Vacuum saturated mass of the specimen (g)

M_{s0} Mass of the dry specimen (g)

A Cross-sectional area of the specimen (mm^2)

d Average specimen thickness (mm)

ρ_w Density of water (g/mm^3)



(a)



(b)

Figure 3.4. (a) Illustration of water-sorptivity test (b) Desiccator used for vacuum saturation

3.4.1.5 Ultrasonic pulse velocity (UPV) test

UPV is an important non-destructive test method used to investigate the state of damage and hence the durability of historic masonry structures, primarily because of the difficulty in performing invasive investigations in the protected monuments (Vasanelli et al. 2017). Direct UPV test was conducted on the stone columns at the site where the transmitting and receiving transducers were placed on opposite surfaces of the column. In the case of brick samples, UPV was conducted on whole bricks along the transverse direction, as illustrated in Figure 3.5. Pulse velocities were estimated from the known dimension traversed by the wave

(i.e., the thickness of cross-section) and the measured time taken by the pulse to travel through the material. Ultrasonic sound waves are used in the test to get an idea of cracks, voids, vaults, and in general, about the overall soundness of materials. Transducers of frequency 55 kHz were used as per the standard ASTM C597-2016 (ASTM Standard C597 2016).



Figure 3.5. Illustration of UPV test on a brick sample

3.4.2 Microstructural characterization

3.4.2.1 X-ray diffraction

Mineralogical composition of all the samples was analysed by X-ray diffraction (XRD) using a Bruker Discover D8 powder diffractometer (shown in Figure 3.6) with 0.5 s/step on scanning from 5° to 90° 2 θ , using Cu K α radiation. The sample preparation for XRD involved powdering of the samples and sieving through a 75-micron sieve. Figure 3.7 shows

the various steps in the sample preparation for XRD followed in this study. The powdered samples were then subjected to X-ray diffraction to identify and analyse the crystalline phases in the material. The output is in the form of a plot with the intensity of the X-ray counts on the Y-axis and diffraction angle 2θ on the X-axis, where 2θ is the angle between incident beam from the source and diffracted beam from the sample. This data is compared with the standard pattern of various known minerals and compounds using the database available from the International Joint Committee on Powder diffraction Standards (JCPDS database). Peaks were identified using this process by X'pert High Score software and quantified later by Rietveld analysis. The Rietveld refinement technique adopts a least squares approach to refine the theoretical line profile in order to match it with the measured profile by various steps. This works by minimising the difference between a calculated profile for the components and the observed data for the material.

In the current study, XRD helps in identifying the major minerals in bricks and stones. In bricks, this knowledge helps to find the raw materials and temperature at which these ancient bricks were fired. This assessment is possible from the identification of the presence/absence of certain minerals, which transform at known temperatures. In the case of stones, identification of minerals from XRD and morphology from SEM work complementarily in understanding the microstructural development of the matrix, which is crucial in determining the durability.

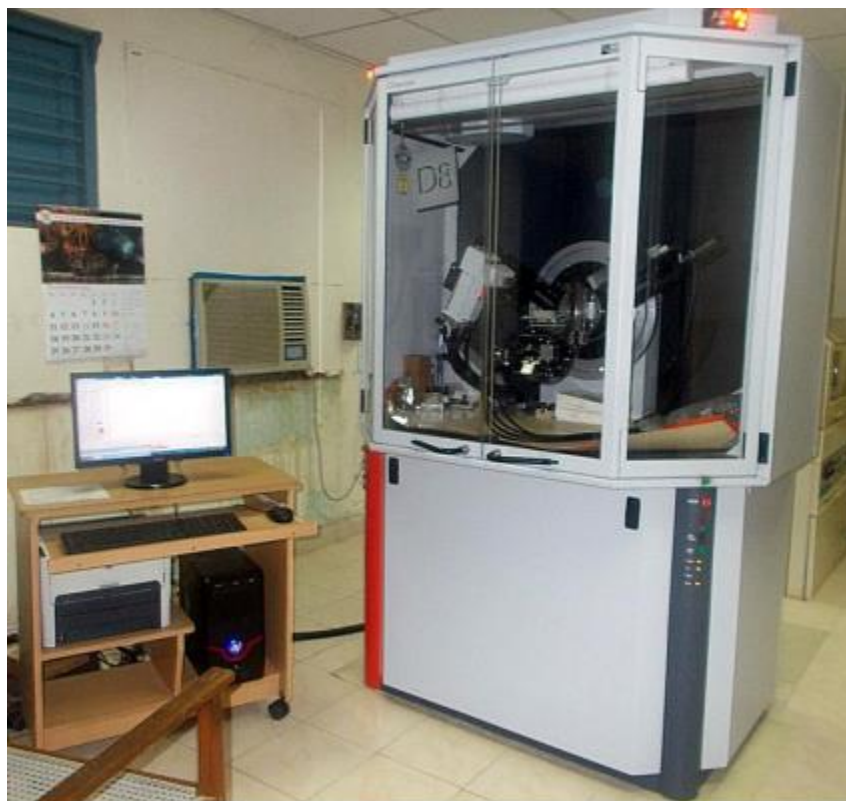


Figure 3.6. X-ray diffractometer

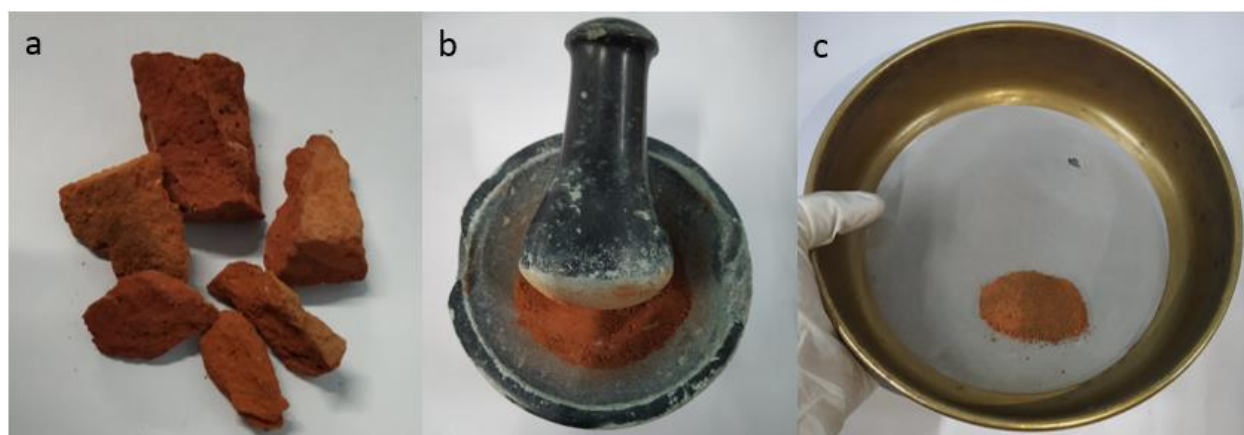


Figure 3.7. Steps in the process of sample preparation for XRD (a) brick chunks (b) powdering the bricks chunks (c) sieving the powder through 75-micron sieve

3.4.2.2 Scanning electron microscopy/EDS

Scanning Electron Microscopy (SEM) is a powerful tool to study the morphological features of stones. An Emcrafts GENESIS 2100 SEM equipment was used in the current study to capture images of the fractured surfaces of the samples, as shown in Figure 3.8. The system was equipped with energy dispersive X-ray analysis or energy dispersive spectroscopy (EDS) to identify the elemental phases on the imaged surface.

High-energy electron beams used in the microscope generate different types of signals when allowed to interact with the specimens. The interactions can produce secondary electrons, backscattered electrons and X-rays. Depending upon the choice of detector, secondary electron (SE) image, backscattered electron (BSE) image or EDS spectra can be obtained. An SE image reveals information about the sample, such as morphology, crystalline structure, and orientation of minerals constituting the sample. A BSE image provides data on the phase composition of the sample from the 2-D greyscale representation. EDS spectra identify the minerals in oxide forms at selected locations from SE/BSE images using the detected X-rays from the sample. Fractured surfaces of the samples of size 5-8 mm were glued to the metallic stubs with carbon tape, and were coated with gold sputtering before viewing in the SEM.

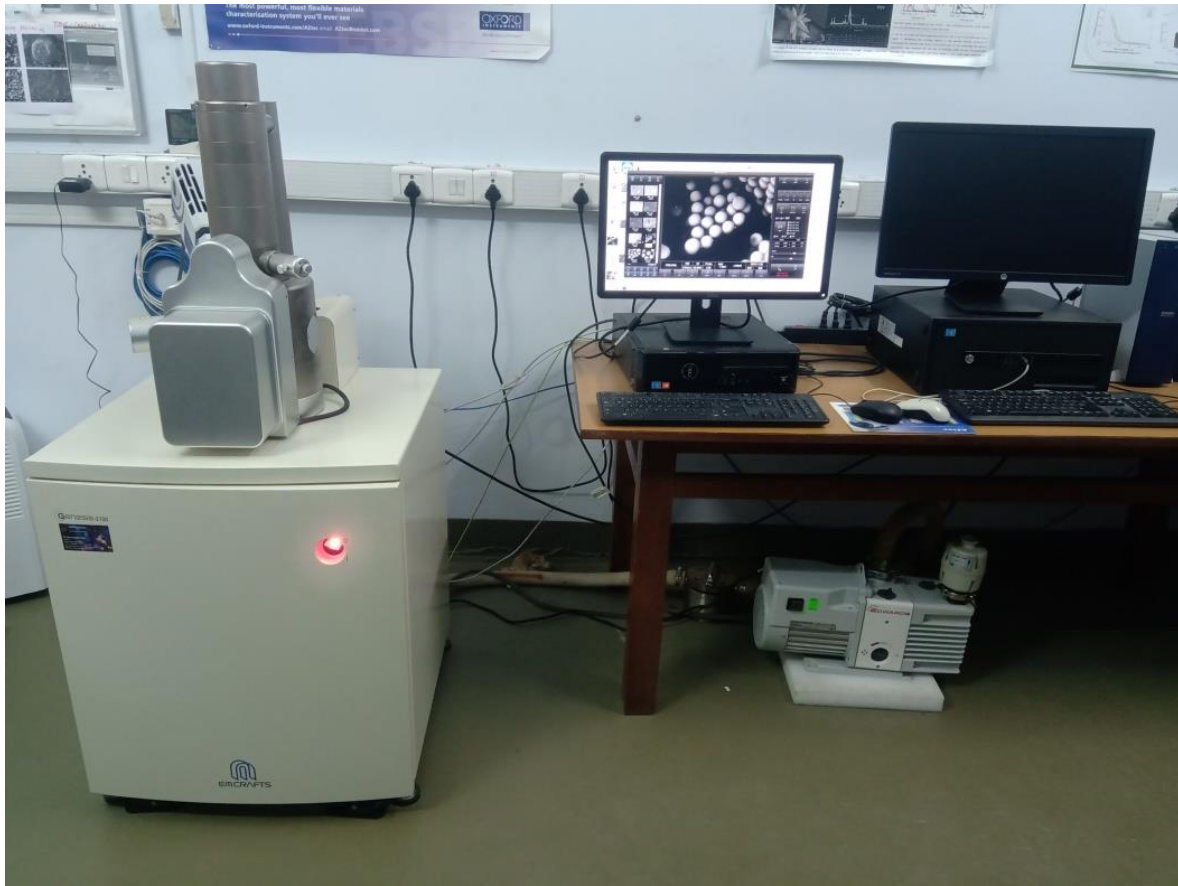


Figure 3.8. Emcrafts SEM equipment

3.4.2.3 Mercury intrusion porosimetry

Mercury Intrusion Porosimetry is an excellent tool, which measures the pore system redistribution and damage objectively, and gives information on the location of salt deposition and extent of the damage. Despite the limitations of the method like ink-bottle effect with pore entry diameter and assumptions regarding contact angle, the technique is widely accepted because of the ease with which the elaborate data can be collected (Lubelli et al. 2018). Mercury Intrusion Porosimetry (MIP) was used as a tool to investigate the total

open porosity and pore size distribution at a microstructural level. The instrument measures the amount of mercury intruded under incremental pressures. Since the pressure is inversely proportional to the pore size, the pore structure features can thus be obtained from this experiment. From the data obtained, cumulative intrusion graph and differential volume intrusion graphs are drawn for each sample. The pore structure parameters, namely critical pore diameter, threshold pore diameter and total pore volume, are found from the graphs for each sample. Critical pore size is the pore diameter that corresponds to the highest frequency of pore sizes, and is obtained as the peak in the differential intrusion curve; threshold pore size is the minimum continuous pore diameter, after which a sudden influx of mercury can be seen in the cumulative intrusion curve. Systems that have finer pore sizes are expected to have lower values for both these parameters. Any deterioration is expected to shift the pores towards coarser sizes. Figure 3.9 shows a typical example of cumulative and differential intrusion curves obtained from MIP, for a Portland cement system which shows the pore parameters (Scrivener, Snellings 2016).

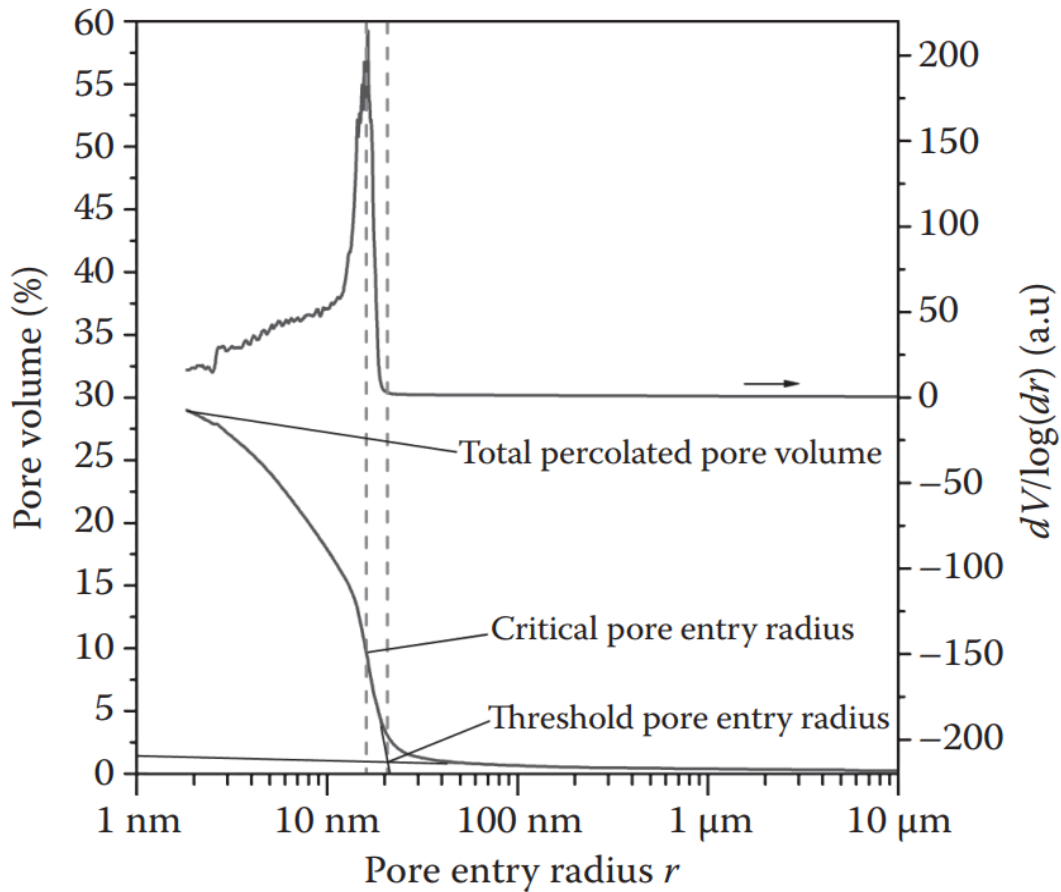


Figure 3.9. A typical example of MIP cumulative and derivative curves for Portland Cement, showing the pore parameters (Scrivener, Snellings 2016)

3-4 small pieces, each around 5 mm and total mass in the range of 0.5-0.8 g were broken from each brick sample for subjecting to MIP, which ensured high exposed surface area and high accessibility for mercury intrusion. 140-440 Pascal porosimeter instrument from Thermo Scientific was used (shown in Figure 3.10), which can measure pore sizes ranging from 100 μm to 3 nm, by increasing pressure from vacuum to 400 MPa.



Figure 3.10. Thermo Scientific Mercury Intrusion Porosimeter

3.4.3 Study of the impact of weathering in samples

3.4.3.1 Natural weathering

Naturally-weathered brick samples of varying conservation states were collected from different sites as specified in section 3.3.1. Among the samples, there were bricks exposed to different salts and showing different kinds of damage patterns, bricks not from salt exposed regions, historic bricks which were heavily weathered even in the absence of salts and bricks that were intact without any weathering traces. In this part of the study, samples weathered naturally with different damage manifestations were analysed, in an attempt to link the kind

of damages with the possible mechanisms in the light of presence/absence of particular salts. Brick samples collected from the Dansberg Fort, T1 and T2 undergoing active deterioration naturally were assessed using microanalytical techniques to explore the role of the pore structure and mineralogy in the deterioration process.

3.4.3.2 Accelerated artificial weathering

Immersion dry-wet cycling with sodium chloride and sodium sulphate salts were conducted on brick and stone specimens as per various standards, which are detailed in the next section. Brick specimens were cubes of side 40 mm, and stones were cubes with sides of 50 mm. Brick samples were limited to cubes of the size of 40 mm because the smallest dimension of most of the historic bricks available was 40 mm. For a more realistic exposure to compare with the naturally weathered samples from the coastal area, samples were exposed to sodium chloride salt spray in a spray chamber in the laboratory. Mass losses and visual damages were documented after each cycle in all cases. This test procedure provides an understanding of the salt weathering resistance of various materials and the role of the microstructure of the materials in controlling the behaviour in the presence of different salts.

3.4.4 Study of the suitability of protective treatments

The objective of this part of the study was to identify the properties determining the efficiency of water-repellent treatments for any historical masonry. The study also aimed at understanding the role of the microstructure of the material in assessing the performance of various protective treatments when exposed to salts. In the first part of the study, the fundamental properties of the water repellent treatments considered were tested using water

drop absorption test, Karstens' pipe test, vapour permeability (breathability) test, and sorptivity test. Once the treatments qualified the particular quality tests, then the performance of the treatments with respect to salt resistance was tested using accelerated salt weathering tests. For all the tests, three numbers of each sample, with uncoated and coated variants were considered. The tests conducted for the evaluation of water repellent treatments are explained in this section.

3.4.4.1 Water drop absorption test (RILEM Test Method - Test No. II.8a, 1980)

In the water drop absorption test, 1 ml of water was dropped from a height of 1 cm on the representative uncoated and coated specimens that were dried to a constant mass at 60 °C. An identical water drop was placed on a glass surface to eliminate the effects of possible evaporation. The reduction in volume in the water drop due to absorption was observed visually after a particular time interval. The time taken for complete absorption of water drop from the surface of each specimen was measured.

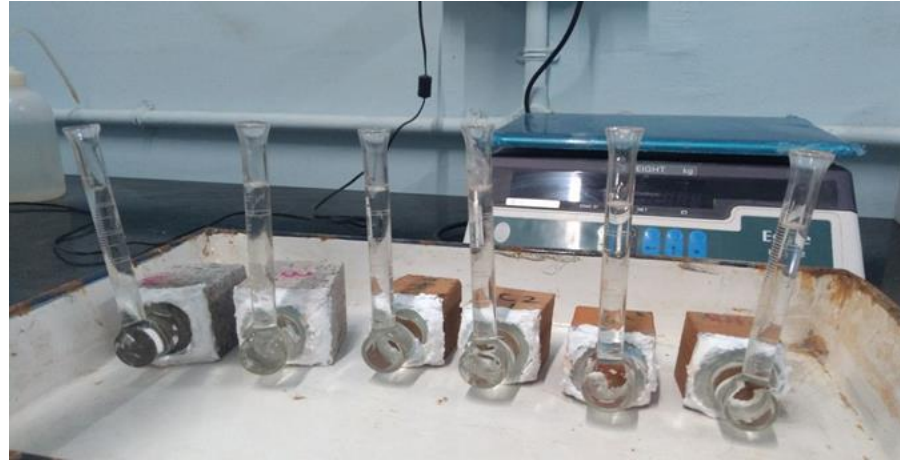
3.4.4.2 Karstens' pipe test (RILEM Test Method - Test No. II.4 1980)

RILEM test no. II.4 was followed to measure the amount of water absorbed under low pressure on a definite surface of porous building material. The apparatus used was a graduated glass tube called Karstens' tube, which was sealed upon the vertical faces of the specimens using acrylic sealants for water tightness. Water was poured into the Karstens' tube attached to the specimens. The drop in water level in the graduated tube was monitored for its absorption at short time intervals. The rate of absorption was compared between

different specimens after plotting the drop in water volume and time elapsed. A typical Karstens' tube and the test setup are shown in Figure 3.11.



(a) Karstens' tube



(b) Test setup in brick specimens

Figure 3.11. Illustration of Karstens' pipe test

3.4.4.3 Vapour permeability test (EN 15803:2010)

In this test procedure, rectangular specimens - uncoated and coated on the bottom side with protective treatments were mounted on top of cups having a particular salt, which constitute a 'measure cell'. The salt solution inside the cups can create RH lower inside the cup than outside, thus facilitating vapour flow through the specimens. The mass change in the cells was then measured periodically until the rate of change of mass was found constant. Figure 3.12 shows the test setup of vapour permeability evaluation. Specimens were prepared as rectangular prisms with thickness 20 mm and surface 70 mm x 70 mm. Coatings were provided for the required specimens in the bottom side, three brush strokes for each. Cups had a circular cross-sectional opening with diameter 50 mm. The acrylic sealant was used to

fix the specimens to the cup tightly. Additionally, the specimens were sealed with adhesive tapes all around to prevent any chances of unwanted vapour leak.



Figure 3.12. Test setup of vapour permeability test showing the measure cells

3.4.4.4 Salt crystallization test

In salt weathering test, the samples were subjected to salt crystallization cycles, in a similar way as in the case of analysing salt weathering resistance of uncoated samples. The mass changes and visible damages occurred to the specimens were recorded at the end of every cycle.

3.5 WEATHERING TEST METHODS

3.5.1 Immersion test according to EN12370

EN12370 is a very commonly used standard for testing porous materials under salt crystallization. This test was used initially for various types of specimens - the fresh, commercially available units, and the historic samples which were found intact and with least

weathering traces. The experiment was conducted for 15 cycles, as mentioned in the standard procedure. This enabled to arrive at initial comparative evaluation of the performance of each material with salt exposure. The samples were exposed to sodium sulphate solution for 4 hours by complete immersion in 14% sodium sulphate decahydrate solution, followed by 16 hours drying at 105 °C and subsequent cooling in room temperature for 4 hours. Then the new dry weight was measured before the next wetting cycle. This process constituted one full cycle, which is 24 hours. During immersion, it was ensured that all specimens are covered by at least 10 mm solution at the top surface. Each lithotype had three specimens, which were in their own containers. The solution was replaced after every 3 cycles. Presently, the standard EN12370 is being criticized for being unrealistic in terms of excessive aggressiveness (Marti 2017). Hence, after understanding the basic pattern of damages in each kind of brick, long term weathering studies were conducted on samples with other standards.

3.5.2 Immersion test according to RILEM V 1.b

When immersion test cycles were also carried out with treated samples with water repellents, the extremely high temperature drying at 105 °C by EN 12370 standard was not preferred, and hence it was decided to adopt the RILEM V1.b procedure. Here, specimens were exposed to 10% sodium sulphate anhydrite solution for 2 hours, followed by drying at 60 °C for 19 hours and subsequent cooling at room temperature for 3 hours. Again, one cycle was 24 hours, and the mass measurements and damage monitoring were carried out after each cycle. The tests were continued for 112 cycles or until the samples were completely disintegrated.

3.5.3 Spraying test according to ASTM B117-11

The salt spray chamber manufactured in the Structural Engineering Laboratory at IIT Madras in accordance with ASTM B117-11 ‘Standard Practice for Operating Salt Spray (Fog) Apparatus’(ASTM B117- 2017) was used for conducting salt spray test for the specimens. The standard ASTM B117 details the conditions and procedures required to maintain the salt spray test chamber. The test environment not only provides a realistic salt exposure atmosphere for the materials to study the effects of salt weathering, but also facilitates study on corrosion of materials. The walk-in chamber is equipped with temperature and humidity controllers. 5% NaCl solution was used to provide atomized spray, which was applied to the specimens in the chamber for five consecutive days, followed by five days of drying. Drying was facilitated using infra-red (IR) lamps of 340 nm @ 1.55 Watts/m², which simulates the effects of sunlight. Figure 3.13 shows the schematic diagram of the chamber. The specifications of the salt spray chamber used are as follows:

- (i) Operating temperature : 35-40 °C
- (ii) Relative Humidity : 95 ± 3%
- (iii) Contaminating solution : 5% NaCl solution
- (iv) pH : 6.5 to 7.2
- (v) Material : Polypropylene reinforced with stainless-steel
- (vi) Air Compressor : 5HP, 200-litre tank pressure capacity with auto cut-off switch

5% NaCl solution was prepared and filled into the reservoir provided in the backside of the chamber. The reservoir with the salt solution is connected to four atomizer nozzles for spraying the humidified salt solution. The air compressor supplies air at a pressure of 12 kg/cm² used for both the humidifier and closing and opening of the chamber door.

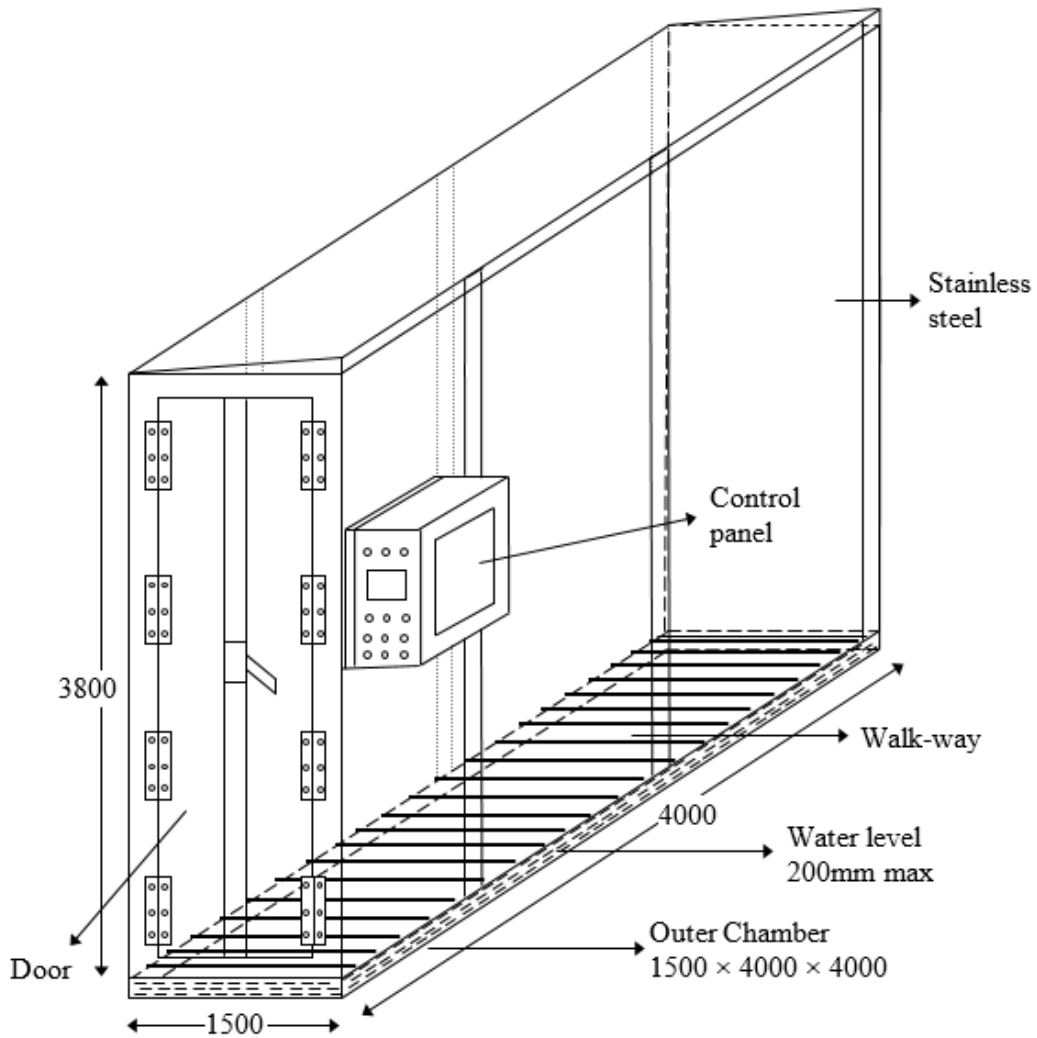


Figure 3.13. Schematic diagram of the salt spray chamber used for the study

Spraying of solution through the atomiser works based on Bernoulli's principle where there is a corresponding pressure drop for an increased fluid velocity, which can be used to draw the next fluid set in the primary flow. The working of atomiser nozzle is illustrated in Figure 3.14. Air from the humidifier is received at the bottom of the atomiser and then blown up. At a certain height from the bottom, there is a cross-sectional area change to facilitate increased velocity as per the Venturi principle. This will result in a reduction in pressure, which draws salt solution through a horizontal pipe connected from the reservoir. Figure 3.15 shows the salt spray chamber used for the test.

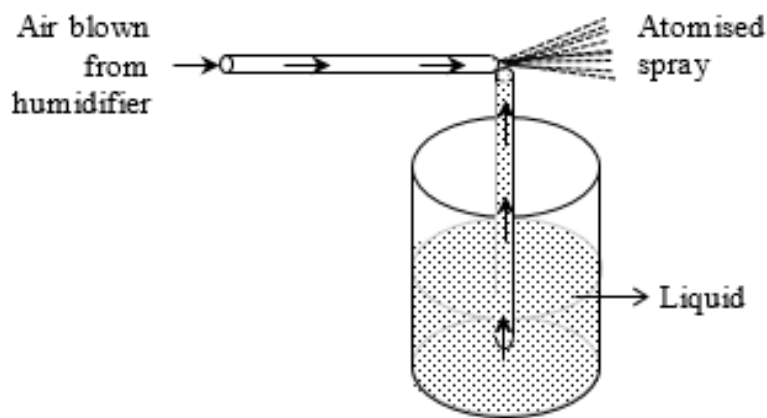


Figure 3.14. Working of atomised nozzle

The specimens, after subjecting to continuous five days of spraying and subsequent five days of drying, were measured for mass changes and monitored for any visible damages. After documenting, the spraying-drying cycles were continued. The exposure was provided for the specimens for 460 days.



Figure 3.15. Salt-spray chamber

3.6 DESALINATION

Desalination is the process of removing the salts from the material - here it is the porous masonry building units. The artificially weathered specimens were subjected to microanalytical characterization techniques, as explained before. However, there can be the presence of salts within the pores, which can influence the results. Hence, the process of desalination was carried out to remove salts from the weathered units and compare those with

the material with salts. Cellulose poulticing was used as the technique for desalination in the study. The study also analyses the effect of cellulose poulticing with respect to different salts and different materials.

Cellulose poulticing is a widespread method of desalination in practice for removal of salts from historic structures. Dry cellulose powder was mixed for 1 minute with water in the ratio 1:4 to form the cellulose pulp. The required water content to provide the poultice with adequate workability depends on the nature and particle size of the particular poultice material. Here, the poultice to water ratio was fixed by trial and error method, on targeting the workability that allows the pulp to mix well, stick to specimens and not flow. The wet poultice was then applied to the surface of the salt weathered specimens with approximately 2 cm thickness on all sides and kept for drying for 2 weeks. The poultice was removed once it was completely dried. The specimens were then washed in water and dried to get desalinated specimens which were later analysed with microstructural characterization techniques. The process of preparation and application of cellulose poultice on specimens was as shown in Figure 3.16. The cellulose powder as such is shown, followed by the mixing of cellulose powder with water to form the pulp (poultice) and then the samples covered by the prepared poultice.



Figure 3.16. Steps followed in the process of poulticing (a) cellulose powder in the dry form (b) mixing of cellulose powder with water to prepare the poultice (c) samples covered with the cellulose poultice left for drying

3.7 SUMMARY

The experimental design, procedures and details of the materials used were explained in this chapter. The details included the samples collected from historic sites and commercial sources, water repellent treatments used in the study, tests used to characterize the samples, and the tests used to evaluate the efficiency of various protective treatments for masonry.

4 CHARACTERIZATION OF MASONRY BRICKS

4.1 INTRODUCTION

Historic building units possess uncertainties with respect to their origin, mineral content, manufacturing etc. The geological and mineralogical nature of any material is critical to understand its process of deterioration. Starting from the visual observations, this chapter unravels the physical, mechanical, chemical and microstructural characteristics of the masonry unit samples - both historic and fresh. These intrinsic properties would connect the microstructure of the matrix and cohesion between the crystal grains to the durability performance.

Physical properties relevant to analyze the conservation state of the materials and weathering were studied, which include water absorption, bulk density, and capillary porosity. Mechanical properties such as compressive strength and ultrasonic pulse velocity were tested. Chemical and mineralogical compositions were analyzed during X-ray diffraction studies and EDS from Scanning Electron Microscopy (SEM). The microstructural understanding was obtained from the morphological details of SEM images and pore size distribution from Mercury Intrusion Porosimetry.






4.2 CHARACTERISTICS OF THE BRICK SAMPLES





The physical, mechanical and chemical properties and microstructural characteristics of all the brick samples considered in the study are presented in this section. Salt crystallization is the crucial damaging mechanism which affects the durability of porous masonry units like bricks. In this section, the role of the pore size distribution of the bricks in resisting salt crystallization was analyzed by subjecting the bricks with different microstructure to accelerated salt weathering tests. Microstructural features were then characterized after weathering to study the mechanism of salt weathering, and its effect on the properties of the material.

4.2.1 Visual observations

Visual observations were documented for all the samples, which included colour and state of external weathering indications if any. Sizes of the samples were measured in cases where whole bricks were obtained. The samples considered are V1, V2, V3, K, T1, T2, which are historic samples and C1, C2 and VN, which are fresh samples. The details of the samples were discussed in detail in Chapter 3, Section 3.2. The fresh samples showed slight differences in colour among each other, which could be because of the variation in raw materials and firing temperature. The sizes of the bricks, colour and texture variations along with visual weathering traces if any are summarized in Table 4.1.

Table 4.1. Visual evaluation of brick samples

	Sample size (mm)	Colour	Visual traces of weathering	Location	Image
V1	165*138*50	Brown	Intact, uniform texture, no weathering	Exterior wall	
V2	150*110*50	Brown	Intact, uniform texture, no weathering	Exterior wall	
V3	168*165*50	Light red-brown	Intact, uniform texture, no weathering traces	Foundation of structure	
K	150*110*50	Light orange-yellow	Edges powdered	Exterior wall	
T1	220*110*50	Orange-red	Showed heavy efflorescence and blistering	Lower portion of masonry wall exposed to sea spray	

T2	220*110*50	Orange-red	Softened and eroded from sides progressively	Partially immersed in sea, subjected to tidal erosive forces	
VN	150*110*50	Brown	Fresh brick	–	
C1	220*110*50	Orange-yellow	Fresh brick	–	
C2	220*110*50	Red-brown	Fresh brick	–	

4.2.2 Physical-mechanical characterization

Physical and mechanical properties of all the brick samples were determined, both for historical and fresh samples. Combining the current weathering state and the observed results of physical-mechanical characterization, certain brick samples were excluded from further accelerated weathering studies. Those historic samples which were in a good conservation

state, with comparable physical-mechanical properties as that of fresh samples, along with the fresh commercial samples were selected for studying the effects of salt crystallization.

Compressive strengths of the bricks were determined at a loading rate of 140 kg/cm²/min as per IS 1077:1992 (Indian Standard IS 1077 1997) and bulk densities of the bricks were obtained from Helium gas pycnometer test and each value was obtained after three iterations with the pycnometer. Water absorption is a critical factor for durability. While higher water absorption can lead to other deterioration mechanisms, deficient water absorption can affect the durability of mortar joints because water will be absorbed into the joints (Ukwatta and Mohajerani 2017).

The results are shown in Figure 4.1. All the historic bricks showed similar water absorption values, in the range of 12-16%, whereas the two new bricks C1 and C2 were found to have extreme high and low values respectively compared to others. When C1 had the highest water absorption value of 17.5%, C2 had it the lowest - 9.8%. Water absorption represents the capillary or water accessible interconnected porosity in the system.

Ultrasonic pulse velocities (UPV) through the different bricks are shown in Figure 4.1 (d). The wave velocities were found to be lower in samples K, T1 and T2, which were observed with visual weathering traces like fissures and cracks.

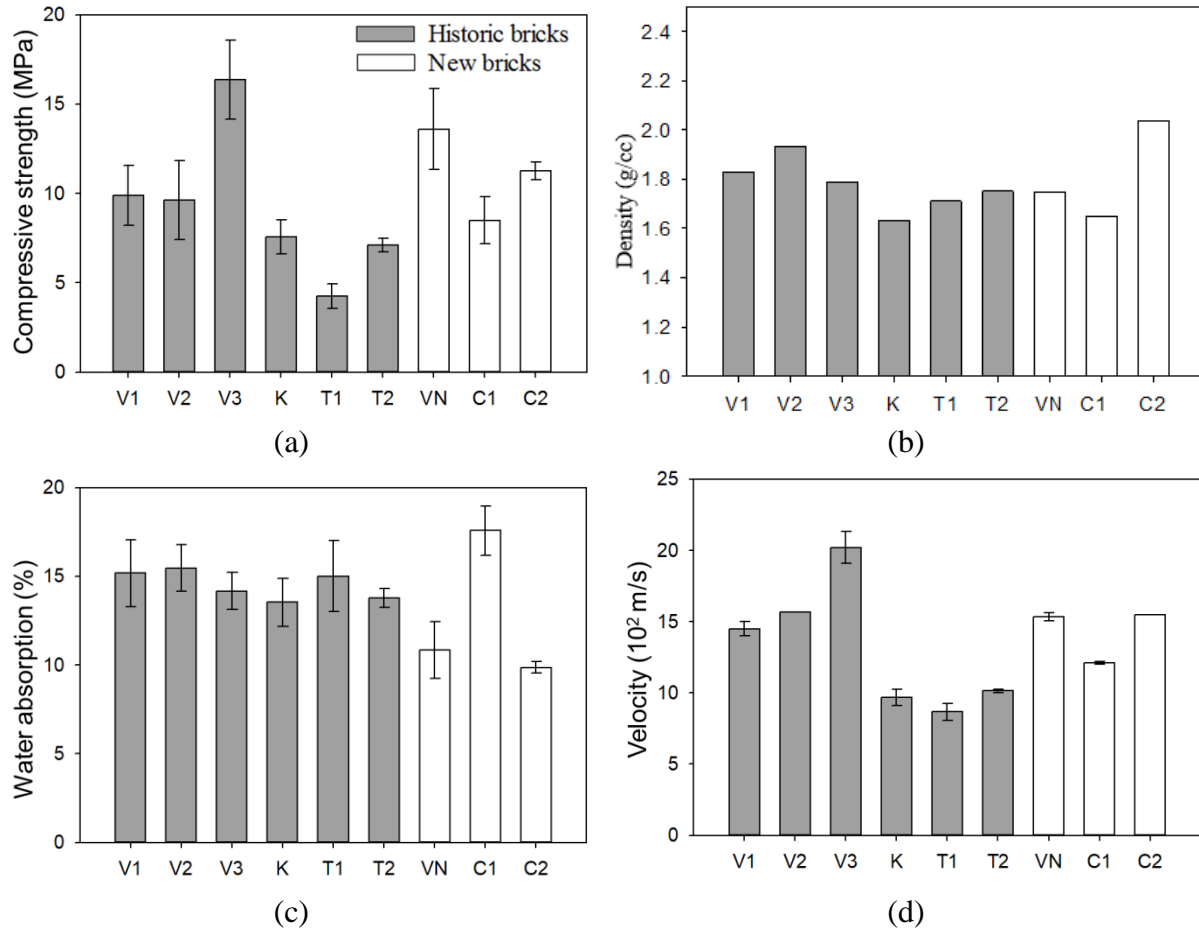


Figure 4.1 (a) Compressive strength (b) Bulk density (c) water absorption (d) UPV

From the test results of compressive strength, UPV, water absorption and density, it was observed that the historic bricks from the temple of Vepathur - V1, V2 and V3 showed outstanding physical properties; these bricks have withstood the tests of time without being affected by the weathering. Measured physical properties are in concordance with the visual observations; the brick samples that showed weathering traces and powdering (samples K, T1 and T2) were found weak in the physical-mechanical tests. Minor inconsistency with respect to compressive strength, density and UPV between bricks which were weathered and

unweathered can be because of the presence of weathering products within the microstructural spaces in the matrix.

Compressive strength of different specimens showed a direct linear correlation with UPV values, but did not show a direct relation with density as expected in normal cases, which could be again because of the presence/absence of weathering products of different densities and other defects/anomalies within. In the case of water absorption, bricks with high strength and high density generally showed lower water absorption. The physical properties were found to be almost matching for the newly made replacement brick (VN) as the ancient bricks V1 and V2 of Vepathur, but the compressive strength was around 35% greater for the new brick.

From the properties observed, T1, T2 and K were found to have weaker physical and mechanical characteristics, and these were already in a weathered state. Hence, all other samples were considered for further accelerated weathering tests, which will be described in section 4.4.

4.2.3 X-ray diffraction

For identifying the mineralogical composition, X-ray diffraction (XRD) technique was used. Firing temperature and raw materials of the bricks were determined from the analysis of mineral composition. Presence of weathering products was also checked from XRD results.

Figure 4.2 shows the X-ray diffractograms of the samples, which reveals their mineralogical constituents. Quartz and alkali feldspars were found as the major minerals present in all the samples. Other minor phases identified were hematite, illite, wollastonite,

paragonite, halite, thenardite, gehlenite, diopside etc. - the mineral type and quantity varied in the samples. These minor minerals provided vital information on the raw materials and firing temperature of the bricks. Quantification of the mineral composition of the samples by Rietveld analysis is given in Table 4.2.

Analysis of the diffractograms can facilitate estimation of the original firing temperature of the bricks, from the absence or presence of various mineral phases (López-Arce et al. 2003). Presence of primary calcite and dolomite in the system indicates the firing temperatures to be less than 800 °C. They decompose to neo-formed mineral phases like diopside and gehlenite on reacting with silicates at temperatures around 800 °C. Hence, the presence of gehlenite and diopside points to a firing temperature of more than 900 °C, and if only gehlenite is found, the temperature is likely to have been above 800 °C. The sampled bricks V3, VN and C2, were assessed to be fired at temperatures well over 900 °C because of the presence of gehlenite and diopside and absence of illite in them. Also, higher background noise was seen in the diffractograms of these samples than the others, which occurs because of the formation of an amorphous phase at very high firing temperatures. This happens when CaO from decomposition reactions acts as a melting agent to facilitate vitrification (Singer and Singer 1963). Presence of calcite in the C2 bricks suggests the formation of secondary calcite. Samples V1 and V2 were probably fired at just over 900 °C, as indicated from the presence of illite, gehlenite and diopside. C1 was identified with the presence of illite, hematite and gehlenite, but no diopside, which indicates a firing temperature between 800 and 900 °C. In samples K, T1 and T2, any neo-formed aluminosilicates like gehlenite or diopside were absent, but the presence of illite and calcite were observed, indicating a firing

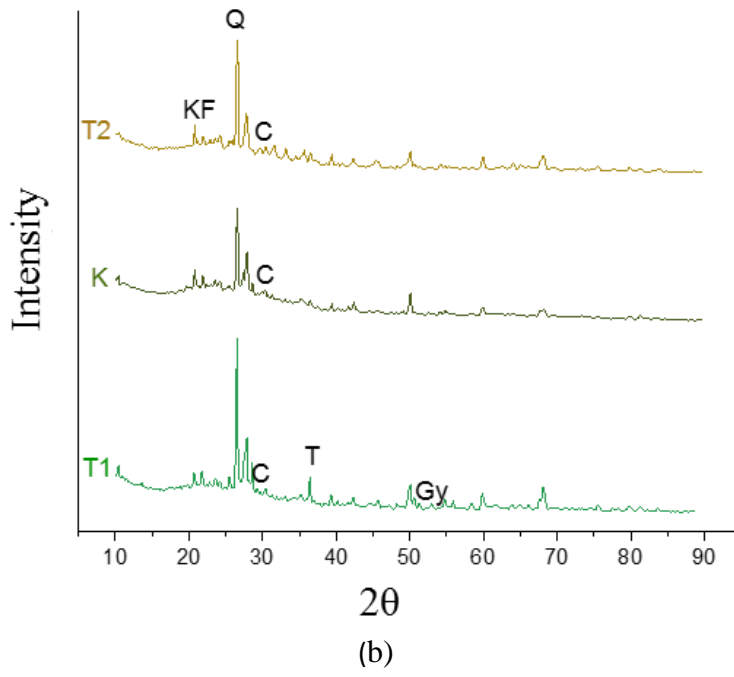
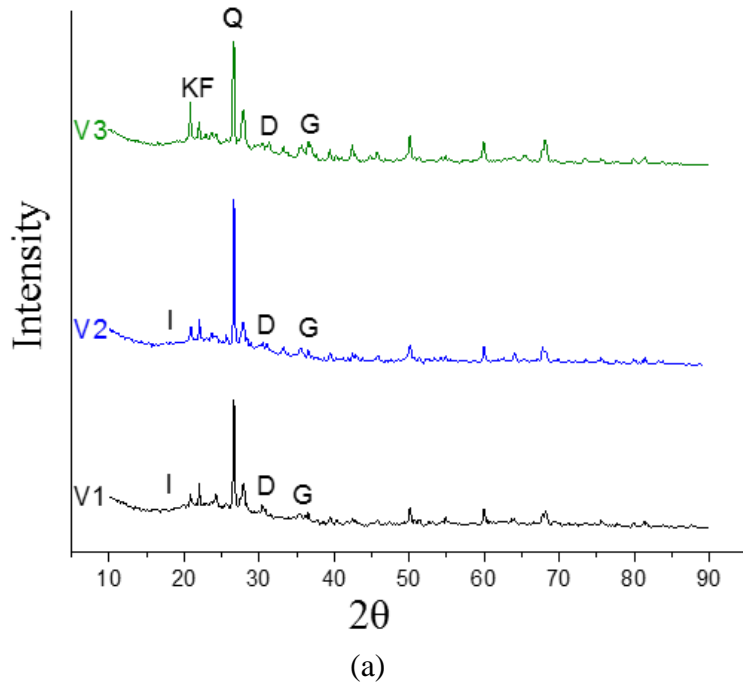
temperature less than 800 °C. Presence of calcite points to the use of Ca-rich clays for the manufacturing of these bricks (K, T1, T2, C2).

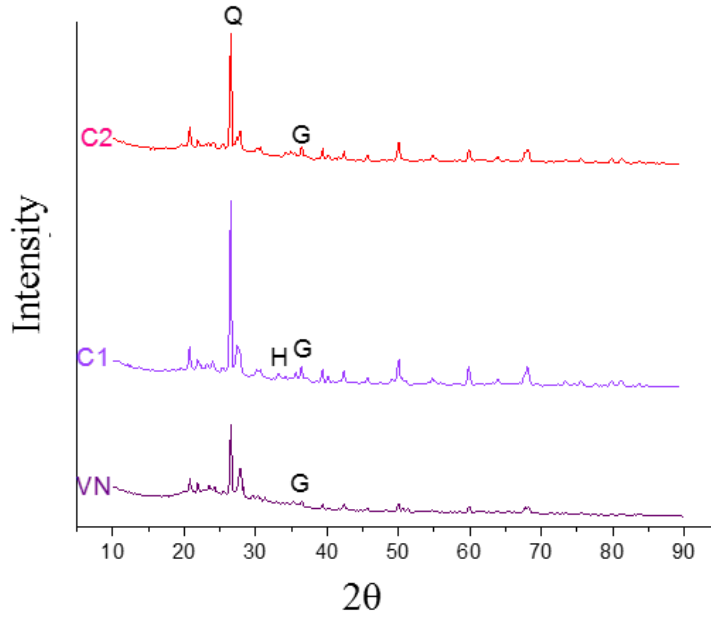
The firing temperatures of the samples analyzed from their mineralogical compositions (Table 4.2) are in concordance with the range of UPV values in the specimens. This could be because of the improved vitrification with firing temperature, which actually creates the brick system to be more intact and sounder, facilitating better traverse of the ultrasonic waves. Also, it could be partially because of the formation of denser mineral phases with increased temperatures (when less dense phases like carbonates or phyllosilicates decompose).

Table 4.2. Mineralogical quantification from XRD data

Sample ID	Firing temperature assessed (°C)	C	Q	KF	NaF	H	D	I	G	W	P	Gy	Ha	T
V1	just above 900	0	39.9	37.8	0	0	3.2	1.2	3	3	12	0	0	0
V2	just above 900	0	50.3	24.1	0	0	2.7	1.8	2.1	8	11	0	0	0
V3	significantly more than 900	0	20.5	70.4	0	0	4.9	0	2.1	0	2.1	0	0	0
K	< 800	1	23.8	1.9	71.9	0.2	0	0	0	0	1.2	0	0	0
T1	< 800	2.1	39.4	45.2	0	0	0	0	0	3	6.1	1.9	1.3	1.2
T2	< 800	1.9	49.4	34.9	0	0	0	0	0	4	6.4	0	3.5	0
VN	significantly more than 900	0	28.9	12.2	43	0	0.4	0	2.1	3.6	10	0	0	0
C1	800-900	0	48	18.4	18.4	1.7	0	7.6	0.9	2	2.9	0	0	0
C2	significantly more than 900	2.2	60.7	14.6	14.8	0	1.5	0	3.0	1.6	2.0	0	0	0

C: Calcite, Q: Quartz, KF: K Feldspar, NaF: Na Feldspar, H: Hematite, D: Diopside, I: Illite, G: Gehlenite, W: Wollastonite, P: Paragonite, Gy: Gypsum, Ha: Halite, T - Thenardite





(c)

Figure 4.2. X-ray diffractograms of the brick samples (a) historic bricks V1, V2, V3 fired at high temperature (b) historic bricks K, T1, T2 fired at low temperature (c) new bricks VN, C1, C2

Q-Quartz; KF-Potassium feldspar; D-Diopside; G-Gehlenite; I-Illite; C-Calcite; T-Thenardite; Gy-Gypsum; H-Hematite

T1 and T2 were the samples collected from a salt exposed environment. Salt weathering (salt crystallisation) is crucial in bricks where saltwater finds its way to the brick pores. But XRD results showed the salt crystallization products were not retained in the material much, even though the associated damage was evident. Salt efflorescence was seen widespread in the samples of T1, due to the alternate dry-wet cycles. The heavy blistering in the T1 samples suggested the presence of crystalline gypsum, which was also confirmed from the X-ray diffractograms. Gypsum typically crystallizes beneath the brick surface, as a result of the reaction of calcium with sulphate salts, which forms the blistering (Lubelli et al.

2004). This phenomenon is more likely in a marine environment because NaCl can directly influence the solubility of gypsum (Price and Brimblecombe 1994) and also act as a catalyst in promoting the reaction between calcite and sulphates to form more gypsum (Laurie and Milne 1927).

4.2.4 Scanning Electron Microscopy

The morphology of weathering traces in the fractured surface of bricks was observed from the SEM images, and the chemistry was studied with the help of EDS.

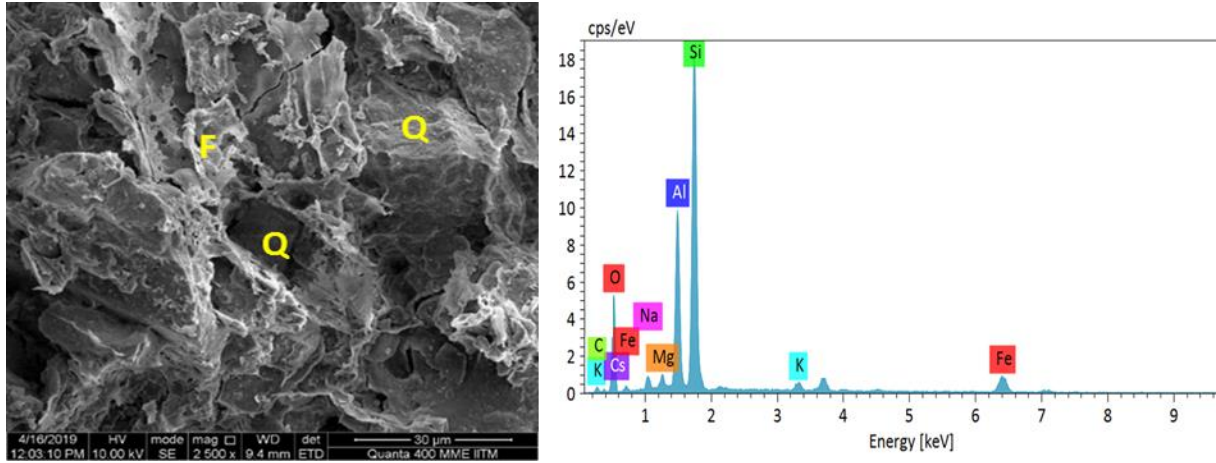
Figure 4.3 (a) and (b) show SEM images of samples C1 and C2 at 2500 X. Both the brick types were characterized by sheet-like phyllosilicates. Typical EDS taken from the image in Figure 4.3 (a) of brick C1 is shown. A clear distinction of the varying degree of vitrification is seen between the two images. While C1 was found with higher porosity, and with the limited interconnection between the feldspar particles, C2 was more vitrified, with low porosity and small pores. This supports the higher firing temperature of C2 and lower firing temperature of C1, assessed from the XRD results (Figure 4.2 and Table 4.2). With a greater degree of vitrification during higher firing temperatures (when temperature is high enough for vitrification to happen), relatively larger rounded pores are created to the detriment of the original porosity with pores of smaller size and irregular morphology (Cultrone et al. 2005a). Phyllosilicates have the tendency to deform and join together after 900 °C, and the further smoothening of grains and modification of pore shapes into elliptical shapes is expected at 1000 °C (Elert et al. 2004). This is visualized in Figure 4.3 (a), and (b), where C2 fired at temperatures close to 1000 °C had phyllosilicates deformed and clumped

together compared to that of C1, which was fired at a lesser temperature. The large and more rounded pores in C1 indicated its excellent salt crystallization resistance whereas C2 with smaller pores suggested its high susceptibility to salt crystallization damage. Hence, rather than the total porosity, the number, size or shape of pores influence to a larger extent the durability of the bricks. The use of Ca-rich clays for manufacturing of C2 brick (from XRD results, Table 4.2) and low-Ca clays for C1 brick also were supposed to have an impact on the resulted pore structure. In case of low-Ca clays (C1 brick), smaller pores between clay particles disappear at higher firing temperatures as a result of melting and coalescence of particles, and larger pores form due to gas release caused by loss of OH⁻ groups in phyllosilicates. However, in case of Ca-rich clays, due to the transformation of calcite into microporous calcium oxide, the resulting pore structure would be different. The further conversion of lime to portlandite could result in localised precipitations. Further, if portlandite reacts with carbon dioxide to form calcite, it could cause lime blowing resulting in a non-uniformly vitrified and fissured system.

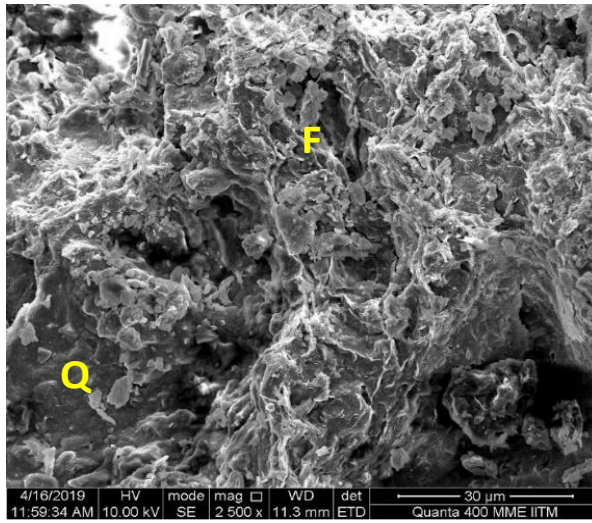
In Figure 4.3 (c) and (d), with the highly vitrified system of V1 and V2 respectively, the deformed minerals filled up the pores/fissures between the quartz crystals, resulting in a more intact matrix. This demonstrates the reason for enhanced strength, density, and UPV values for the heritage bricks from Vepathur temple. A low porosity with smaller sized pores, mostly of size less than 1 μm in the well-packed matrix are seen from the images of V1 and V2, which indicates poor salt crystallization resistance in the system. However, these bricks were not exposed to a salt crystallization prone environment, but only to load, age and other anthropogenic factors like pollution and heating and hence had no visible degradation. V3

bricks, from a different location at same site, even though showing excellent physical and mechanical performance, had a different microstructure. They were well vitrified with highly dense structure but with larger pores. Commonly seen pore sizes close to 5 μm in V3 are shown in Figure 4.3 (e). This formation of modified elliptical larger pores in a well-vitrified system suggests that V3 bricks could have been fired at temperatures more than or close to 1000 °C. VN bricks, which were made to replace the V1 and V2 types, with similar properties, showed a similar microstructure too, as seen in Figure 5f where feldspar particles diffuse into the gaps between and over quartz crystals. K showed only physical weathering with the presence of fractures and fissures. Samples T1 and T2 showed chemical weathering, but of different degree. In these low temperature-fired bricks, i.e. K and T1, the persistence of the sheet-like structure of phyllosilicates, very low particle-interconnectivity and extensive fissuring were seen (Figure 4.3 (g) and (i)). In Figure 4.3 (h), T2, in spite of being fired at low temperature, lacked fissuring, which is expected from its good strength properties. Evidence of corrosion-dissolution process giving rise to recrystallization of tabular elongated calcite crystals was seen in sample T2, near the edges of quartz and feldspar crystals, which could have also helped the bricks to have increased strength in spite of the continuous erosive forces. Secondary calcite covering up space and pores in between major mineral grains is shown in Figure 4.3 (h). The elemental analysis EDS, presented alongside, shows the possible presence of calcite, halite, quartz and feldspars. Figure 4.3 (i) and (j) shows SEM images of T1, which was attacked by sulphates and showed blistering. Gypsum nodules of diameter 10 μm to more than 50 μm were abundantly seen, and one such nodule is magnified in Figure 4.3 (j). These sub-spherical gypsum nodules, which were the saline crypto-

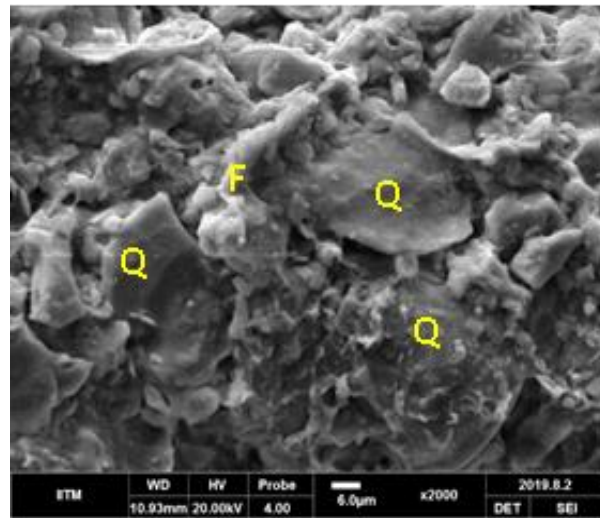
efflorescence seen inside T1 bricks, would have formed because of the precipitation and crystallization of sulphate salts inside pores.



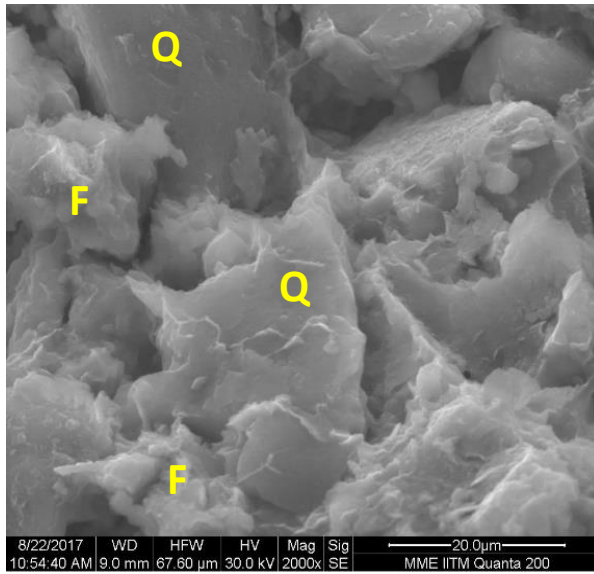
(a) C1



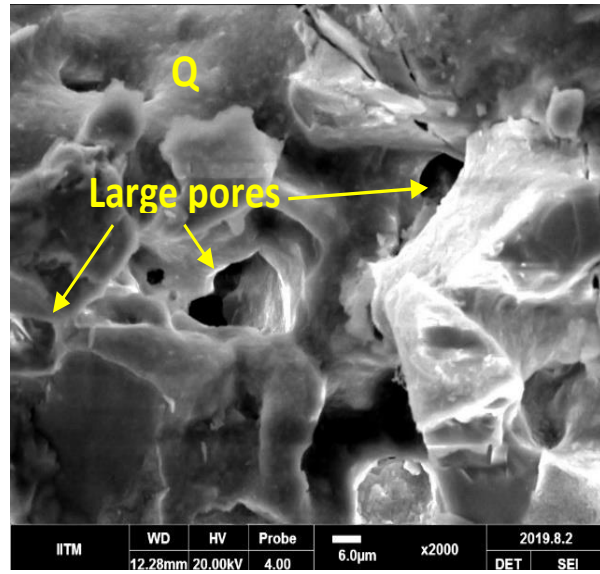
(b) C2



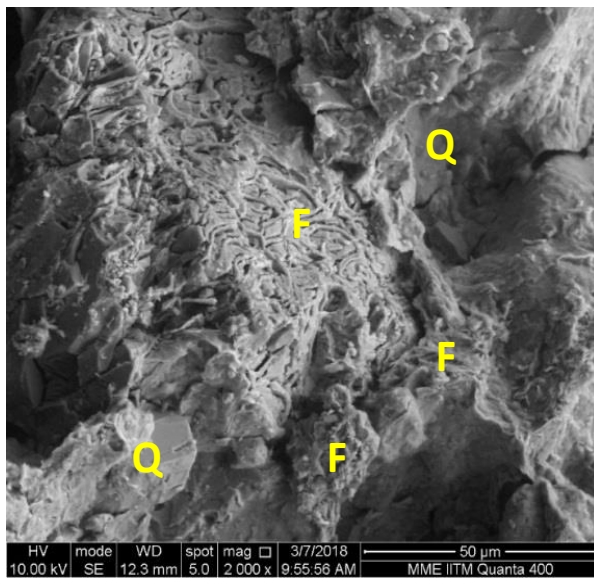
(c) V1



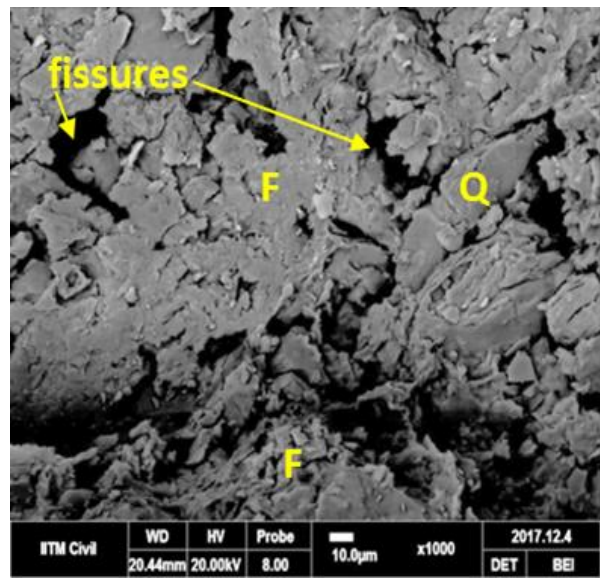
(d) V2



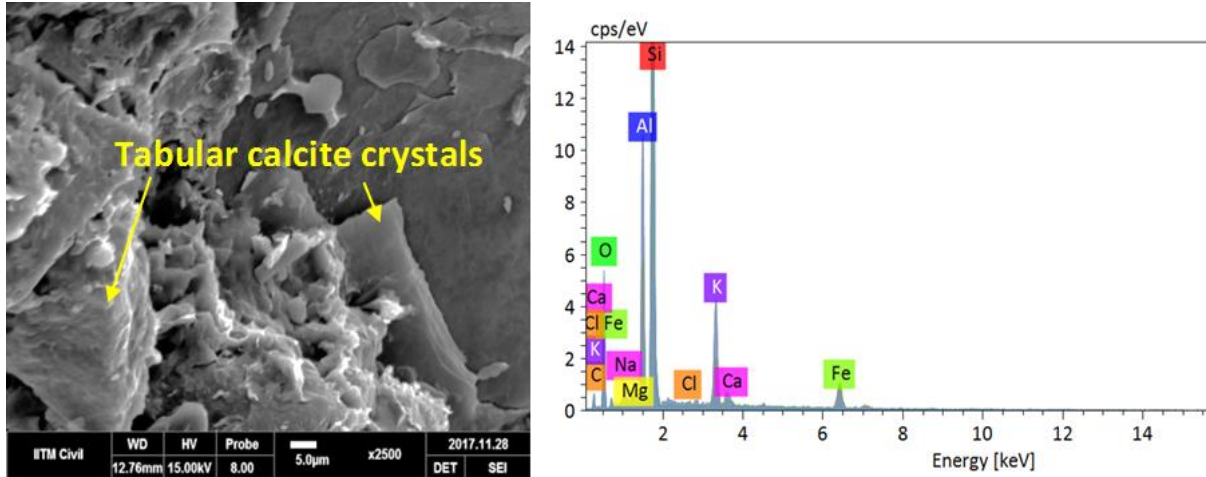
(e) V3



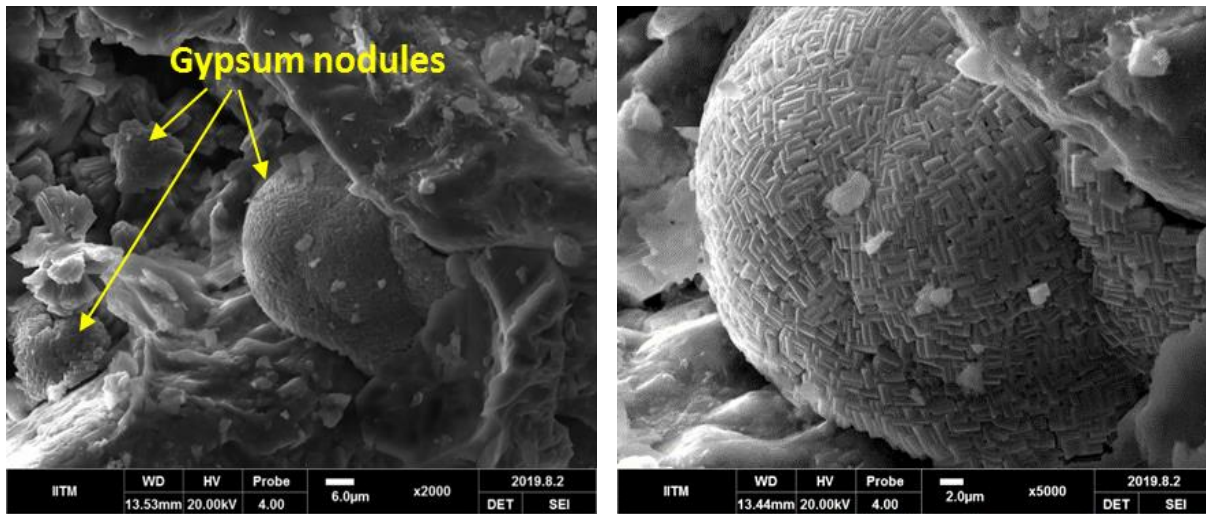
(f) VN



(g) K



(h) T2



(i) T1

(j) Gypsum nodule in T1

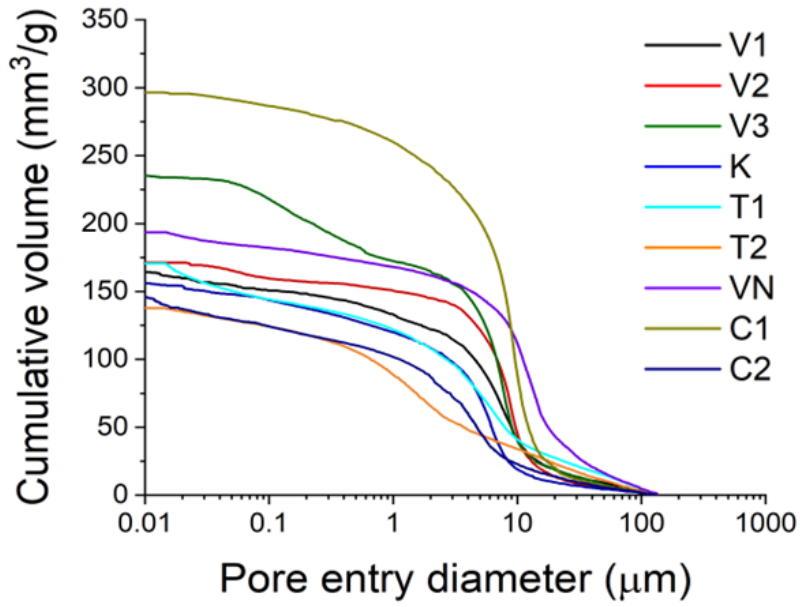
Figure 4.3. SEM images of the samples: (a) C1, fired at just above 900 °C showed vitrified matrix but with larger pores; (b) C2 fired at temperature much higher than 900 °C showed a denser matrix with smaller pores; (c) V1 (d) V2, both are less weathered historic brick samples, with the pores filled with deformed feldspar particles; (e) V3, well vitrified historical sample with macropores; (f) VN, the replacement brick made for ancient brick V2 and V1 showing a similarly dense matrix with diffusing feldspar into pores; (g) K, the poorly baked brick sample with heavy fissuring and poor interconnectivity; (h) T2 with recrystallized precipitates of carbonates filling in the large fissures due to poor baking; (i) T1 with gypsum nodules; (j) A gypsum nodule in T1

F: Feldspar, Q: Quartz

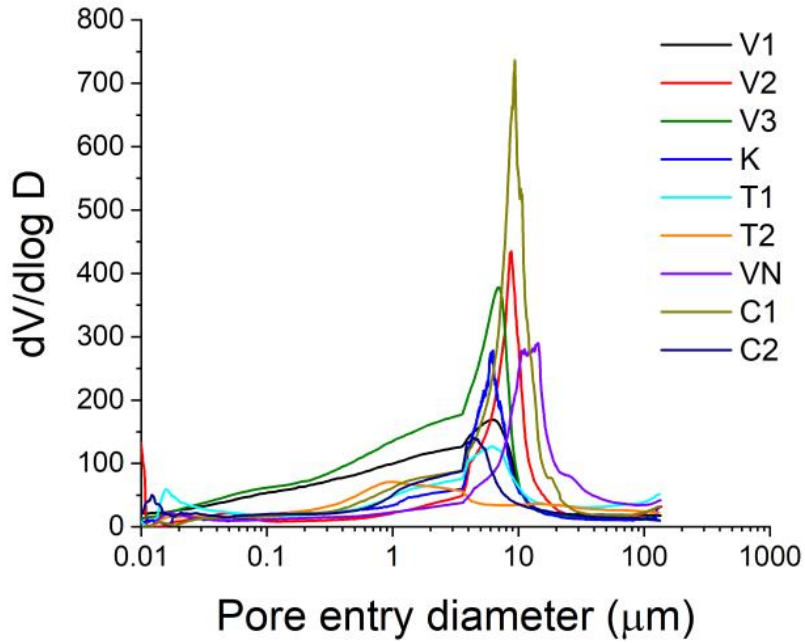
4.2.5 Mercury Intrusion Porosimetry (MIP)

The cumulative volumetric intrusion curves and differential intrusion graphs for the brick samples using the data from MIP tests are presented in Figure 4.4 (a) and (b) respectively. The pore parameters of a typical curve from MIP data are threshold pore entry diameter, critical pore entry diameter and total intrusion volume. Threshold pore entry diameter is the minimum continuous pore diameter in the material, which can be obtained as the intersection point of the two tangent lines drawn on the cumulative intrusion curve (Scherer 2004b). Critical pore entry diameter is the pore size corresponding to the maximum mercury intrusion, obtained as the peak from the differential intrusion graph.

Figure 4.4 (a) and (b) rightly complement the results of physical properties. The highly vitrified denser structure of C2, indicated from its high strength, density and UPV values is supported by the smallest threshold pore entry diameter and corresponding least cumulative intruded volume, and vice-versa in case of C1. The distribution of V1, V2, V3, VN, K looked similar and intermediate between the extreme characteristics of C1 and C2. VN was found distinctively more porous than C2 from the MIP data; however, their strength values are similar from Figure 4.1. This could possibly be attributed to the mineralogical differences observed from the XRD results (Table 4.2). While VN has some quartz and a majority of feldspar, C2 shows the opposite. Even though brick samples K were found with external weathering traces like powdered edges, MIP results showed that the interior pore structure was not affected. The critical pore diameter or total intrusion did not represent any pore system disintegration.



(a)



(b)

Figure 4.4 (a) Cumulative intrusion curves; (b) Differential intrusion curves from MIP data

Since samples T1 and T2 were exposed to extreme saline conditions, the differences seen in the behaviour could be attributed to the action of salt in the pores - deposition or crystallization damage. T2 had a denser structure with least cumulative volume and critical pore entry diameter. In addition to the above-mentioned result, the physical properties measured also point to the fact that despite being subjected to continuous erosive forces, the core of the bricks are not deteriorated, and indeed found stronger and denser than other samples. A demarcating difference was found in the pore distribution between T1 and T2, even if they are of the same source, age and of the same site, but exposed to different salts. The critical pore diameter of T1 is 6.27 μm , indicating a greater extent of damage compared to T2 where critical pore size is 1.01 μm . T1 was not in direct contact with the sea, hence less exposed to NaCl compared to T2. Also, from the XRD results (Table 4.2), the presence of sulphate salts (gypsum and thenardite) was observed in T1. Sodium sulphate causes crystallization damage due to its high supersaturation, which leads to the disintegration of the pore system (Scherer 1999; Scherer 2004b; Tsui et al. 2003). T2 was more exposed to NaCl, which has a low crystallisation pressure due to low supersaturation value. Hence instead of causing crystallization damage, NaCl crystals get deposited in the pores and fill them when exposed to such a salty environment, decreasing the porosity.

4.3 EFFECT OF NATURAL SALT WEATHERING ON BRICKS

In this section, analysis of brick samples collected from a historic fort on the seashore - T1 and T2 are presented, which were typical examples of bricks affected by natural salt

crystallization. The brick masonry fort shows partial or complete damage at different parts along its stretch, where the sea has encroached and immersed some portion of it. The scenario provides scope for a better understanding of the mechanism and characteristics of clay bricks with severe salt damage. Two locations of the same structure showed entirely different kind of damage. Detailed characterization of these differences seen in the samples could provide more insights into the variation in the mechanisms with varying sources of damage. After analysing the physical-mechanical properties, microanalytical techniques were used to explore the role of the pore structure and mineralogy in the deterioration process.

4.3.1 Visual observations

The T1 bricks were collected from dry walls at a lower level, close to the ground where it is more exposed to both moisture and salts (both sulphates and chlorides). The selected walls were facing the sea but had no direct contact with the sea. Sample T2 was from wet bricks, which were partially or fully immersed in the sea and under continuous erosive forces of the splashing waves. The bricks in the wall where T1 was collected showed heavy efflorescence and blistering. The T2 bricks did not show any efflorescence but were softened and eroded from the sides progressively. Even though no efflorescence was found, crystallization happened beneath the surface, which is termed as sub-florescence. Full bricks which are representative were removed carefully using a chisel and hammer. A few specimens which got damaged during the process were discarded. Figure 4.5 shows the locations where the samples were collected.



Figure 4.5. (a) Brick wall showing T1 bricks (b) T2 sample bricks which were partially immersed in seawater

4.3.2 Physical and mechanical characterization

Table 4.3 shows the results of compressive strength, water absorption, bulk density and moisture content measured for samples T1 and T2. Moisture content was calculated from the differences between mass of samples as collected and after drying them in the oven at 40 °C until attaining constant weight. Even though T2 was subjected to more sea salts and erosive forces, it possessed more strength than T1 due to its comparatively less porosity, as seen from the lower water absorption values. This could be attributed to the presence of more NaCl in T2 bricks, which is highly soluble, and thus quickly penetrates into the pores and gets crystallized inside upon drying. The crystallized salt inside the pores can make the brick denser, but the crystallization can also cause expansion, cracking, and damage of the system (Foraboschi and Vanin 2014). However, the T2 bricks did not show cracking damage, but only softening and progressive degradation from the surface. The T1 bricks, where both

chlorides and sulphates were present, had more porosity, less strength, and more deterioration. Sodium sulphate, upon changing its phase from thenardite to mirabilite causes a volumetric expansion, and this creates inter granular cracks that weaken the system. Besides hydration and expansion, the higher solubility of sulphates causing very high supersaturation and resulting in increased crystallization pressure and precipitation of salts is also a crucial damage mechanism (Flatt et al. 2014).

Table 4.3. Physical and mechanical properties of the natural salt-attacked samples

Sample	Moisture content (%)	Compressive strength (MPa)	Water absorption (%)	Bulk density (g/cm ³)
T1	7	4.2	15.5	1.89
T2	30	10.1	11.5	2.02

4.3.3 Mineralogical characterization

Mineralogical compositions of the samples were analyzed using X-ray diffraction. From the peak analysis in the XRD patterns, quartz and K-feldspar were found as the major peaks in both sets of samples. High-temperature phases like diopside and gehlenite were not detected, which indicates a low-temperature firing of the bricks. This could have resulted in more porous, weak bricks that promote easy deterioration in adverse environments. The major peaks identified are shown in the diffractograms in Figure 4.6.

Table 4.4 shows the quantification of phases from XRD studies using Rietveld refinement. Halite and thenardite were found in both the bricks, with an increased amount of halite in the T2 bricks. The T1 bricks, which were not in direct contact with the sea, possessed gypsum, whose presence was suggested from the blistering observed in the bricks. Conversion of thenardite (Na_2SO_4) to mirabilite ($\text{Na}_2\text{SO}_4 \cdot 10\text{H}_2\text{O}$) was confirmed in T1 bricks which were dry. The mirabilite phase has a higher volume than thenardite, and the transformation causes expansion and internal cracks.

The sample T1 was collected from the coastal region where the temperatures range between 25 °C in the night and 40 °C in the day most of the time. Thenardite is the only stable phase at temperatures greater than 32 °C. So, thenardite crystallizes directly from the solution at these temperatures (Flatt, 2002). On the other hand, mirabilite is stable at temperatures below 32 °C. However, the crystalline phase of mirabilite crystallizing directly from the solution is stable with respect to dehydration only at relative humidity greater than 70 %. Tranquebar being a coastal region, the relative humidity increases to more than 75%. This facilitates direct precipitation of mirabilite and also the dissolution-mediated phase transformation of thenardite to mirabilite. Furthermore, the mechanism of crystallization in natural systems is heterogeneous, nucleating from imperfections and dust (multiple phases), rather than the homogeneous crystallization from pure solution (two-phase) as suggested by phase diagram (Carlos Rodriguez-Navarro, 2000). Heterogeneous crystallization results in non-equilibrium crystals of thenardite along with equilibrium crystals of mirabilite. Therefore, the reasons for the presence of both the mirabilite and thenardite simultaneously in T1 bricks can be summarized as,

- Surrounding temperature varying across a wide range (both less than and greater than the phase transition point of 32 °C)
- High relative humidity (stabilizing crystalline mirabilite)
- Dissolution-mediated phase transformations
- Heterogeneous (multiple-phase) crystallization

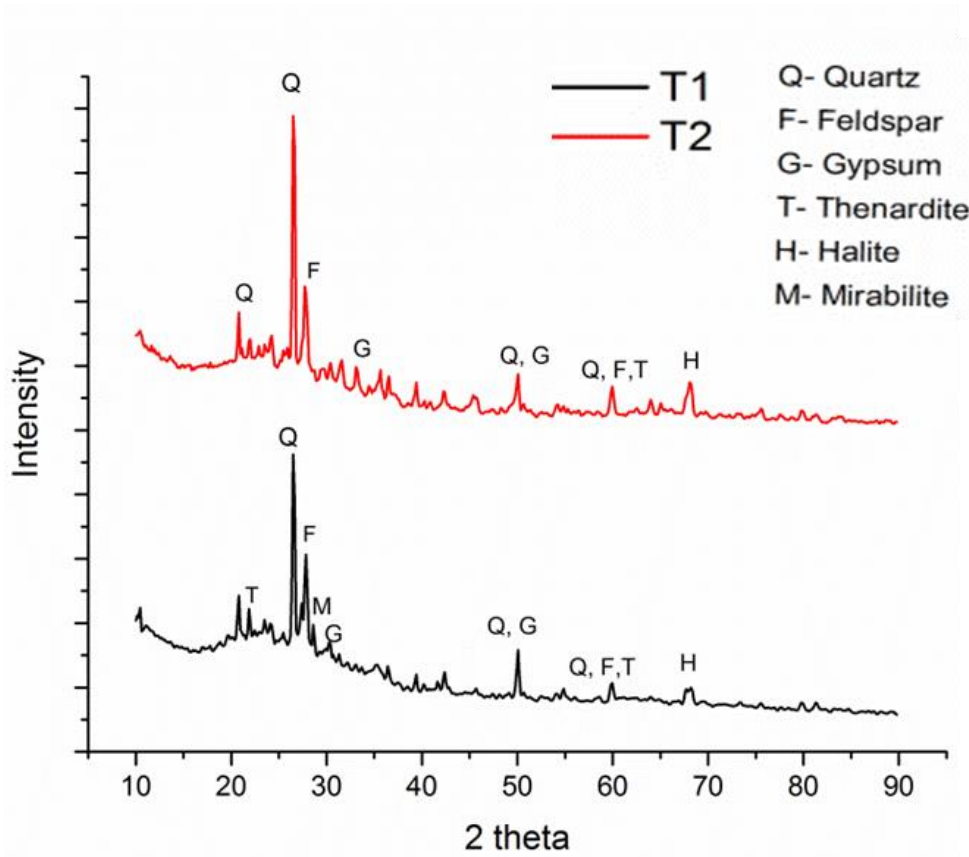


Figure 4.6. Diffractograms showing the peaks of major mineral phases of T1 and T2 samples

Table 4.4. Quantification of mineral phases in bricks T1 and T2

Minerals	T1	T2
Quartz	47.1	61.8
K feldspar	32.7	28.3
Calcite	1	2.8
Halite	1.9	2.1
hematite	1.9	0
Gypsum	3.6	0.8
Thenardite	4.6	4.2
Mirabilite	7.2	0
Diopside	0	0
Gehnelite	0	0

4.3.4 Pore structure and pore size distribution

Mercury Intrusion Porosimetry was used to study the porosity and pore size distribution of the samples. Figure 4.7 shows the range of pore sizes in the bricks, as measured by MIP. Chloride crystal growth within the pores causes superficial mass loss and generation of microcracks within the system in the initial stage, resulting in an increase in porosity. But later, the crystal growth in pores decreases the porosity (Scherer, 2004). The T2 bricks showed lesser porosity than the dry T1 bricks. NaCl being more soluble and mobile easily penetrates into the pores and gets crystallized. The crystallization pressure of NaCl is comparatively lesser than Na₂SO₄. Thus, it can be concluded that the NaCl crystals filled up the pores and reduced the porosity in T2 bricks. The sulphate crystallization results in volumetric expansion inside the pores, which increases the stress and induces cracks. These microcracks increased the porosity in the case of T1, the dry bricks possessing both chlorides and sulphates. In Table 4.5, the study on pore diameter ranges shows that the relative percentage of pores less than 0.05 μm is more for T1 bricks, whereas it is much lesser in the case of T2 bricks. This indicates that the effect of sulphate crystallization is not pronounced

on pores smaller than $0.05\ \mu\text{m}$. But in T1 bricks, the NaCl crystallization has happened in the pores smaller than $0.05\ \mu\text{m}$ also. Because of the smaller ionic size and high mobility, NaCl can enter into pores smaller than $0.05\ \mu\text{m}$ and crystallize there.

Table 4.6 shows the pore structure parameters obtained from the test. The critical pore diameter of T1 is $6.27\ \mu\text{m}$, indicating the greater extent of damage inside compared to T2 where critical pore size is $1.01\ \mu\text{m}$. From analyzing the pore structure parameters in Figure 4.7, it is seen that the critical pore diameter has shifted to a larger size for T1 bricks. Critical pore size is the most common pore size among all the pores in the system.

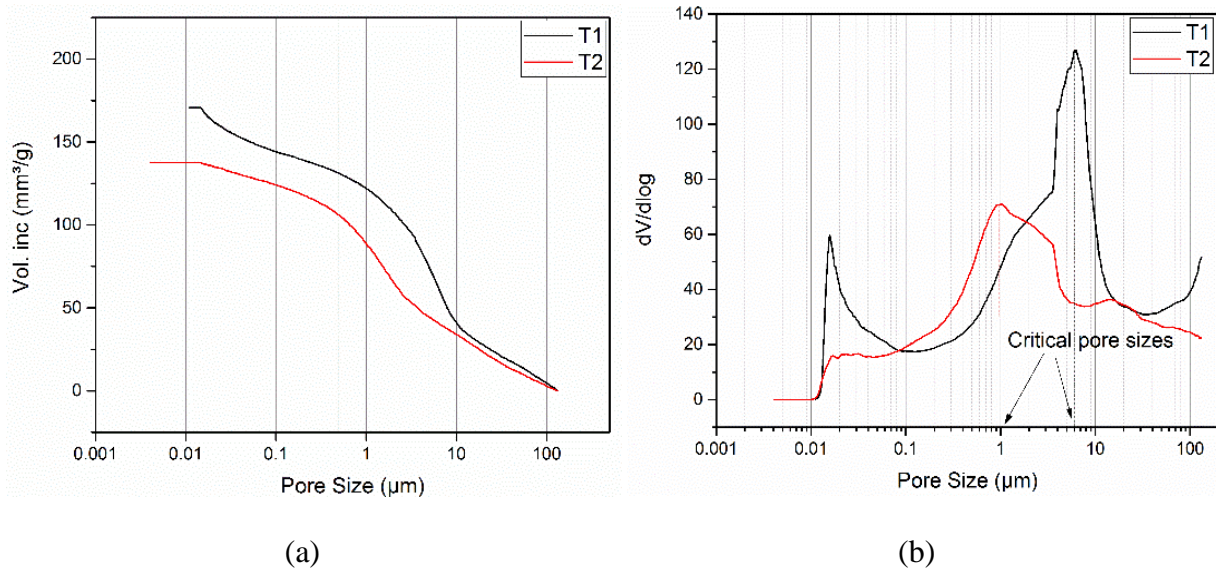


Figure 4.7. (a) Cumulative intrusion curves from MIP (b) Differential intrusion curves showing the critical pore diameter

Table 4.5. Relative proportions (as % volume) of various pore sizes

Pore diameter ranges μm	Relative volume percentage	
	T1	T2
100.0000-10.0000	19.69	22.64
10.0000-1.0000	43.28	39.93
1.0000-0.3000	7.43	17.81
0.3000-0.2000	1.83	3.46
0.2000-0.1000	2.62	4.34
0.1000-0.0500	3.30	3.38
0.0500-0.0100	10.87	6.31

Table 4.6. Pore parameters obtained from MIP

Properties	T1	T2
Porosity by Hg intrusion (%):	35.29	27.88
Threshold pore diameter (μm):	8.01	2.5
Critical pore diameter (μm):	6.27	1.01

4.4 EFFECT OF ARTIFICIAL SALT WEATHERING ON THE BRICKS

4.4.1 Accelerated salt weathering cycles as per EN12370

The performance of bricks with various microstructures on exposing to the salt solution was studied by subjecting the specimens primarily to accelerated salt weathering tests using the most commonly adopted procedure of EN 12370. 40 mm size cubes were prepared out of the bricks and subjected to 15 numbers of cycles. Each test cycle comprised of 2 h of immersion

of specimens in a 14% solution of sodium decahydrate followed by 16 hours of drying in an oven at a temperature of 105 °C and subsequent cooling for 6 hours in room temperature. Mass changes were documented for the samples after each day (each cycle), and Figure 4.8 shows the mass changes of the samples throughout the 15 cycles.

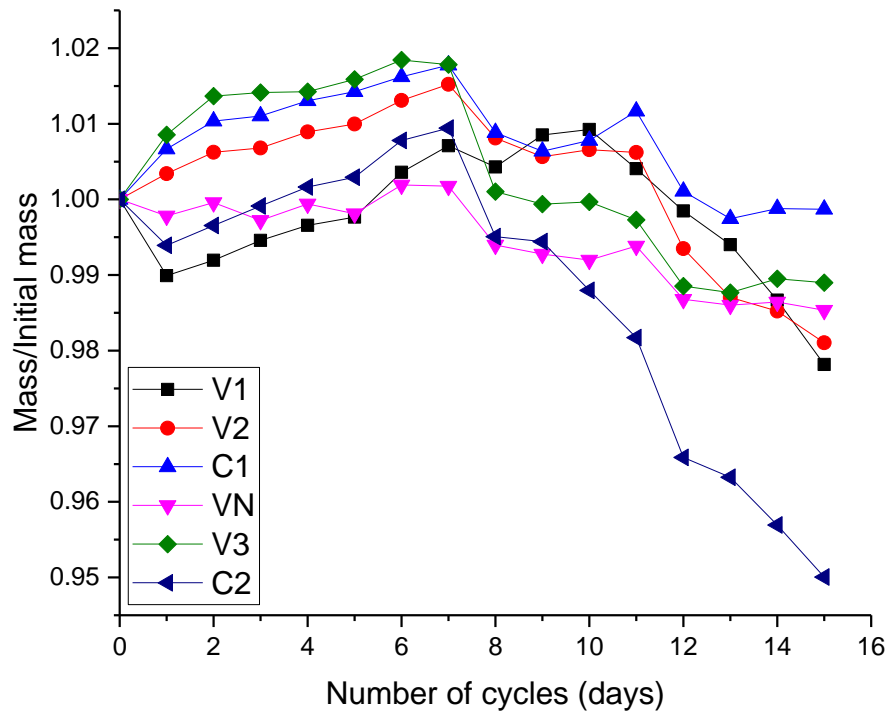


Figure 4.8. Mass changes for the samples during accelerated salt weathering (for 15 cycles)

All the specimens had a mass gain period, followed by a period of mass loss. The mass gain was due to continuous deposition of salt crystals in the pores of the material. All the graphs showed single points at which the mass of the specimen was the highest. Beyond that peak, none of the samples showed an increase in mass. Thus, this point can be considered as the time of onset of damage in the samples. The point of onset of damage varied depending upon the material or its microstructure. This can be explained in terms of

salt crystallization in a porous material as follows. There is always a competition between mass gain due to salt deposition and mass loss due to deterioration. During the mass gain phase, the processes of crystal nucleation, dissolution of small crystals, ion transport and generation of a high supersaturation dominate in majority of the pores. On the other hand, due to the amount of salt deposited during the mass gain phase, during the wetting cycles of the mass loss phase, a high supersaturation is generated, as a result of which crystal growth and the development of transient crystallization pressure followed by material failure dominates in most of the pores.

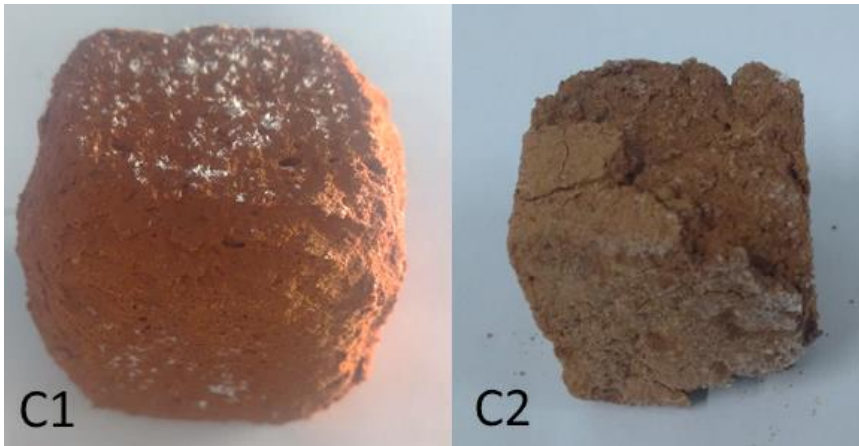
Figure 4.9 shows the image of specimens at various stages of weathering test. Among all the samples, visual observations of the damage and the mass loss data showed that C1 was the brick sample which was least affected by the salt exposure, and C2 was one most affected. Signs of deterioration like roughening of surface and deposition of powder around the samples were visible even before the beginning of mass loss phase. For C1, the deterioration pattern was uniform, without any spalling or flaking. The samples became more rounded in shape with progressive, slow and homogeneous deterioration as damage progressed. On the other hand, the mass loss and deterioration were found to be the maximum in C2 where a heterogeneous and deep damage was observed only after the 6th cycle. Figure 4.9 (c) shows the homogeneous deterioration pattern of C1 and heterogeneous damage of C2 after 15 cycles. C1, the lower density brick when subjected to salt solution eventually resulted in homogeneous distribution of salt inside the material, which is confirmed from the uniform progressive damage patterns.



(a) Specimens before subjecting to salt weathering test



(b) Specimens after 6 cycles of salt weathering test



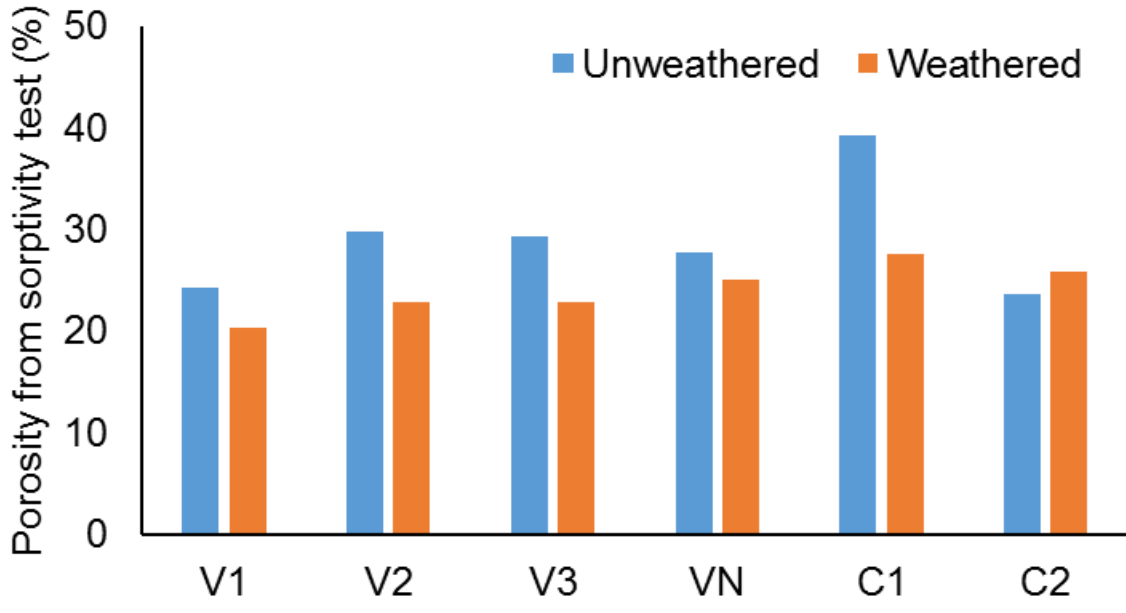
(c) C1 and C2 after 15 cycles of weathering

Figure 4.9. Visual changes of the specimens during salt weathering test

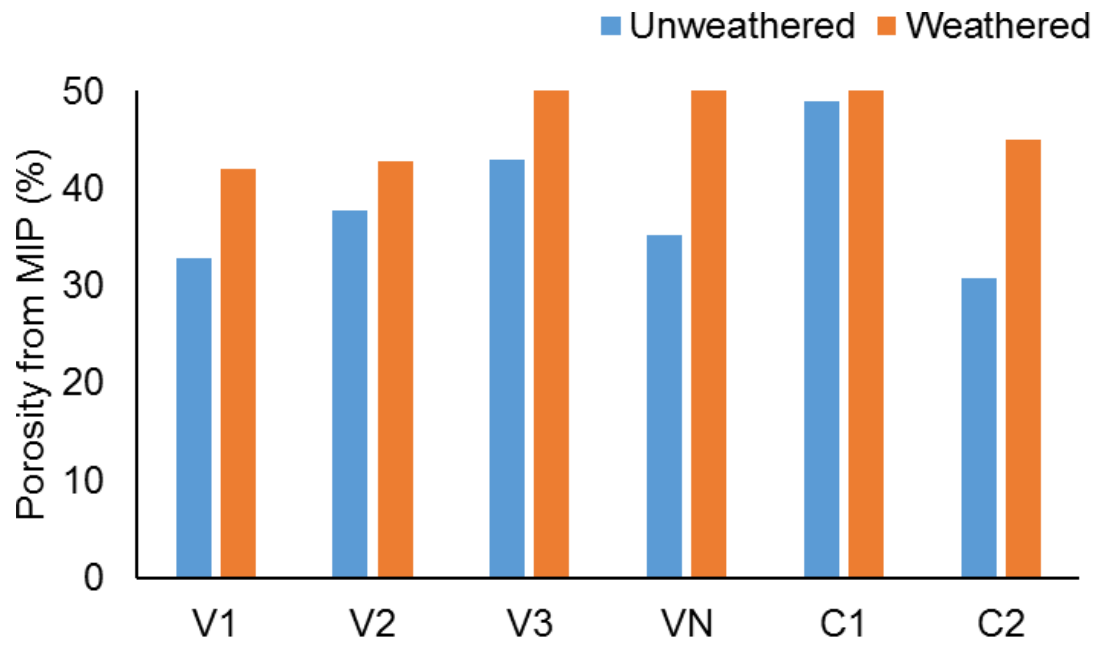
The nature of damages and mechanism of salt crystallization in each material can be directly corroborated with their physical and microstructural properties described in the previous sections. As indicated from the physical properties, C2 is having the densest and highly vitrified structure, which is evident from its least cumulative intruded volume and corresponding small threshold pore entry radius from the MIP results. The differential intrusion curve (Figure 4.4. b) also points towards the same indication, from the minimum critical pore size diameter of C2 among all other brick samples. C1, which is the other commercial brick sample, is at the opposite end, showing the maximum intrusion and very large critical pore diameter. The other brick samples V1, V2, V3 and VN fall in between C1 and C2 with respect to the pore distribution; further, samples V1, V2, V3 and VN showed almost similar distribution.

4.4.2 Porosity evaluation after weathering test

Total porosities were calculated for the specimens by sorptivity test and MIP, which is shown in Figure 4.10. The total porosities calculated for weathered and unweathered samples using MIP and sorptivity tests provide information related to the pores affected by weathering. When assessed by water sorptivity test (which measures only the water-accessible porosity), the porosities were found to decrease after salt weathering for all the samples. Whereas, the porosity values obtained from MIP tests exhibited an opposite trend with the weathered samples being more porous than the unweathered. MIP gives the total porosity which includes microporosity too, until a size of 3 nm. Hence, the data clearly shows that macropores or capillary pores get decreased on weathering because of the salt deposition, whereas more micro-fissures get generated.



(a) From water-sorptivity test



(b) From MIP

Figure 4.10. Comparison of porosities calculated for brick before and after weathering test

4.5 SUMMARY

The chapter discussed the characteristics of each type of brick sample with respect to physical, mechanical and microstructural properties. The characteristics investigated were then connected to the salt weathering resistance of the corresponding materials. Effect of natural weathering on bricks was studied by analysing historic samples collected from areas with heavy exposure to salt. More controlled studies were then conducted by subjecting bricks to artificial accelerated weathering studies in the laboratory. Further analyses of weathered samples helped in correlating the microstructural features to the salt weathering mechanism that could happen inside the pore system.

The detailed characterization of brick samples provided objective data that help to understand the quality of various bricks from India and its relation with performance over prolonged exposures. Basic correlations between the raw materials, firing temperature and the development of microstructure was clarified by analysing these wide range of brick types. The presence of non-calcium clays and high firing temperature as observed from the XRD and SEM results was found responsible for the better vitrification degree in the ancient bricks (V1, V2, V3), which provided the excellent weathering resistance and physical-mechanical properties. The historic sample K with low vitrification showed high fissuring towards the surface, which is a characteristic of the presence of Ca-rich clays and low firing temperature. However, the core was unweathered, because it was not exposed to an aggressive salt-rich environment. Non-Ca clays and firing temperatures as high as 900 °C makes the system resistant to salt crystallization damage with the formation of large rounded pores ($> 1 \mu\text{m}$), as in the case of new commercial brick C1. New bricks fired at very high temperature (C2) did

not show pore parameters corresponding to good salt weathering resistance, even though they exhibited enhanced strength properties. So, raw material composition (i.e. Ca or non-Ca clays) is equally important as firing temperature in determining weathering resistance of a brick. Gypsum crystallization was identified as the cause for the blistering and powdering effect in the ancient bricks (T1) that were fired at lower temperature and had Ca clays in them, which also increased the weathering susceptibility. However, the same brick exposed to chlorides (T2) instead of sulphates did not show weathering, but improved strength and porosity.

The results from the study on naturally weathered bricks suggest that the combined action of chloride and sulphate salt attack causes more damage than chloride alone. This is proved from higher porosity, lesser strength and blistering effects of the brick samples near the seashore, as compared to those from bricks directly from the splash zone. The bricks which were immersed had a considerable loss of cross-section due to the combined action of NaCl effect and erosive action of water. But the comparatively lesser porosity and increased compressive strength of the T2 bricks showed them to be in a better condition than the T1 bricks. This was due to the high solubility and mobility of NaCl which enters deep into the finer pores and gets crystallized, thus closing up the pores. The volumetric expansion during the crystallization process is very less for NaCl compared to sodium sulphate. The difference in the behaviour of sodium sulphate is due to the larger crystallization pressure when it changes the phase from thenardite to mirabilite. From the study on relative volume percentage of various pore sizes, it is concluded that sodium sulphate has a limitation in crystallizing in pores smaller than $0.05\ \mu\text{m}$, whereas NaCl can influence even those pores.

Accelerated weathering studied on brick specimens revealed the significance of pore structure in determining the salt crystallization resistance of a material. Among all the brick samples studied, the highly porous C1 was found to be the most resistant sample when exposed to sodium sulphate solution, with progressive homogeneous material loss from the surface. C2, the high strength dense brick performed the worst with the salt exposure, with deep cracking and sudden failure. This clearly demonstrated that more than the entry of salt solutions inside the material, it was the availability of crystallization spaces inside, which were in the range of micropores, that created the damage.

From understanding the microstructural characteristics of the bricks, it is clearly understood that the pore sizes and their distribution are the principal factors in determining the resistance of the material towards salt weathering. In the next chapter, the characteristics studied for two different stone types are presented, which have different pore structures. This would help to generalize the role of microstructure, especially porosity, pore size and pore structure of any masonry unit, in controlling the durability of the structure.

5 CHARACTERIZATION OF MASONRY STONES

5.1 INTRODUCTION

The previous chapter discussed the characteristics of bricks and the role of the microstructure in determining the durability of the material, primarily for understanding the deterioration mechanisms of heritage masonry. Natural stones are the other common building material used for the construction of historic monuments. Hence, there is a need to understand the properties of stones and compare the findings obtained from studying the brick masonry with stones to provide a more comprehensive understanding of the behaviour of masonry units.

Stones are basically classified into three categories based on their origin, as igneous, sedimentary and metamorphic. Again, there are subdivisions based on texture, mineral composition etc. The rate and nature of weathering are determined by the rock-forming minerals and their morphological distribution in the microstructure of the matrix. In order to validate the role of pore structure and pore size distribution in controlling the durability of the material, two different stones of extremely different pore structures are selected for the study- (i) Granite- with a low porosity and small-sized pores among most rock types and (ii) Coral stone- with a high porosity and large-sized pores.

5.2 CHARACTERISTICS OF THE STONE SAMPLES

5.2.1 Introduction to the nature of stones

Granite is a plutonic leucocratic igneous rock. It is formed essentially with an equigranular crystalline assemblage of quartz and feldspars with minor amounts of micaceous minerals. The equigranularity arises out of its formation from a hot molten mass called magma. During the course of formation and further crystallization, the younger minerals (quartz) form in the interstices of the older formed minerals (Deer et al. 1992).

Coral limestones are very common building materials in ancient stone and masonry structures along the coasts of East Africa, Malaysia, and throughout the settlements of Indian Ocean, the Arabian Sea and the Red Sea (Ochieng 2012; Orbasli 2009). They are organic sedimentary rocks formed out of coral reefs in a marine ecosystem by polyps, which are multicellular organisms. The calcareous exoskeleton contains the deposition of aragonite mineral by the polyps, sourced from the calcium and carbonate ions they acquire from the marine surroundings. On their extinction, polyps leave behind the hard exoskeleton of calcareous carbonates which forms the coral stones later (Ochieng 2012). The concern of protection of coral reefs is supported by many regulations and policies including Coral Reef Conservation Act of 2000, Indian Wildlife (Protection) Act and more, which has resulted in a strict restriction on the further mining of coral stones (Sehgal 2006).

5.2.2 Visual observations

Visual observations were documented from the site from which samples were collected, which depicts the current weathering state. In-situ measurements were obtained from columns in the structure. Depending on the exposure difference between various columns, there were differences in weathering states observed.

The granite samples were collected from Meenakshi Sundareswarar Temple, a 14th century stone temple at Madurai, Tamil Nadu. Small pieces of weathered samples were collected from highly weathered portions from a particular column. The weathering caused a reduction in the dimension of the columns as the surface showed flaking, delamination and spalling. Granite samples from a new quarry which had previously been used as a replacement for the damaged columns in the near past were also collected to compare with the properties of the granite in the structure and to study the general characteristics of granite as a masonry material. Typical columns with and without weathering signs are shown in Figure 5.1.



(a)

(b)

Figure 5.1. (a) Granite column showing flaking and delamination as weathering signs (b) An unweathered granite column from the same structure

Coral stones were collected from Sri Ramanathaswamy temple, built before 16th century, and located in Rameshwaram Island, Tamil Nadu, India, which is located in the Bay of Bengal. The particular coral stone used in the structure was from a fringing reef coral formation, which is the most common type of reef seen and being used for construction purposes. Currently, the structure is in a partly deteriorating stage at some locations. The types of distress and extent of damages observed in the structural elements were documented and classified as: no damage/minor/major/extreme categories with increasing order of extent of distress (area or volume) with each category. A few columns were found with no

prominent weathering traces or damages, but sometimes with very slight smoothing of edges and they were categorized under “no damage” group. Minor damages were the surface damages on the columns such as spalling of plaster, blackening and presence of algae due to dampness, staining and other damages seen exclusively in the plaster. Moderate damages were those not responsible for any structural failure, which include loss of profile as a result of ridge formation, rounding off, material loss and alveolation (deeply pitted honey-combed structure due to closely spaced cavity formation). Major damages were those structural damages that disturb the loading pattern of the structure such as heavy loss in profile due to erosion and improper conservation by the introduction of new and incompatible materials like brickbats in cement mortar in the structure during renovations. Extreme damages were those structural damages that were more severe than the major damage problems, which can adversely affect the structural stability of the building. Figure 5.2 shows examples of coral stone columns with no damage, minor damage and major damages in the structure. Figure 5.3 shows some cases of extreme damages seen in different coral columns.



Figure 5.2. Coral stone columns showing damages of different degree (a) no damage (b) minor (spalling of plaster) (c) major (usage of improper incompatible brickbats leading to deterioration)

The columns in the Northern and Western sides of the cloister, which were more exposed to wind and moisture, exhibited heavy deterioration in the plaster, deep ridge formation in the columns, formation of pores and holes on the capitals. The columns renovated during 1975 with cement mortars had deep horizontal cracks at the bottom (Figure 5.3 (b)), which are formed due to extreme structural damage. The original lime plastering in the columns was effective in protecting the coral stones to an extent, even though the plaster faced heavy deterioration, but which is expected in a sacrificial coat. Line formation, which further developed as ridges, resulting slowly in the powdering of the stone, was a common deterioration pattern found in the columns. The action of wind and lack of waterproofing

treatment to the roof, which resulted in rainwater seepage, were considered as the major causes for the deterioration observed from the primary visual analysis.

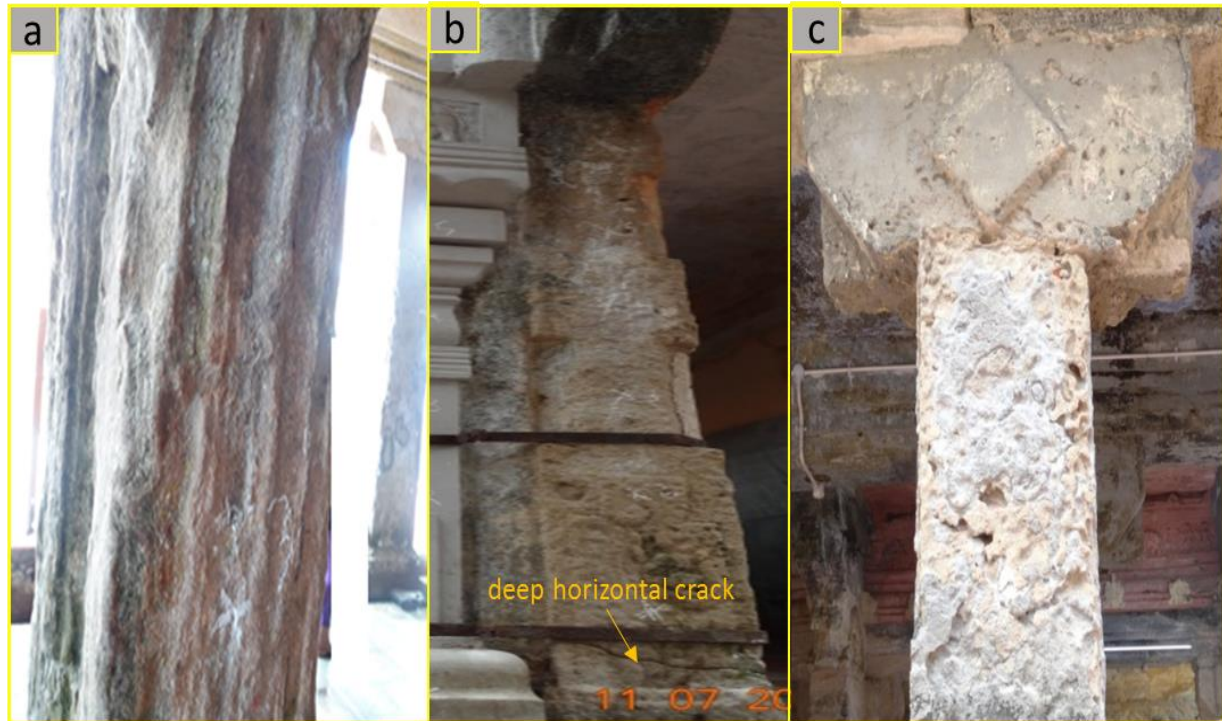


Figure 5.3. Examples of extreme damages in the columns (a) heavy ridging (b) deep cracking (c) fissures and loss of section

5.2.3 Physical-mechanical characterization

5.2.3.1 Compressive strength

Compressive strength of the granite was measured as per the testing procedure given in IS 1121:2013. The test was conducted on granite stone cubes from columns without any weathering traces and also cubes collected from a quarry near to the site. Table 5.1 and Table 5.2 show the compressive strength determined for three specimens of granite cubes, each for

samples from the site and that from the nearby quarry, respectively. The average compressive strength of granite was found as 134 MPa and 155 MPa for the specimens from site and quarry respectively. Cubes were tested in both parallel and perpendicular direction, and it was found that the direction of loading had no impact on the compressive strength of granite.

Table 5.1. Compressive strength of granite cubes collected from the site

Specimens	Length L (mm)	Breadth B (mm)	Depth D (mm)	Failure load (N)	Compressive strength (MPa)
1	52.92	52.27	46.47	291800	116
2	52.80	52.71	48.29	369300	143
3	52.50	52.54	51.98	383800	142
Average					134
Standard deviation					15

Table 5.2. Compressive strength of granite cubes collected from the nearby quarry (fresh granite)

Specimens	Length L (mm)	Breadth B (mm)	Depth D (mm)	Failure load (N)	Compressive strength (MPa)
1	52.92	52.27	52.68	359100	130
2	52.80	52.71	52.48	423900	152
3	52.50	52.54	52.44	504400	183
Average					155
Standard deviation					27

For coral stones, the compressive strength was measured on 5 dry specimens and 5 wet specimens, and the average values observed were 66 MPa and 59 MPa respectively (with a standard deviation of 12 and 21 MPa respectively), but no variation was seen between the dry and wet stones. Dry and wet cubes were considered for the testing because of the concern

of the highly porous nature of the coral stones. The dry stone specimens were prepared for testing by placing the neatly dressed stone cubes in an oven at 75 °C for 48 hours and cooled to normal room temperature. The wet stone specimens were prepared by immersing the dressed stone cubes in the water for 4 hours and then wiping the surface dry. Cubes were tested in both parallel and perpendicular direction, and it was found that the direction of loading had no significant impact on the compressive strength of coral stones. At failure load, the specimens were crushed, broken into conical shaped wedges and flakes and powdered like sand. Figure 5.4 shows the failure of a typical coral stone cubical specimen in compression. Table 5.3 and Table 5.4 shows the calculation of compressive strength for the coral stones from the test, for dry and wet specimens, respectively.



Figure 5.4. Failure of a coral stone cube under compression

Table 5.3. Compressive strength of dry coral stone cubes

S No	Length L (mm)	Breadth B (mm)	Depth D (mm)	Failure load (N)	Compressive strength (N/mm ²)	Load Direction
1	100	93	96	778325	84	Parallel
2	100	98	93	635296	65	
3	100	94	96	641652	68	
4	96	95	100	451858	50	Perpendicular
5	97	100	98	630332	65	
Average						66
Standard Deviation						12

Table 5.4. Compressive strength of wet coral stone cubes

S No	Length L (mm)	Breadth B (mm)	Depth D (mm)	Failure load (N)	Compressive strength (N/mm ²)	Load Direction
1	96	96	96	688005	75	Parallel
2	98	98	98	337346	35	Parallel
3	98	98	100	809139	84	Parallel
4	98	98	101	574474	60	Perpendicular
5	102	102	95	414227	40	Perpendicular
Average						59
Standard Deviation						21

5.2.3.2 Bulk density

Bulk densities of the samples were obtained using Helium gas pycnometer test, and each value was obtained after three iterations with the pycnometer. Three samples were tested for measuring the bulk density of granite, and the average value was 2.66 g/cm³ with a standard deviation of 0.01.

The bulk density of coral stone was tested on three samples using Helium gas pycnometer, and the average value was found as 2.21 g/cm³ with a standard deviation of 0.03.

5.2.3.3 Water absorption

The water absorption was measured as per the standard IS 1124-2017 (Indian Standard IS 1124 1974) for both granite and coral stones. Six samples were tested for both the stones. The average value for granite was 0.11%, and that of coral stones was found to be between 14 and 18%. The individual values are given in Table 5.5.

Table 5.5. Water absorption values for granite and coral stones

Sample No.	Water absorption (%) for granite	Water absorption (%) for coral stones
1	0.10	14.2
2	0.11	14.9
3	0.10	16.9
4	0.12	14.8
5	0.12	15.0
6	0.11	15.8
7	0.11	17.3
8	0.11	17.0
9	0.10	18.0
10	0.12	16.6
11	0.12	16.6
12	0.10	15.2

5.2.3.4 Capillary porosity

Capillary porosity (%) was calculated from the water sorptivity test which was carried out on 12 cubical samples of granite and coral stones of 50 mm side as per the South African Durability Index testing procedure manual - Part 3 (Durability Index Testing Procedure Manual 2018). The capillary porosity of granite calculated was low, with an average value of 0.07%. For coral stones, the capillary porosity was found to be varying between 8.5% and 13.4%, with CoV (coefficient of variation) of 14.3%. The values are given in Table 5.6.

Table 5.6. Capillary porosity for granite and coral stone specimens

Sample No.	Capillary porosity of granite (%)	Capillary porosity of coral stone (%)
1	0.05	8.9
2	0.04	12.1
3	0.04	12.6
4	0.05	13.4
5	0.06	13.0
6	0.06	8.6
7	0.06	11.2
8	0.04	9.6
9	0.05	11.6
10	0.05	9.5
11	0.06	12.7
12	0.04	11.9

5.2.3.5 Ultrasonic Pulse Velocity Test

Ultrasonic pulse velocity was measured in cubes of 50 mm size for both granite and coral stone, with testing being done on six specimens each. The values of UPV measured are given in Table 5.7 for both the stone samples. The average value was 6200 m/s for granite samples and 4150 m/s for coral stone samples.

Table 5.7. Ultrasonic pulse velocity (m/s) for granite and coral stone specimens

Sample No.	UPV for granite (m/s)	UPV for coral stone (m/s)
1	6500	3700
2	6510	4590
3	5720	3640
4	6200	4100
5	6150	4370
6	6120	4490

5.2.4 X-ray diffraction

5.2.4.1 Mineral composition in granite

XRD patterns confirmed the presence of quartz and feldspars as the major components in all the samples. This is expected mostly in all the Indian granites. Feldspars can be categorized into two types - alkali feldspar (potassium feldspar which can be of different crystal structures like monoclinic and triclinic) and plagioclase feldspars (sodium feldspar or albite- $\text{NaAlSi}_3\text{O}_8$; calcium feldspar or anorthite- $\text{CaAl}_2\text{Si}_2\text{O}_8$). The granite used in the structure was typically having a slight pink trace because of the presence of a large amount of potassium feldspar, which was confirmed from quantification of XRD phases. Mafic minerals like biotite, hematite and hornblende were found in minor quantities. The approximate percentage of the components are - feldspars (around 70%), quartz (around 20%), biotite (5%), hornblende (3%), magnetite and other accessory minerals to 2%. Samples collected were found to be A-type granite based on the chemical composition. The quantification of the phases using Rietveld refinement is presented in Table 5.8. The diffractograms are shown in Figure 5.5.

Table 5.8. Quantified data for the composition of minerals in granite

Minerals	Quantified amount (%)
Quartz	27.0
Ca feldspar	19.7
Na feldspar	27.9
K feldspar	16.8
Biotite	06.3
Hornblende	01.2
Magnetite	01.1

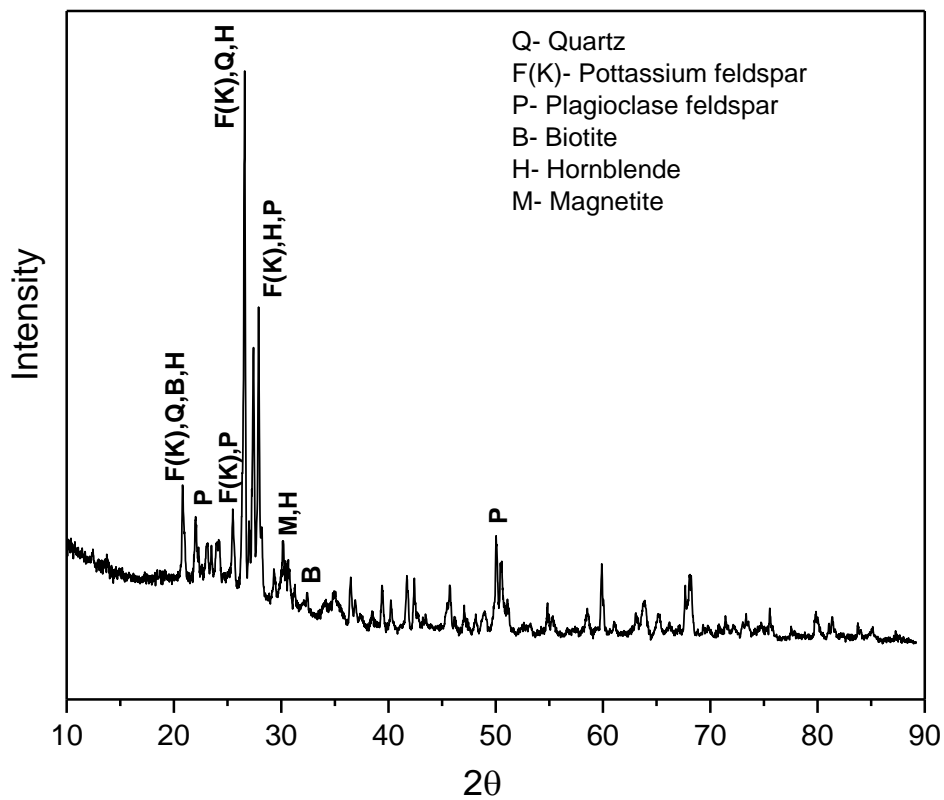


Figure 5.5. X-ray diffractogram of granite stone used for the study

5.2.4.2 Mineral composition in coral stone

Figure 5.6 shows a typical diffractogram for coral stone samples collected from the site. The particular sample was procured from a column in the major damage category. Major minerals in the coral stone were found as quartz, calcite, magnesian calcite, and aragonite. Aragonite and calcite are two different forms of calcium carbonate, which differ in structure, symmetry and crystal shape. Both are from skeletons of marine organisms, where aragonite is having a higher dissolution tendency than calcite. That would be the reason that aragonite was found in a lesser quantity than calcite. Magnesian calcite ((Ca,Mg)CO₃) is a variant of calcite containing randomly substituted magnesium carbonate within a disordered calcite lattice. It can also be called Mg-rich calcite as the calcite content is more than 96% (Wang et al. 2017). Minor amounts of halite (NaCl) were also encountered. But no mineralogical differences were observed among the different samples, suggesting the absence of any chemical reactions involved in the deterioration processes that have occurred in the stone over the years. Quantified data for the mineral composition is shown in Table 5.9.

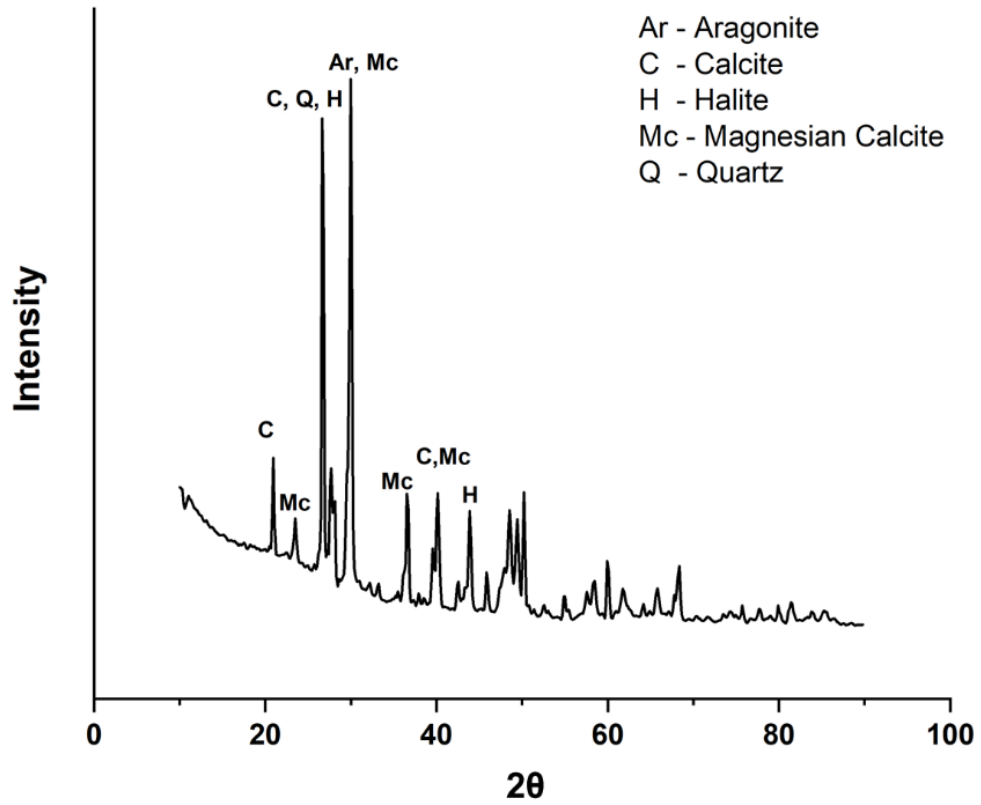


Figure 5.6. X-ray diffractogram of coral stone showing the major peaks

Table 5.9. Quantified data for composition of minerals in coral stone

Minerals	Quantified amount (%)
Aragonite	7.2
Mg-Calcite	49.0
Calcite	18.6
Halite	1.2
Quartz	24.0

5.2.5 Scanning Electron Microscopy

The morphology of weathering traces in the fractured surface of stones, and general microscopic features of those stones were observed from the SEM images, and the chemistry was studied with the help of EDS.

5.2.5.1 Morphological features in granite

Secondary electron mode images were captured on gold-coated fractured representative samples of granites. Quartz (Q) and feldspars with conchoidal fractures (F) were seen as the major components for all the categories of samples. In the weathered samples (Figure 5.7 and Figure 5.8), heavy atmospheric deposition (D), mainly dark deposits (in the microscopic range and also some at macroscopic levels) were found. Deposits were seen in crevices in quartz and feldspar crystals and also along the intergranular boundaries. Considering the position of the columns identified with heavy weathering as the ones placed near the eastern entrance of the hall in the particular site, and the weathered portion being the lower parts especially near the pedestal area of the columns, the cause for the heavy weathering seen can be the atmospheric pollution, human interference, temperature variations etc.

Presence of mafic minerals like biotite and hornblende was observed, as shown in Figure 5.9. Biotite is the dark mica that forms flat, sheet-like crystals that cleave into smooth flakes.

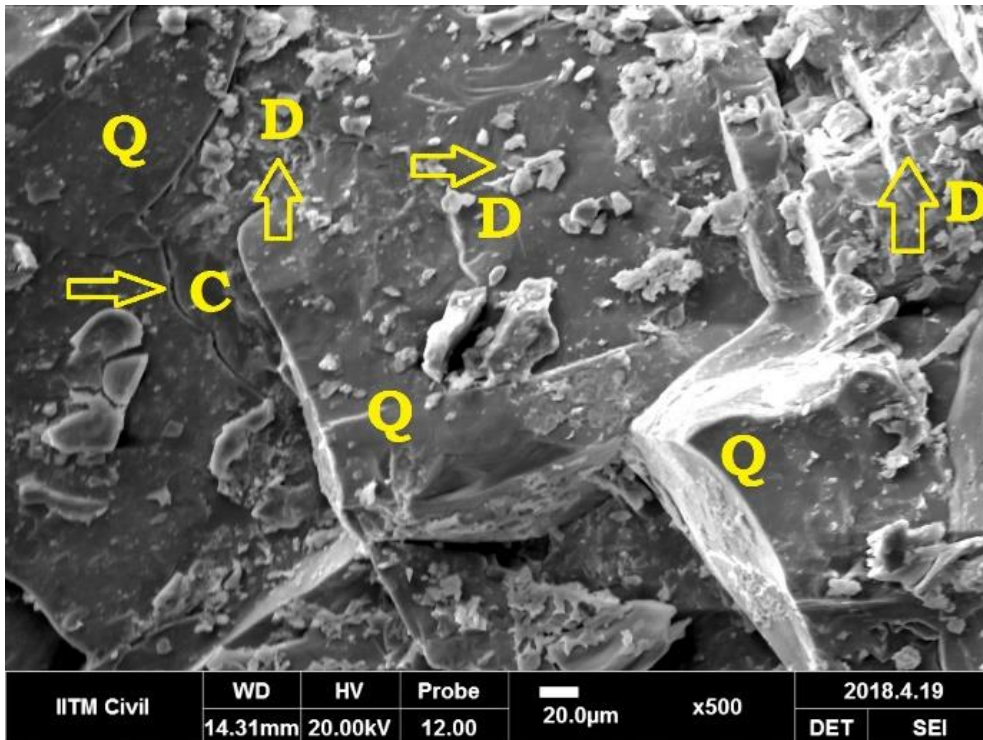


Figure 5.7. SE image of weathered granite

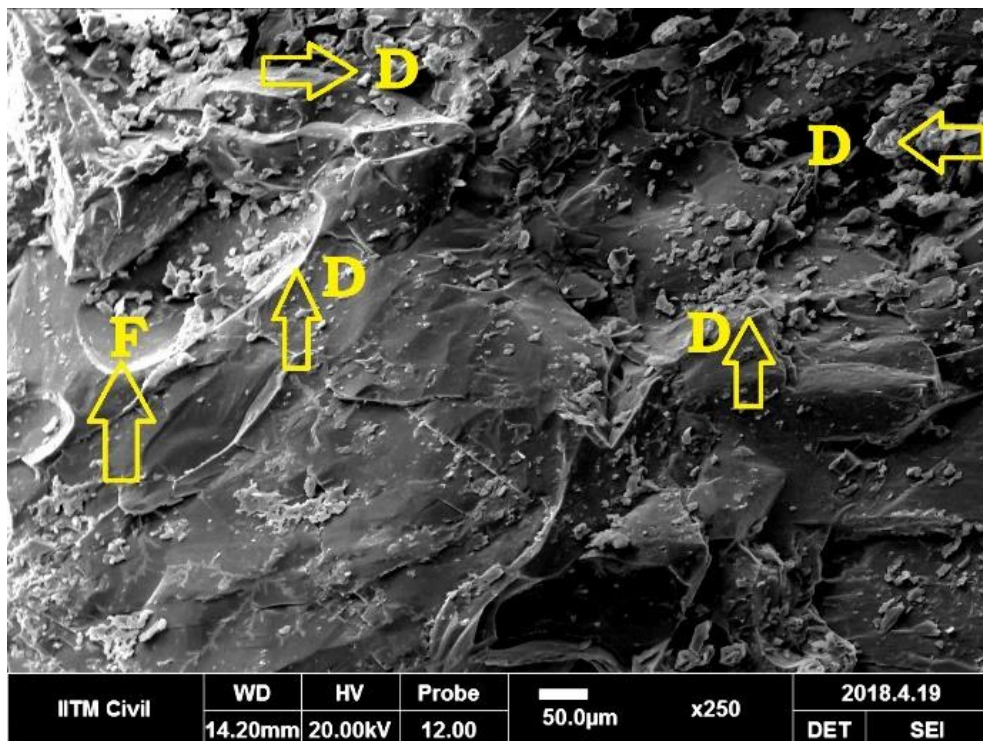


Figure 5.8. SE image of weathered granite depicting atmospheric depositions

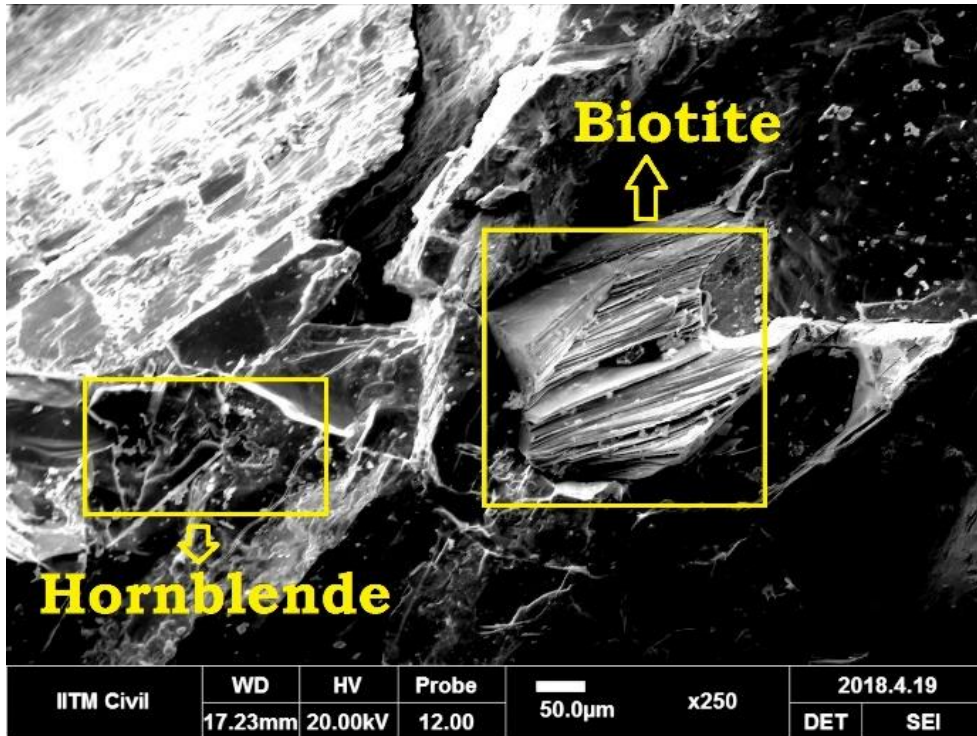
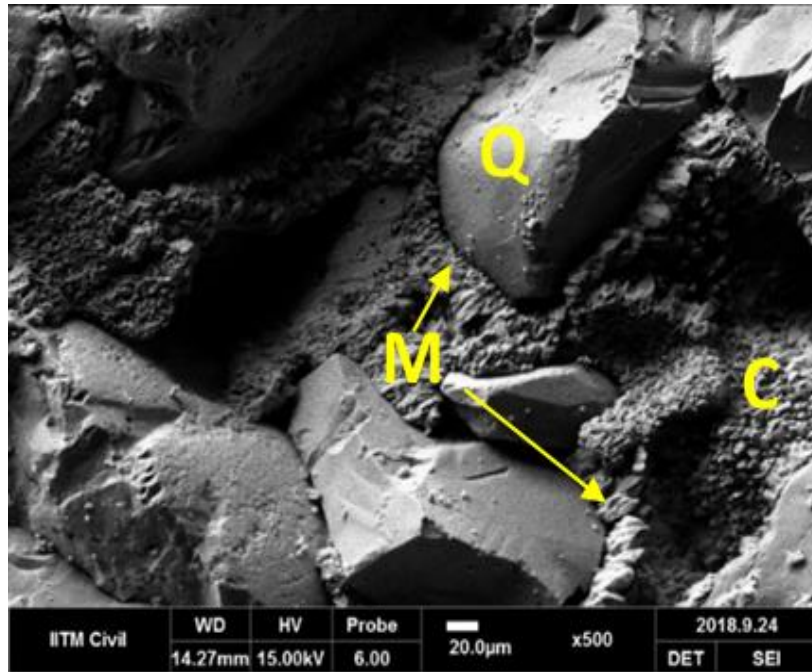


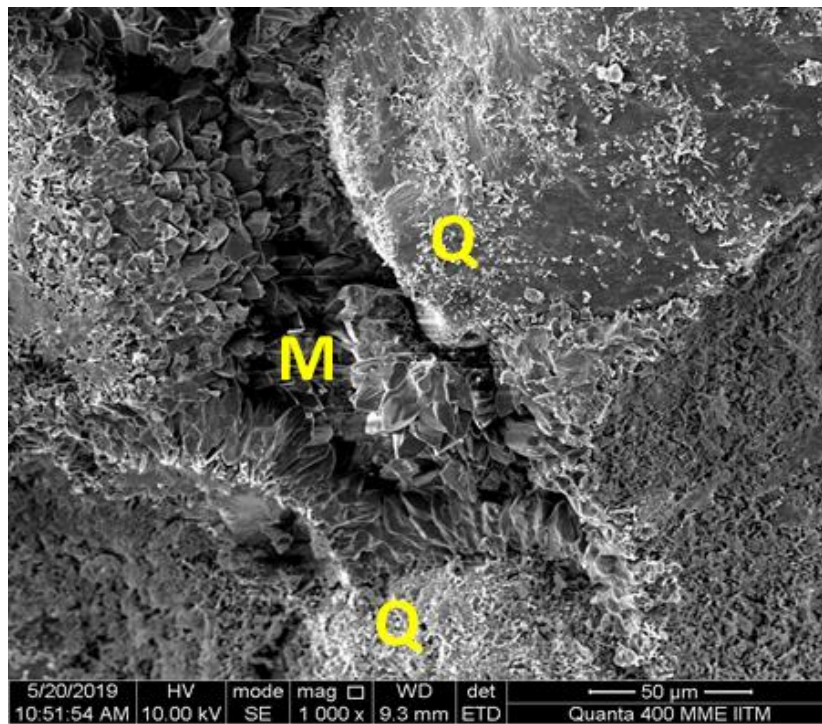
Figure 5.9. Biotite and hornblende in an unweathered granite sample

5.2.5.2 Morphological features in coral stone

Quartz grains of size greater than 100 µm were found distributed in the microstructure, which was surrounded by a more porous matrix, as shown in Figure 5.10 (a). At a higher magnification, the porous and less dense distribution of magnesian calcite in the matrix between quartz grains was observed, as shown in Figure 5.10 (b). The magnesian calcite lining the quartz grains was found to possess a flower-petal like morphology, as shown in Figure 5.11.



(a)



(b)

Figure 5.10. SEM images of coral stone (a) Quartz grains (Q) lined by magnesian calcite (M) along with calcite (C) (b) less dense distribution of magnesian calcite around quartz grains

The distribution of calcite crystals was observed, and the chemical composition identified by EDX is illustrated in Figure 5.12. The habit of the calcite crystals was found as prismatic at higher magnification, as seen in Figure 5.13 (a). On closer observation, white projected dots were observed all over the calcite crystals, which can be signs of corrosion (as the tested samples were naturally weathered ones and pure calcite does not show such characteristics), as shown in Figure 5.13 (b). The distribution of magnesian calcite and the prismatic but dendritic habit of calcite crystals along with the pores can be associated with the low density and high porosity of the coral stones.

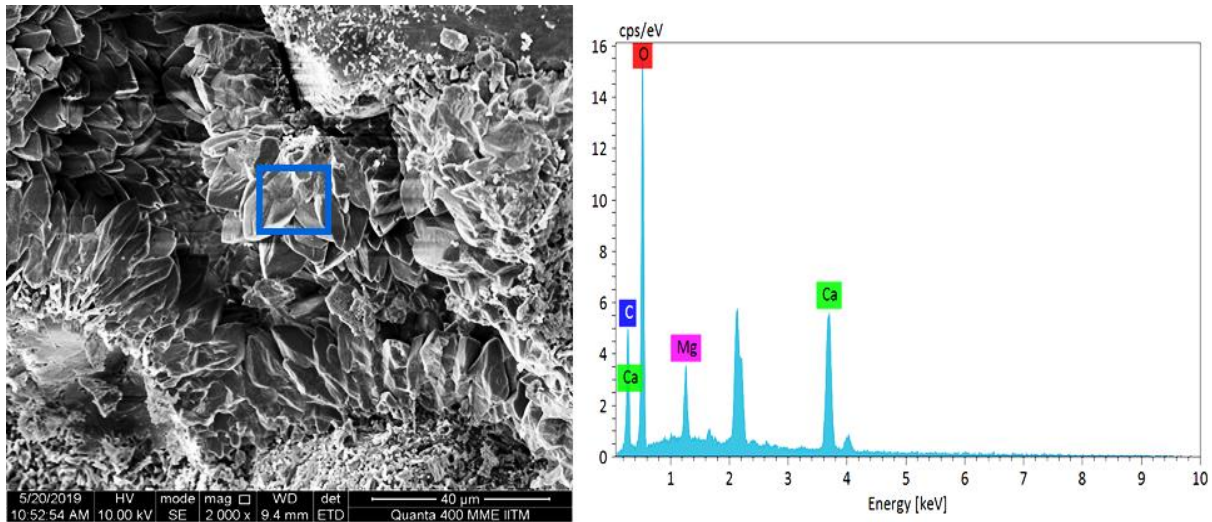


Figure 5.11. Petal-like lining of magnesian calcite around the quartz grains

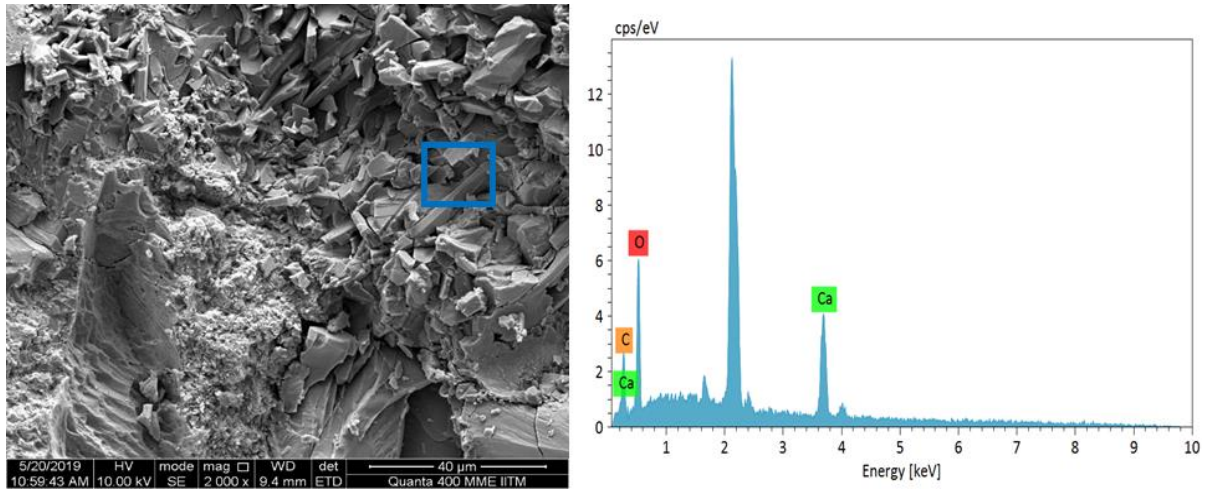
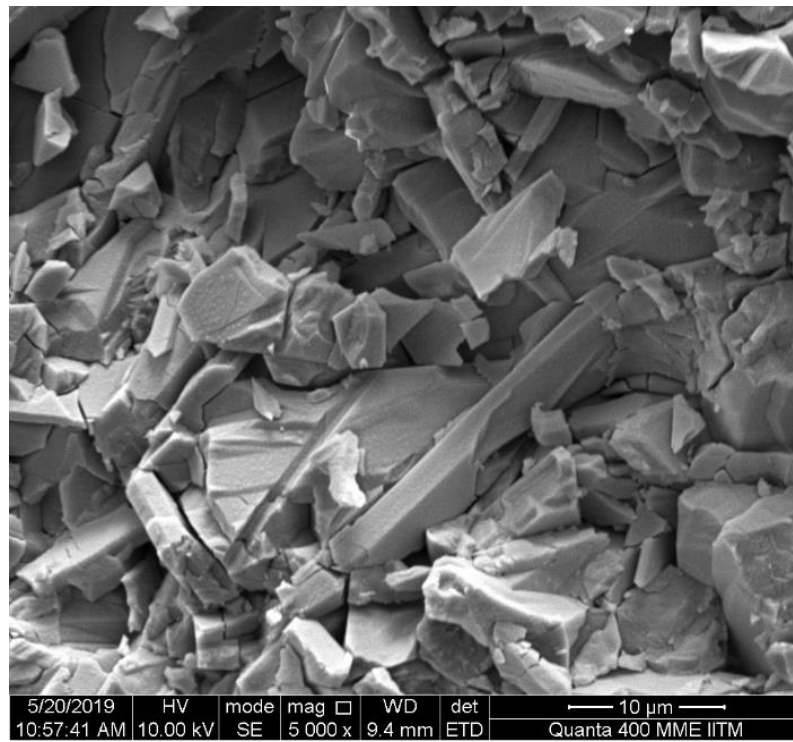
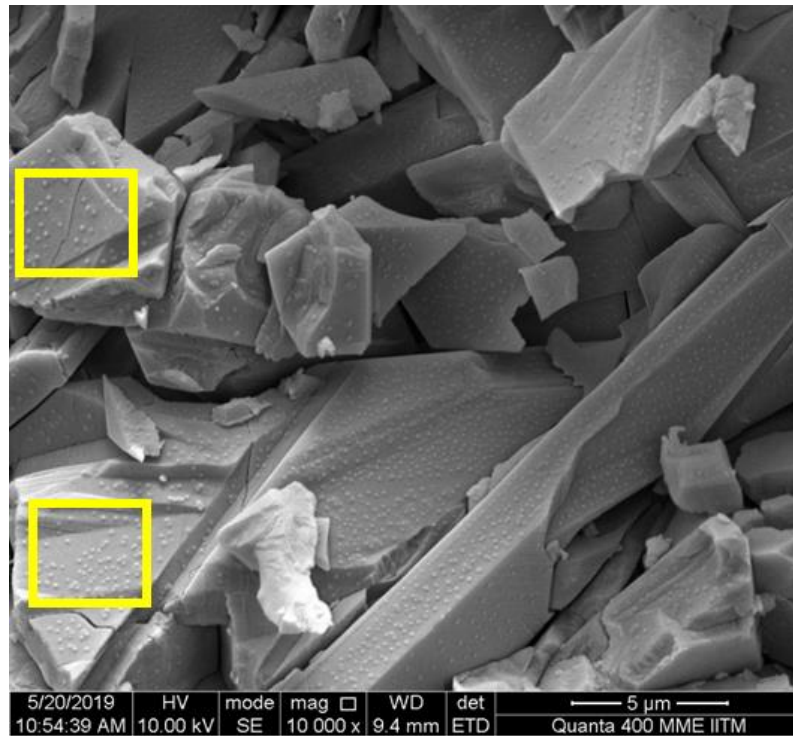


Figure 5.12. Distribution of prismatic crystals of calcite in the coral stone microstructure



(a)



(b)

Figure 5.13. (a) Prismatic calcite crystals (b) A magnified view elucidating the habit of calcite crystals showing corrosion pits

5.2.6 Thin section petrography

5.2.6.1 Petrographical features of granite samples

The petrographic images of granite are presented in Figure 5.14, captured on thin sections under crossed polarized light (CPL) and plane-polarized light (PPL). The petrographic images captured using CPL assist in identifying the minerals by their interference colours, extinction properties and relief. Whereas, the PPL images assist in tracing mafic (usually dark) minerals and cleavages. Figure 5.14 (a) and (b) represent petrography of unweathered granite under CPL and PPL respectively. The petrographic image illustrates hypidiomorphic, tiled and granular texture of granite. Figure 5.14 (c) and (d) represent thin section images in CPL and PPL of weathered granite sample. Granite texture is holocrystalline and rich in

potash feldspar with a conchoidal fracture. Quartz is also present in the system. Mineral compositions were found comparable to both weathered and the unweathered granite. The samples appear to be light pink granite stones. Other accessory minerals are less than 2% in a section. According to Goldich's weathering series, granite stones with a high proportion of amphibole mineral hornblende are highly prone to rapid weathering (Deer et al. 1992). Hence, the variety of samples subjected to the study can be said to have more resistance to weathering.

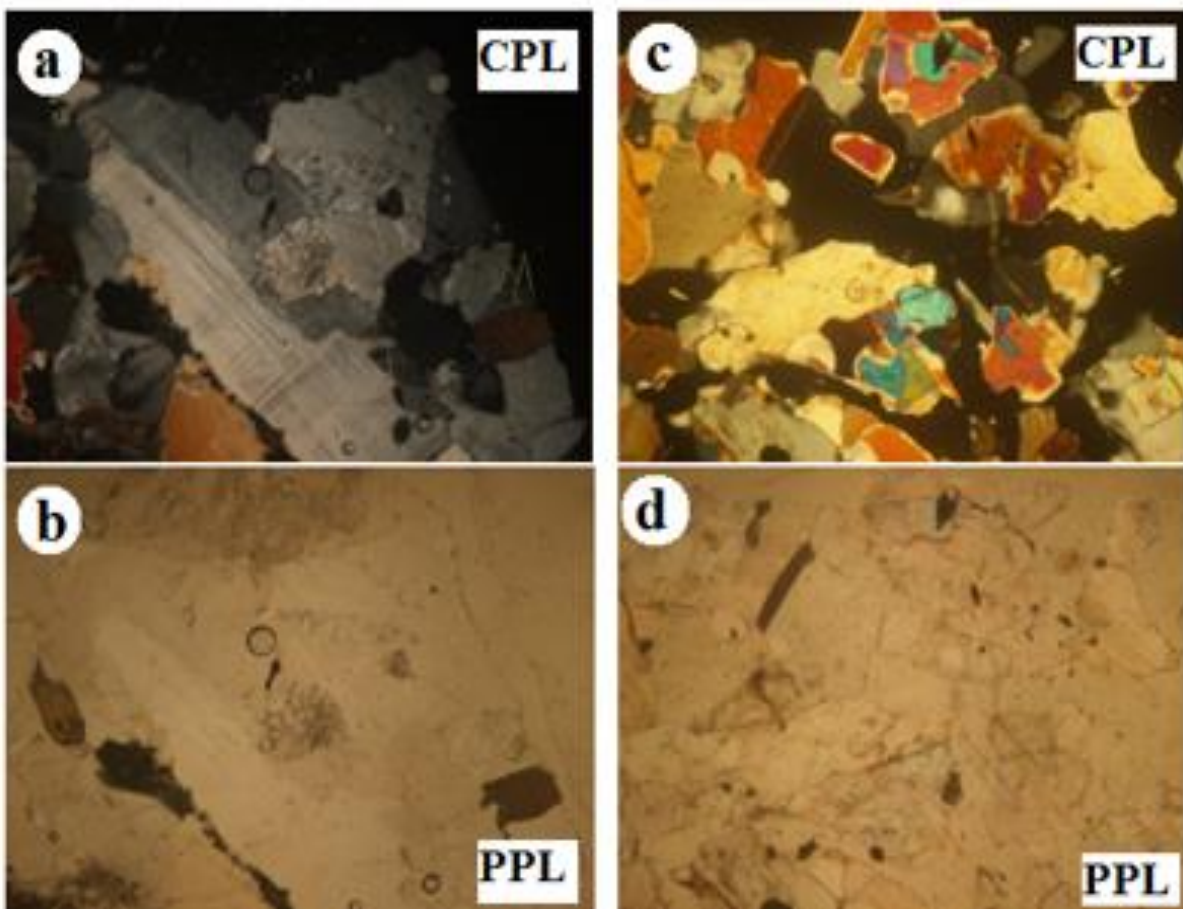
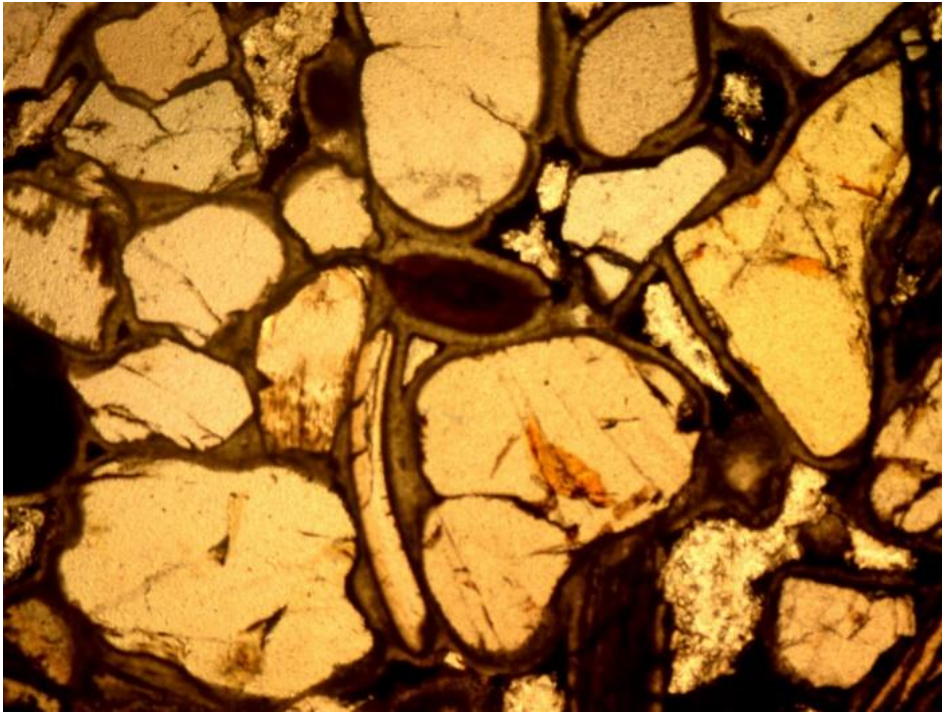


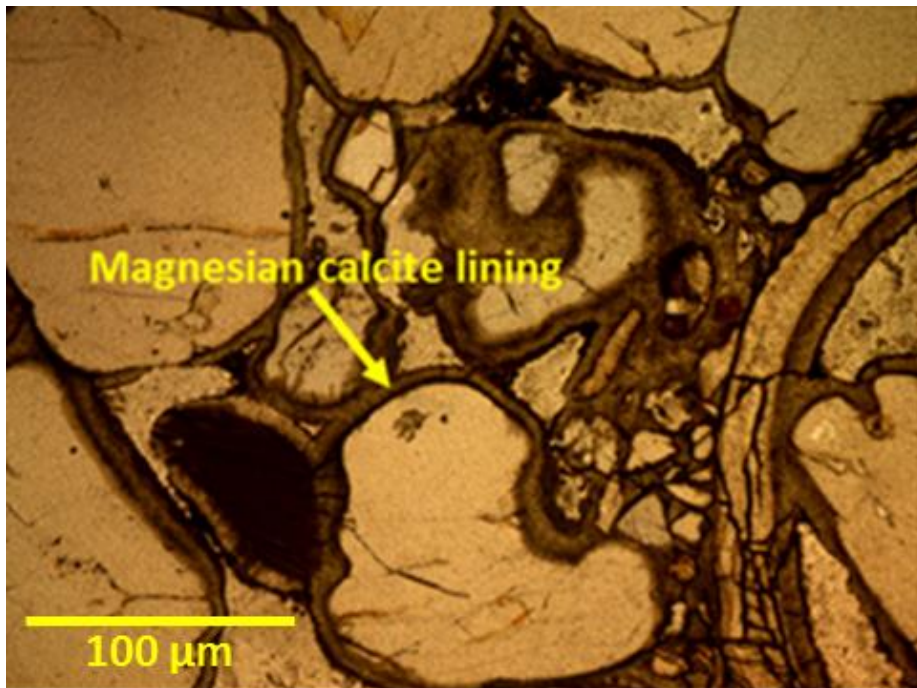
Figure 5.14. Petrographic images: (a&b) Unweathered granite (c & d) Weathered granite

5.2.6.2 Petrographical features of coral stone samples

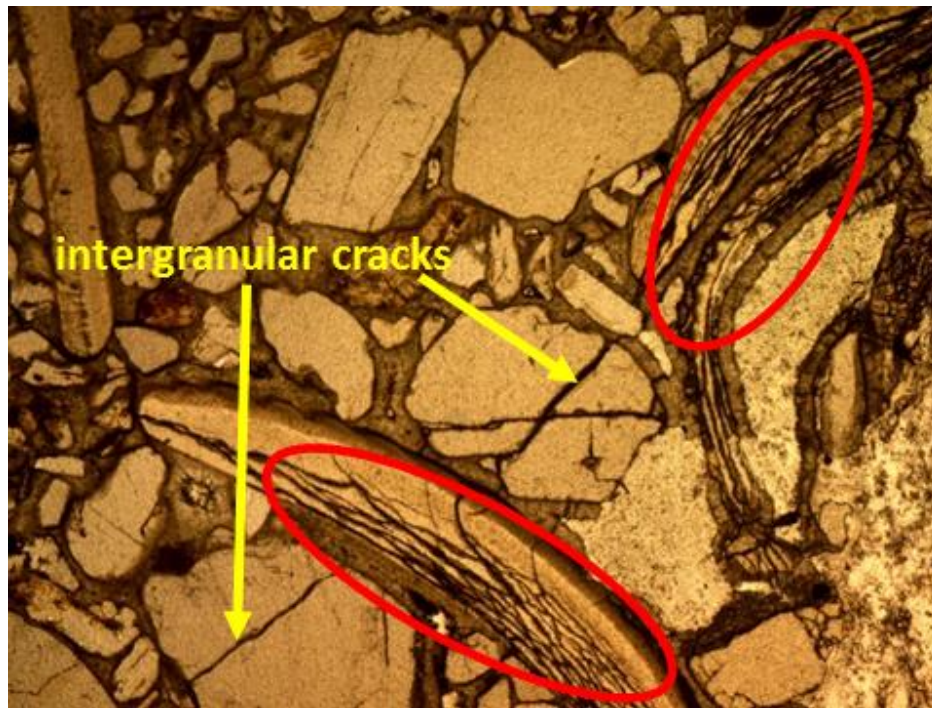
From the thin section-petrographical analysis, the images taken in the plane-polarized light guide in tracing the cleavages and microcracks in the minerals and their relief properties. The coral stone (with least weathering traces) observed with the polarized light microscope showed characteristics similar to a fine-grained limestone with pores having foraminifer (a unicellular planktonic organism with chalky shell) calcareous fossils (Figure 5.15 (a)). Also, the quartz and calcite grains were found intact and clear, with no intergranular cracks. The prominent carbonate nature is confirmed, and the material is found to be highly porous. The quartz crystals were found to be lined with a material of lesser density throughout, which is clearly illustrated in Figure 5.15 (b), which is again from samples which were having no weathering traces. Compared to the undamaged coral stone, the sample from the surface of a weathered coral stone column from the site shows a more disrupted texture (Figure 5.15 (c)). The degradation mechanisms were elucidated from the petrographic image (Figure 5.15 (c)) as inter mineral cracks and cleavages (marked with yellow pointers in the figure). The prismatic calcite grains exhibited longitudinal parallel crack patterns (marked with red ellipses in Figure 5.15 (c)).



(a)



(b)



(c)

Figure 5.15. Plane polarized petrographic images of coral stones (a) least weathered sample (b) calcite grains lined by magnesian calcite (c) sample from a weathered column surface

5.2.7 Mercury Intrusion Porosimetry (MIP)

5.2.7.1 Porosity and pore structure of granite

From the MIP data obtained, cumulative intrusion (Figure 5.16) and differential volume intrusion graphs (Figure 5.17) were drawn for granite samples which were unweathered and naturally weathered from the structure. The pore structure parameters, namely critical pore diameter, threshold pore diameter and total pore volume, were found from the measurements. The unweathered granite samples had a very low porosity value of 1.7%. A unimodal differential intrusion curve was obtained for this sample with a critical pore diameter of

0.0104 μm . A narrow band of pore sizes was observed, ranging from 0.001 to 0.05 μm . The pore parameters of all the samples as measured by MIP are given in Table 5.10.

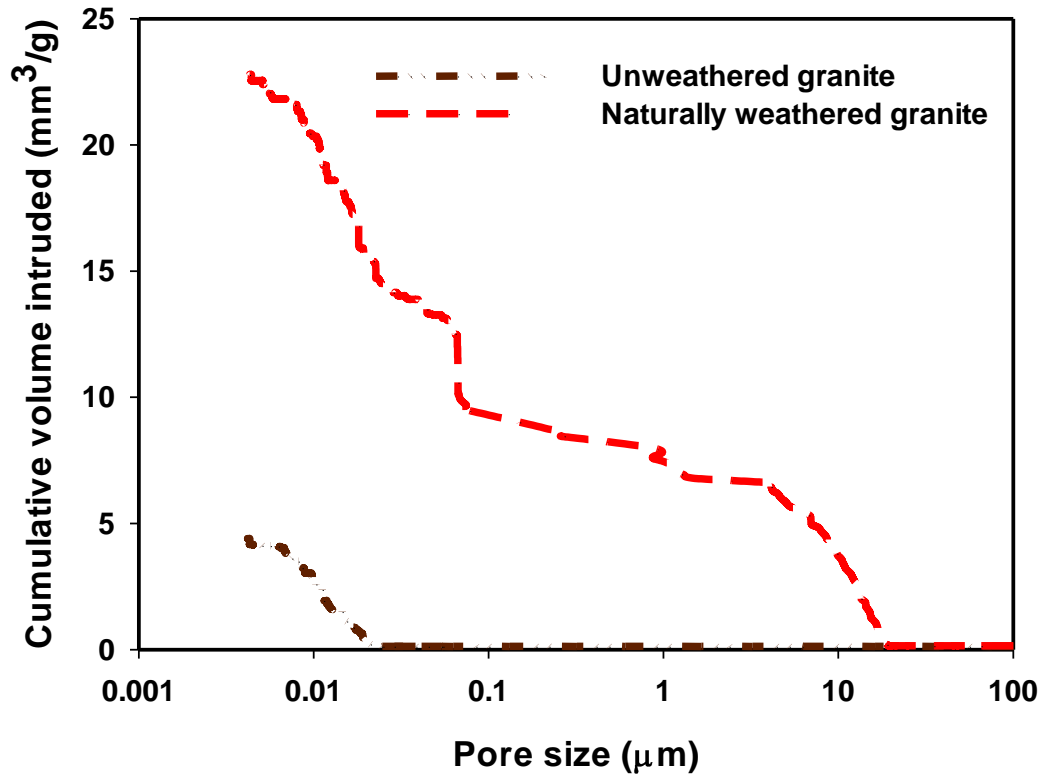


Figure 5.16. Cumulative intrusion curves for granite samples

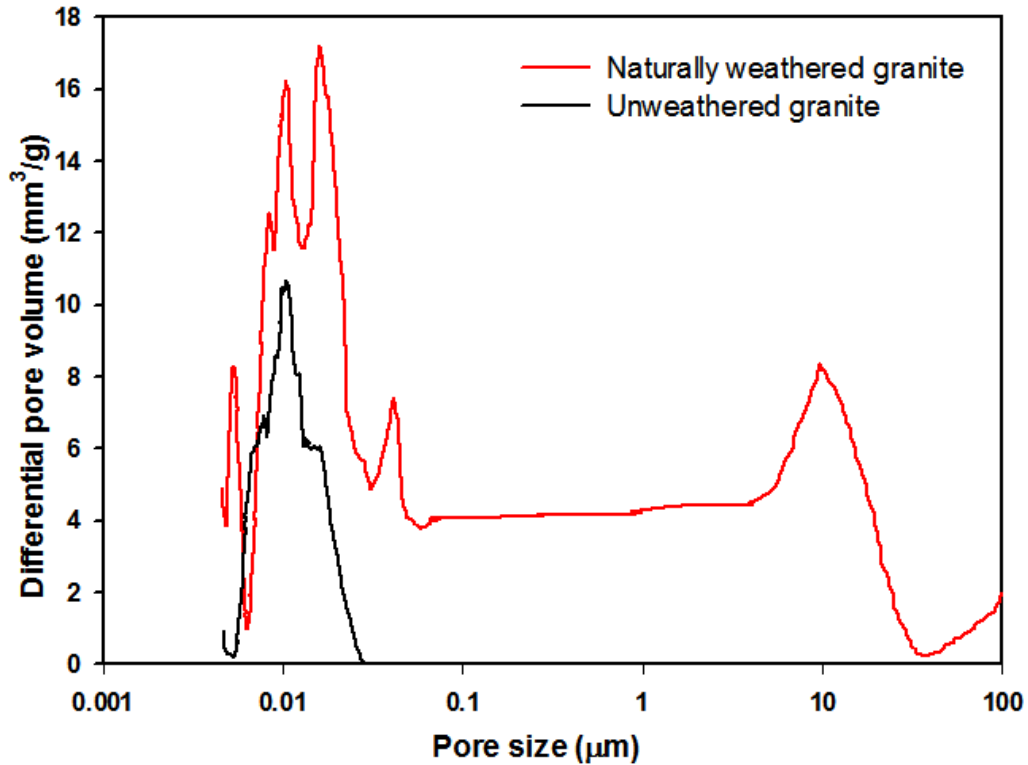


Figure 5.17. Differential intrusion curves for granite samples

The extent of damage and microcracking in the weathered sample was clearly captured from the variation of porosity and widening of the pore ranges, especially the occurrence of larger pores with severe damages. In weathering, maybe due to temperature gradient effect, stress, and human factors over a long span of time, cracks were formed. An extensive weathering was observed only in a few columns and in the pedestal portion, and the sample subjected to MIP was collected from such a weathered surface of a column. Also, multiple peaks were observed in the differential intrusion curve, indicating that different sizes of new pores had formed, and the range of pore sizes was widened in the cumulative

intrusion curve. This is indicative of the extent of random disintegration that occurred with damage.

Table 5.10. Pore parameters of the granite samples

Pore parameters	Unweathered	Naturally weathered
Porosity (%)	1.70	9.69
Critical pore diameter (μm)	0.010	0.004
Threshold pore diameter (μm)	0.02	20.29
Bulk density (g/cm^3)	2.63	2.71

Table 5.11. Relative volume fractions of different pore size ranges in granite

Pore diameter ranges (μm)	Relative fraction (%)	
	Unweathered	Naturally weathered
100-10	0	15.46
10-1	0	16.23
1-0.1	0	8.41
0.1-0.05	0	16.19
0.05-0.01	58.99	30.40
0.01-0.005	30.94	9.46
0.005-0.001	7.05	3.19

5.2.7.2 Porosity and pore structure of coral stone

The cumulative volume intrusion curve and differential pore volume curve for a typical coral stone sample are shown in Figure 5.18, in which the critical pore size is marked for better

understanding. The critical pore diameter, which is obtained as the peak of the differential curve is the pore diameter corresponding to the maximum volume intrusion. Systems with finer pores are expected to have reduced values for critical pore size and total pore volume, whereas when subjected to any deterioration, the pores shift towards coarser sizes. The total porosity was found to have a very high value of 17.45% compared to the porosity of granite of less than 2%.

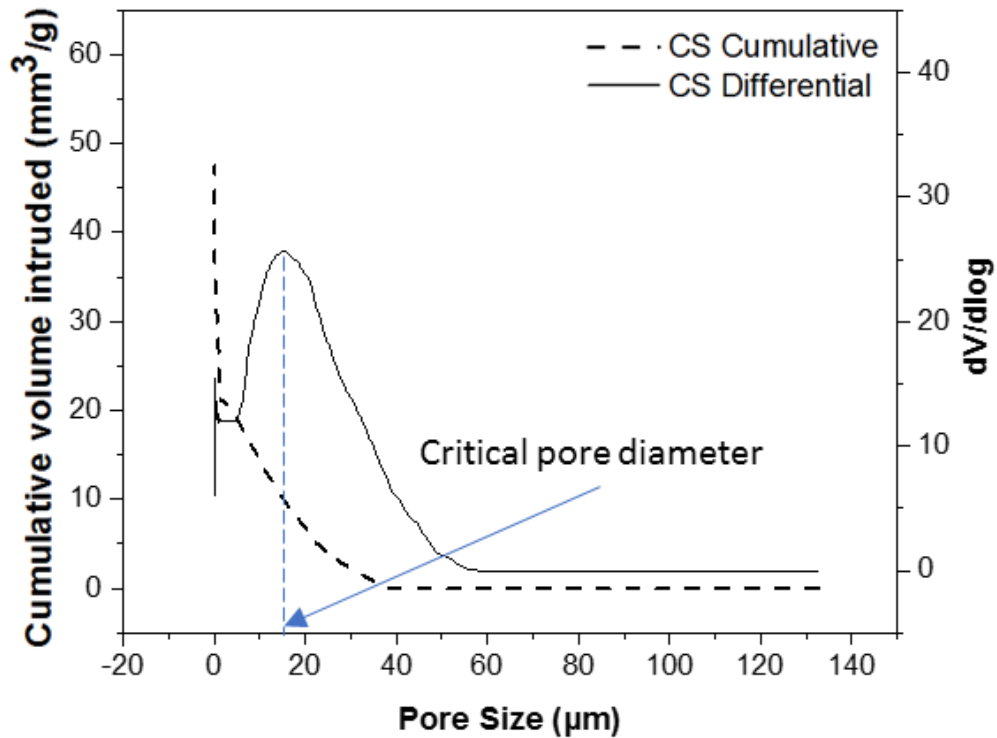


Figure 5.18. Cumulative and differential intrusion curves for a typical coral stone sample

The critical pore diameter in a typical coral stone type used in the current study is found close to 15 µm, which is also higher compared to other types of rocks such as granite,

limestone, sandstone, etc. which are common building units (Molina et al. 2011). Also, the assessment of the relative volume fractions of pores of different size ranges indicates that more than 70% of the total pores had a diameter more than 0.5 μm , from Table 5.12. These pores can be classified as macropores, where the susceptibility for salt crystallization is the least. In the smaller (sub-micron) pores, the growing salt crystals repel against the confined pore walls generating stresses (crystallization pressure) and hence initiate damage (Scherer 2004a). Thus, the pore characteristics indicate that despite the coral stone structures being seen mostly in areas of salt exposure due to the local availability, the chances of salt crystallization to occur inside the matrix of coral stones are much lesser. However, this needs to be confirmed by subjecting the samples to accelerated salt weathering tests.

Table 5.12. Relative volume fractions of pores of various size ranges for coral stone sample

Pore diameter ranges (μm)	Relative volume fraction of pores (%)
100-10	29.92
10-1	21.18
1-0.5	19.85
0.5-0.1	7.3
0.1-0.05	3.22
0.05-0.01	9.28
0.01-0.005	8.31
0.005-0.001	0.94

5.3 EFFECT OF ARTIFICIAL SALT WEATHERING ON THE STONES

The performance of stones on exposure to salt solution was studied by subjecting the specimens to accelerated salt weathering tests using the most commonly adopted procedure of EN 12370. 50 mm size cubes were prepared out of the stones - both granite and coral stone, and subjected to alternate dry-wet cycles with two different salt solutions separately - sodium sulphate and sodium chloride. Three specimens of each type of stone were used for the test. Each test cycle comprised of 2 hours of immersion of specimens in a 14% solution of sodium decahydrate followed by 16 hours of drying in an oven at a temperature of 105 °C and subsequent cooling for 6 hours in room temperature. In the case of sodium chloride exposure, 15.6% NaCl solution was used for immersing the specimens. Mass changes were documented for the samples after each day (each cycle).

5.3.1 Performance of granite in salt exposure

Figure 5.19 shows the granite specimens before the test, and after sodium sulphate and sodium chloride weathering, respectively. Figure 5.20 and Figure 5.21 show the mass changes along 110 cycles of salt weathering with sodium sulphate and sodium chloride salts respectively, for three specimens in each case. Long term studies were conducted using granite because 15 cycles of testing as per the standard did not result in any damage in granite specimens. However, the smaller pore sizes observed from MIP data suggested chances of salt crystallization due to high supersaturations that can be reached inside those pores. But the granite specimens did not show any visual signs of damages throughout the long-term test cycles for both sodium sulphate and sodium chloride, except the salt efflorescence in the case of sodium chloride test. Comparing to graphs from sodium sulphate

test, spread or variations in mass in each cycle was more in the case of chloride exposure test. This could be because of the high salt efflorescence, which was found on the external surface of the samples. The salt weathering tests on granite suggest the high resistance of the granite stone against salt weathering damages. This could be because of the high grain strength of the material, which is able to resist the crystallization pressure that develops inside.

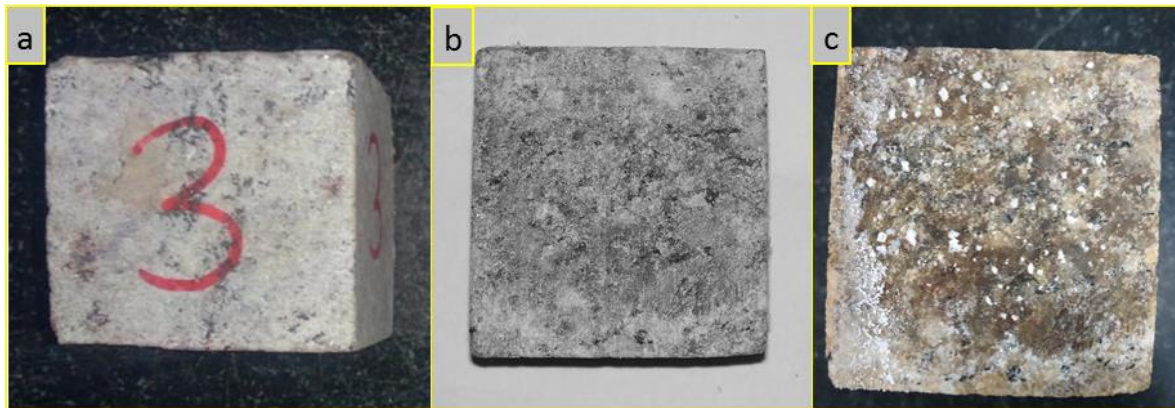


Figure 5.19. Images of granite specimens (a) before salt weathering (b) after sulphate exposure (c) after chloride exposure

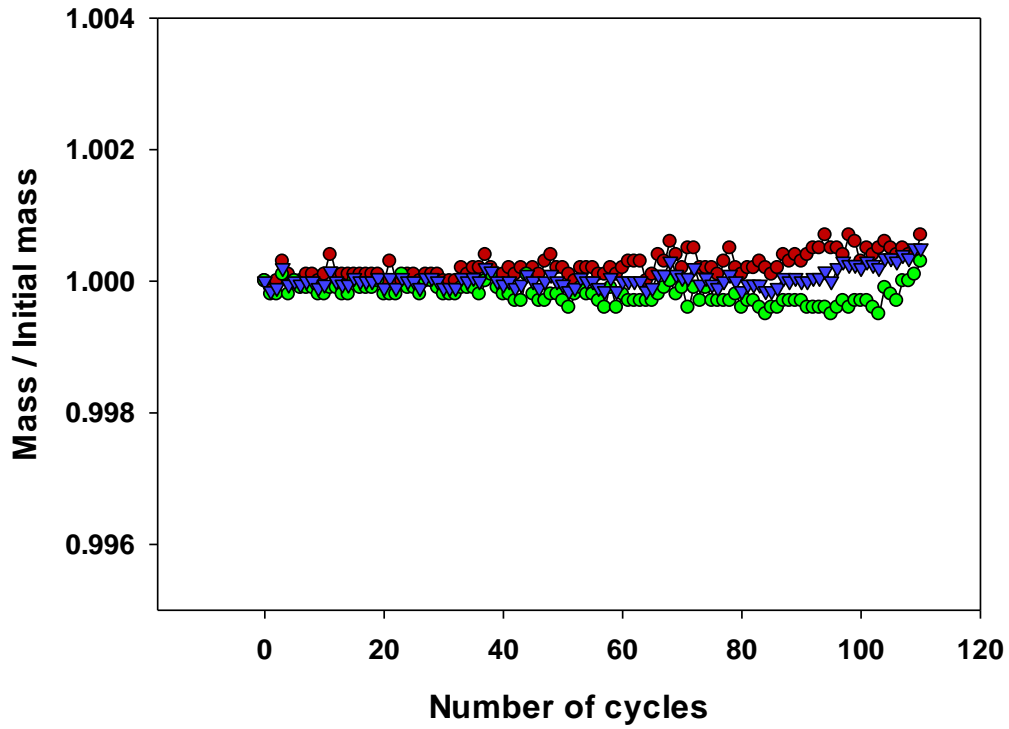


Figure 5.20. Mass change for granite samples under sodium sulphate salt weathering cycles

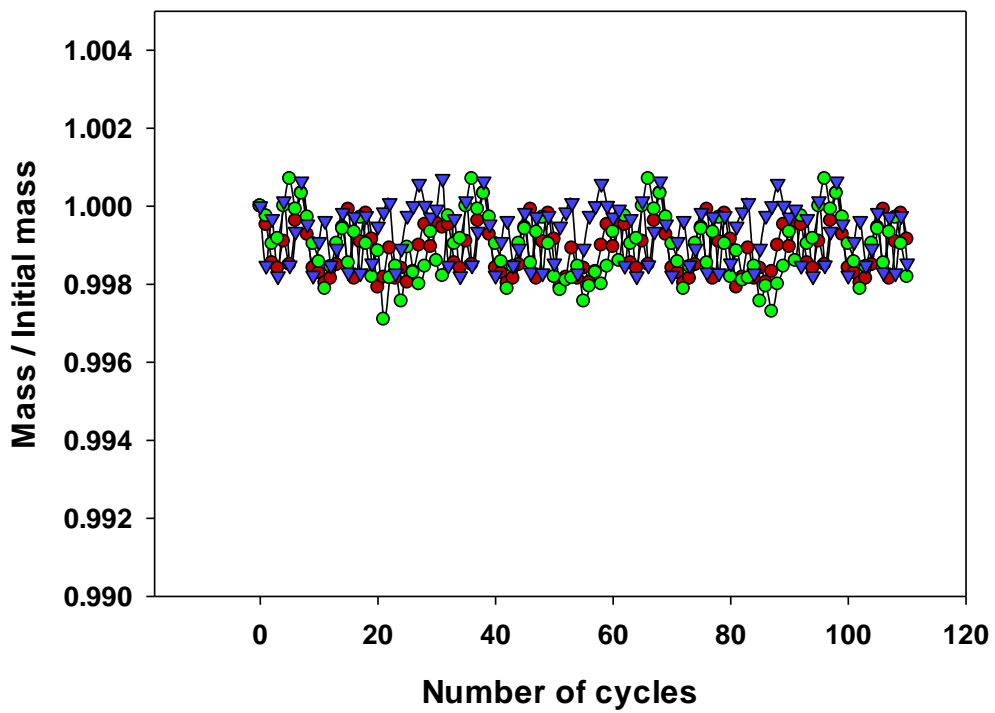


Figure 5.21. Mass change for granite samples under sodium chloride salt weathering cycles

Because of the observation of no damage in the samples after such a long exposure time, microstructural changes within the matrix were not studied.

5.3.2 Performance of coral stones in salt exposure

Three coral stone cubes, each of dimension 50 mm, were tested for both sodium sulphate weathering test and sodium chloride weathering test. Mass changes and damage patterns were documented for the 15 cycles of testing. Figure 5.22 shows the coral stone specimens before the test, and after sodium sulphate and sodium chloride weathering tests, respectively.

The mass changes with respect to the number of weathering cycles for Na_2SO_4 and NaCl solution are shown in Figure 5.23 (a) and (b) respectively. There was an initial mass gain in both cases due to the sudden salt deposition inside the pores, followed by a competitive phase of mass gain/loss. No continuous mass loss phase was observed, which would denote the onset of degradation due to salt crystallization in any of the specimens. For both the tests, no other physical changes were noticed.



Figure 5.22. Coral stone specimens a) before subjecting to artificial weathering cycles b) after subjecting to Na_2SO_4 exposure c) after subjecting to NaCl exposure

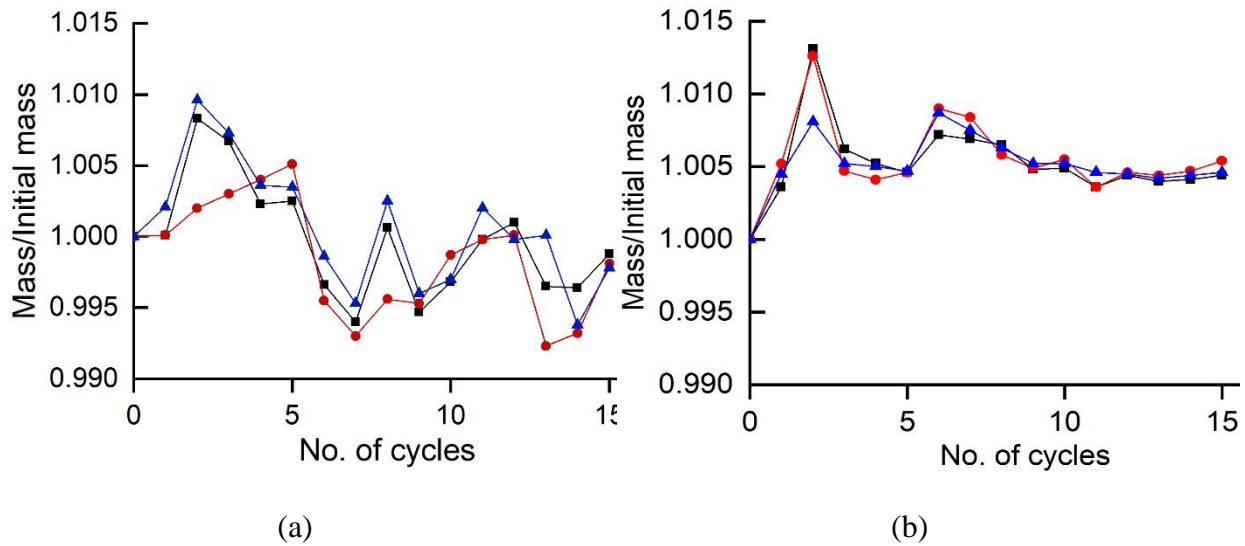


Figure 5.23. Mass change for the specimens (a) with Na₂SO₄ exposure (b) with NaCl exposure

With sodium sulfate solution, after the 15 weathering cycles, samples were observed with a minor change in the surface texture and a smoothening of corners (see Figure 5.22 a and b). The slight change in the appearance of the surface could have occurred because of the formation of thenardite crystals as a thin layer covering the external surface, which seals the pores. In the case of NaCl solution exposure, the specimens did not show any changes with respect to its geometry, but remarkable efflorescence/crusts were seen at a macroscopic scale on the external surface, which were easily removable (Figure 5.22 c). The salt crystals were more visible in the case of NaCl as the halite crystals are much larger in size than the thenardite crystals (Vázquez et al. 2015). The coral stones were found to possess a good salt weathering resistance in the exposures of both NaCl and Na₂SO₄ solutions, which are the common threats in salt weathering.

Compressive strength was measured after subjecting to these weathering cycles. The average compressive strength of specimens exposed with sodium sulphate was 65 MPa with a standard deviation of 3 MPa, and that of sodium chloride exposure was 70 MPa with a standard deviation of 4 MPa. The difference in strength was negligible after the salt exposures. Results suggest that the bulk of the material was not affected by damages/cracks due to accelerated salt weathering.

After 15 dry-wet cycles, because of the peculiar highly porous nature of the material and the curiosity to observe the alteration in the microstructure that would have occurred within the material, microanalytical studies were conducted. For that, samples were taken from the weathered specimens. Analysing the porosity and pore distribution in the coral stones before and after subjecting them to accelerated weathering studies gives insights into the mechanisms of action of salts within the material and the consequence on the durability of the stone. The cumulative volume intrusion curve and differential pore volume curve for coral stones before and after accelerated sodium sulphate weathering are shown in Figure 5.24, and the pore parameters - critical pore size and total pore volume, are marked. Results with respect to sodium sulphate are used to compare with original specimens to understand the extent of damage because only sodium sulphate exposure resulted in slight damages for the specimens. The critical pore diameter, which is obtained as the peak of the differential curve is the pore diameter corresponding to the maximum volume intrusion. Systems with finer pores are expected to have reduced values for critical pore size and total pore volume, whereas when subjected to any deterioration, the pores shift towards coarser sizes. The aged but undamaged sample is denoted as CS and accelerated weathered sample is denoted as

CSW in the graph in Figure 5.24. Even though there is a slight increase in the total intruded volume for the weathered sample, the difference in the critical pore diameter is negligible, indicating the absence of a noticeable disintegration of pore structure at the microstructure level. The total porosity was found to have a very minor increase of 17.45% to 17.86% upon subjecting the samples to accelerated weathering.

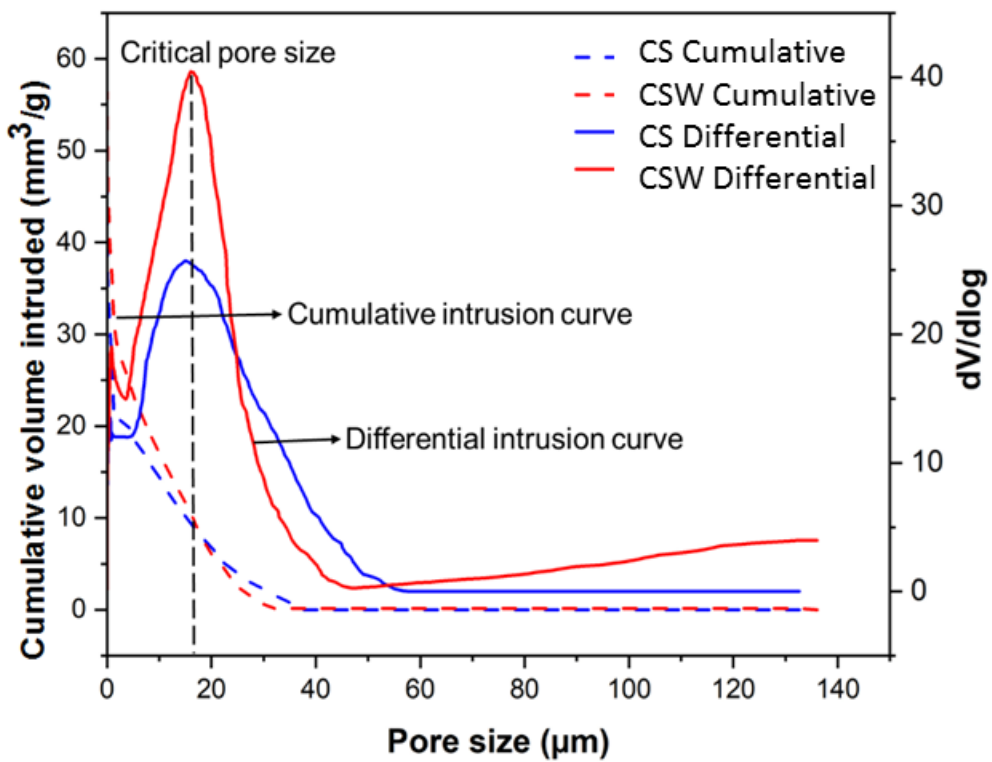


Figure 5.24. Curves from MIP data for natural undamaged coral stone and accelerated weathered coral stone

Table 5.13 shows the relative pore volumes in different size ranges before and after accelerated weathering with sodium sulphate solution. The results are similar for both the as-received sample and accelerated weathered sample. Around 27% of the total porosity consisted of pores between 10 and 100 μm , and more than 70% of total pores were greater than 1 μm . The chances of salt crystallization damage to occur in these macro-pores are low because it is difficult to sustain high crystallization pressure in larger pores.

Table 5.13. Pore size ranges for coral stone samples before and after accelerated weathering tests (with sodium sulphate)

Pore diameter ranges (μm)	Relative volume fraction of pores (%)	
	Received as such sample (CS)	accelerated salt weathered (CSW)
100-10	26.92	27.47
10-1	21.18	29.16
1-0.5	9.85	8.81
0.5-0.1	11.3	11.99
0.1-0.05	5.22	4.46
0.05-0.01	13.28	9.07
0.01-0.005	11.31	4.02
0.005-0.001	0.94	4.76

The combined effect of the pore-distribution being in the macropore range and the good grain strength, as exhibited by the mechanical characteristics, aids the damage-free behaviour of coral stones in a salt environment. Figure 5.25 shows an SEM image on the coral stone sample after the accelerated weathering cycles with NaCl. Here, NaCl crystals

were found to have a preferential deposition in the highly porous (with macropores) magnesium calcite region, which cannot cause any crystallization pressure/damage to the pore wall.

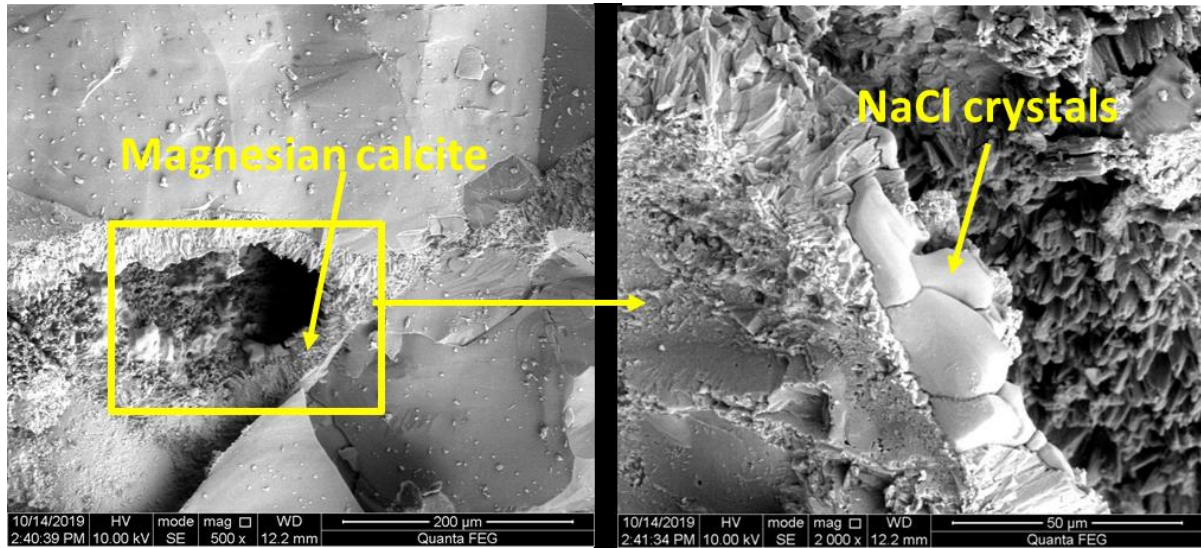


Figure 5.25. SEM image depicting preferential deposition of NaCl crystals over magnesian calcite

From the analysis of microstructure after the accelerated weathering tests of 15 cycles, it was understood that the pore sizes were in the macro-range for coral stones, which led to minimal salt crystallization damage. It would be practically challenging to fill the large pores with growing crystals to get the restraining effect from walls, which would subsequently cause crystallization pressure or further damages. 15 exposure cycles with highly concentrated salts resulted in no signs of damage, for which the cause and processes were analysed deeply with micro-analytical tools. If the exposure time would be extended, damages due to crystallization pressure are not expected, but damages may arise due to

erosional activities only. Hence the weathering cycles were interrupted and stopped after 15 cycles for coral stone specimens.

5.4 SUMMARY

The key role of pore sizes and porosity was understood from the test results on bricks in the previous chapter. Hence, in this chapter, the evaluation of two types of stones with extremely different pore parameters was conducted in order to establish the significance of pore parameters in general, in any masonry material. Physical and mechanical characterization studies for both the stones - granite and coral stone - were supported further with microanalytical studies. The performance of the materials with respect to salt crystallization was examined by subjecting the materials to artificial salt weathering studies. The mechanism of salt crystallization was understood in each case from the material behaviour with accelerated weathering tests, and the known microstructure. This helped in establishing the role of pore size and pore structure in a masonry unit in determining the durability performance.

Granite stone showed excellent mechanical properties with high strength and low water absorption. Further, microstructural analysis supported the remarkable mechanical performance with the densely packed microstructure revealed through SEM images and very low porosity observed from MIP. Long-term accelerated weathering tests with highly deleterious sodium sulphate salt solution on granite specimens exhibited the remarkable resistance of the material towards salt crystallization. The very low permeability, i.e., the low

accessibility for the liquids to get into the pores, along with the high grain strength could be the factors that prevent the onset of any damages in granite due to salt crystallization.

Physical and mechanical characterization of coral stones emphasized the good grain strength, low density, high capillary porosity and high water-absorption values, which were corroborated with the microanalytical studies. Coral stone samples subjected to both sodium sulfate and sodium chloride salt solutions separately were found with no noticeable deterioration after 15 wetting – drying cycles. The impressive salt weathering resistance observed with artificial weathering studies was supported by the detailed pore structure analysis data from MIP. The reason for the low susceptibility of coral stones towards salt crystallization was found as the prominence of macropores in the system (more than 70% of the total pores were of size greater than 0.5 μm). The substantial strength of the grains would have assisted in resisting the crystallization pressures caused by salt crystallization in the smaller fraction of micro-porosity.

6 SELECTION AND EVALUATION OF PROTECTIVE TREATMENTS

6.1 INTRODUCTION

The treatments to historic structures are often applied without proper scientific study, and without identifying the actual intention and the properties of the chemicals involved. If not selected and applied properly, it can cause deleterious actions, and it will be difficult to remove them from the surface properly if they fail. Although the application of water repellents has several advantages (hydrophobicity, reduced capillary absorption, etc.), the ultimate aim of the treatment is to improve the durability of the brick. As learnt from the previous chapters, degradation by salt crystallization has been identified as the most damaging mechanism for masonry units. It is also evident that the mechanism and the extent of damage by salt crystallization depend, to a great extent, on the pore size distribution and the environmental conditions. Thus, the prominent deterioration mechanism itself depends on the characteristic microstructural properties (pore size distribution, pore connectivity, etc.) of the substrate. Hence, water repellent treatments aimed at improving the durability of the bricks should be studied for their compatibility with different types of substrates.

In this chapter, the effect of the pore structure of bricks on the performance of different water repellents applied to them in salt weathering conditions is investigated. The

water repellent coatings selected for the study are also characterized and evaluated for their required properties according to standard recommendations. Only the brick samples were subjected to study the performance of water repellent treatments and not the stone samples. Since both the stone samples (granite and coral stones) proved non-deteriorating with the preliminary salt exposure experiments due to the peculiarities in their microstructural and physical properties, a study of the behaviour of water repellent treatments using the stone samples cannot provide the required information. The aim of this particular section of the study was to analyse the alterations in the process of salt-crystallisation and the deteriorations with the application of various water-repellents, which would be efficiently visualized with high-response systems like bricks.

Bricks V1, VN, C1 and C2 were selected for conducting the study. Other brick samples K, T1 and T2 were discarded from subjecting to accelerated weathering cycles since they were already in an extremely weathered state. VN, C1 and C2 were specimens prepared from fresh brick samples, and V1, even though historic, had physical-mechanical properties much similar to the fresh brick samples. Throughout the chapter, specimen C1 coated with the silicone-based coating is named as C1-SC, and C1 coated with the acrylic siloxane-based coating is named as C1-AS. The uncoated sample of the set is named as C1 itself. Similar nomenclature is followed for other brick specimens too.

6.2 BASIC PROPERTIES OF PROTECTIVE TREATMENTS

Since the purpose of protective treatment in these cases is to prevent the entry of salt and water, the treatment to choose is a water repellent coating. Properties expected from an ideal treatment material are:

- Reduced water absorption or absorption of other liquids
- Vapour permeability or breathability
- Good adhesion to the material
- Transparent and causing no discolouration to the substrate material

Two popular, commercially available and most commonly used masonry protective treatments were selected for the study - a silicone-based water repellent treatment (SC) and an acrylic-siloxane based water repellent (AS). This section details the application of the water-repellents and tests conducted to identify the properties of the treatment with respect to the basic requirements before evaluating their salt weathering resistance.

6.2.1 Application of water repellent treatments

Brick cubes of 40 mm sides were oven-dried to constant mass by keeping in the oven at a temperature of 60 °C. After cooling, three numbers of specimens from each lithotype were left uncoated, coated with silicone-based water repellent and next set coated with acrylic-siloxane based water repellent. Although the RILEM procedure recommends impregnation of water repellent by immersion, the treatments were applied using a brush. This was done to resemble the field conditions. Three brushstrokes were applied to all the six faces of the

cubes. Second stroke was provided in a direction perpendicular to first and third stroke. Brushing was selected as the application method as it is the most commonly used procedure in masonry conservation practice, and also because it is not supposed to give any drastic colour change (Franzoni et al. 2014; Graziani et al. 2016). In the actual field conditions, all the six faces cannot be coated due to accessibility issues, and none of the uncoated faces (inaccessible) is expected to be in direct contact with the salt solution as in an accelerated weathering test. Hence, leaving any face uncoated during the immersion test in such small samples would result in unrealistic damage.

The tests used to evaluate the water repellency and breathability of the treatments are:

- Waterdrop absorption test (RILEM Test Method - Test No. II.8b)
- Water Sorptivity test (South African Durability Index testing procedure manual)
- Karstens' pipe test (RILEM Test Method - Test No. II.4, 1980)
- Breathability test (RILEM Test No. II.2, 1980)

6.2.2 Waterdrop absorption test

The uncoated brick samples - C1, C2, V1 and VN - absorbed the entire drop of water placed on them immediately. The silicone-coated samples absorbed a small amount of water after 24 hours. The acrylic siloxane coated samples had absorbed the entire water after 24 hours. But the surface was still wet. This behaviour was similar for all the tested bricks (C1/C2/V1/VN). Hence, both the considered treatments were found to have essential water repellency. This is the most straightforward initial test to screen a good water repellent treatment for brick masonry. Figure 6.1 shows the water drop over a typical uncoated and coated (with acrylic-

siloxane water repellent) substrate, photographed after 1 hour of placing the water drop over the substrate.

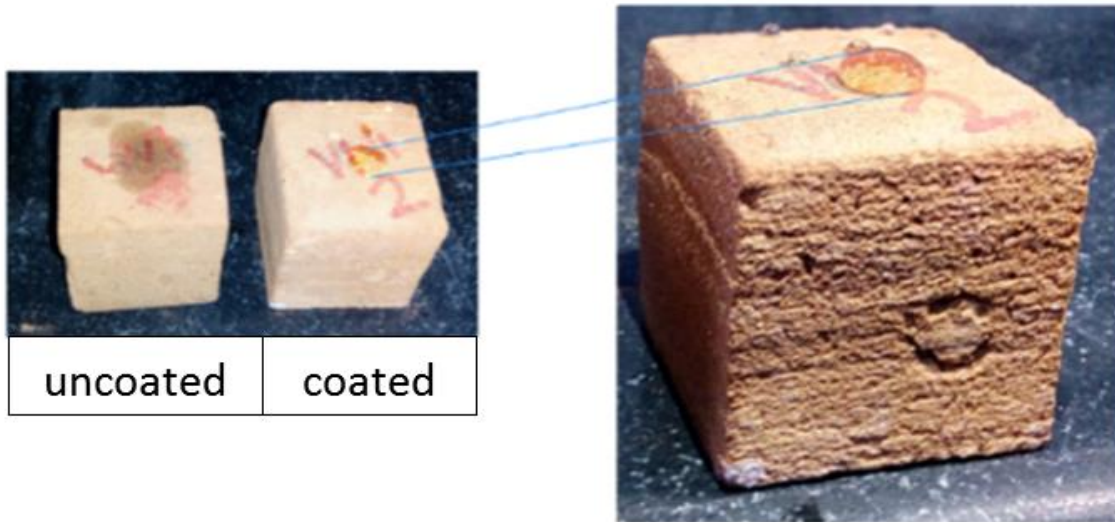


Figure 6.1. Illustration of water drop absorption test

6.2.3 Water Sorptivity test

Water sorptivity test was performed following the South African procedure outlined in the Durability Index testing procedure manual (“Durability Index Testing Procedure Manual” 2018), and the water-accessible porosity values (capillary porosity) for the bricks were also determined. Figure 6.2 shows the variation of capillary porosity with each brick type, for uncoated and coated samples with two different types of water repellent treatments. For the coated samples, actual capillary porosity inside cannot be obtained by this test, but it measures the current water-accessible porosity. Still, this test was used to comparatively analyse the two different type of coatings in preventing the entry of water inside the pores

during the process of sorptivity test. The results showed that the water absorption into the capillary pores reduced with both the coatings for all samples. Among the two different coatings, silicone-based coating (SC) had the least capillary porosity values observed from sorptivity test, indicating that silicone-based coating was capable of repelling more water than the acrylic-siloxane based coating.

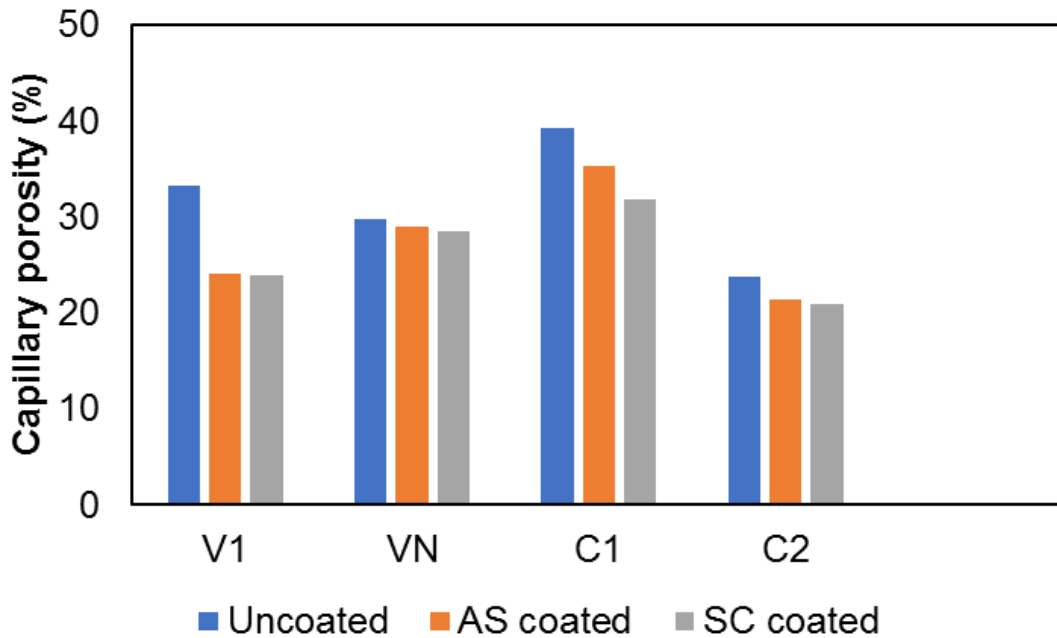


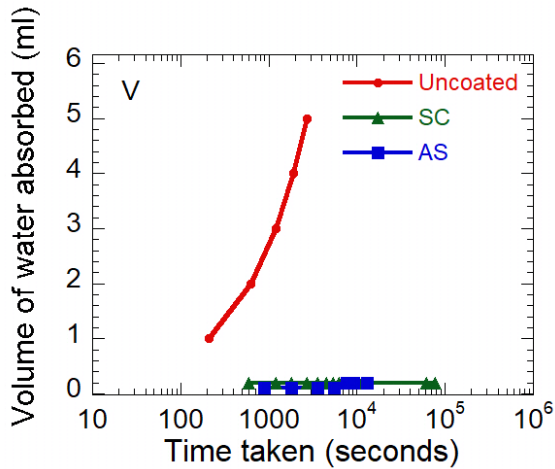
Figure 6.2. Variation of capillary porosity for specimens with different coatings

6.2.4 Karsten tube test

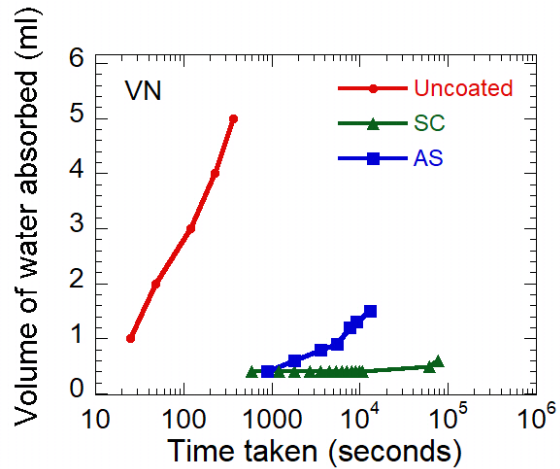
The results of Karsten tube test are evaluated based on the volume of water absorbed with respect to time elapsed. Uncoated and coated brick samples were tested. Figure 6.3 shows the graph between the volume of water absorbed and time in each case. The following observations were made from the data:

- In historic bricks (V1), acrylic siloxane-based coating (AS) reduced the rate of absorption by about 100 times, whereas, silicone-based coating (SC) reduced it by about 1000 times, compared with uncoated samples.
- In the VN bricks, acrylic siloxane-based coating (AS) reduced the rate of absorption by 100 times approximately, whereas, silicone-based coating (SC) reduced it by 10000 times.
- In commonly available non-wire-cut bricks (C1), the acrylic siloxane-based coating (AS) reduced the water absorption rate by around 1000 times, whereas, silicone-based coating (SC) reduced it by 10000 times.
- In wire-cut bricks (C2), the rate of absorption was reduced roughly by 1000 times by both the coatings.

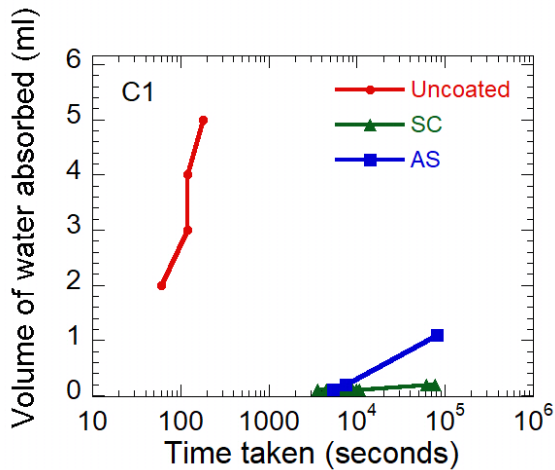
In general, in relatively more porous materials (V1, VN and C1), the silicone-based water repellent performed better than the acrylic siloxane-based water repellent in terms of reducing the rate of water absorption. On the other hand, both the water repellents were found to have similar performance when applied to the less porous material C2.



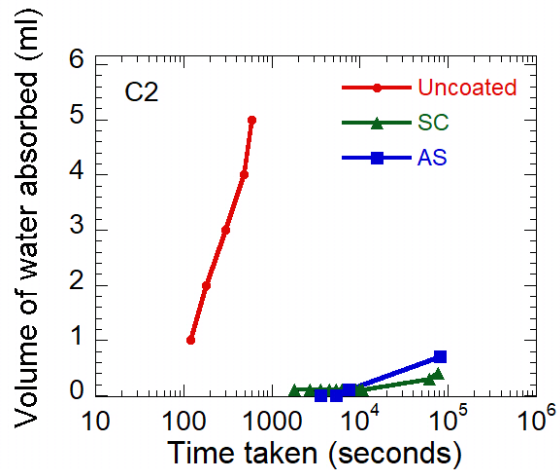
(a) V



(b) VN



(c) C1



(d) C2

Figure 6.3. Water absorption by Karsten tube test

Bricks fired at a low temperature have a low degree of vitrification and high porosity. So, they have relatively larger open pores at the surface. This effectively increases the depth of penetration of silicone-based water repellent, thus reducing the water absorption rate significantly. Acrylic-siloxane based coatings were less effective in this aspect of water

repellence, and the reason could be the cracking tendency of acrylic siloxane coatings as reported by Stefanidou and Karozou (2016). They observed that silicone-based water repellent coatings had a profound penetration depth when applied on common bricks fired at a low temperature ($< 900\text{ }^{\circ}\text{C}$). On the same type of bricks, they found acrylic siloxane-based coatings to have a cracking tendency when observed using microscopic studies, on accelerated weathering test. On the other hand, in relatively less porous bricks, the number of large pores available at the surface is not adequate to ensure good penetration of the silicone-based coating. So, they had a similar performance as the acrylic siloxane-based coating in reducing the rate of water absorption.

6.2.5 Breathability test

The vapour permeability of the water repellent coatings is critical since the porous masonry units need to allow the water vapour to get in and out. Otherwise, vapour can get blocked inside the pores and result in causing additional stress. The test was conducted on uncoated, SC coated and AS coated samples of C1 and C2 bricks which had the extreme values for porosities and mechanical properties. The mass of the measuring cell in the vapour permeability cell as per UNI EN 15803 (2015) was measured every 24 hours for 36 days, and the plot is shown in Figure 6.4. The test confirmed that both of the selected water repellent coatings provide breathability to the systems. None of the coatings was found to be blocking the movement of vapour.

From the graphs, the results are then expressed by a parameter called S_d , which is the equivalent air layer thickness (which can provide the same amount of resistance to vapour transmission as that of the specimens).

$$S_d = \frac{\pi^{ar} \cdot A \cdot \Delta P}{G} \quad (6.1)$$

where π^{ar} is the diffusion coefficient for water vapour in air at atmospheric pressure, A (m^2) is the test area of the specimen, ΔP (Pa) is the vapour pressure differential between the top and bottom surfaces of the specimen, and G (kg/s) is the rate of water vapour flow across the specimen in steady-state conditions.

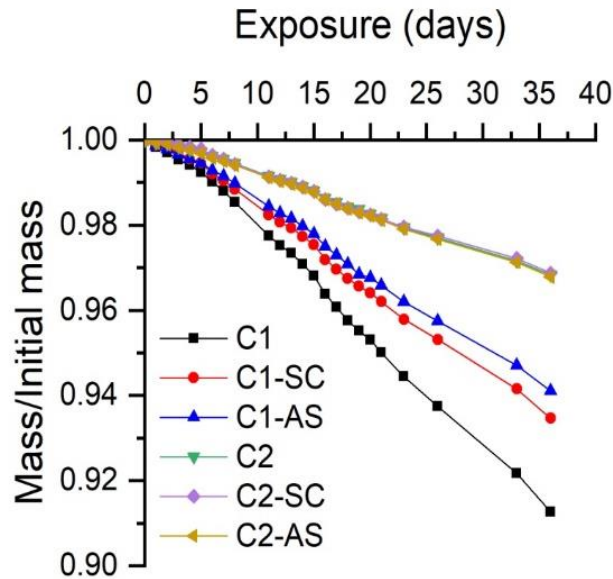


Figure 6.4. Mass variation of the measure-cell with time

S_d values calculated are shown in Table 6.1. The results show that silicone-based coatings are comparatively providing less breathability than the acrylic-siloxane based

treatment (as indicated by the higher air layer thickness), which was not well captured from the graphs.

Table 6.1. Equivalent air layer thickness values (S_d)

Samples	S_d (m)
C1	0.49
C1-SC	0.67
C1-AS	0.58
C2	1.79
C2-SC	2.25
C2-AS	2.01

6.2.6 The penetration depth of treatments

The penetration depth of both types of water-repellent treatments was measured using their property of hydrophobicity. Cubical specimens of 40 mm size were coated with the coatings using three brush strokes, on all the four peripheral sides of the specimens. The specimens were then cut open into two equal parts with a depth of 20 mm, followed by dipping in the water as illustrated in Figure 6.5, so that the cut inner surface is allowed to get in touch with water. Hydrophobicity of the treatments facilitated the identification of the depth of penetration through visual observation at the cut surface when wetted with water.

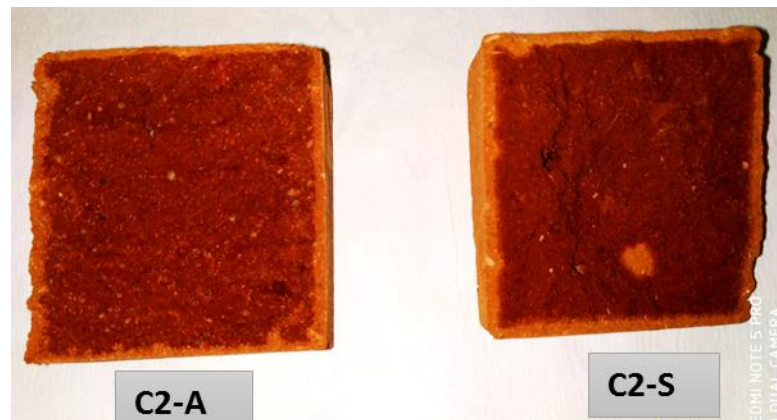


Figure 6.5. Illustration of cut specimen wetting with water to find penetration depth

For specimens C1-SC and C1-AS, no wetting of the specimens occurred when immersed in water, which suggested a minimum penetration depth of 20 mm for both the coatings in C1 brick. Whereas in C2 specimens, a wetted interior square and a dry exterior lining were observed as shown in Figure 6.6, which shows the depth at which treatments could penetrate. C2-SC showed a depth of penetration of 2 mm and the penetration depth for C2-AS specimen was measured as 1.5 mm. C1 being a highly porous brick, both the treatments were found to penetrate to the full depth of the specimens. However, the high density and low porosity of C2 brick could have caused the low penetration depth of both the treatments in C2 specimens.



(a)



(b)

Figure 6.6. Cut-surfaces of specimens wetted in water, showing the penetration depth of treatments

6.3 ACCELERATED SALT WEATHERING TESTS

Uncoated and differently coated samples were subjected to artificial weathering, with an objective to analyse the efficiency of the different coatings and to see if there is any possible

relationship between the performance of coatings and microstructure of the bricks. Salt weathering resistance was tested by exposing the specimens to sodium sulphate solution and sodium chloride solution separately. Since coated specimens were also used for the test, RILEM Test no. V 1. b (RILEM V 1.b, 1980) was followed in which drying of the specimens is recommended at 60 °C. The other standard EN12370 recommends 105 °C for drying, which could harm the layer of protective treatment.

After drying, the uncoated and coated brick specimens of 4 cm side cubes were completely immersed in the salt solution. Two parallel thin plastic sticks were provided at the bottom of each cube to avoid the bottom surface contact of specimens with the container. As per the RILEM recommendation, 10% Na₂SO₄ anhydrate was used as the solution. Na₂SO₄ was selected for the weathering studies as it is the most deleterious salt with respect to heritage porous masonry materials and also because of its abundance. Since sodium chloride is a less damaging salt and damage due to crystallization pressure is not a significant concern, only samples C1 and C2 (which showed the two extremes of behaviour with respect to salt weathering resistance – as seen previously in Chapter 4) were considered for NaCl weathering test. The test was conducted to identify and compare the response of the different type of bricks with sodium chloride and sodium sulphate exposure. 15.6% sodium chloride solution was used to immerse the cubical specimens in wet cycles, and the rest of the procedure was kept the same as that of sodium sulphate weathering test. The initial mass and dimensional measurements of the specimens were noted before subjecting to weathering cycles.

Soaking was done for 2 hours in the laboratory which was set at a temperature of 27 °C and relative humidity of 50%. This was followed by drying at 60 °C for 19 hours (overnight), to facilitate the wet-dry cycles. Then the specimens were cooled at room temperature for 3 hours. After each cycle of 24 hours, the mass change and visual signs of deterioration were documented. The solution in the container was replaced after every three days. The cyclic tests were continued until the specimens were damaged entirely, or for 120 cycles, whichever occurred earlier.

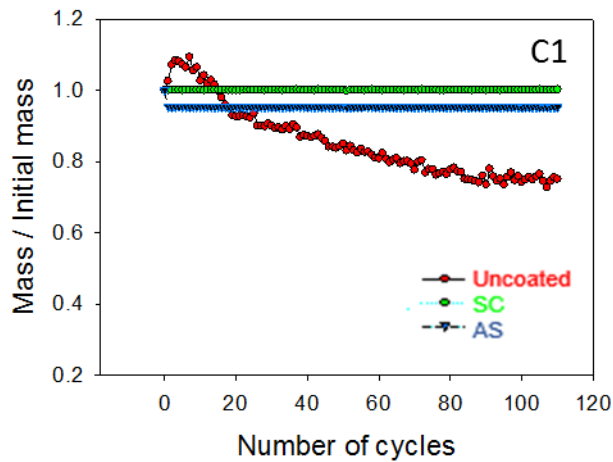
After completion of the weathering cycles, samples from the weathered specimens were analysed using MIP, along with the unweathered samples. Samples for MIP were collected from a depth of about 2 mm from the surface. The pore redistribution on salt weathering was assessed in detail from the MIP data, on calculating the relative volume fraction of pores in particular size ranges. The significance of pores of a particular size that are conducive for the crystallization process inside the material was studied using comparative analysis on pore data of unweathered and weathered samples.

6.3.1 Mass changes on accelerated weathering

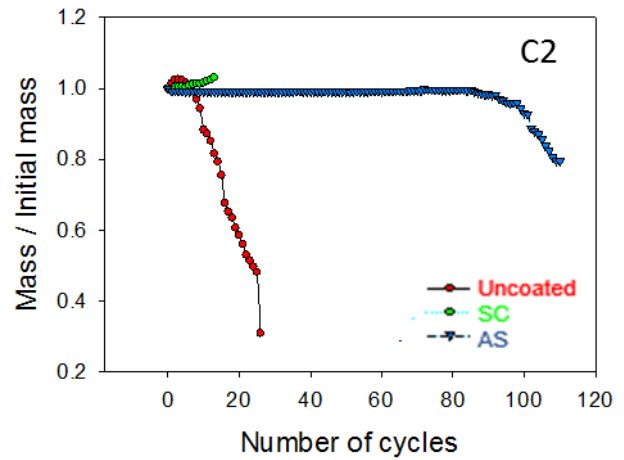
Mass loss was used to quantify the extent of deterioration in building units in addition to the visible damage observed. The performance of the coatings varied with the type of material they were applied on.

6.3.1.1 Exposure to sodium sulphate solution

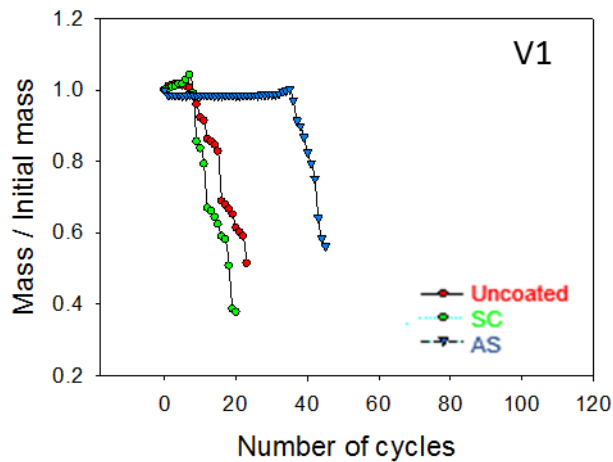
Figure 6.7 (a)-(d) show the mass variation of the uncoated, silicone-coated, and the acrylic siloxane coated samples of the four types of materials studied. Each data point is an average of three readings.



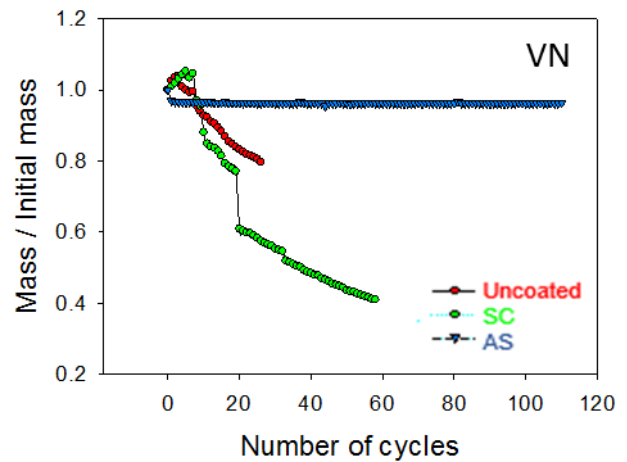
(a) C1



(b) C2



(c) V1



(d) VN

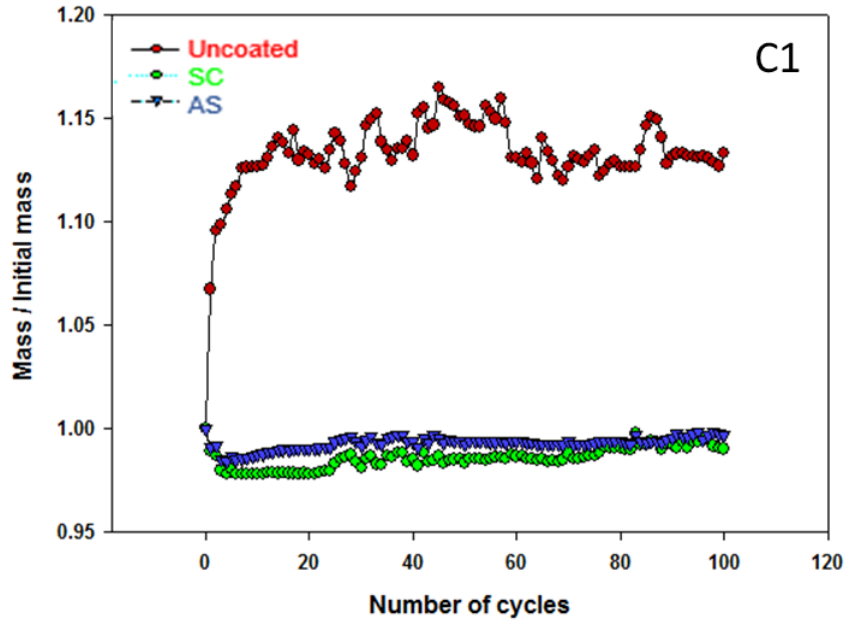
Figure 6.7. Mass changes with increasing wet-dry cycles with Na_2SO_4 solution

C1 and C2 showed the extreme behaviours with respect to mass loss and visible damages, with both uncoated and coated variants. Specimens V1 and VN had intermediate behaviour, owing to the porosity and pore structure being intermediate to that of C1 and C2. Uncoated C1 had a very low but progressive mass loss, whereas C1-AS and C1-SC specimens did not show any significant mass differences throughout the long-term test. For C2, the uncoated sample showed progressive mass loss but at a very fast rate. While coated with the acrylic-siloxane based coating (C2-AS), the mass loss was resisted remarkably throughout the cycles. Meanwhile, C2-SC specimens had a sudden mass loss without any warning at around 15 cycles, which was much lower weathering resistance than that of C2 left uncoated.

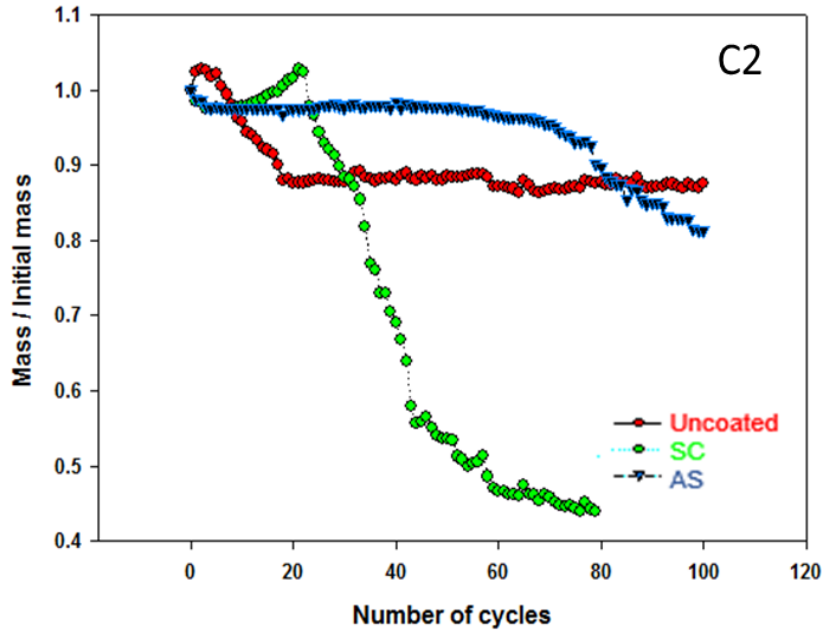
6.3.1.2 Exposure to sodium chloride solution

From the sodium sulphate weathering test, it was observed that the commonly available bricks fired at low temperatures (C1) and the wire-cut bricks fired in a modern kiln (C2) exhibited the two extreme cases of damage pattern. Sodium chloride weathering tests were carried out with these samples following the procedure as RILEM V 1.b, but using a 15.6 % solution of sodium chloride in water. Figure 6.8 shows the mass variation of the uncoated, silicone-coated, and the acrylic siloxane coated samples of the brick types C1 and C2. The uncoated samples of C1 and C2 exhibited slow mass increase up to the 60th cycle, although both showed visible signs of damage to different extents. The mass gain due to salt accumulation dominated the mass loss due to damage of specimens. C1-SC suffered no damage, but C2-SC underwent sudden mass loss as in the case of sodium sulphate exposure.

The mass of these specimens remained constant throughout the test for both the brick types coated with acrylic siloxane coating (C1-AS and C2-AS).



(a)



(b)

Figure 6.8. Mass changes with increasing wet-dry cycles with NaCl solution

6.3.2 Visual observations of damages

6.3.2.1 Exposure to sodium sulphate solution

All the uncoated specimens had an early onset of damage (within 10 cycles of immersion). Signs of deterioration like roughening of surface and deposition of powder around the samples were visible even before the beginning of the mass loss phase. For C1, the deterioration pattern was uniform, without any spalling or flaking. Whereas, the mass loss and deterioration were found to be the maximum in C2 where heterogeneous and deep damage was observed after the 6th cycle itself.

The specimens coated with the silicone-based coating (SC) exhibited distinguishable results. Except for the commonly available non-wire-cut bricks fired at a relatively lower temperature (C1), all the samples coated with the silicone-based coating (SC) underwent severe damage in the very early stages. There was no visible sign of warning except for the bulging that occurred only by the end of the drying phase that preceded the immersion phase, during which sudden, severe damage was observed. Heritage bricks (V1– SC) and the bricks made to replace them (VN – SC) showed unforeseen damage by spalling of intact flakes of thickness approximately 3 mm from all faces of the specimen. As the coating had fallen out along with these flakes, the remaining portion of brick deteriorated in the same pattern as the uncoated ones. The wire-cut brick specimen coated with the silicone-based coating (C2 – SC) broke into several pieces, without any warning, during the immersion phase. Even after it broke, the surface remained intact and smooth. Figure 6.9 and Figure 6.10 show the damages incurred to the variants of C1 and C2 specimens, respectively, after 20 cycles of weathering tests.



Figure 6.9. Damage state of specimens C1, C1-SC and C1-AS respectively after 20 weathering cycles



Figure 6.10. Damage state of specimens C2, C2-SC and C2-AS respectively after 20 weathering cycles

Every specimen coated with the acrylic siloxane-based coating (AS) performed very well in the weathering test, with negligible mass gain or loss at least up to the 100th cycle. The heritage brick specimen coated with acrylic-siloxane based coating (V1- AS) also performed very well up to 40th cycle, which was much better than the other two specimens of the same material that deteriorated severely even before the 20th cycle. Significant efflorescence was found on the surface of every acrylic-siloxane coated sample by the end of drying in almost every cycle.

Despite the better performance of the silicone-based coating (SC) in the Karsten tube test, the silicone – coated samples suffered the most considerable damage in salt crystallization test. Acrylic siloxane – coated samples performed relatively better because the acrylic siloxane-based coating acted only as a water repellent, without completely clogging the pores on the surface. The silicone-based coating had a greater depth of impregnation (around 2.5 mm, as deduced from the thickness of spalled flakes) and blocked almost all the pore entries on the surface. Due to accidental damage or erroneous application of the coating, especially with commonly used brushing method of application, there could have been discontinuities in both the coatings that served as salt solution entry points. The bulk of both types of samples got saturated with the salt solution that entered through these entry points. Subsequently, the coating AS only reduced the rate of moisture transmission from the interior to the exterior of the bricks, whereas, the coating SC blocked the entire passage. Due to reduced rate of moisture transmission, the evaporation front, and thereby the salt crystallization front was drawn to the surface, causing no damage to the AS – coated bricks. This can be substantiated by the occurrence of significant efflorescence on the AS– coated samples. On the other hand, moisture got entrapped in the bulk, unable to diffuse across the impregnated SC – coating. Evaporation occurred within the bulk of the material causing sub-florescence. When these crystals grew, they induced tensile stresses in the material by exerting crystallization pressure. As a result, the damage was sudden.

C1, the lower density brick when subjected to the salt solution eventually resulted in a homogeneous distribution of salt inside the material, which is confirmed from the uniform progressive damage patterns. The damage is somewhat similar with the application of the

coating AS, which has a cracking tendency (Stefanidou and Karozou 2016) that prevents complete sealing of the brick surface. Hence breathability is allowed for the porous material even though the solution enters inside material through some defects. In the other case, for the denser brick material C2 or with the completely sealing silicone coating (SC), salts entering will be mostly accumulated in certain places without getting distributed, resulting in the pores getting more filled. The filled pores eventually result in higher crystallization pressures, and hence more damage (Flatt et al. 2017). The C2, V1 and VN samples coated with silicone-based coating bulged and chunks got removed from the core showing a thin layer of salt deposition or deterioration from the surface (measuring 2-3 mm). Figure 6.11 shows the damaged surface of the brick C2 when coated with silicone-based and acrylic based coatings. A thin film being cracked and removed can be observed in acrylic-siloxane coated sample (AS) at 60 days of exposure, where once the film is completely removed, the specimen deteriorated like the uncoated ones. Figure 6.12 is the SEM image of the surface of specimen C2-AS after 60 days of weathering, which reveals the cracking over the thin layer of coating. Figure 6.13 again shows the case of the sudden rupture of the specimen (VN) without any warning when coated with silicone-based treatment (SC).



(a) Sudden rupture of C2 treated with SC coating at 15 cycles



(b) The thin layer of the film gets cracked and removed for C2 treated with AS coating at 60 cycles

Figure 6.11. Comparison of damage patterns with silicone-based (SC) and acrylic-based (AS) coatings

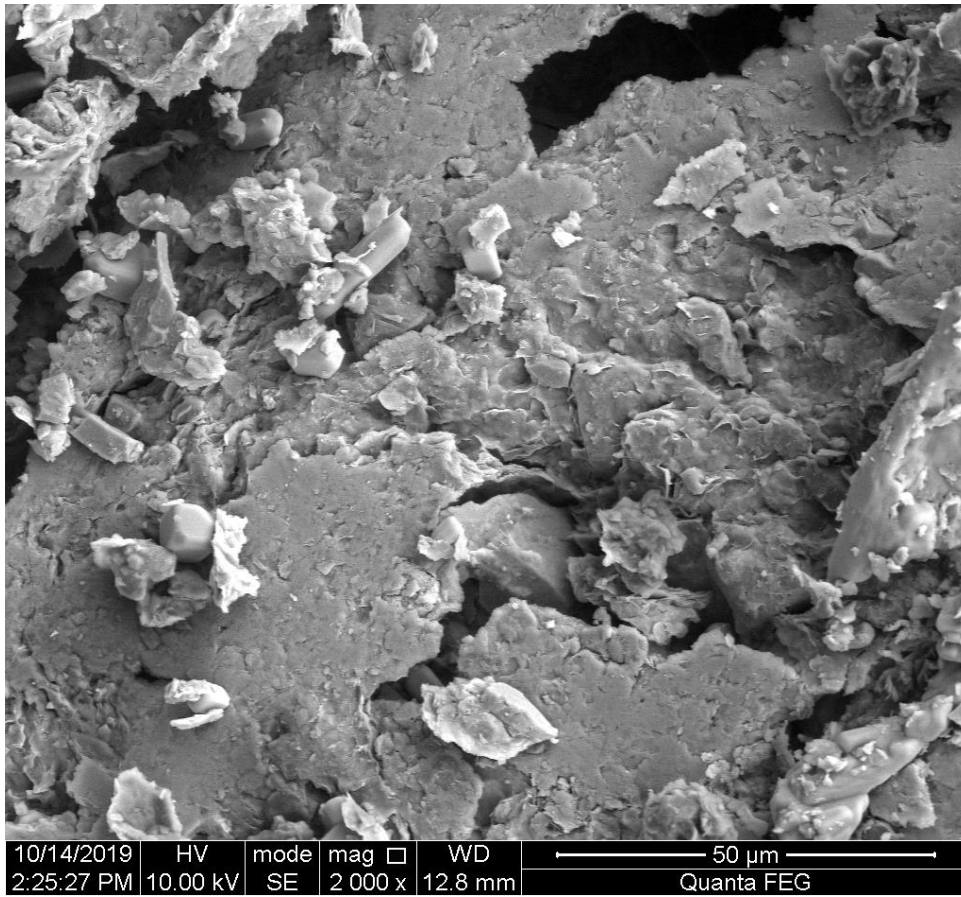


Figure 6.12. Surface of C2-AS specimen showing cracking of the acrylic-siloxane based coating



Figure 6.13. Sudden rupture of VN- specimen after 7th, 8th and 9th cycle respectively

Among all brick samples, the highly porous C1 – SC brick suffered the least damage. This could be due to a higher fraction of macropores. In a big sized pore, a crystal can undergo unrestrained growth, without exerting any crystallization pressure. A better degree of pore interconnection also helps in draining out supersaturation from smaller pores by ion transport, thereby dissipating the transient crystallization pressure. Due to the presence of a good network of large connected pores, the salt solution can easily be transported to the surface. As a result, even the highly porous C1 – SC sample performed very well in the salt weathering test.

Two different morphologies of crystals were found in the test. Long needle-shaped crystals were found in the crevices and the surfaces of degraded bricks dried at 60 °C, whereas, white layers of powdery crystals were found in the edges of broken chunks of bricks saturated with salt solution that were left to dry in the lab at 27 °C (Figure 6.14). These needle-shaped crystals should not be misunderstood to be the cause of the damage. As pointed out by Scherer (2004 b), needle-shaped crystals are a result, and not the cause, of damage. When a crack develops in the brick, the solution film becomes discontinuous. As the crystals cannot grow in lateral directions due to unavailability of pore solution, unidirectional film-fed growth leads to needle-shaped crystals.

It was also observed that the crystals, when formed in the laboratory at 27 °C, did not cause any damage to the brick. Instead, they built up to a thick deposit on the broken edges of the brick. This is because the drying at 27 °C involves a slow rate of evaporation. The solution had enough time to migrate to the surface and then crystallize. However, while drying at 60 °C, the rate of evaporation is very fast, and the solution does not have enough

time to migrate to the surface. The broken edges of the brick have many imperfections. As heterogeneous nucleation is favoured in the sites of imperfections, extensive crystallization was found at the edges rather than the flat surfaces. This is in accordance with the studies of Navarro and Doehne (Rodriguez-Navarro and Doehne 1999) on the crystallization of sodium sulphate.



(a) Long needle-shaped salt crystal
efflorescence



(b) Dense white powdery efflorescence

Figure 6.14. Different morphologies of salt crystals seen in efflorescence

6.3.2.2 Exposure to sodium chloride solution

Figure 6.15 and Figure 6.16 show the images of each type of specimen before and after 90 days of salt weathering with NaCl exposure. The damage pattern in the uncoated C1 was

homogeneous with granular disintegration. On the other hand, the damage pattern observed in the uncoated sample of C2 was heterogeneous with more visible signs of damage like powdery surface and rounding of edges. Another vital feature exhibited by the uncoated samples was massive efflorescence, that was uniformly distributed over the surface of C1 and non-uniformly distributed over C2.



(a) Before weathering



(b) After 90 cycles of weathering

Figure 6.15. C1, C1-SC and C1-AS specimens respectively before and after weathering

The C1 samples coated with the silicone-based coating (C1-SC) suffered little or no damage up to the 60th cycle, while the wire-cut brick samples coated with the silicone-based coating (C2-SC) underwent sudden damage with cracking, like their behaviour in sodium sulphate weathering test. This was followed by a period of rapid mass loss.

Both the samples coated with the acrylic-based coating (AS) performed very well in the sodium chloride weathering test. No visible sign of deterioration was observed in the samples until the 35th cycle, after which C2-AS began showing very mild signs of damage, and C1-AS showed none.



(a) Before weathering



(b) After 90 cycles of weathering

Figure 6.16. C2, C2-SC and C2-AS specimens respectively before and after weathering

However, the extent of mass loss and the severity of damage was found to be much less than that in the sodium sulphate weathering test in all the samples, regardless of their coating, if present. Other striking points of difference between the two test results are the massive efflorescence in the case of NaCl even at a high rate of evaporation and the continuous mass gain. The difference is due to the difference between the mechanisms of deterioration by the two salts.

It follows from the studies of Navarro et al. (1999) that sodium chloride tends to crystallize at the solution – vapour interface, unlike sodium sulphate that crystallizes rapidly in the bulk of its solution. In building materials, this interface is at the surface. That is why massive efflorescence was observed. Sodium chloride cannot sustain high supersaturations before crystal nucleation, unlike sodium sulphate that can generate very high supersaturations due to dissolution mediated phase transformation. As a result, the crystallization pressure exerted by sodium chloride is much lower than sodium sulphate.

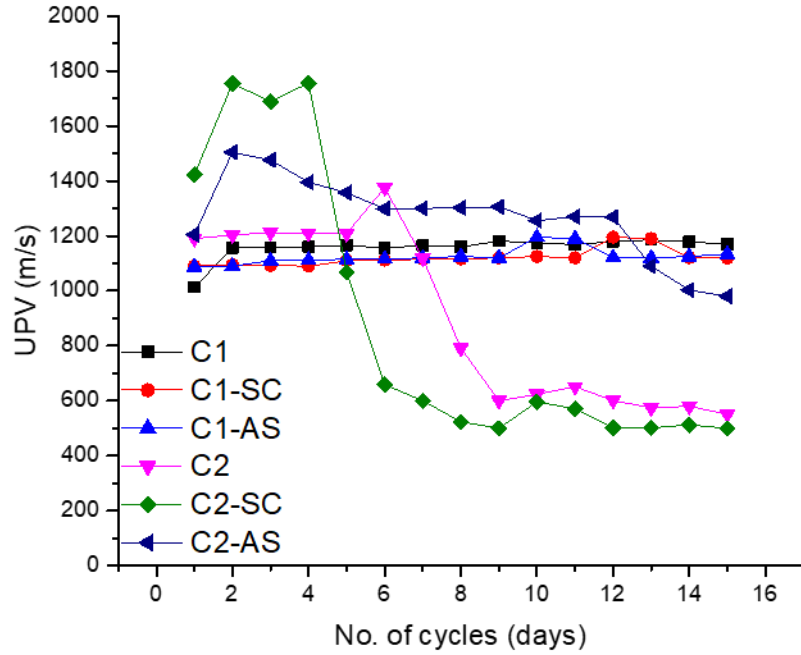
The continuous mass gain is because of sodium chloride crystals filling the micropores. Due to this, a net decrease in porosity is expected by the end of the sodium chloride weathering test. This is against the notion just established from sodium sulphate weathering test, that crystallization is favoured in a bigger pore against the adjacent smaller pores. It is because the surface tension of a saturated solution of sodium chloride salt is higher than the surface tension of the sodium sulphate solution. Subsequently, the capillary suction (rise) in smaller pores is very high for NaCl. The NaCl solution is thus easily drawn to the smaller pores due to capillary suction, and the salt slowly gets deposited there. In the

case of sodium sulphate, the solution flow due to capillary suction is slower than the rate of evaporation of sodium sulphate solution, which would result in subflorescence with damage.

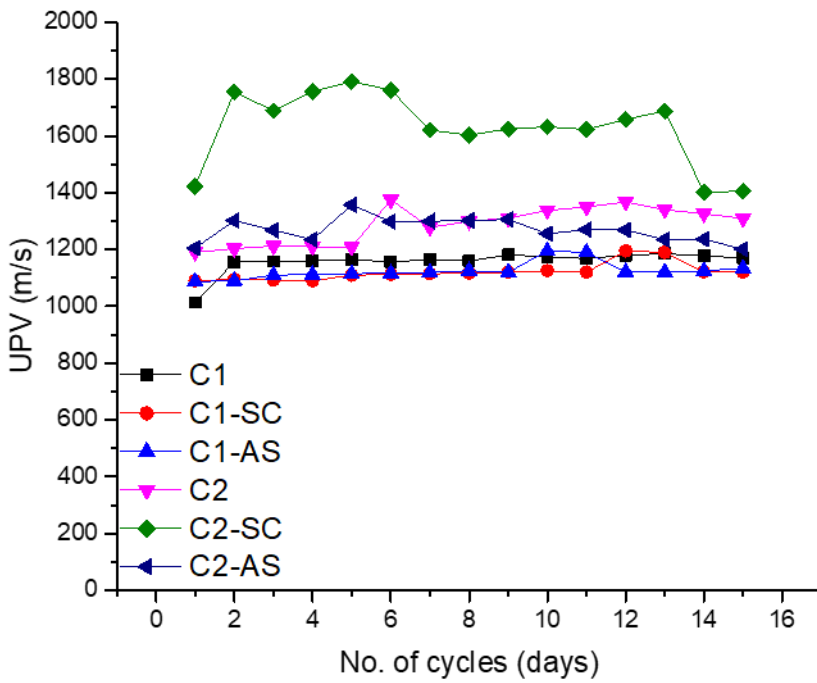
It is probably due to the same reason that the highly porous C1-SC suffered negligible damage, unlike C2-SC in the chloride weathering test. The capillary suction in large open pores of C1-SC is very weak (as it inversely depends on pore diameter). So, crystallization occurred near the surface resulting in minimum damage.

6.3.3 UPV measurements

UPV was measured for all the specimens- coated and uncoated after each drying cycle for 15 consecutive cycles (days). After 15 days of weathering, some of the specimens lost most of the surfaces, and some other specimens disintegrated into several pieces; hence the UPV readings were disrupted. Figure 6.17 shows the UPV readings for C1 and C2 specimens (both uncoated and coated variants) taken during sodium sulphate and sodium chloride exposure, respectively. It shows that the velocities become stable with uniform salt depositions inside the pores. However, this trend was seen applicable only before the onset of larger cracks. Hence, UPV represents the degradation only once larger cracks are formed, and not with the formation of microcracks and fissures, which would get filled with salts. The trend is similar with both NaCl and Na₂SO₄.



(a) Sodium sulphate weathering



(b) Sodium chloride weathering

Figure 6.17. UPV variation for the specimens during weathering

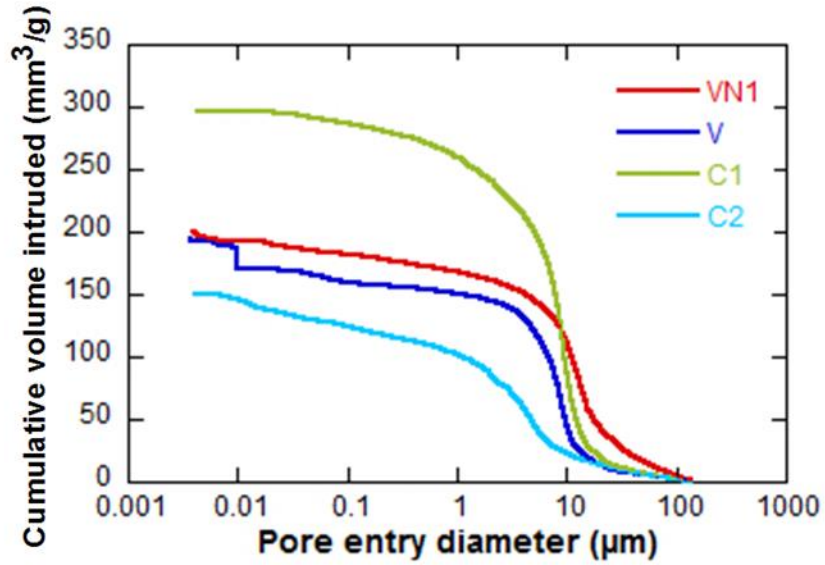
6.3.4 Modification of pore structure on accelerated weathering

There are serious limitations with respect to consideration of mass change as the only way to keep track of the damage. Mass change is not observed in those cases when damage occurs as cracking without any material loss. Such damage can be identified by studying the pore structure. Mercury Intrusion Porosimetry is an excellent tool, which measures the pore system redistribution and damage objectively, and gives information on the location of salt deposition and extent of the damage.

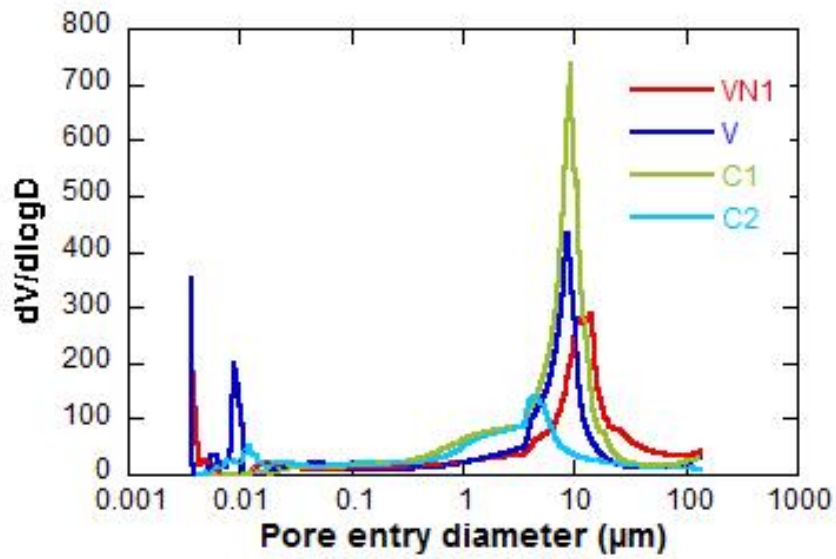
6.3.4.1 Exposure to sodium sulphate solution

The cumulative intrusion and differential intrusion curves for the unweathered samples, which were later subjected to accelerated weathering with sodium sulphate solution are shown in Figure 6.18. As indicated from the physical properties, C2 has the densest and highly vitrified structure, which is evident from its least cumulative intruded volume and corresponding small threshold pore entry radius. The differential intrusion curve also points towards the same indication, from the minimum critical pore diameter of C2 among all other brick samples. C1, which is the other commercial brick sample, is at the opposite end, showing the maximum intrusion and very large critical pore size diameter. The other brick samples V and VN fall in between C1 and C2 with respect to the pore distribution; further, both V and VN showed almost similar distribution. From the MIP results of the unweathered bricks, it is evident that C2 is distinctly less porous as compared to VN. However, it can be seen from the strength data, that both these bricks almost had the same level of strength – this could possibly be attributed to the difference in the mineralogy of the bricks that was

described in the XRD results during characterization of the materials in Chapter 4. While C2 has a majority of quartz and some feldspar, the opposite trend is seen for VN.



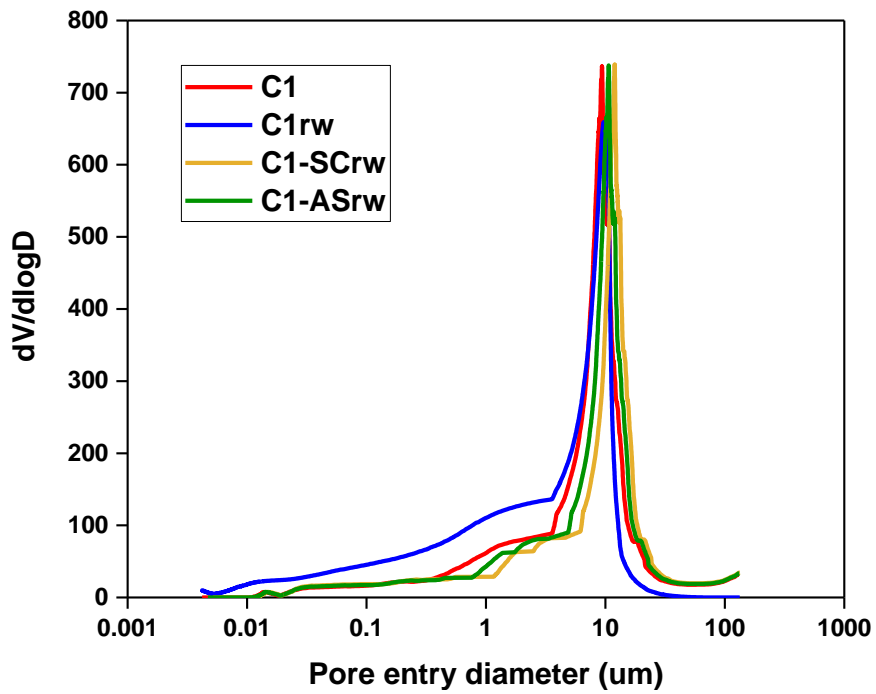
(a)



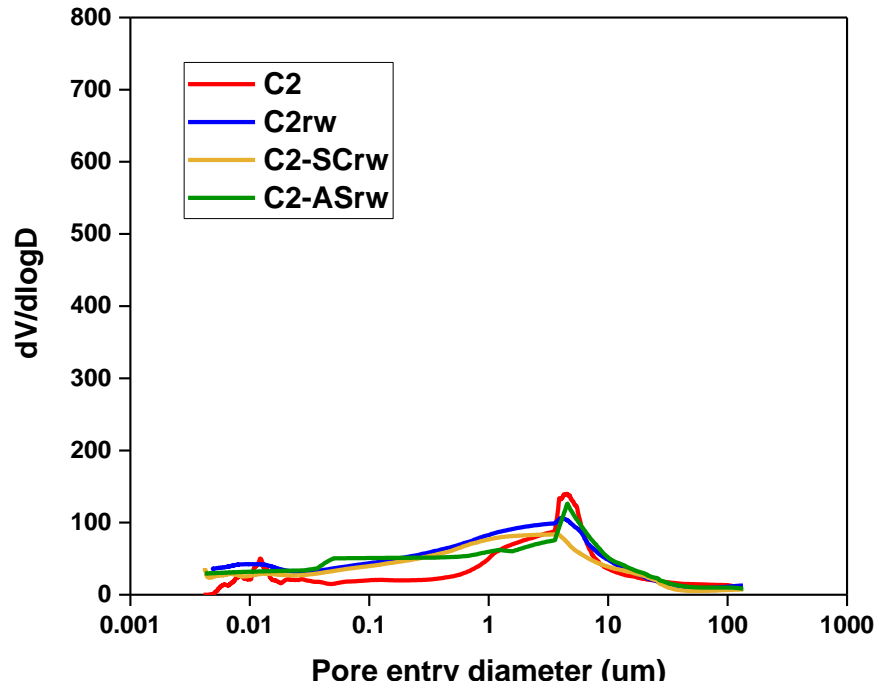
(b)

Figure 6.18. (a) Cumulative intrusion curves (b) Differential intrusion curves

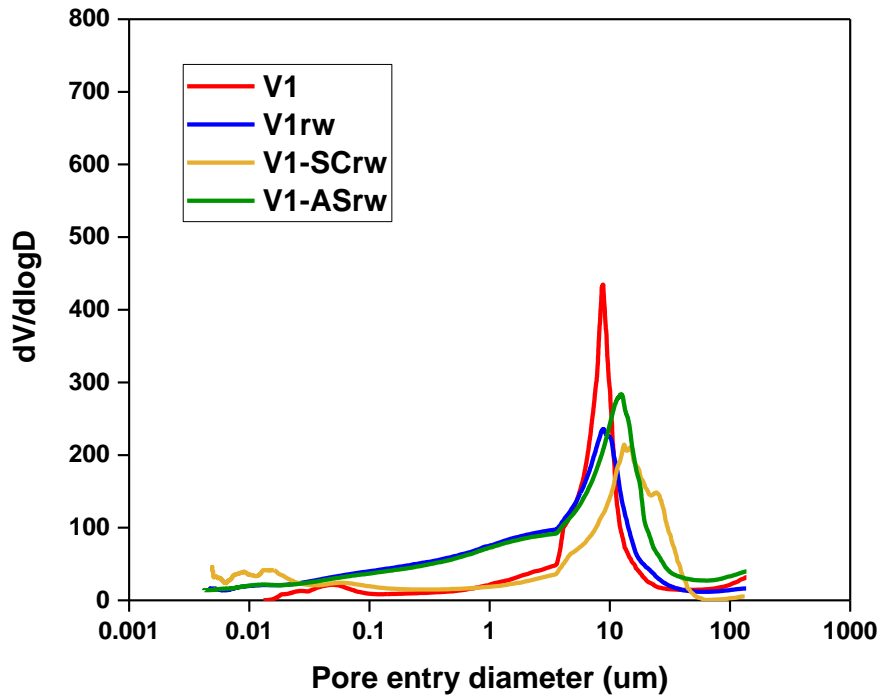
Evaluation of the effectiveness of different coatings is shown in Figure 6.19 (a) - (d) through the differential intrusion curves. Each figure compares the differential intrusion curves of unweathered and weathered samples- coated and uncoated. Only the cases C1 and C2 are being discussed in detail since these are representative of the typical behaviours of two different microstructures.



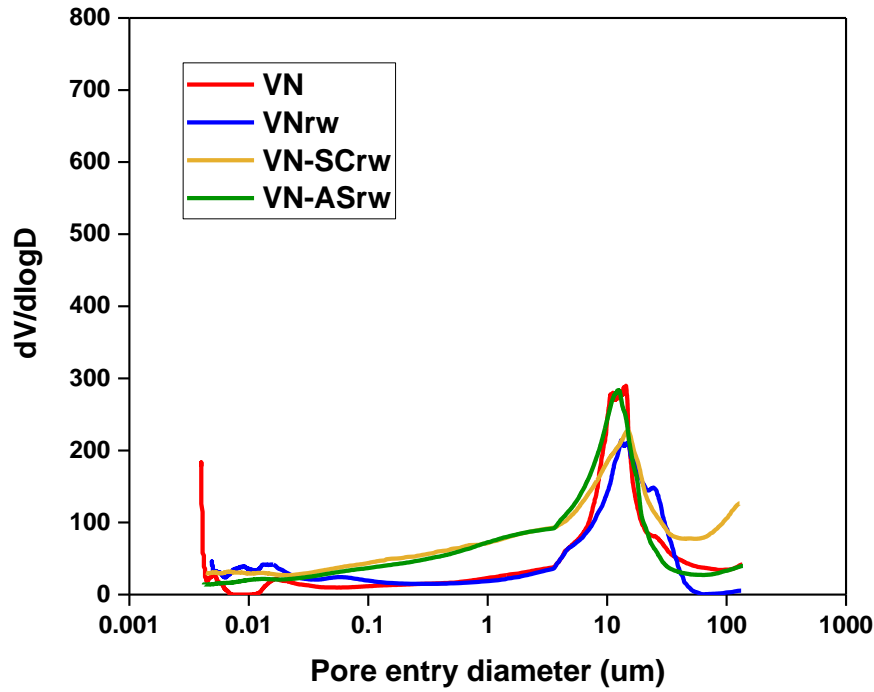
(a)



(b)



(c)



(d)

Figure 6.19. Comparison of differential intrusion curves for unweathered and weathered specimens with coatings with Na_2SO_4 (a) for C1, (b) for C2

C1rw indicates the brick C1 after weathering, C1-SCrw denotes the brick C1 which is treated with the silicone-based coating (SC) after weathering, and C1-ASrw refers to brick C1 treated with acrylic-siloxane based coating (AS) after weathering. The nomenclature pattern is similar to the other specimens.

In C2, where the fraction of smaller pores was high, a reduction in the amount of pores was observed because of the possible deposition of large amount of thenardite and mirabilite precipitates. Whereas for C1 where a larger fraction of capillary pores or macropores was present, the pore-redistribution suggests much lesser precipitation inside the pores, but more towards the surface of the bricks - detected as efflorescence. Thus, the pore

size redistribution data from MIP here confirms that efflorescence was more seen on bricks with larger pores where chances for sub-florescence was less, which was previously suggested from the visual damage mapping. If the differential intrusion graphs of salt weathered samples are subtracted from the differential intrusion graphs of fresh samples in each case (from Figure 6.19), the remaining portion denotes the pores filled with the salt, which is very high in case of C2 and almost negligible in case of C1. This supports the observation from Benavente et al. (2004). Also, the critical pore sizes were almost unaffected between unweathered and weathered samples. A minimal reduction of critical pore diameters for samples C2, V and VN was observed, which indicates that a large share of the most common sized pores was slightly filled by the crystals of sodium sulphate.

The relative volume fractions of pore sizes in various ranges were plotted using the data obtained from MIP for the various brick samples, and are shown in Figure 6.20. C1 denotes the sample collected from C1 specimen before subjecting to accelerated weathering, and C1rw denotes the sample collected from the same specimen after subjecting it to accelerated weathering with sodium sulphate solution according to the standard procedure in RILEM V 1.b, 1980. This analysis indicates an important implication of the salt crystallization mechanism and the associated pore sizes to it. Comparison of particular range of pore sizes in any type of specimen before and after weathering (say comparing C2 and C2rw), an increase in the volume fraction of macropores (pores sizes 100-10 μm) indicates the new cracks formed, while a decrease in the pores between 10-1 μm could be due to the combined effect of increase in relative volume of pores $> 10 \mu\text{m}$ and possible salt deposition. Pores in size ranges between 1-0.2 μm were understood as the most noteworthy, where the

phenomenon of salt crystallization would have occurred. The pores in that particular range (1-0.2 μm) constantly faced a decrease in volume fraction of pores during weathering, possibly because of the deposition of sodium sulphate crystals during the crystallization process. The pores of size less than 0.2 μm were found to be unaffected (without any reduction in volume fraction) with respect to any formation of crystals in them. Though a slight increase in these pores (smaller than 0.2 μm) was observed in most samples, this could be due to the salt crystal deposition in other pores, which would decrease the size of some pores to sizes less than 0.2 μm .

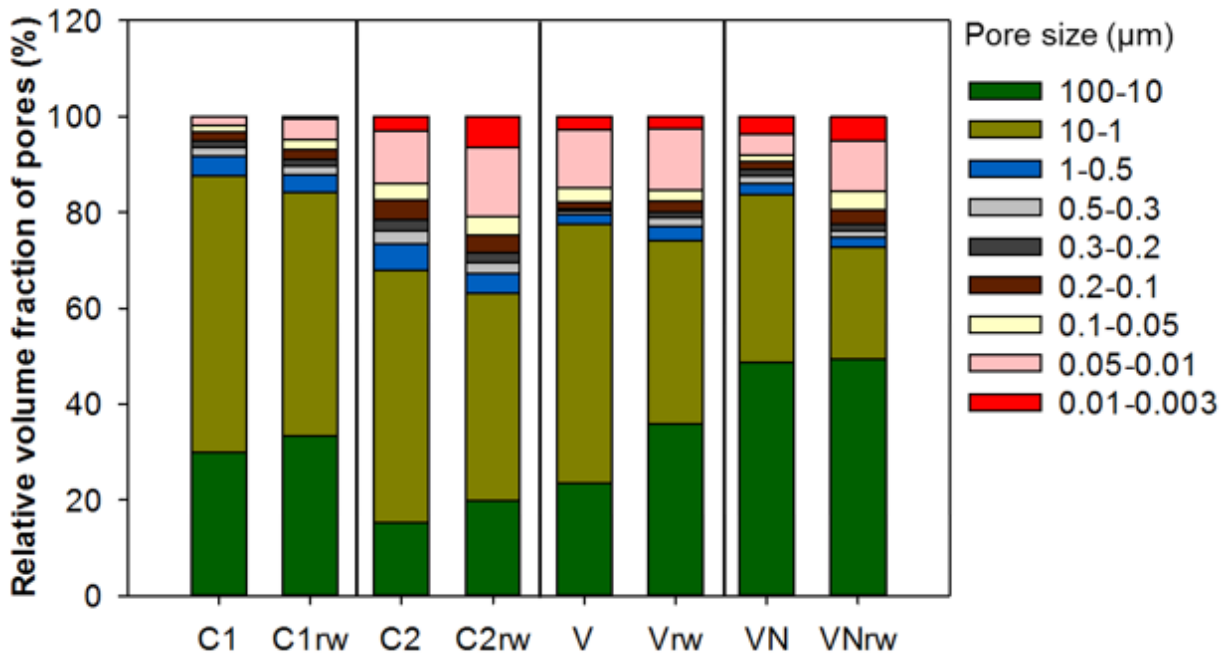


Figure 6.20. Relative volume fraction of pores of various size ranges for unweathered and weathered samples

6.3.4.2 Exposure to sodium chloride solution

Figure 6.21 (a) and (b) shows the differential intrusion curves for the specimens C1 and C2, respectively. For C1, as expected from the similarities in the visual damage patterns between sulphate weathering and chloride weathering, the curves were very identical with each other. The curves for both the coated specimens (C1-SC and C1-AS) curves were overlapping with that of unweathered C1 specimen. This indicates both the coatings could prevent any action of weathering on the material and preserve the material as such even after 100 days of severe exposure - with no difference among the type of coating. Unlike the case of sulphate weathered specimens, uniform salt deposition occurred in uncoated C1 specimens when subjected to weathering cycles, which shows a difference in the 'C1-cl' curve. In the case of samples from brick C2, critical pore size of the curve for C2-AS cl is overlapping with that of uncoated C2. This observation again indicates the higher efficiency of AS coating compared to that of SC. The weathered samples, which were uncoated and those coated with silicone-based treatment (C2-SC) exhibited overlapping differential curves.

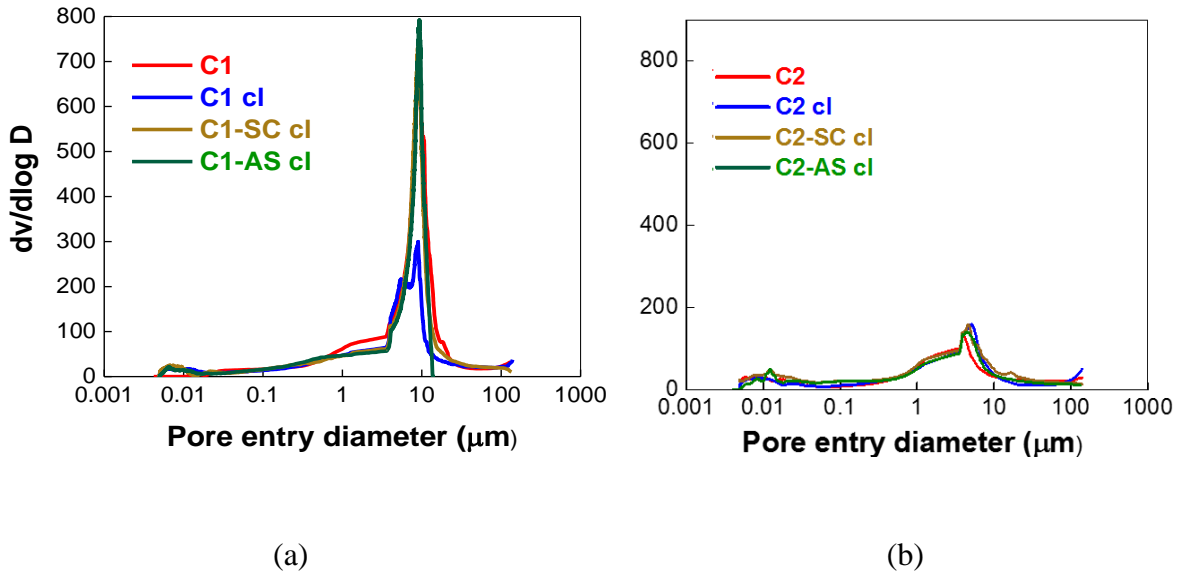


Figure 6.21. Comparison of differential intrusion curves for unweathered and weathered specimens with coatings with NaCl (a) for C1, (b) for C2

6.4 DESALINATION OF WEATHERED SPECIMENS

Poulticing using cellulose pulp was applied on artificially weathered samples for desalination, to remove the salts inside the pores. As the deposited salts are removed, this process would facilitate quantifying the actual damage by opening up all the fissures formed during crystallization damage. The effect and efficiency of the desalination process using cellulose poulticing were studied using Scanning Electron Microscopic imaging and porosity measurements with Mercury Intrusion Porosimetry.

6.4.1 Scanning Electron Microscopy

The effect of desalination on weathered samples was examined by capturing SEM images on samples before and after desalination. Cellulose poulticing was found practical in removing

salts from the pores, for both sodium sulphate and sodium chloride salts, which is illustrated in the SEM images shown in Figure 6.22 - Figure 6.24.

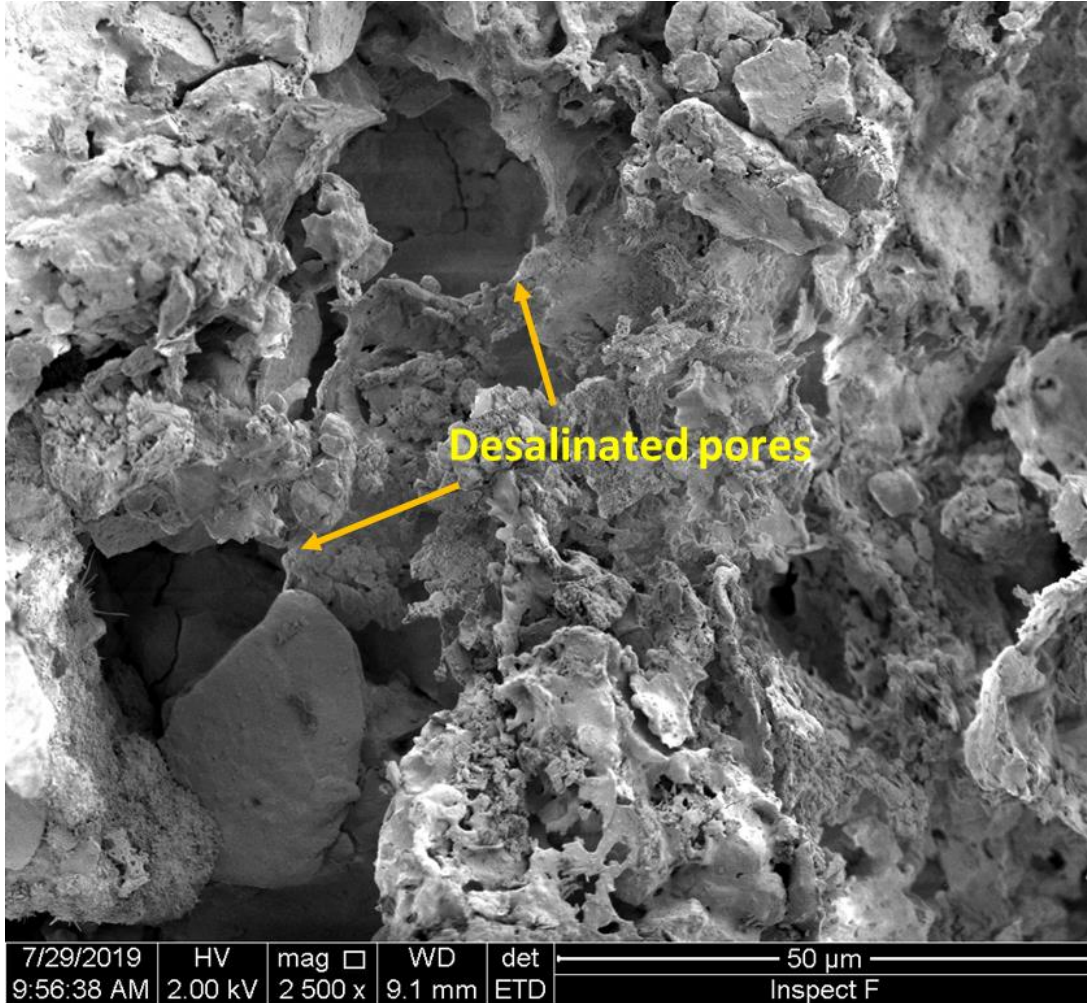
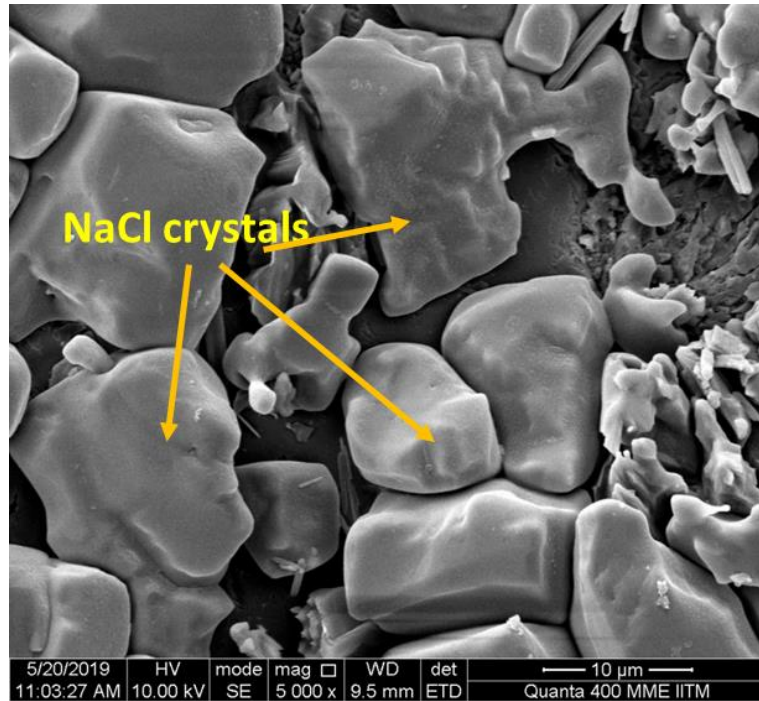


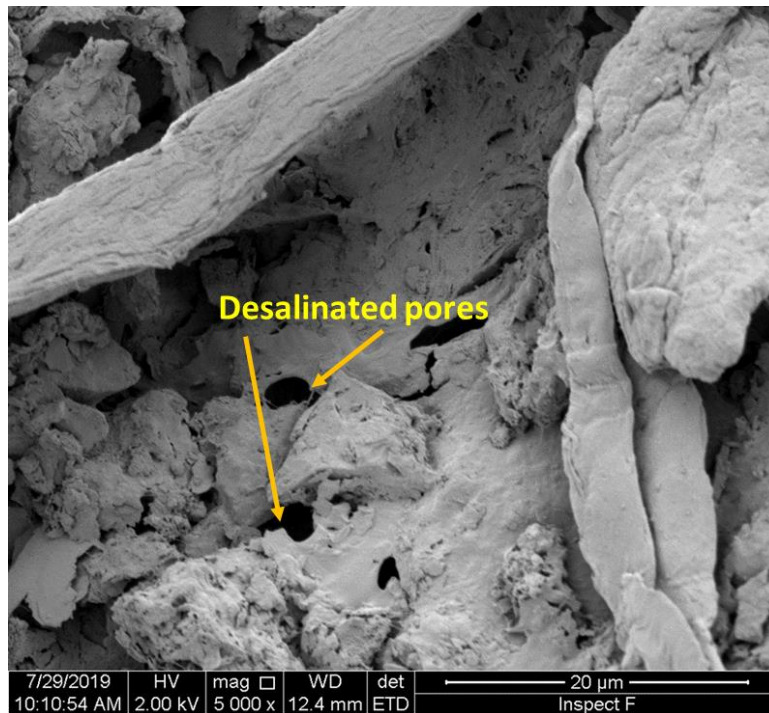
Figure 6.22. Interior of weathered (with Na_2SO_4) C2-SC sample after desalination

Figure 6.22 shows the interior of a weathered (with Na_2SO_4 exposure) C2-SC sample after desalination (sample was taken at a depth of 3-5 mm from the surface). Larger pores opened up without any salts in them are observed in this figure, which is indicative of the

efficiency of cellulose poulticing in removing the sodium sulphate salts from the bricks. The poulticing was also applied in samples subjected to NaCl weathering. Figure 6.23 shows the surface of a weathered sample (C1) with NaCl exposure, before and after desalination. The weathered surface clearly exhibited larger NaCl crystals almost completely covering the exposed area. The image of the sample surface after desalination showed that the NaCl crystals were completely removed from the surface, and in addition, new small pores were opened up from which salts would have possibly removed. Figure 6.24 shows SEM images taken on desalinated samples collected 3-5 mm deep from the surface of a weathered uncoated C2 sample (with NaCl). The large group of micropores observed shows that NaCl could deposit in pores of such smaller sizes, and poulticing could remove NaCl salts even from these small pores. However, SEM images are insufficient to quantify the efficiency of salt removal fully.

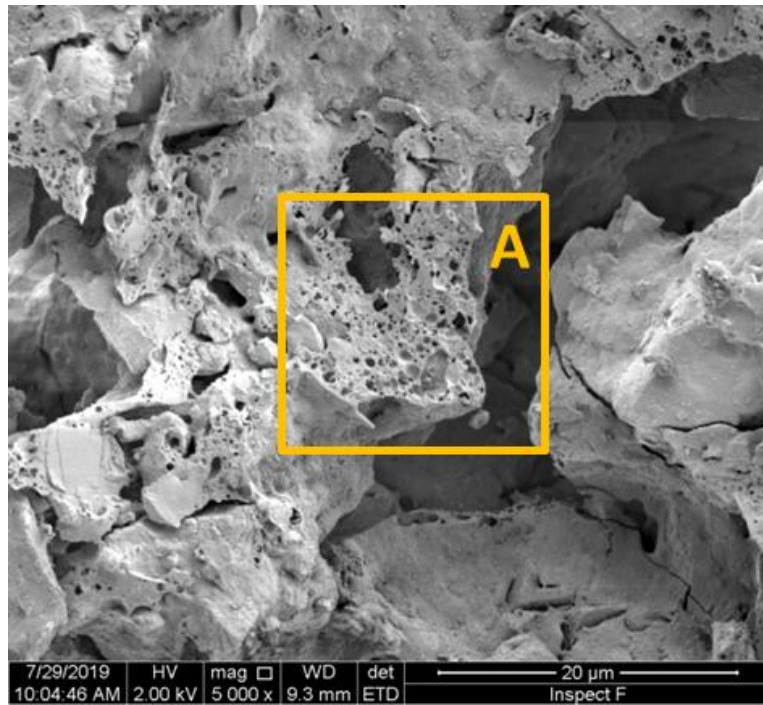


(a) Surface of a weathered uncoated C1 sample showing NaCl crystals



(b) Surface of the sample after desalination showing pores opened-up

Figure 6.23. Surface of weathered (with NaCl) uncoated C1 sample before and after desalination



(a) Interior of the desalinated sample showing micropores



(b) Magnified view of 'A' marked in the previous figure

Figure 6.24. Interior of weathered (with NaCl) uncoated C2 sample after desalination

6.4.2 Porosity measurements

From the assurance that cellulose poulticing practically works for both Na_2SO_4 and NaCl salts, Mercury Intrusion Porosimetry was carried out in the desalinated samples to identify the actual pore structure and pore distribution on weathering, excluding the effect of possible salt deposition.

Total porosities were measured for each specimen - before weathering, after accelerated weathering and after desalination of accelerated weathered specimens, using MIP. The total porosities were then compared for each type of specimen and in different salt solutions (Na_2SO_4 and NaCl) to evaluate the efficiency of poulticing in desalination, as shown in Figure 6.25. Comparing the change in porosities on desalination among sulphate weathered samples and chloride weathered samples, it is observed that cellulose poulticing is more efficient in removing sodium sulphate salts than sodium chloride salts. Due to the greater occurrence of macropores in the case of C1 samples, sodium sulphate salt crystallization and deposition is not highly favoured. The reason is the dissolution-mediated phase transformation of sodium sulphate to reach supersaturations in smaller pores. This is evident from the observation of the negligible difference in total porosity values before and after desalination in C1, C1-SC and C1-AS samples as seen from Figure 6.25 (a). C2, with its inherent micropores and newly formed micro-fissures on weathering, facilitated easy crystallization and precipitation of sodium sulphate salts, which were then removed on desalination. Whereas, the difference between total porosities before and after desalination in case of chloride affected samples are much higher (Figure 6.25 b). This is because NaCl salt does not face phase transitions, but gets precipitated and deposited on evaporation. Hence, a

remarkable number of macropores in C1 would get filled with NaCl salts. The accumulated NaCl salts from C1 were then removed on desalination resulting in an increase of up to 13% total porosity.

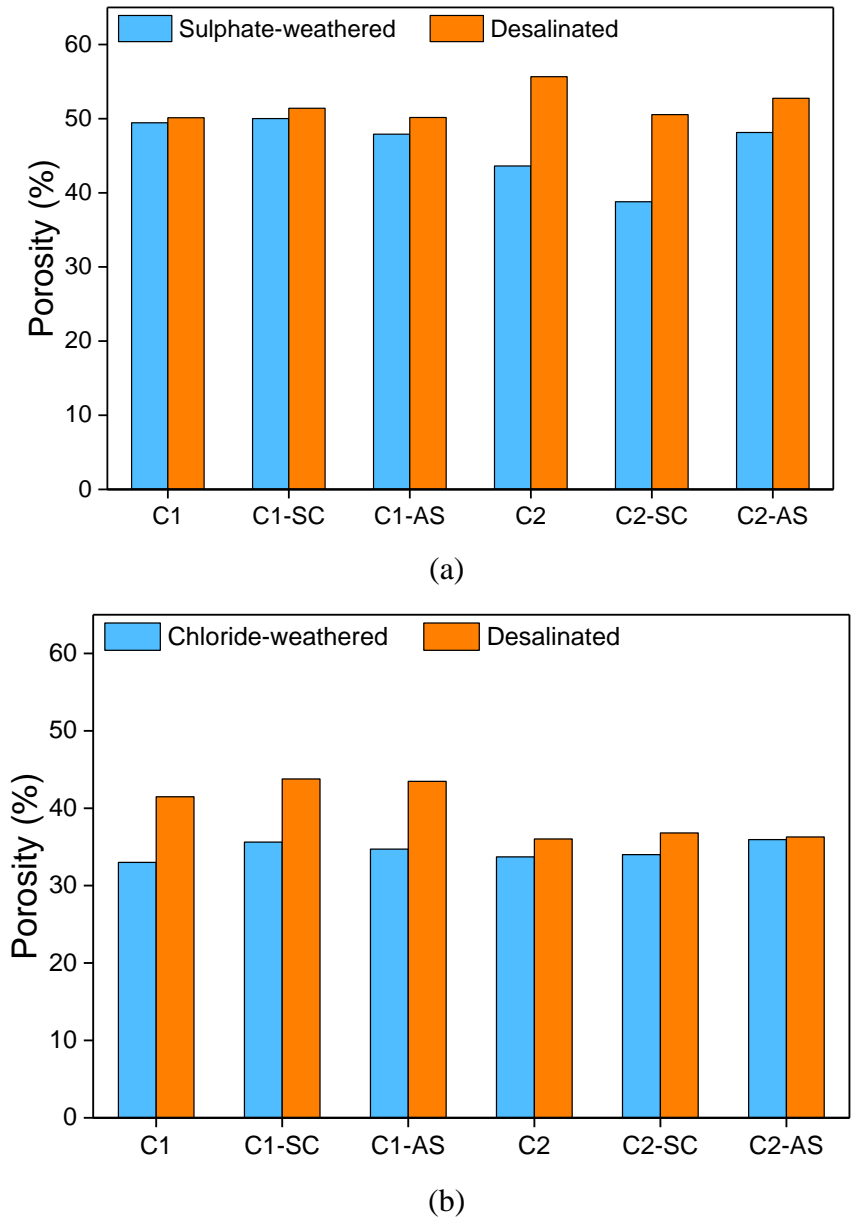


Figure 6.25. Comparison of total porosity values before and after desalination on (a) Samples weathered with sodium sulphate (b) Samples weathered with sodium chloride

In the case of C2, the exposure of sodium chloride solution resulted in the deposition of NaCl crystals in the larger portion of micropores which are abundant in the C2 system. Smaller ionic size and easy mobility of NaCl aids its deposition in micropores. Much higher capillary action is required to remove these salts from the micropores- which would result in a decreased efficiency of desalination in C2 bricks when affected with NaCl.

6.5 SODIUM CHLORIDE SPRAY TEST

6.5.1 Mass changes and visual damages

Mass changes were measured for the coated and uncoated specimens subjected to NaCl spray in the spray chamber after every 15 days, for a period of 460 days, and are shown in Figure 6.26. No noticeable disintegration had occurred to any of the samples after the 460 days of wet-dry spray test. This could be because of the lesser intensity of the spray test, with respect to the concentration of NaCl solution and the low temperature at which drying was facilitated. Drying at low temperature could prevent salt crystallization inside the pores, and move the mechanism towards evaporation and subsequent efflorescence formation on the external surface of the material. Though there was no disintegration of specimens, mass changes were observed which, along with the visual damages, can represent the salt weathering resistance of various specimens. No significant mass change was observed for all the specimens irrespective of the coating category, for the first 50 days of spray test. After 50 days, mass variations were exhibited by specimens C2 and C2-SC. The sudden mass increase in the few specimens was followed by mass loss and degradation in the next 100 cycles. The

specimens degraded were the same kind that showed heavy deterioration in both the cases of sodium sulphate and sodium chloride immersion weathering tests (following RILEM V 1.b standard). Specimen C2 was found to have a low weathering resistance than C1. With respect to the type of coatings, long-term spray test shows that C2-SC degrades at a faster rate than C2 uncoated. C2-AS (C2 when coated with acrylic siloxane coating) showed a high resistance and stability in mass, indicating that acrylic siloxane-based treatment could protect the material from salt weathering. C1 specimens, both uncoated and coated variants had a stable mass without any noticeable degradation throughout the cycles.

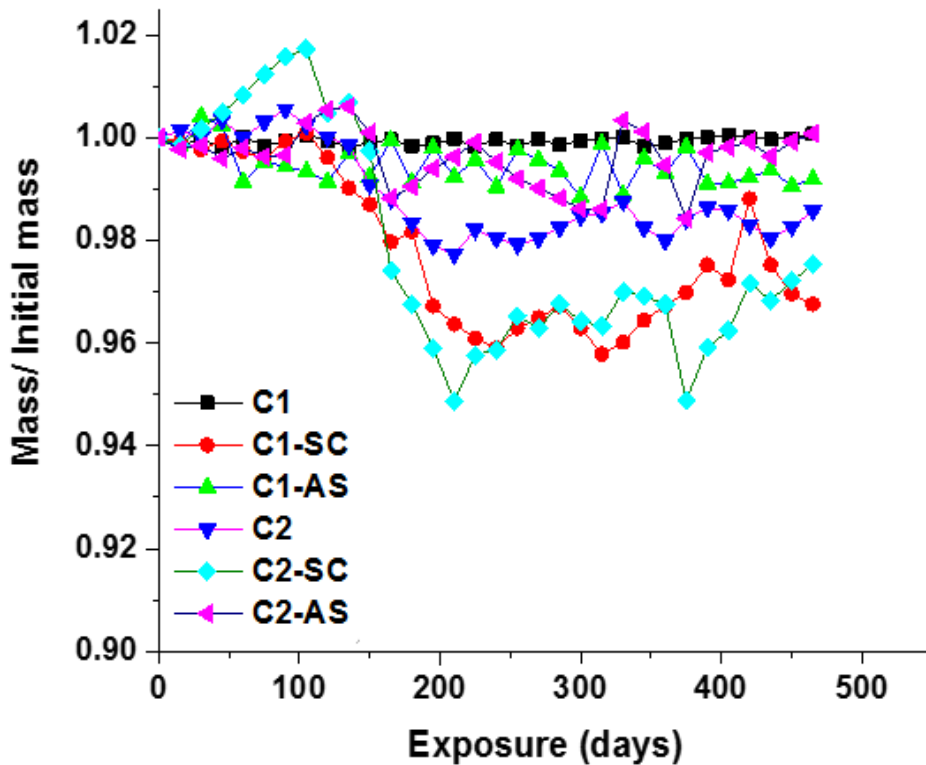


Figure 6.26. Mass changes with increasing exposure with NaCl spray

Figure 6.27 shows the images of specimens after 460 days of NaCl spray test. Similar to the observation from mass changes, no significant deterioration was observed in any of the samples, though heavy efflorescence was seen in both the uncoated variants of C1 and C2 specimens.



(a) Specimens C1, C1-SC and C1-AS respectively



(b) Specimens C2, C2-SC and C2-AS respectively

Figure 6.27. Images of specimens after 450 days of NaCl spray test

6.5.2 UPV measurements

Ultrasonic Pulse Velocity was measured for the specimens C1 and C2 - coated and uncoated after every 15 days, for a period of 450 days of sodium chloride spray test, and the variation is shown in Figure 6.28. Due to the absence of any destructive damage to the samples throughout the study, no major disruption was seen in the UPV readings too. After 150 days of weathering, specimens C2-SC and C2 showed a slight decrease in the UPV values, which is related to the mass loss shown by them.

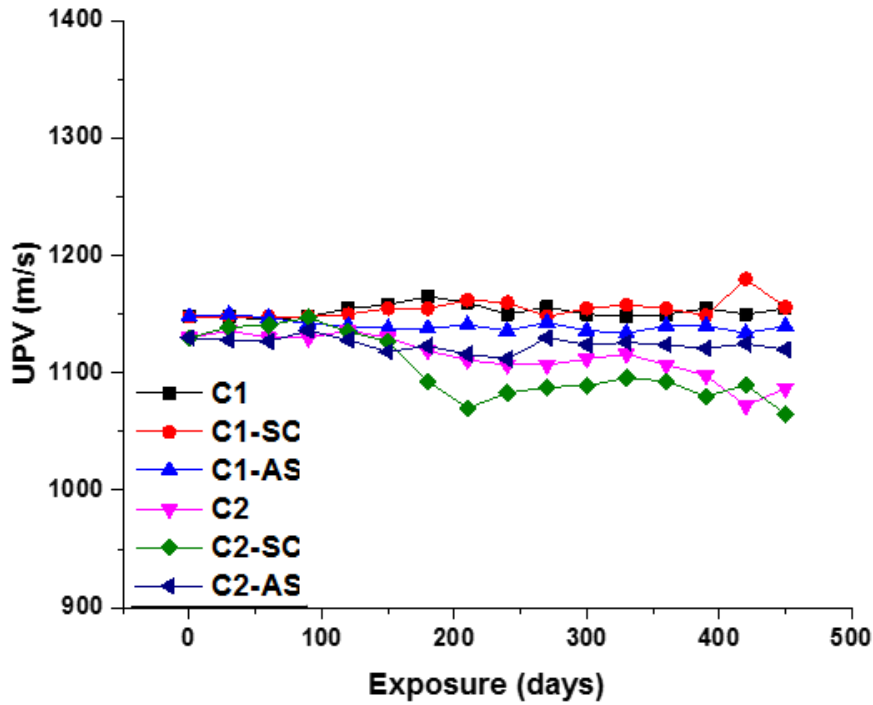
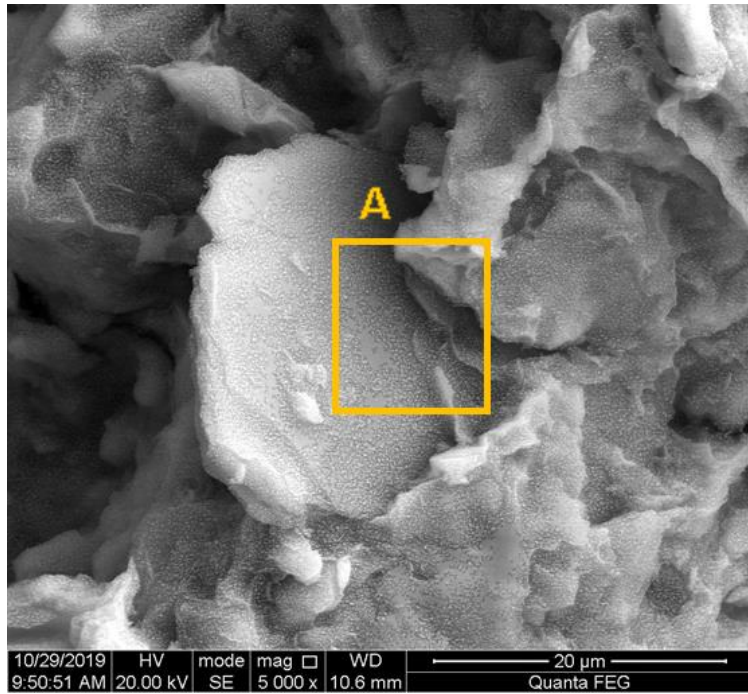


Figure 6.28. Ultrasonic pulse velocity values for the specimens during NaCl spray test

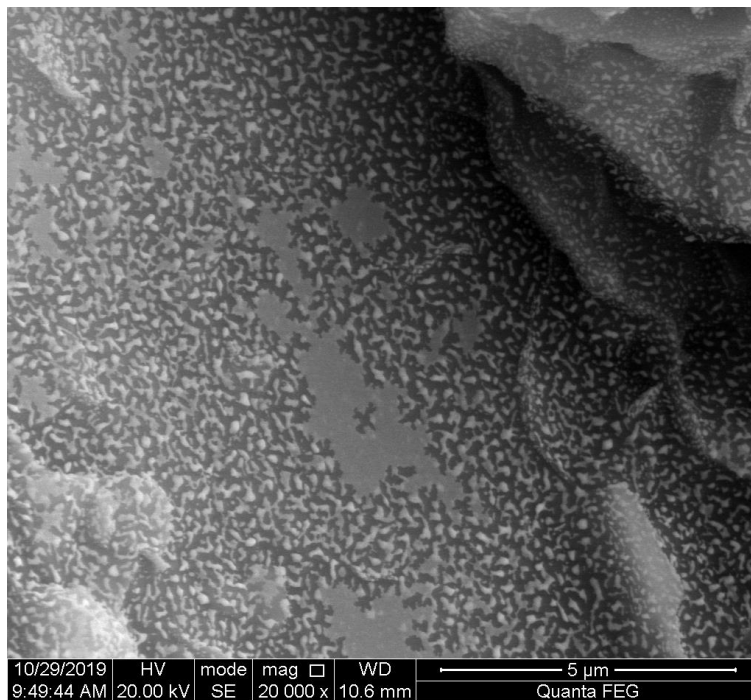
6.5.3 Microstructure modification

6.5.3.1 Scanning Electron Microscopic images

SEM images did not show any micro-fissures or intra-granular or intergranular cracks in the microstructure of the specimens subjected to NaCl spray. Salt deposition was observed, but neither covering all the pores nor filling the pores completely. Figure 6.29 (a) shows an SEM image captured for C1 specimen after the salt spray test. Much smaller precipitates of NaCl were observed over the surfaces of quartz grains - at the nanoscale. Figure 6.29 (b) is a magnified view of the area 'A' marked in Figure 6.29 (a). This formation would have happened because of the controlled atomized spray technique used to provide NaCl exposure to the specimen. Here, the precipitates were evenly distributed on the surfaces, and not preferentially inside the pores - diminishing the chances of any damages. Figure 6.30 shows macropores in sample C1, which is very clearly seen as unfilled by salt crystals. The salt deposition was not observed on most of the pores, which further removes the chances of growth restraint to crystals, causing stresses to pore-walls. Figure 6.30 (b) is the magnified view of area 'B' marked in Figure 6.30 (a). Even the thickest of the efflorescence observed in the exterior surface of specimens showed much smaller NaCl crystals clubbed together, as shown in Figure 6.31, rather than the larger (5-10 μm) octahedral NaCl crystals of sharp boundaries as observed in the case of NaCl immersion weathering test (Figure 6.23 a). This observation again indicates the difference in the crystal morphology of NaCl produced in immersion weathering test and spray type of weathering test.

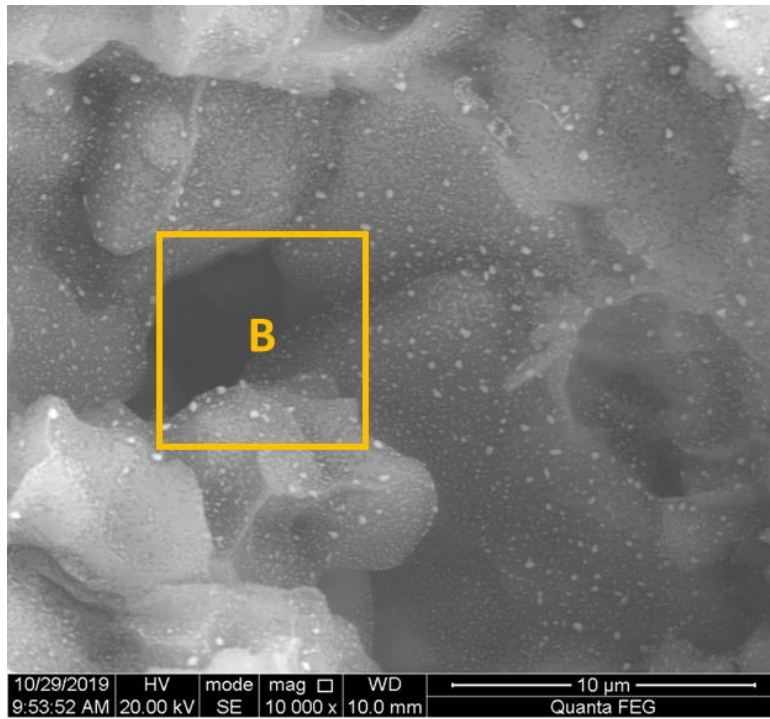


(a)

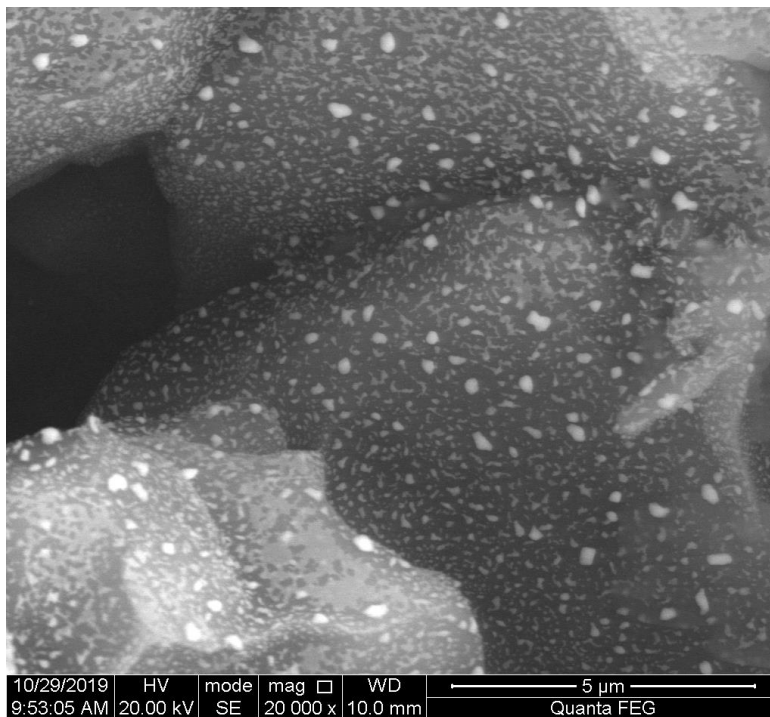


(b)

Figure 6.29. SEM image of C1 specimen after being subjected to NaCl spray test



(a)



(b)

Figure 6.30. SEM image showing the larger unfilled pores in C1 samples after salt spray test

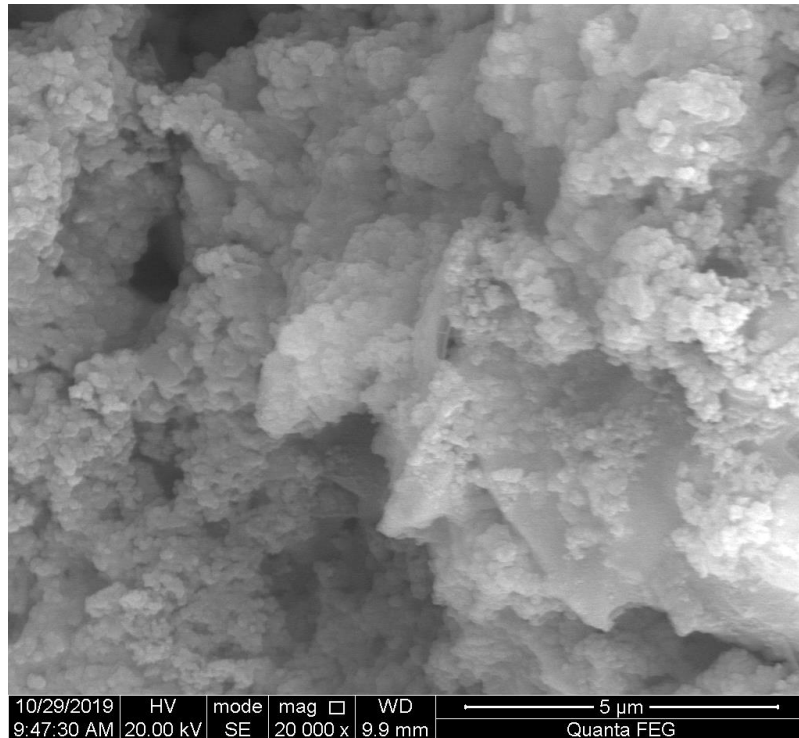
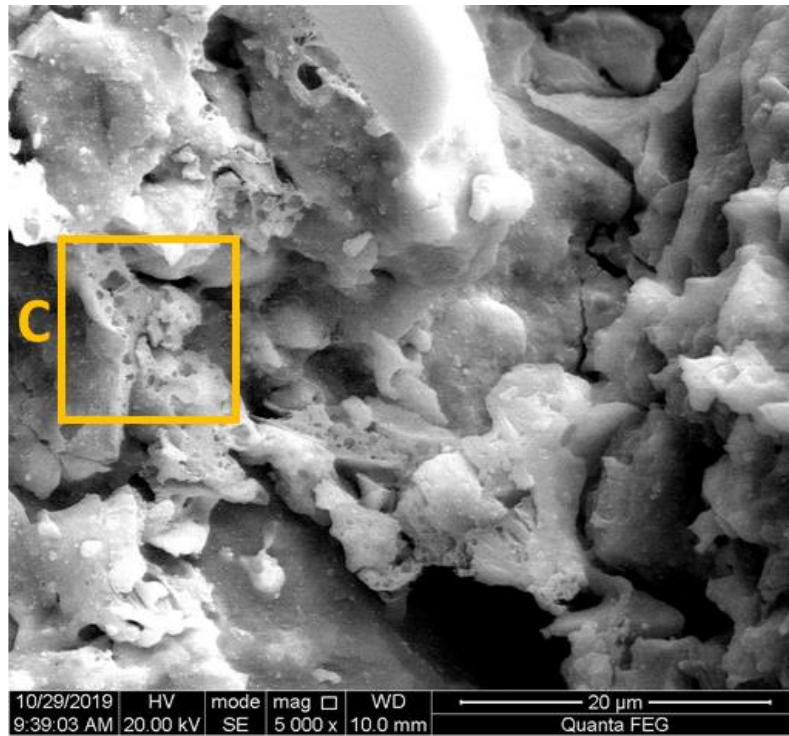
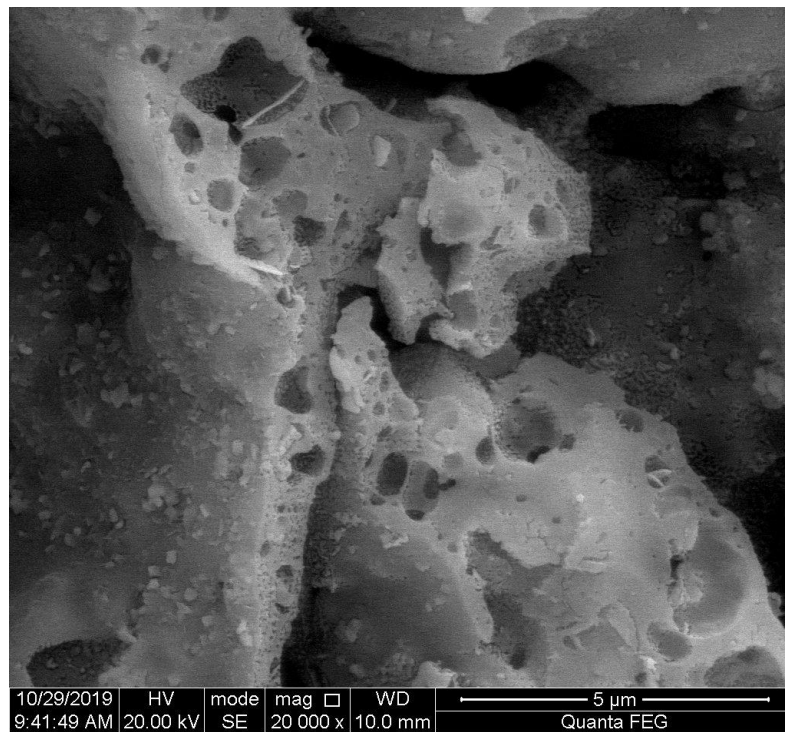


Figure 6.31. NaCl efflorescence in the exterior surface of a specimen subjected to salt spray test

Cellulose poulticing for desalination was applied in the specimens which underwent the long-term salt spray test. The effect of cellulose poultice desalination was found to be similar in the case of NaCl spray test, to that of NaCl immersion weathering test as per RILEM V 1.b 1980. The newly opened pores due to salt removal were found to be non-uniformly distributed, showing a preferential absorption of salt crystals from pores at certain locations inside the brick matrix, and not at other parts. Figure 6.32 shows the opened pores due to desalination in sample C1, which was subjected to NaCl spray test. Figure 6.32 (a) shows the non-uniformity in the distribution of opened pores due to desalination, and Figure 6.32 (b) shows the magnified view of area 'C' magnified from Figure 6.32 (a), which shows the opened desalinated pores.



(a)

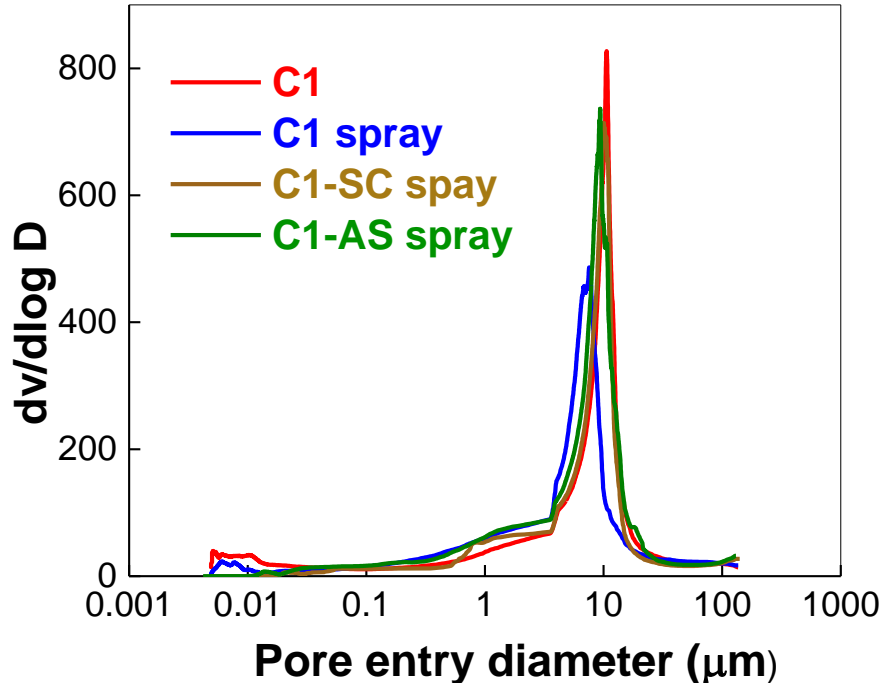


(b)

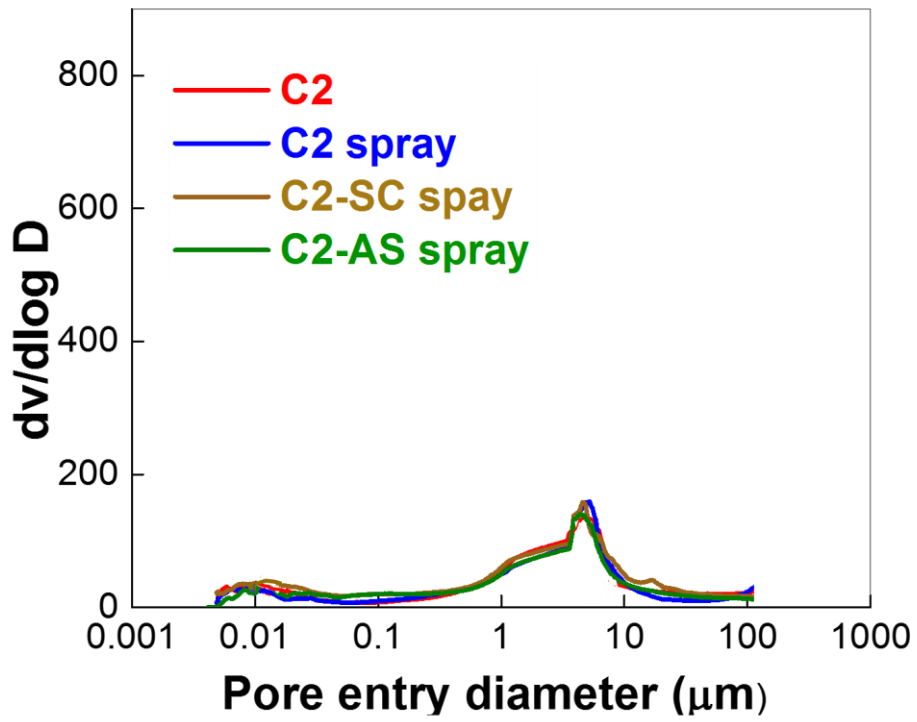
Figure 6.32. Desalinated pores in sample C1 weathered with NaCl spray test

6.5.3.2 Pore parameters

Figure 6.33 (a) and (b) show the MIP differential intrusion curves for C1 and C2 respectively, with uncoated, silicone-coated (SC) and acrylic-siloxane coated (AS) specimens, which were subjected to 450 days of NaCl spray test. C1 is the curve for uncoated-unweathered specimen, C1 spray denotes the specimen which was uncoated but subjected to weathering by salt spray, 'C1-SC spray' and 'C1-AS spray' denote the specimens which were coated with silicone-based treatment and acrylic-siloxane based treatment respectively and then subjected to weathering by salt spray. The curves were similar to that of the specimens that underwent the immersion type of weathering by NaCl. The curves were very identical and overlapping with each other for coated and uncoated variants of each brick - C1 and C2. No disruptions in the curves were seen because of the lack of significant damages in the material with the NaCl spray. The total critical pore size and total porosity were almost the same with unweathered and weathered specimens from the same kind of brick.



(a)



(b)

Figure 6.33. Differential intrusion curves for specimens subjected to NaCl spray test

The relative volume fractions of pores of each size range were calculated for unweathered specimens and the weathered specimens. Figure 6.34 shows a comparison of the relative percentage of volume fraction of different pore sizes for the various samples when weathered with NaCl spray test (Figure 6.34 a) and NaCl immersion test (Figure 6.34 b). C1 and C2 refer to the samples which are Unweathered. C1-spray and C2-spray denote the samples weathered with NaCl spray and C1rw and C2rw indicate the samples weathered with NaCl immersion test as per RILEM V 1.b recommendations. It can be seen that there is a reduction in the larger pores ($> 10 \mu\text{m}$) with NaCl immersion weathering due to salt deposition in those pores, but which did not occur in case of NaCl spray test. The increased relative fraction of macropores in the case of spray test is only reflected from the alterations occurring at the micropore level. This observation again emphasises the formation of larger NaCl crystals in the case of immersion test, which is practically not happening in the case of actual NaCl spray that represents a more realistic scenario.

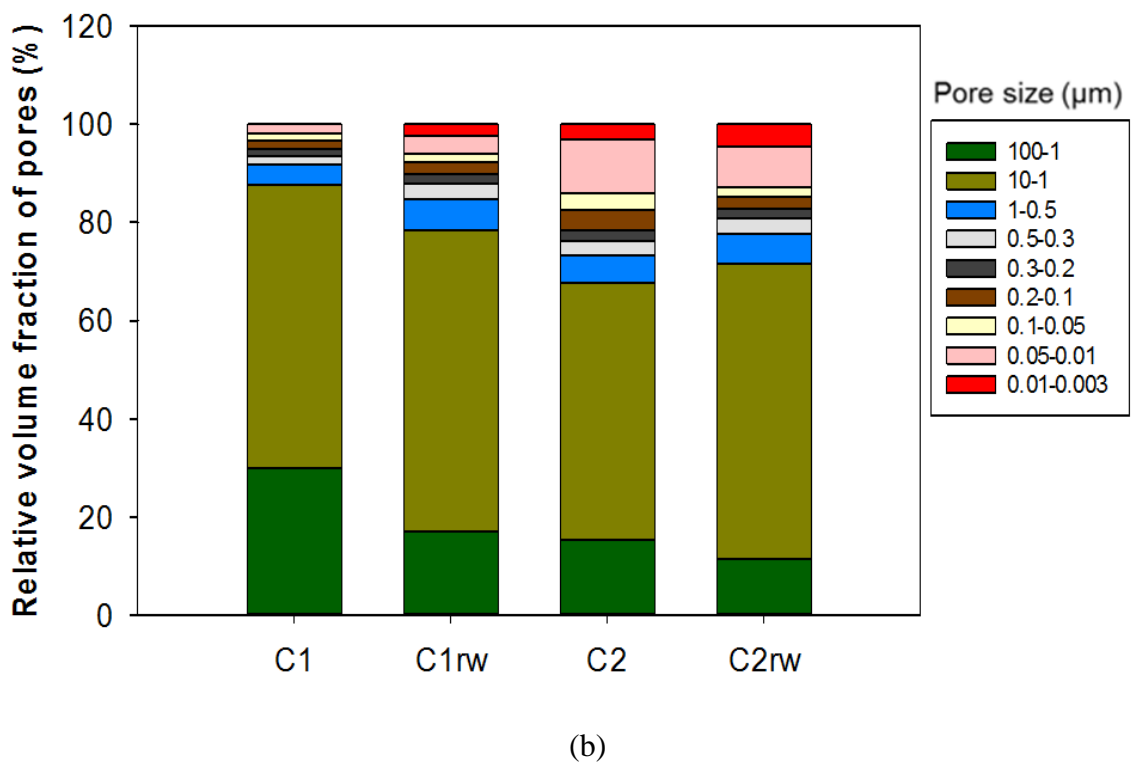
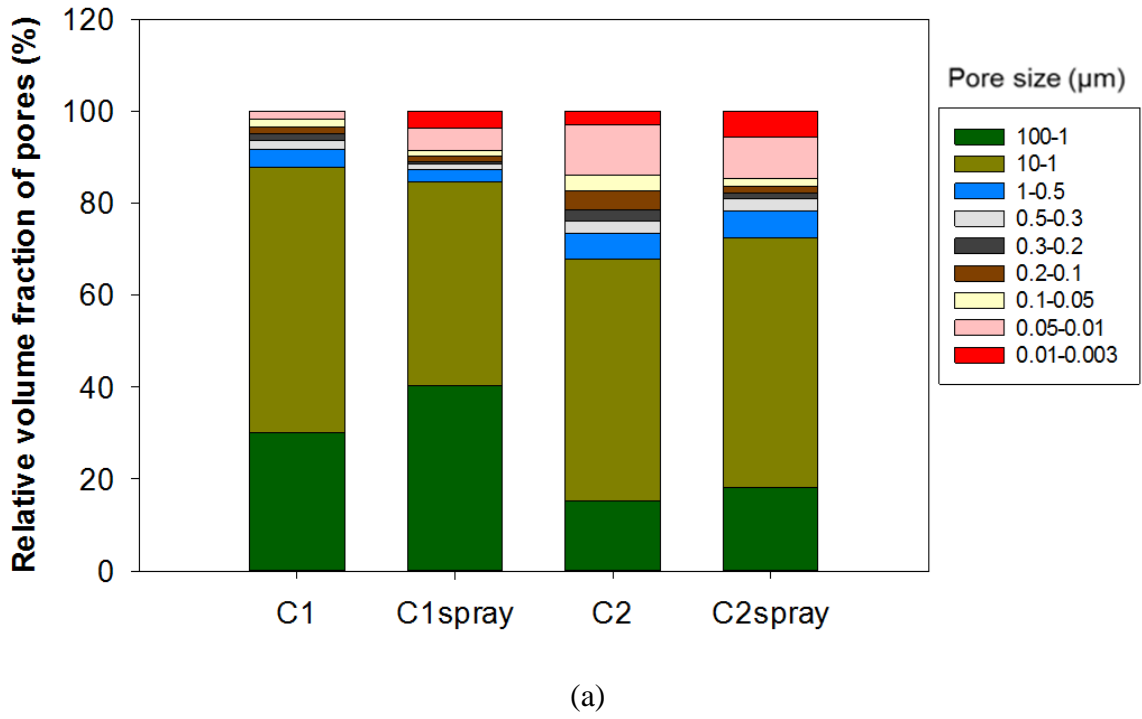


Figure 6.34. Relative volume fraction of pores in different size ranges

6.6 SUMMARY

This chapter presented a comprehensive study on the concerns to be addressed in choosing a protective treatment for preventing damage in masonry structures, especially when the structure is exposed to salt. Two different, but most commonly used and commercially available water-repellent treatments were used for the study - a silicone-based and an acrylic-siloxane based coating. In the first part of the chapter, the essential properties to be looked at for an ideal water repellent treatment were discussed and evaluated for the particular treatments used in the study. The tests included water-drop absorption test, Karstens' tube test, water sorptivity test and vapour permeability test. The two treatments - silicone-based and acrylic-siloxane based, were found to be qualified to be used as water-repellent protective treatments over masonry units. Though, among the two, silicone based treatment was found to have the lower water absorption property than acrylic-siloxane based treatments from the preliminary tests.

In the next part of the chapter, the efficiency of the treatments was analysed experimentally towards salt weathering resistance, for various types of bricks for a duration of 112 days (112 wet-dry cycles). This was implemented by conducting accelerated weathering tests by exposing coated brick specimens to sodium sulphate and sodium chloride salt solutions separately with alternate dry-wet cycles as per RILEM V 1.b test procedure. Sodium sulphate was considered for the apparent reason that it is the most deleterious salt among the common exposures for a masonry structure. And, sodium chloride was also studied in view of its wide availability in natural environment. The performance of the treatments towards salt weathering resistance was found contradictory to that of its water-

repellence. Acrylic-siloxane based treatment was found to be providing a high salt weathering resistance to the substrate material, due to its property of cracking with salt exposure. On the other hand, the silicone-based coating blocked many pores, causing the specimens to be in a sealed condition. Thus, crystallization stress was created and retained within the material leading to further damages. It could be concluded from the study that there exists a relationship between the properties of water-repellent treatment chosen and the pore structure of the substrate (brick) material, to provide the required salt weathering resistance. For a material (brick in this case) which is more prone to salt crystallization damage (due to a large amount of smaller pores), the treatment provided should not be one which blocks the pores. This would enhance the damage compared to the material left uncoated.

Desalination of the salt-weathered specimens was executed using cellulose poulticing, and the efficiency was compared between the removal of sodium sulphate and sodium chloride salt crystals. Through SEM imaging and analysis of pore structure using MIP in the specimens, it is demonstrated that this process of desalination is more efficient in removing sodium sulphate salts, especially in materials with more micropores. If the material is mostly comprised of macropores, desalination by cellulose poulticing is equally efficient to remove sulphate and chloride salts. Variations with respect to different coatings were tested but were not captured significantly in these results, since possibly the layer of treatments would have been removed mostly at the end of weathering cycles - when the desalination treatment was applied.

The artificial accelerated weathering test on the same kind of specimens was also administered with NaCl spray test, which is more realistic, in a salt spray chamber constructed as per the recommendations of ASTM B117 (ASTM International standard B117 2017). The visible damages were almost negligible after the end of continuous dry-wet cycles for 450 days. The uncoated variants of all specimens showed heavy efflorescence, but no material damage. The coated specimens did not exhibit any kind of complete destruction as in the case of immersion weathering test, other than the minor powdering of C2 specimens (with more micropores) coated with the silicone-based coating. The reason was observed as the difference in the morphologies of crystals getting precipitated in each case. This observation is important because it implies that the damage does not occur for the material as fast as observed from the accelerated weathering test by immersion. However, the trends (the comparative behaviour showing the least salt-resistant combination and well-resistant combination of protective treatment and substrate) are the same in both spray test and immersion test. Hence the detailed analysis from the immersion test studies could be used for a better understanding of the mechanism of salt crystallization and protection, and the final conclusions from the study can definitely help in choosing the right treatment for the substrate material to obtain the required performance in realistic conditions. The right choice of protective treatment to a masonry structure in a salt-exposed environment is essential to minimise further interventions in future.

7 GENERAL DISCUSSIONS

7.1 INTRODUCTION

This chapter provides a discussion on the significance of the major learnings from the thesis. The significant results from all the previous chapters are compiled, and the role and contributions of the microstructure of the masonry materials in determining their durability are discussed. The importance of microstructure has been identified in various domains of interest within masonry materials. The first part of the study unravelled the characteristics of various masonry units through different microanalytical techniques, so that the state of conservation, the physical-chemical-mechanical properties and information regarding the origin of the material could be traced. In the second and third phases of the study, the role of microstructure in the process of salt crystallisation in the materials and protective methods against salt crystallisation were analysed respectively.

7.2 DEVELOPMENT OF A FRAMEWORK FOR CHARACTERISING HISTORIC MASONRY MATERIALS

Techniques are well-developed and established to analyse the pore distribution, mineralogy and morphological features of materials. The choice of techniques, the way of analysis and interpretation of results generally varies for different materials, depending on the nature of

the material, weathering state and purpose of investigation. Hence, there exists no standard methodology which can be adopted to characterise a historical masonry unit- so that the details about their origin, current weathering state and performance can be understood and documented.

Visual inspection gives the first hint or options to identify a material. The colour, texture and approximate density (from the weight) can provide various possible options for different stone types or the class of brick it can be. Further information on the origin/source of any historical building material is to be reckoned from mineralogical and compositional identification - which can be studied in the laboratory using techniques like XRD or XRF. The minerals and their compositions are indicative of the types of stones, once the first clues are obtained from visual inspections. In the case of fired clay bricks, the presence or absence of particular minerals reveals the type of clay (low-calcium clays or calcium-rich clays) used for their production and the temperature at which they were fired. Enough literature is available to identify the firing temperature from mineralogical identification using the temperature-dependent phase transitions. For example, the presence of calcite and dolomite suggests that the bricks were fired at lower temperatures, of less than 800 °C. The calcite and dolomite react with silicates as the temperature rises to transform into neo-formed phases like gehlenite and diopside. Likewise, there are several known mineral transformations, which can help to access the maximum temperature reached during the time of firing for the brick. Gaining accurate knowledge on the origin of a material is important for choosing similar new/replacement materials for existing structures. In the case of bricks, manufacturing new bricks of similar properties may be required at times, which demands robustness.

There can be multiple variants for the same type of stone - for example; there are many types of granite and limestone. In such conditions, identifying the exact type of that particular stone requires additional information than the mineral composition. Morphological features and orientation and distribution of specific mineral grains would help in this regard. Scanning electron microscopy is one such advanced tool which can provide 3D images, where different minerals, pores and their distributions can be visualised. In the current study, after confirming the mineral compositions, the morphological visualisation carried out using SEM clearly differentiated a coral stone from other types of limestones through its peculiar structure with quartz grains lined by flower-shaped magnesian calcite.

Once the type of material and information regarding the origin are known, a historical building material is to be studied for its weathering state. SEM images can provide information on the occurrence of weathering products and cracks within the microstructure. A combined analysis of the presence of weathering products and analysis of pore structure gives a better understanding of the state of weathering. MIP (Mercury Intrusion Porosimetry) facilitates the quantification of porosity and pore-related parameters of a material. A shift in critical pore size from the expected values for that particular material and widening of the differential intrusion curve indicates the extent of disintegration.

Besides the information on origin, morphology and pores, these techniques can also indicate the durability performance of any material. It is found in the current study and also reported prior, that smaller pores of size $< 1 \mu\text{m}$ predominate when the bricks are fired at temperatures less than $900 \text{ }^\circ\text{C}$. At temperatures above $900 \text{ }^\circ\text{C}$, bricks with low-Ca clays exhibited an increase in the number of pores $> 7 \mu\text{m}$ size, whereas no significant changes are

expected for bricks made with for Ca-rich clays. The size of pores in the system is closely related to the durability of the bricks. The desired pore system for a masonry material to be used in a salt-exposed environment is suggested in the study. Materials with most micropores have a high susceptibility to salt crystallisation damage. The thesis shows that salt crystallisation by sodium sulphate salt is more predominant in the pores of sizes varying from 1 μm to 0.2 μm . Hence, knowing the combination of firing temperature and raw materials helps in assessing the salt weathering resistance of the material. For optimal performance, a fired clay brick with high resistance to salt-weathering can be designed/manufactured using high firing temperature and low-Ca clays.

Figure 7.1 shows the framework proposed for the characterisation of historic masonry material, to extract information on its origin, to document its weathering state and predicting the durability performance.

This framework would be helpful in the following cases:

- Documentation of the material-details and weathering state of historic structures
- Efficient choice of restoration works on the existing material
- Manufacturing new/replacement material for partial replacement or reconstruction in a historic structure.
- Predicting the durability of the existing material in terms of resistance towards salt-crystallisation.

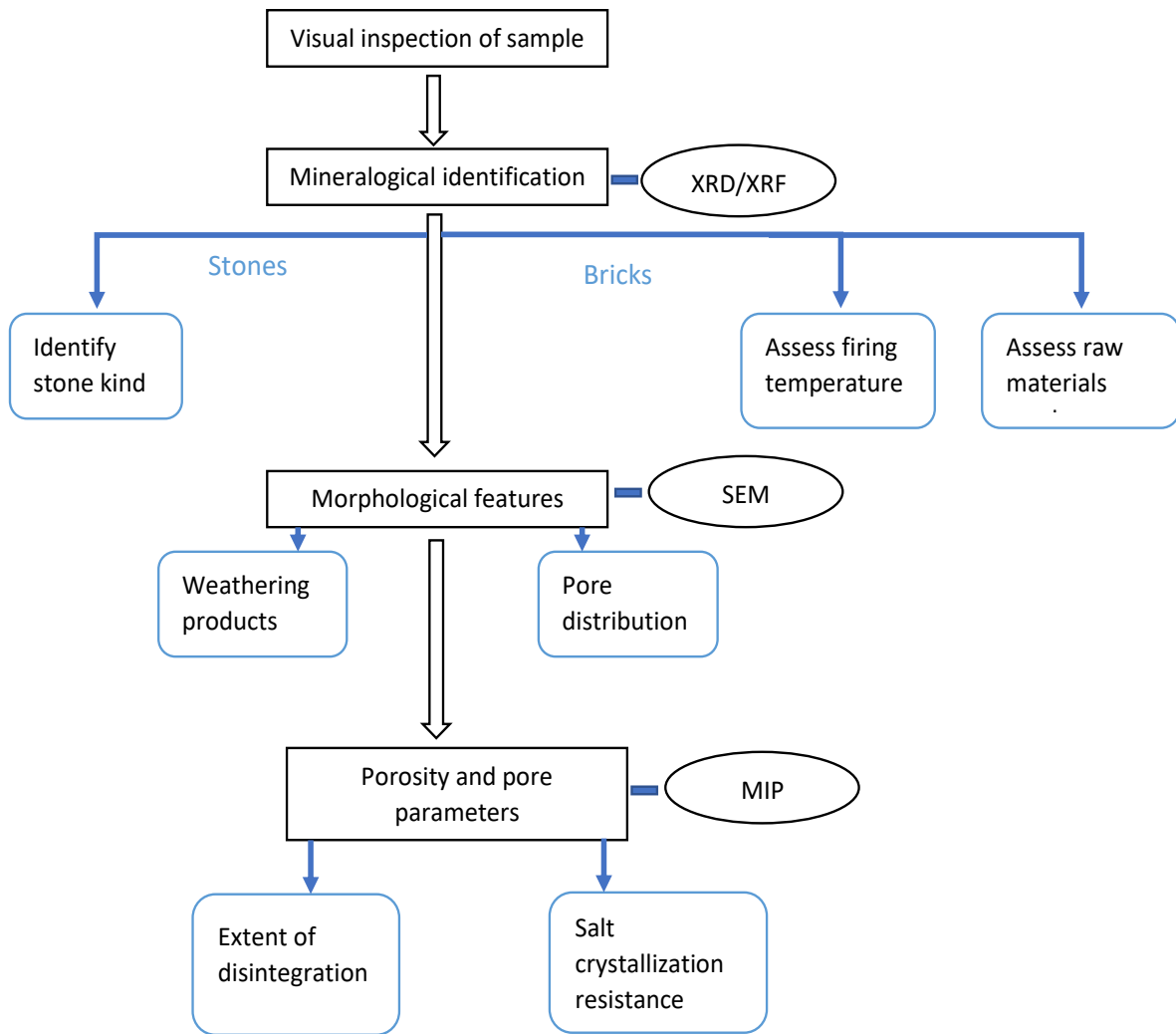


Figure 7.1. Framework for characterising historic masonry materials

7.3 FACTORS CONTROLLING THE SALT CRYSTALLISATION PROCESS

Salt solutions enter the brick or stone through the openings (outer pores) and occupy the pores inside. Eventually, salt crystallisation and/or generation of a high supersaturation may occur due to evaporation of water, a sudden drop in temperature, or due to dissolution mediated phase transformation. When a crystal in contact with a highly supersaturated solution grows in a pore, such that its growth is restrained by the pore walls, tensile hoop stresses are induced in the material supporting the pore. If the stress is high enough to exceed the tensile strength of the material, the building unit undergoes damage. The major factors which are capable of altering the mechanism of this process of salt crystallisation, as observed from the current study are explained here.

7.3.1 Size of the pores

The crystallisation pressure generated during the nucleation of salt inside the pores is more substantial in smaller pores. This happens due to the difference in geometry of the crystal in a small and a sufficiently big pore. When the pore is small, the crystal is restrained from growing in some directions by the pressure from the pore and grows in the unrestrained directions to a depth. In the unrestrained portions of the pore wall, the crystal attains a large curvature not greater than what is allowed by the existing supersaturation. However, the curvature of the crystal remains very low in the restrained pore walls, where it is not balanced with the existing high supersaturation. A crystallisation pressure forms at such areas to maintain/regain this balance, which acts on pore-walls, and is of a damaging nature. On the other hand, if the pore is big enough to accommodate the growing crystal, the free energy due to supersaturation is balanced by the curvature alone, without generating harmful

stresses. In the current study, it is found that among all the different types of bricks analysed, C1 which was the brick sample with larger pores was the most resistant towards salt crystallisation, whereas C2 - which was the brick with maximum number of pores with size $< 1 \mu\text{m}$ was found heavily deteriorating in the long-term dry-wet cycles with the sodium sulphate salt.

Figure 7.2 shows the relative volume fractions of all the brick samples studied for the different range of pore sizes. C1 refers to the sample collected from brick C1, and C1w refers to the C1 sample after subjecting to accelerated weathering cycles with sodium sulphate salt solution. It was understood from visual inspection and mass changes, that C1 was the most resistant brick towards salt weathering and C2 was the least resistant among all the samples tested. This analysis on correlating with the figure (Figure 7.2) clearly shows that it is the microporosity (pores in the range of $1 \mu\text{m}$ to $0.2 \mu\text{m}$) that controls the salt crystallisation and further damage in each case. Despite the very high porosity of C1, the least fraction of pores in this range ($1 \mu\text{m}$ to $0.2 \mu\text{m}$) among all other bricks protected the specimens from damages due to salt crystallisation. In the case of C2, the total porosity was the least among all other brick samples, but the relative volume fraction of pores between 1 and $0.2 \mu\text{m}$ was the maximum for C2. This resulted in the highest degree of deterioration for C2 brick. Thus, the pore size ranging from ' $1 \mu\text{m}$ to $0.2 \mu\text{m}$ ' can be defined as a "critical pore-size range for salt crystallisation".

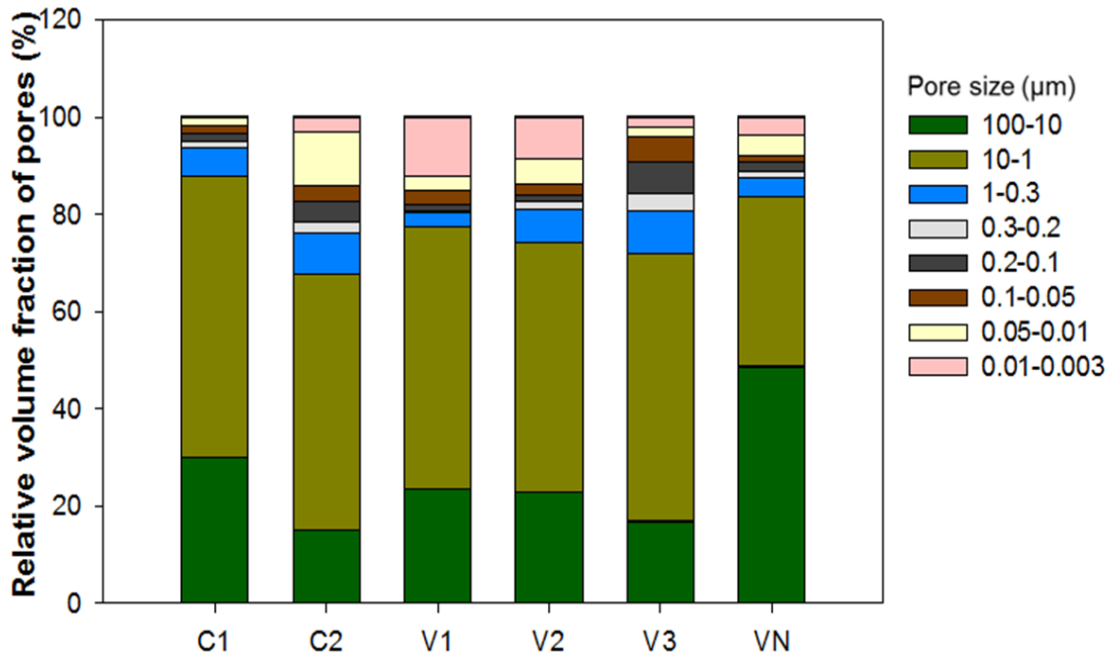


Figure 7.2. The relative volume fraction of pores of different sizes in various brick samples

7.3.2 Pore-interconnection

Several experiments have confirmed that as a stressed crystal is at a higher chemical potential than an unstressed one, the former dissolves spontaneously to supply ions for the growth of the latter when both are in contact with the same pore solution (Flatt, 2002). Therefore, crystallisation stress is a transient phenomenon that is experienced only until a crystal has nucleated in an adjacent connected bigger pore. Thus, the crystallisation pressure in a pore is smaller if the pore is closer to a bigger pore or the free surface, provided that the pore solution provides a continuous matrix for ion transport. Figure 7.3 represents a pore-network in a material, where crystal A is formed in a smaller pore which is connected to a larger pore, where crystal B is formed. The growth of crystal A is restrained in the smaller pore, whereas

B is free to grow in the larger pore. In this case, crystal A would dissolve to supply ions to the larger pore, facilitating the growth of crystal B. This phenomenon is theoretically suggested by Flatt (2002) and experimentally illustrated in the current study in case of coral stone.

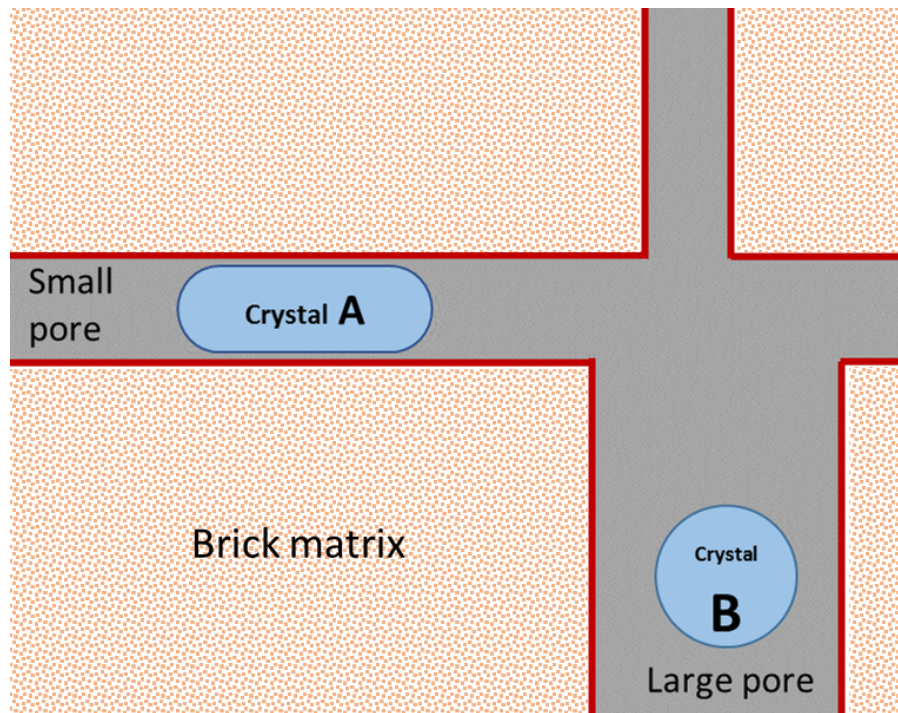


Figure 7.3. Representation of crystal formation in an interconnected pore-network

In the current study, the coral stone was found to have remarkable resistance towards salt crystallisation. Observations of the original microstructure of the coral stone and the modifications in microstructure with accelerated salt weathering indicated that the aforementioned draining of supersaturation due to highly interconnected porosity is the reason for this resistance. The microstructure of coral stone observed from SEM imaging showed quartz grains lined with a very porous opened flower-petal like magnesian calcite,

which provides good interconnectivity. The matrix is filled with calcite and aragonite too, which contribute to the smallest of the pores in the system. During accelerated weathering by exposing to NaCl solutions in the study, salt crystals were found to have preferential nucleation on the magnesian calcite portion, which provides the high porosity to the system with the larger pores. The draining of supersaturation here prevents the nucleation in the smaller pores in calcite region, but facilitates the crystallisation in magnesian calcite - which cannot cause any crystallisation pressure/damage to the pore wall.

7.3.3 Nature of salt

Sodium sulphate has been prescribed to be used as the deteriorating agent by various laboratory salt degradation tests due to its highly damaging nature. Even though at a given supersaturation, the crystallisation pressure due to sodium chloride is much higher than that due to sodium sulphate, the damage due to sodium sulphate is very high as compared to sodium chloride. This can be attributed to the temperature-dependent solubility of sodium sulphate, and the dissolution-mediated phase transformations undergone by the salt.

Sodium chloride tends to crystallise at the solution–vapour interface, unlike sodium sulphate that crystallises rapidly in the bulk of its solution. In building materials, this interface is at the surface. Because of this reason, massive efflorescence was observed in all the cases with uncoated specimens in the study. Sodium chloride cannot sustain high supersaturations before crystal nucleation (due to its very high solubility), unlike sodium sulphate that can generate very high supersaturations due to dissolution-mediated phase

transformation. As a result, the effective crystallisation pressure exerted by sodium chloride is much lower than by sodium sulphate.

In the current study, specimens subjected to sodium sulphate exhibited quick deteriorations, with sudden failure at times, whereas specimens exposed to sodium chloride showed a much slower rate of deterioration. Also, the mass gain was predominant for a considerable number of cycles initially due to NaCl salt deposition inside the pores instead of mass loss in the case of exposure to sodium sulphate. Despite the lesser damaging nature of NaCl, the results from the study indicate that long-term exposure of the materials to NaCl could render damage to the material which should be considered/treated in a similar way as that of sodium sulphate exposure. The extent of damage was found lesser with NaCl exposure, but the variation of damage patterns was found according to the durability characteristics of the material. Hence, materials which are inherently prone to salt weathering are essential to be protected effectively irrespective of the type of salt.

7.3.4 Strength of the material

Even with a pore structure that facilitates high crystallisation pressure, damage does not occur if the crystallisation pressure generated at the pore wall is resisted well by the tensile strength of the grains. Granite was found to be unaffected by the long-term weathering cycles despite the smaller size of pores in it. Very high grain strength of the material could be the prior reason for the resistant nature of granite in this case. Very low permeability also would have supported this cause.

7.3.5 Temperature and rate of evaporation

Other factors which are known to be influencing the crystallisation of salt are temperature and humidity. These are experienced during the laboratory testing of accelerated salt weathering in the samples, but not quantified as it was out of the scope of this study. Temperature plays a crucial role in salts that have highly temperature-dependent solubility like the mirabilite phase of sodium sulphate. It was shown in the experimental results that when the samples were allowed to dry at 27 °C after the wetting phase during dry-wet cycling with sodium sulphate, heavy efflorescence was formed at the corner and edges of the sample. However, during the recommended drying (at 60 °C), sub-florescence was predominant, and even small efflorescence on uncoated samples was not localised. If the rate of evaporation is very high that discontinuities are introduced in the pore solution, ion transport is not continuous, and crystallisation stress develops. Higher the rate of evaporation, greater is the crystallisation pressure.

7.4 PRESERVATION STRATEGIES

Investing in the preservation of built heritage enhances the economic and cultural resources of a society. Major masonry structures are either built of stone or brick. Both the materials undergo deterioration with different mechanisms, subject to the weather and exposure conditions. Considering the various possibilities of degradation and the uncertainties about the materials in the heritage structure, their preservation is mostly tedious and complicated.

Managing and conserving built heritage is thus a multi-disciplinary process, where multiple variables are to be adequately studied.

The most common preservation strategy being followed for historic masonry structures is the usage of treatments (consolidants, water-repellents, surface-compensation mortars (when mortar or plaster is used to smoothen surface), etc.). The ideal characteristics of the treatments are transparency, ease of usage, cost, least water-absorption, non-reactivity and safety in handling. The current study proposes that the compatibility between the treatment and the substrate material with respect to performance characteristics is the most important criterion. Defining compatibility is complex because it is to be determined based on the particular type of exposure which the structure faces. And this complexity could be the reason why it is ranked low among the various selection criteria. In the current work, salt exposure was the condition on which the detailed study was conducted because salt crystallisation is identified as the most crucial damaging mechanism for porous masonry structures. This can be extended to various other exposure conditions also.

The experimental results showed that for a porous material where the majority of pore sizes are not in the critical range for salt crystallisation ($1\ \mu\text{m}$ to $0.2\ \mu\text{m}$), a water-repellent could be chosen for the system based on its fundamental requirements such as least water-absorption, transparency, breathability (vapour permeability), reversibility and non-reactivity. However, if the substrate material is having the majority of its pores in size range of $1\ \mu\text{m}$ to $0.2\ \mu\text{m}$, the material itself is considered as prone to salt-weathering. In such cases, selection of water-repellent treatment is very crucial. The treatment should reduce the water absorption, without blocking any of the pores. If the treatment blocks the pores, an accidental

intrusion of the salt solution inside the material will cause sudden damages due to internal stresses generated. A conceptualisation of the bonding of an ideal water-repellent to the substrate, in this case, is represented in Figure 7.4.

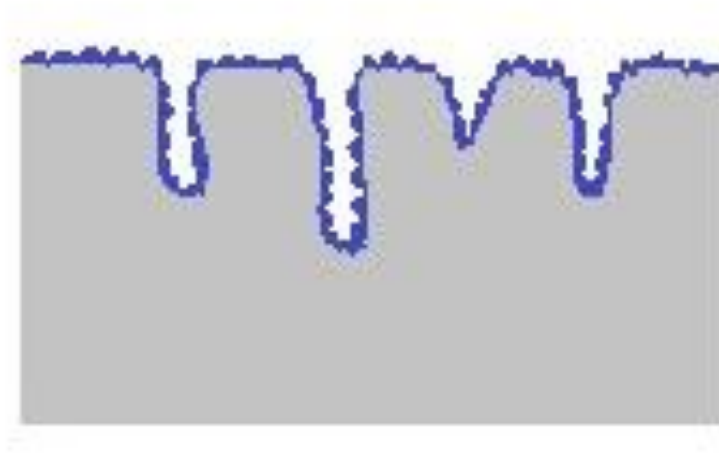


Figure 7.4. Conceptualisation of the bonding of an ideal water-repellent to the substrate

The bonding of a water-repellent as conceptualised in Figure 7.4 again reduces its efficiency when the depth of penetration is high, eventually allowing salt solution inside pores where pore sizes are further reduced by the presence of treatment. In such cases, in addition to the unblocking of pores, another desired quality of the water-repellent to be used for a material prone to salt crystallisation is the formation of micro-cracks in the layer of water-repellent itself during the salt-exposure. Many literatures have identified this property not as a ‘desired quality’ but a demerit. The formation of micro-cracks in the layer of treatment would help the release of the internal stresses and thus reduce the risk of sudden

damages in the system due to crystallisation pressure. If salt crystallisation is not a risk to be considered in a location, the choice of treatment can be based on their efficiency in repelling water.

An effective choice of treatment eventually makes the preservation more sustainable. It reduces the chances of frequent future interventions to the structure, thus reducing the consumption of resources and resulting emissions. Environmental issues regarding production and use of various protective treatments are not addressed properly, which can be carried out by analysing the process in the life-cycle of the various products using LCA (Life-cycle assessment). Once that information is available, the sustainability factor of each product can be another selection criterion.

When a masonry structure affected with salt is to be preserved, desalination is recommended prior to the application of the treatment. Removal or reducing the salt content within the material can be carried out in different ways. Washing with water and poulticing are common techniques among these. Washing with water may only remove the salts present on the external surface. Poulticing for desalination is a process where the pulp (example: cellulose) applied over the masonry material is allowed to dry, and it absorbs salts which can be removed on complete drying. One condition to be satisfied with poultice selection is to ensure a residue-free removal. The efficiency of the procedure has to be tested. The study showed that cellulose poulticing has a reduced efficiency in removing sodium chloride salts from materials with more tortuous and smaller pores (in C2 brick with a significant amount of pores less than 3 μm). But the efficiency was not compromised on removing sodium sulphate salts. The reason could be the deposition of NaCl crystals in much smaller pores due

to their smaller size, from where the capillary force required to remove the salts is very large. For materials with larger pores, cellulose poulticing was found as an effective method of desalination in removing both sodium sulphate and sodium chloride salts.

Preservation strategies for an existing building which is affected by the salt can be briefly listed in three steps:

- (i) Characterisation of the existing masonry material and the salts present in the system
- (ii) Removal/reduction of salt in the system (desalination)
- (iii) Providing compatible repair methods/treatments

Other strategies suggested from the study, in light of the importance of breathability of the porous masonry units, are:

- (i) Adopting measures to control the temperature and humidity variations in historic structures, at least wherever possible, such as inside halls. This would prevent the temperature and relative humidity dependent phase transitions of salt like sodium sulphate, which is quite dangerous for masonry units.
- (ii) Installing breathable vents/openings in historical structures which are more exposed to salt and moisture, to facilitate the release of internal stresses and prevent mobilisation and crystallisation of salts.

7.5 SUMMARY

This chapter presented the practical significance of the outputs from the study, and a conceptualisation of the learnings compiled together. A framework was given for the

characterisation of historic masonry units of any conservation state, to understand the material properties and performance in a minimum number of tests. This framework would help in providing a sequence of tests, with the vital information about the material which can be extracted from the various tests. Also, the major factors which were found to be controlling the process of salt crystallisation and the resulting damages, as observed during different stages of the thesis work and with various materials, were compiled together in this chapter. A proper understanding of these factors and a closer look at them together could help in reducing/mitigating the damages due to salt crystallisation. Thus, the restoration process of historic structures is effectively benefitted from a better understanding of the science behind the microstructure of the material and salt crystallisation.

8 CONCLUSIONS

8.1 INTRODUCTION

The current interdisciplinary research work attempted to generate new knowledge from experimental data, on the significance of microstructure of ancient masonry units and their implications on performance requirements. This study was subdivided into different phases, which sought to achieve the following objectives:

- (i) Investigating the characteristics of historic masonry units from India and linking the properties to the performance
- (ii) Understanding the alteration in the mechanism of salt crystallisation for different materials with the change in microstructure
- (iii) Evaluating the efficiency and compatibility of protective treatments for historic masonry.

These objectives were met through a process of understanding and critically reviewing the available literature followed by essential laboratory experiments. In-situ investigations on heritage masonry units such as bricks and stones, combined with detailed characterisation using physical and microanalytical tests provided the material properties. Laboratory accelerated salt weathering tests with different salts further provided the durability performance of the materials. The implications of each of the physical, chemical and

microstructural properties on the performance are established through this study. Strategies for efficiently choosing the protective treatments were also suggested through a comprehensive experimental program which analysed the fundamental properties and compatibility requirements of a protective treatment to be provided for any masonry unit.

8.2 CHARACTERISATION OF HISTORIC MASONRY UNITS

Samples collected from historical and commercial sources were subjected to physical, mechanical, chemical and microstructural characterisation to trace the knowledge on their origin and behaviour. The study was conducted on different types of bricks and stones.

8.2.1 Characteristics of bricks

The state of conservation of various historic bricks collected from different time periods was analysed using characterisation methods, and compared with the characteristics of different new commercial bricks. The study provides objective data that help to understand the quality of various bricks from Southern India and its relation with performance over prolonged exposures. The following conclusions are drawn from the characterisation studies conducted on a wide range of brick samples:

- (i) The presence of non-calcium clays and high firing temperature as observed from the XRD and SEM results was responsible for the better vitrification degree in the ancient bricks (V1, V2, V3), which provided the good weathering resistance and physical-mechanical properties.

- (ii) The historic sample K with low vitrification showed high fissuring towards the surface, which is a characteristic of the presence of Ca-rich clays and low firing temperature. However, the core was unweathered because it was not exposed to an aggressive salt-rich environment.
- (iii) Non-Ca clays and firing temperatures as high as 900 °C make the system resistant to salt crystallisation damage with the formation of large rounded pores ($> 1 \mu\text{m}$), as in the case of new commercial brick C1.
- (iv) New bricks fired at very high temperature (C2) did not show pore parameters corresponding to good salt weathering resistance, even though they exhibited enhanced strength properties. So, raw material composition (i.e. Ca-rich or non-Ca clays) is equally important as firing temperature in determining weathering resistance of a brick.
- (v) Gypsum crystallisation was identified as the cause for the blistering and powdering effect in the ancient bricks (T1) that were fired at lower temperature and had Ca clays in them, which also increased the weathering susceptibility. However, the same brick exposed to chlorides (T2) instead of sulphates did not show weathering, but improved strength and porosity.

Replacement of brick units during restoration work demands compatibility between the existing and newly replaced materials, which is captured in this work with respect to raw materials and firing temperature. These factors alter the pore structure, which controls the durability and breathability of bricks. Thus, a methodology was established in the current

study to characterise heritage bricks for their properties and performance, and to select suitable replacement materials when necessary.

8.2.2 Characteristics of stones

The pore sizes and their distribution are found as the principal factors in determining the performance characteristics of bricks exhibiting different weathering states. With that background, two separate stone types were selected for analysing the characteristics - (i) granite stone - which has a very low porosity with small pores, but high strength, and (ii) coral stone, with high porosity and large pores. This helped in establishing the role of microstructure, especially porosity, pore size and pore structure of any masonry unit, in controlling the durability of the structure. The major conclusions drawn from this part of study are as follows:

- (i) Granite stone showed excellent physical - mechanical properties in terms of high strength and low water absorption. Further, microstructural analysis supported the remarkable mechanical performance with the densely packed microstructure, which was revealed through SEM images and very low porosity observed from MIP.
- (ii) Long-term accelerated weathering tests with highly deleterious sodium sulphate salt solution on granite specimens exhibited the remarkable resistance of the material towards salt crystallisation. The very low permeability, i.e., the low accessibility for the liquids to get into the pores, along with the high grain strength could be the factors that prevent the onset of any damages in granite due to salt crystallisation.

When the tensile strength of the grains is sufficient to resist any crystallisation pressure being generated to the pore wall, no damages are initiated.

- (iii) Physical characterisation of coral stones emphasised the low density, high capillary porosity and high water-absorption values, which were in line with the further microanalytical studies.
- (iv) Coral stone samples subjected to both sodium sulphate and sodium chloride salt solutions separately were found with no noticeable deterioration after 15 wetting – drying cycles.
- (v) The reason for the low susceptibility of coral stones towards salt crystallisation was found as the prominence of macropores in the system (more than 70% of the total pores were of size greater than 0.5 μm).
- (vi) Large interconnectivity of pores was found in the peculiar microstructure of the coral stone through SEM images. This facilitated a draining of supersaturation from the smaller pores located in the calcite portion to the larger pores in the magnesian calcite lining of the quartz, resulting in preferential nucleation of salt crystals over there. Crystallisation in the larger pores of magnesian calcite was observed in SEM images, which would prevent any generation of crystallisation pressure and further damages.

8.3 SALT CRYSTALLISATION IN POROUS MASONRY UNITS

A comprehensive study was conducted on investigating the concerns to be addressed in choosing a protective treatment for preventing damage in masonry structures, especially

when the structure is exposed to salt. Two different, but most commonly used and commercially available water-repellent treatments were used for the study - a silicone-based and an acrylic-siloxane based coating. The conclusions are limited to the particular varieties (types) of bricks, granite and coral stones used in the study. The major conclusions from the study are as follows:

- (i) Among the various brick samples studied, the highly porous C1 was found to be the most resistant sample when exposed to sodium sulphate solution, with progressive homogeneous material loss from the surface. C2, the high strength dense brick performed the worst with the salt exposure, with deep cracking and sudden failure. This clearly demonstrated that more than the entry of salt solutions inside the material, it was the availability of crystallisation spaces inside, which were in the range of micropores, that created the damage.
- (ii) Detailed analysis of pore distribution within the samples, and the subsequent monitoring of the damage patterns and the rate of deterioration showed that samples with a large volume fraction of pores smaller than $0.2\ \mu\text{m}$ were more prone to salt crystallisation damage. The salt deposition was seen from pores smaller than $10\ \mu\text{m}$, where a combined effect of salt deposition and formation of micro-fissures was observed in pores smaller than $0.2\ \mu\text{m}$. With further analysis of volume fraction of pores of different sizes, the study proposes a critical range of pore size for causing salt crystallisation, which is from $1\ \mu\text{m}$ to $0.2\ \mu\text{m}$.
- (iii) Protective water repellent coatings should be selected based on the exposure conditions of the masonry and properties of the masonry unit. Silicone-based

coatings, which proved to be better water repellent from the Karsten tube test, were found to be more detrimental to the brick samples in the presence of sodium sulphate than the brick surfaces left uncoated. Acrylic siloxane-based coatings, because of the fact that they could allow more breathability to the material because of their cracking tendency in salt exposure, resulting in an increase in the salt weathering resistance of relatively less porous brick samples to a considerable extent in the presence of sodium sulphate solution.

- (iv) Bricks with larger pores and least micro-porosity, which intrinsically possessed good salt crystallisation resistance, performed better with both the coatings, with no difference observed with the change in coatings (in case of C1). In other words, if the substrate has sufficient porous space for unrestrained crystallisation with a good degree of pore connectivity to the exterior to reduce the supersaturation, then the protective treatment should be aimed at rendering maximum impermeability to water, as moisture entrapment will not be a problem - provided the water repellent is qualified for vapour permeability property from preliminary tests. On the other hand, under the same exposure and drying conditions, substrates with a more significant fraction of small pores should be treated with protective coatings that ensure a good moisture transmission, making the surface hydrophobic but not impervious. It is because such materials promote the growth of restrained crystals, whose damaging effect can be reduced only by providing good ion transport channels. Therefore, since the performance of any water-repellent coating has been found to vary with the

properties of its substrate, it is necessary to consider the substrate microstructure among the other factors while making a choice in the selection of treatment.

(v) The damaging nature of NaCl has always had a disagreement in the research community due to the lack of long-term exposure data. In the current study, long-term exposure for NaCl was conducted using immersion type of testing and salt-spray testing. Mass depositions were found predominating for NaCl because of its low crystallisation pressures, resulting mostly in decreased porosities and fewer damages. However, in the long run, the damaging pattern was similar for NaCl and Na₂SO₄ among the range of sample types used indicating the similar choice of restoration strategies for effective conservation.

(vi) NaCl salt spray test resulted in significantly lesser mass loss of the material than the case of NaCl immersion test. Still, the pore structure, pore redistribution, action of salts in pores and effect of desalination was similar in both cases. This indicates that all the damages observed and studied from accelerated studies are exaggerated, but help in the purpose of understanding the mechanisms. Thus, the preservation strategies decided based on the study are conservative in nature. They would be ideal and work more efficiently in real cases than the observations made from the accelerated tests

(vii) The process of desalination was found around 74% more efficient in removing sodium sulphate salts, in materials with more micropores (pore size < 1 µm), demonstrated from SEM images and analysis of pore structure using MIP in the

specimens. If the material is mostly comprised of macropores, desalination by cellulose poulticing is equally efficient to remove sulphate and chloride salts.

8.4 MAJOR CONTRIBUTIONS

The following are the major contributions that resulted from the present thesis work:

8.4.1 Scientific contributions

- (i) A framework for characterisation of historic bricks of any conservation state to understand their properties and performance was developed.
- (ii) A better understanding of the damage mechanisms of salt crystallisation on masonry units was provided.
- (iii) Pore size in the range of 1 μm to 0.2 μm was identified as critical for salt-crystallisation. Any material with more number of pores in this range would tend to promote salt crystallization if it is exposed to salt-rich environment.
- (iv) Even though NaCl is less damaging, with the support of experimental data the study showed that the efficiency of preservation strategies to be adopted for masonry structures should be the same in case of sodium sulphate exposure and sodium chloride exposure.
- (v) A connection between the performance of any protective treatment and the microstructure (pore distribution) of the substrate material was effectively demonstrated.

8.4.2 Engineering contributions

(i) Significance of the brick processing (choice of raw materials and firing temperature) on the durability performance of the material was articulated. Bricks shall be fired at temperature $> 900\text{ }^{\circ}\text{C}$ and preferably manufactured with low-calcium clay for ensuring the minimum standard strength and the right vitrification to form large rounded pores for obtaining resistance to salt weathering.

(ii) Suggestions for the efficient selection of suitable water repellent coatings.

— For material with larger pores (pore size $> 1\text{ }\mu\text{m}$), treatments can be selected based on their water permeability, whereas the material with more micropores should be protected with treatment providing high moisture transmission.

(iii) Suggestions on the application of desalination process

— Desalination with cellulose poulticing is recommended for removing sodium sulphate salts from any masonry material, and sodium chloride salts from materials with a lesser fraction of micropores (such as granite and bricks with more microporosity). Desalination is recommended to be applied on salt-affected masonry before the application of water-repellent treatments.

8.5 RECOMMENDATIONS FOR FURTHER RESEARCH

- (i) To make the results of the work more relevant in practice, the efficiencies of the choices of treatments, and desalination procedures should be studied in wallets which combine masonry units and mortar.
- (ii) The effectiveness of the treatments and applicability of the selection criteria suggested should be tested and confirmed with wallet combinations of bricks with different mortars- lime and cement. This kind of approach would be useful in practical restoration works.
- (iii) The current study was limited to the analysis of two different water-repellents. The work can be extended to action of other water-repellents and consolidants which can be applied to masonry. Water repellents can have the limitation of sacrificial performance in long run when salt precipitation occurs underneath the treatment. In cases where an increase in mechanical properties is needed and a little compromise on pore structure is possible (like in marbles, limestones etc.), action of inorganic consolidants can be preferred and need to be explored more in this line.
- (iv) The study should be extended to more types of rocks with varying combinations of microstructure and strength. Sandstones and limestones have intermediate porosity and pore sizes to that of granite and coral stones. Hence, the mechanisms of damage would be interesting to analyse and complimentary with that of bricks.

(v) A model that predicts the crystallisation pressure and damages which can be incurred to the material need to be developed which can be applied to different environmental types and different materials.

REFERENCES

- Abell A.B., Willis K.L., D. A. L. (1999). “Mercury intrusion porosimetry and image analysis of cement-based materials.” *Colloid Interface Science*, 211, 39–44.
- Ahmed, F. S. (2011). *A Comprehensive History of Medieval India: From Twelfth to the Mid-Eighteenth Century*. Pearson Education India, India.
- Aldeeky, H., and Al Hattamleh, O. (2018). “Prediction of Engineering Properties of Basalt Rock in Jordan Using Ultrasonic Pulse Velocity Test.” *Geotechnical and Geological Engineering*, 36, 3511–3525
- Aligizaki K.K. (2006). “Pore Structure in Cement-based Materials. Testing, Interpretation and Requirements.” *Taylor and Francis Group*, New York.
- Alves, C., Figueiredo, C., and Mauricio, A. (2017). “A Critical Discussion of Salt Weathering Laboratory Tests for Assessment of Petrological Features Susceptibility.” *Procedia Earth and Planetary Science*, 17, 324–327.
- Amoroso G.G., V. F. (1983). “Stone Decay and Conservation.” *Elsevier*, Amsterdam.
- Angeli, M., Benavente, D., Bigas, J. P., Menéndez, B., Hébert, R., and David, C. (2008). “Modification of the porous network by salt crystallization in experimentally weathered sedimentary stones.” *Materials and Structures/Materiaux et Constructions*, 41(6), 1091–1108.
- Anovitz L.M., D. R. C. (2015). “Characterization and analysis of porosity and pore

- structure.” *Rev. Mineral. Geochem.*, 80, 61–164.
- Antonelli, F., Cancelliere, S., and Lazzarini, L. (2002). “Minero-petrographic characterisation of historic bricks in the Arsenale , Venice.” *Journal of Cultural Heritage*, 3, 59–64.
- Anupadma, R. (2009). “Study on weathering and structural characteristics of granite and sandstone monuments in Tamil Nadu.” IIT Madras, India.
- ASTM Int. (2017). “ASTM-B117: Standard Practice for Operating Salt Spray (Fog) Apparatus.” *ASTM International*, 1–12.
- ASTM International. (2016). “ASTM C597 Standard Test Method for Pulse Velocity Through Concrete.” *ASTM International*.
- Bagde, M. N. (2016). “Characterization of failure modes and planned stabilization measures for the Ajanta caves in India.” *International Journal of Rock Mechanics and Mining Sciences*, 81, 12–18.
- Benavente, D., Cura, M. G. del, Fort, R., and Ordoñez, S. (1999). “Thermodynamic modelling of changes induced by salt pressure crystallization in porous media of stone.” *Journal of Crystal Growth*, 204, 168–178.
- Benavente, D., García Del Cura, M. A., Bernabéu, A., and Ordóñez, S. (2001). “Quantification of salt weathering in porous stones using an experimental continuous partial immersion method.” *Engineering Geology*, 59(3–4), 313–325.
- Benavente, D., García del Cura, M. A., García-Guinea, J., Sánchez-Moral, S., and Ordóñez,

- S. (2004). "Role of pore structure in salt crystallisation in unsaturated porous stone." *Journal of Crystal Growth*, 260(3–4), 532–544.
- Benavente D., L. Linares-Fernández, G. Cultrone, E. S. (2006). "E. Sebastián, Influence of micro-structure on the resistance to salt crystallisation damage in brick." *Materials and Structures*, 39, 105–113.
- Cardiano, P., R. C. Ponterio, S. Sergi, S. Lo Schiavo, P. P. (2005). "Epoxy-silica polymers as stone conservation materials." *Polymers*, 46(6), 1857–1864.
- Centre, U. W. H. (2005). "Basic Texts of the 1972 World Heritage Convention." France.
- Charola, A. E., Rørig-dalgaard, I., Chwast, J., and Elsen, J. (2017). "Salt crystallization tests : Focus on their objective." *Proceedings of 4th International Conference on Salt Weathering of Buildings and Stone Sculptures*, Potsdam, Germany, 1–10.
- Cnudde V., M. N. B. (2013). "High-resolution X-ray computed tomography in geosciences: a review of the current technology and applications." *Earth-Science Reviews*, 123, 1–17.
- Cole, and Hardy, H. (1885). *Preservation of National Monuments - First Report of the Curator of Ancient Monuments in India for the year 1883-84*. Calcutta.
- Coletti, C. (2016). "Bricktech: assessment for the use of waste in the brick production. Petrophysical characterization of new mix designs and optimization of the firing conditions." *Plinius*, 42, 20.
- Coletti, C., Cultrone, G., Maritan, L., and Mazzoli, C. (2016a). "Materials Characterization Combined multi-analytical approach for study of pore system in bricks : How much

porosity is there ?” *Materials Characterization*, Elsevier Inc., 121, 82–92.

Coletti, C., Cultrone, G., Maritan, L., and Mazzoli, C. (2016b). “Combined multi-analytical approach for study of pore system in bricks: How much porosity is there?” *Materials Characterization*, 121, 82-92.

Correns, C. (1949). "Growth and dissolution of crystals under linear pressure", *Discussion Faraday Society*, Volume 5.

Cueto N., Benavente D., Martínez-Martínez J., M. A. G.-C. (2009). “Rock fabric, pore geometry and mineralogy effects on water transport in fractured dolostones.” *Engineering Geology*, 107, 1–15.

Cultrone, G., and Madkour, F. (2013). “Evaluation of the effectiveness of treatment products in improving the quality of ceramics used in new and historical buildings.” *Journal of Cultural Heritage*, Elsevier Masson SAS, 14(4), 304–310.

Cultrone, G., and Sebastián, E. (2008). “Laboratory simulation showing the influence of salt efflorescence on the weathering of composite building materials.” *Environmental Geology*, 56(3–4), 729–740.

Cultrone, G., Sebastián, E., Elert, K., de la Torre, M. J., Cazalla, O., and Rodriguez-Navarro, C. (2004). “Influence of mineralogy and firing temperature on the porosity of bricks.” *Journal of the European Ceramic Society*, 24(3), 547–564.

Cultrone, G., Sebastián, E., and De La Torre, M. J. (2005a). “Mineralogical and physical behaviour of solid bricks with additives.” *Construction and Building Materials*, 19(1),

39–48.

Cultrone, G., Sidraba, I., and Sebastián, E. (2005b). “Mineralogical and physical characterization of the bricks used in the construction of the ‘Triangul Bastion’, Riga (Latvia).” *Applied Clay Science*, 28(1–4), 297–308.

De Bonis, A., Cultrone, G., Grifa, C., Langella, A., Leon, A. P., Mercurio, M., and Morra, V. (2017). “Different shades of red: the complexity of mineralogical and physico-chemical factors influencing the colour of ceramics.” *Ceramics International*, 43, 8065–8074.

De Kock, T., De Boever, W., Dewanckele, J., Boone, M. A., Jacobs, P., and Cnudde, V. (2015). “Characterization, performance and replacement stone compatibility of building stone in the 12th century tower of Dudzele (Belgium).” *Engineering Geology*, Elsevier B.V., 184, 43–51.

Deer, W., Howie, R., and Zussman, J. (1992). "An Introduction to The Rock Forming Minerals". *Pearson Education Limited*, Essex, UK.

Diamond, S. (2000). “Mercury porosimetry: an inappropriate method for the measurement of pore size distributions in cement-based materials.” *Cement and Concrete Research.*, 30, 1517–1525.

Di Benedetto C., Cappelletti P., Favaro M., Graziano S.F., Langella A., Calcaterra D., Colella A.. (2015). “Porosity as key factor in the durability of two historical building stones: Neapolitan Yellow Tuff and Vicenza Stone.” *Engineering Geology*, 193, 310–319.

- Dorey R.A., Yeomans J.A., P. A. S. (2002). “Effect of pore clustering on the mechanical properties of ceramics.” *European Ceramic Society Report*, 22, 403–409.
- Dunning, J. D., and Huf, W. L. (1983). “The effects of aqueous chemical environments on crack and hydraulic fracture propagation and morphologies.” *Journal of Geophysical Research*, 88, 6491–6499.
- “Durability Index Testing Procedure Manual.” (2018), University of Cape Town and University of the Witwatersrand, Johannesburg.
- Elert, K., Cultrone, G., Navarro, C. R., and Pardo, E. S. (2003). “Durability of bricks used in the conservation of historic buildings — influence of composition and microstructure.” *Journal of Cultural Heritage*, 4(2), 91–99.
- Elert, K., Jose, M., Cultrone, G., Sebastia, E., Cazalla, O., and Navarro, C. R. (2004). “Influence of mineralogy and firing temperature on the porosity of bricks.” 24, 547–564.
- Emery, S. N. D., and Charola, A. E. (2007). “Coatings on Brick Masonry: Are they Protective or Can They Enhance Deterioration?” *Journal of the American Institute for Conservation*, 46(1), 39–52.
- EN-12370:1999. (1999). “Natural stone test methods: Resistance to salt crystallization.”
- Eric, D., and Price Clifford A. (2010). *Stone Conservation an Overview of Current Research*, 2nd ed.; *The Getty ConservationInstitute: Los Angeles, CA, USA*, 2010; pp. 20–24
- Espinosa, R. M., Franke, L., and Deckelmann, G. (2008). “Model for the mechanical stress

- due to the salt crystallization in porous materials.” *Construction and Building Materials*, 22(7), 1350–1367.
- Ferrero A.M., Migliazza M., A. S. (2009). “Theoretical modelling of bowing in cracked marble slabs under cyclic thermal loading.” *Construction and Building Materials*, 23, 2151–2159.
- Fitzner, B., Heinrichs, K., Kownatzki, R. (1995). “Weathering forms-classification and mapping.” *Denkmalpflege und Naturwissenschaft, Natursteinkonservierung I*. Ernst and Sohn, Berlin, 41–88.
- Fitzner, B. (1988). “Porosity properties of naturally or artificially weathered sandstones.” *Proceedings of the VIth international congress on deterioration and conservation of stones*, Torun, 236–245.
- Flatt, R., Aly Mohamed, N., Caruso, F., Derluyn, H., Desarnaud, J., Lubelli, B., Espinosa Marzal, R. M., Pel, L., Rodriguez-Navarro, C., Scherer, G. W., Shahidzadeh, N., and Steiger, M. (2017). “Predicting salt damage in practice: A theoretical insight into laboratory tests.” *RILEM Technical Letters*, 2, 108.
- Flatt, R. J. (2002). “Salt damage in porous materials: How high supersaturations are generated.” *Journal of Crystal Growth*, 242(3–4), 435–454.
- Flatt, R. J., Caruso, F., Sanchez, A. M. A., and Scherer, G. W. (2014). “Chemo-mechanics of salt damage in stone.” *Nature Communications*, Nature Publishing Group, 5, 1–5.
- Foraboschi, P., and Vanin, A. (2014). “Experimental investigation on bricks from historical

- Venetian buildings subjected to moisture and salt crystallization.” *Engineering Failure Analysis*, Elsevier Ltd, 45, 185–203.
- Franke, L., and Reimann-Oenel., R. (2001). “Untersuchung des Einflusses von Lasuren auf die Lebensdauer von Natursteinfassaden.” *International Journal for Restoration of Buildings and Monuments*, 7(1), 27–46.
- Franzen, C. (2004). “Moisture sorption of natural building stone.” *Proceedings of the 10th International Congress on Deterioration and Conservation of Stone, ICOMOS*, Sweden, Stockholm, 75–82.
- Franzoni E., Sassoni E., (2011). “Correlation between microstructural characteristics and weight loss of natural stones exposed to simulated acid rain.” *Sci. Total Environ.*, 412-413,278–285.
- Franzoni, E., Pigino, B., Leemann, A., and Lura, P. (2014). “Use of TEOS for fired-clay bricks consolidation.” *Materials and Structures*, 47(7), 1175–1184.
- Franzoni, E., Sassoni, E., Scherer, G. W., and Naidu, S. (2013). “Artificial weathering of stone by heating.” *Journal of Cultural Heritage*, Elsevier Masson SAS, 14(3 SUPPL), e85–e93.
- Gomes, V., Dionísio, A., and Pozo-Antonio, J. S. (2017). “Conservation strategies against graffiti vandalism on Cultural Heritage stones: Protective coatings and cleaning methods.” *Progress in Organic Coatings*, Elsevier, 113(June), 90–109.
- Graziani, G., Sassoni, E., and Franzoni, E. (2016). “Experimental study on the salt

- weathering resistance of fired clay bricks consolidated by ethyl silicate.” *Materials and Structures*, Springer Netherlands, 49(7), 2525–2533.
- Griffin, P. S., Indictor, N., and Koestler, R. J. (1991). “The biodeterioration of stone: a review of deterioration mechanisms, conservation case histories, and treatment.” *International Biodeterioration*, 28(1–4), 187–207.
- Grossi, C.M., Brimblecombe, P., Harris, I. (2007). “Predicting long term freeze–thaw risks on Europe built heritage and archaeological sites in a changing climate.” *The Science of the Total Environment*, 377, 273–281.
- Hall C., W. D. H. (2009). “Water Transport in Brick. Stone and Concrete.” *CRC Press: Taylor and Francis Group*, UK.
- Hitchcock, D. H. and M. (2005). “The Politics of World Heritage.” *Cromwell press*, London.
- Indian Standard IS 1121- Part 1. (Reaffirmed 2017). “Determination of strength properties of natural building stones — methods of test.” (January 2013).
- Indian Standard IS 1124. (1974). (Reaffirmed 2017). "Determination of water absorption, apparent specific gravity and porosity of natural building stones.”
- Indian Standard. (1997), Reaffirmed 2002. “IS 1077 Common Burnt Clay Building Bricks-Specification.” .
- Jetson Ronald A., Prasad, A.M., Menon, D., Menon, A., Magenes, G. (2008). “Seismic vulnerability of south Indian temples.” *6th Structural Engineering Convention*, Chennai.
- Jin, P., Zhang, Y., Wang, S., Yang, X., and Zhang, M. (2017). “Characterization of the

- superficial weathering of bricks on the City Wall of Xi ' an , China.” *Construction and Building Materials*, Elsevier Ltd, 149, 139–148.
- Jordan, M. M., Montero, M. A., Meseguer, S., and Sanfeliu, T. (2008). “Influence of firing temperature and mineralogical composition on bending strength and porosity of ceramic tile bodies.” *Applied Clay Science*, Elsevier B.V., 42(1–2), 266–271.
- Kasthurba, A.K., Santhanam, M., Achyuthan, H. (2007). “Investigation of laterite stones for building purpose from Malabar region, Kerala state, SW India: Part-1: Field studies and profile characterisation.” *Construction and Building Materials*, 21(1), 73–82.
- Kollerathu, A.J., Sethumadhavan, K., Menon, A. (2016). “Modelling and seismic analysis of existing masonry structures.” *X International Conference on Structural Analysis of Historical Constructions*, Leuven.
- Kronlund, D., Lindén, M., and Smått, J. H. (2016). “A polydimethylsiloxane coating to minimize weathering effects on granite.” *Construction and Building Materials*, Elsevier Ltd, 124, 1051–1058.
- Lal, B. . (1949). “Sisupalgarh 1948: An Early Historical Fort in Eastern India.” *Ancient India*, 5, 62–105.
- La Russa, M. F., Ruffolo, S. A., Belfiore, C. M., Aloise, P., Randazzo, L., Rovella, N., Pezzino, A., and Montana, G. (2013). “Study of the effects of salt crystallization on degradation of limestone rocks.” *Periodico di Mineralogia*, 82(1), 113–127.
- Laurie, A., and Milne, J. (1927). “The evaporation of water and salt solutions form surfaces

- of stone, brick and mortar.” *Proceedings of the Royal Society of Edinburgh*, 47, 86–92.
- Laycock, E. . (2002). “Ten years of frost testing at Sheffield Hallam University.” *Construction and Building Materials*, 16, 195–205.
- Lopez-Arce, P., and Garcia-Guinea, J. (2005). “Weathering traces in ancient bricks from historic buildings.” *Building and Environment*, 40(7), 929–941.
- López-Arce, P., Garcia-Guinea, J., Gracia, M., and Obis, J. (2003). “Bricks in historical buildings of Toledo City: Characterisation and restoration.” *Materials Characterization*, 50(1), 59–68.
- Lu, Z., and Zhou, X. (2000). “The waterproofing characteristics of polymer sodium carboxymethyl-cellulose.” *Cement and Concrete Research*, 30(2), 227–231.
- Lubelli, B., Cnudde, V., Diaz-Goncalves, T., Franzoni, E., van Hees, R. P. J., Ioannou, I., Menendez, B., Nunes, C., Siedel, H., Stefanidou, M., Verges-Belmin, V., and Viles, H. (2018). “Towards a more effective and reliable salt crystallization test for porous building materials: state of the art.” *Materials and Structures/Materiaux et Constructions*, Springer Netherlands, 51(2), 1–21.
- Lubelli, B., Van Hees, R. P. J., and Groot, C. J. W. P. (2004). “The role of sea salts in the occurrence of different damage mechanisms and decay patterns on brick masonry.” *Construction and Building Materials*, 18(2), 119–124.
- Lubelli, B., Hees, R. P. J. van, and Nijland, T. G. (2014). “Salt crystallization damage: how realistic are existing ageing tests?” *AMS '14 Proceedings of the Int. Conference on*

Ageing of Materials and Structures, 2(1), 103–111.

Ludovico-Marques, M., and Chastre, C. (2012). “Effect of salt crystallization ageing on the compressive behavior of sandstone blocks in historical buildings.” *Engineering Failure Analysis*, Elsevier Ltd, 26, 247–257.

Luque, A., Cultrone, G., Mosch, S., Siegesmund S., Sebastian, E., Leiss, B. (2010). “Anisotropic behaviour of White Macael marble used in the Alhambra of Granada (Spain) The role of thermohydric expansion in stone durability.” *Engineering Geology*.

Maage M. (1980). “Frost resistance and pore size distribution in bricks. Materials and Structures.” *Materials and Structures*, 17, 345–350.

Mack, R. C., and Grimmer, A. (2000). “Assessing Cleaning and Water-Repellent Treatments for Historic Masonry Buildings.” Preservation Briefs No. 1, National Park Service, Washington DC.

Marti, C. B. (2017). "The use of integrative approaches to characterize new mechanisms of toxicity of pollutants in the aquatic environment", Universitat Politècnica de Catalunya.

Mate, M. S. (1969). “Building in ancient India.” *World Archaeology*, 1(2), 236–246.

Mathews, M.S., Menon, A., Chandran, S. (2003). “Rehabilitation and retrofit of earthquake damaged monuments in Gujarat.” *Special volume on conservation of stone objects*, The Commissioner of Museums, Chennai.

Menon, A. (2014). “Heritage Conservation in India: Challenges and New Paradigms.” *SAHC2014 – 9th International Conference on Structural Analysis of Historical*

Constructions, (October), 14–17.

Menon, A. (2017). “Tracing Two Decades of Research at IIT Madras on Historical Structures.” *71st RILEM Annual week and ICACMS 2017*, Chennai.

Meskill, L. (2013). “UNESCO’s World Heritage Convention at 40: Challenging the Economic and Political Order of International Heritage Conservatio.” *Current Anthropology*, 54(4), 483–494.

Ministry of Culture - Government of India, World Heritage, Tangible Heritage in India, accessed 04 May 2020, < <https://www.indiaculture.nic.in/world-heritage> >

Mohammed Haneefa, K., Divya Rani, S., Ramasamy, R., and Santhanam, M. (2019). “Microstructure and geochemistry of lime plaster mortar from a heritage structure.” *Construction and Building Materials*, Elsevier Ltd, 225, 538–554.

Molina, E., Cultrone, G., Sebastián, E., Alonso, F. J., Carrizo, L., Gisbert, J., and Buj, O. (2011). “The pore system of sedimentary rocks as a key factor in the durability of building materials.” *Engineering Geology*, Elsevier B.V., 118(3–4), 110–121.

Munday, C. J. & M. (2001). “Blaenavon and United Nations World Heritage Site Status: Is Conservation of Industrial Heritage a Road to Local Economic Development.” *Regional Studies*, 35(6), 585–590.

Nicholson D.T.. (2001). “Pore properties as indicators of breakdown mechanisms in experimentally weathered limestones.” *Earth Surf. Process. Landf.*, 26, 819–838.

Noor-E-Khuda, S., and Albermani, F. (2019). “Mechanical properties of clay masonry units:

- Destructive and ultrasonic testing.” *Construction and Building Materials*, 219, 111–120.
- Ochieng, O. P. (2012). “University of Nairobi- Department of Civil and Construction Engineering, "An Investigation into the Durability, Weathering And Strength Properties Of Coral Stone" A project submitted as a partial fulfillment for the requirement for the award of the degree of master of science”, Nairobi.
- Orbasli, A. (2009). “The conservation of coral buildings on Saudi Arabia’s northern Red Sea coast.” *Journal of Architectural Conservation*, 15(1), 49–64.
- Ordenez, S., Fort, R., and Garcia del Cura, M. A. (1997). “Pore size distribution and the durability of a porous limestone.” *Quarterly Journal of Engineering Geology*, 30, 221–230.
- Palmer, T. (2008). “Understanding the weathering behaviour of Caen Stone.” *Architectural conservation*, 14(3), 43–54.
- Peters, T., and Iberg, R. (1978). “Mineralogical Changes During Firing of Calcium-Rich Brick Clays.” *American Ceramic Society Bulletin*.
- Pope, G. A., Meierding, T. C., Paradise, T. R., and Montclair, U. (2002). “Geomorphology ’s role in the study of weathering of cultural stone.” *Geomorphology*, 47, 211–225.
- Price, C., and Brimblecombe, P. (1994). "Preventing salt damage in porous material", *Preprints of the Contributions to the Ottawa Congress Preventive Conservation Practice, Theory and Research*.
- Rani, S. D., Deb, M., Santhanam, M., and Gettu, R. (2016). “Evaluation of repair mortar

- materials for old monuments in southern India.” *Proceeding of International Conference on concrete repair, rehab and retrofitting*, Germany, 631–635.
- RILEM. (1980). “Recommended tests to measure the deterioration of stone and to assess the effectiveness of treatment methods, Test V.1a—crystallization test by total immersion (for untreated stone); Test V.1b—crystallization test by total immersion (for treated stone); T.” *Materials and Structures*, 13(75), 175–253.
- Robert J. Flatt. (2002). “Salt damage in porous materials : how high supersaturations are generated.” *Journal of Crystal Growth*, 242, 435–454.
- Robinson, G. C. (1982). "Conservation of Historic Stone Buildings and Monuments", *National Research Council Report 1982*. Washington DC.
- Rodriguez-navarro, C. (1997). “Origins of honeycomb weathering : The role of salts and wind.” *GSA Bulletin*; v. 111, no. 8; 1250–1255.
- Rodriguez-Navarro, C., and Doehne, E. (1999). “Salt weathering: influence of evaporation rate, supersaturation and crystallization pattern.” *Earth Surface Processes and Landforms*, 24(3), 191–209.
- Rodriguez-Navarro, C., Doehne, E., and Sebastian, E. (2000). “How does sodium sulfate crystallize? Implications for the decay and testing of building materials.” *Cement and Concrete Research*, 30(10), 1527–1534.
- Rozenbaum, O., L. Barbanson, F. Muller, and A. B. (2008). “Significance of a combined approach for replacement stones in the heritage buildings’ conservation frame.”

Comptes Rendus—Geoscience, 340(6), 345–355.

Russell S. A. (1927). *Stone preservation committee report*. London.

Saidov, T. A., Pel, L., and Kopinga, K. (2017). “Sodium sulfate salt weathering of porous building materials studied by NMR.” *Materials and Structures*, Springer Netherlands, 50(2), 145.

Sanjurjo-Sánchez, J., Gomez-Heras, M., Fort, R., Alvarez de Buergo, M., Izquierdo Benito, R., and Bru, M. A. (2016). “Dating fires and estimating the temperature attained on stone surfaces. The case of Ciudad de Vascos (Spain).” *Microchemical Journal*, Elsevier B.V., 127, 247–255.

Santhakumar, A., Mathews, M.S., Thirumurugan, S., U. R. (2010). *Seismic retrofitting of Historic Masonry Buildings*. 991–996.

Sassoni, E., and Franzoni, E. (2014). “Influence of porosity on artificial deterioration of marble and limestone by heating.” *Applied Physics A: Materials Science and Processing*, 115(3), 809–816.

Scherer G.W. (1999). “Crystallization in pores.” *Cement and Concrete Research*, 29 (August 1998), 1347–1358.

Scherer, G. W. (2004a). “Factors affecting crystallization pressure.” *International RILEM Workshop on Internal Sulfate Attack and Delayed Ettringite Formation*, (September), 139–154.

Scherer, G. W. (2004b). “Stress from crystallization of salt.” *Cement and Concrete Research*,

34(9), 1613–1624.

Scrivener K.L., Snellings R., B. L. (2016). *A Practical Guide to Microstructural Analysis of Cementitious Materials*. CRC Press, Taylor & Francis Group.

Sehgal, R. (2006). “Legal Regime towards Protecting Coral Reefs An International Perspective and Indian scenario.” *Law, Environment and Development Journal*, 2(2), 183–195.

Seuba J., Deville S., Guizard C., A. J. S. (2016). "Mechanical properties and failure behavior of unidirectional porous ceramics". *Scientific Reports*, vol. 6, Article number: 24326 .

Sharma, P. K., Khandelwal, M., and Singh, T. N. (2007). “Variation on physico-mechanical properties of Kota stone under different watery environments.” *Building and Environment*, 42(12), 4117–4123.

Shu, C. X., Cantisani, E., Fratini, F., Rasmussen, K. L., Rovero, L., Stipo, G., and Vettori, S. (2017). “China’s brick history and conservation: laboratory results of Shanghai samples from 19th to 20th century.” *Construction and Building Materials*, Elsevier Ltd, 151, 789–800.

Singer, F., and Singer, S. (1963). "Industrial Ceramics", *Chapman & Hall*, London.

Stefanidou, M., and Karozou, A. (2016). “Testing the effectiveness of protective coatings on traditional bricks.” *Construction and Building Materials*, Elsevier Ltd, 111, 482–487.

Steiger, M. (2005a). “Crystal growth in porous materials - I: The crystallization pressure of large crystals.” *Journal of Crystal Growth*, 282(3–4), 455–469.

- Steiger, M. (2005b). "Crystal growth in porous materials - II: Influence of crystal size on the crystallization pressure." *Journal of Crystal Growth*, 282(3–4), 470–481.
- Tite M.S., Y. M. (1975). "Scanning electron microscopy of fired calcareous clays." *Transaction of the British Ceramic Society*, 74, 19–22.
- Török, Á., & Píkryl, R. (2010). "Current methods and future trends in testing, durability analyses and provenance studies of natural stones used in historical monuments." *Engineering Geology*, 115(3–4), 139–142.
- Tsakalof, A., Manoudis, P., Karapanagiotis, I., Chryssoulakis, I., and Panayiotou, C. (2007). "Assessment of synthetic polymeric coatings for the protection and preservation of stone monuments." *Journal of Cultural Heritage*, 8(1), 69–72.
- Tsui, N., Flatt, R. J., and Scherer, G. W. (2003). "Crystallization damage by sodium sulfate." *Journal of Cultural Heritage*, 4(2), 109–115.
- Tulliani, J. M., Serra, C. L., and Sangermano, M. (2014). "A visible and long-wavelength photocured epoxy coating for stone protection." *Journal of Cultural Heritage*, Elsevier Masson SAS, 15(3), 250–257.
- Uğurlu Sağın, E., and Böke, H. (2013a). "Characteristics of bricks used in the domes of some historic bath buildings." *Journal of Cultural Heritage*, 14(3 SUPPL), 73–76.
- Uğurlu Sağın, E., and Böke, H. (2013b). "Characteristics of bricks used in the domes of some historic bath buildings." *Journal of Cultural Heritage*, 14(3 SUPPL), 73–76.
- Ukwatta, A., and Mohajerani, A. (2017). "Characterisation of fired-clay bricks incorporating

biosolids and the effect of heating rate on properties of bricks.” *Construction and Building Materials*, Elsevier Ltd, 142, 11–22.

UNESCO World Heritage Convention, Heritage sites in India, accessed 04 May 2020, <
www.whc.unesco.org/en/statesparties/IN>

UNI-EN-15803. (2015). “Conservation of cultural property Test methods - Determination of water vapour permeability.”

Varas-Muriel, M. J., Pérez-Monserrat, E. M., Vázquez-Calvo, C., and Fort, R. (2015). “Effect of conservation treatments on heritage stone. Characterisation of decay processes in a case study.” *Construction and Building Materials*, 95, 611–622.

Varatharajan, A., Vignesh, S., Prasanth, C.S. and Menon, A. (2012). “Assessment and strengthening of multi-tiered masonry towers in South India.” *The VIII International Conference on Structural Analysis of Historical Constructions*, Poland.

Vasanelli, E., Calia, A., Luprano, V., and Micelli, F. (2017). “Ultrasonic pulse velocity test for non-destructive investigations of historical masonries: an experimental study of the effect of frequency and applied load on the response of a limestone.” *Materials and Structures/Materiaux et Constructions*, Springer Netherlands, 50(1), 1–11.

Vázquez, P., Menéndez, B., Denecker, M. F. C., and Thomachot-Schneider, C. (2015). “Comparison between petrophysical properties, durability and use of two limestones of the Paris region.” *Geological Society, London, Special Publications*, 416(March), SP416--15.

- Vicente, M. A., & Rives, V. (2000). "Weathering and decay of granitic rocks : its relation to their pore network." 32, 555–560.
- Vos, B. H. (1978). "Hygric methods for the determination of the behavior of stones." *UNESCO-RILEM International Symposium "Deterioration and Protection of Stone Monuments,"* Paris, 1–19.
- Wang, X., Shui, Z., Yu, R., Bao, M., and Wang, G. (2017). "Effect of coral filler on the hydration and properties of calcium sulfoaluminate cement based materials." *Construction and Building Materials*, Elsevier Ltd, 150, 459–466.
- Wendler, E., and Charola, A. (2008). "Water and its interaction with porous inorganic building materials." *Hydrophobe V 5th International Conference on Water Repellent Treatment of Building Materials*, 74, 57–74.
- Whiteley, P., Russman, H. D., and Bishop, J. D. (1977). "Porosity of building materials — a collection of published results." *Journal of Oil and Colour Chemists' Association*, 60, 142–150.
- Winkler E.M.. (1997). "Stone in Architecture - Properties, Durability", *Springer-Verlag Berlin Heidelberg*, 3rd Edition.
- World weather online, accessed 04 May 2020 <www.worldweatheronline.com>
- Yu, S., and Oguchi, C. T. (2010). "Is sodium sulphate invariably effective in destroying any type of rock?" *Geological Society, London, Special Publications*, 333(1), 43–58.
- Zdravkov B.D., Čermák J.J., Šefara M., J. J. (2007). "Pore classification in the

characterization of porous materials: a perspective.” *Cent. Eur. J. Chem.*, 5, 385–395.

Zhang, Z. J., Cheng, Q. M., Yang, J., and Hu, X. L. (2018). “Characterization and origin of granites from the Luoyang Fe deposit, southwestern Fujian Province, South China.” *Journal of Geochemical Exploration*, Elsevier, 184(April 2017), 119–135.

LIST OF PUBLICATIONS BASED ON THIS THESIS

Refereed Journals

1. **Swathy Manohar**, Manu Santhanam, Naresh Chockalingam (2019) “Performance and microstructure of bricks with protective coatings subjected to salt weathering”, Construction and Building Materials, Volume 226, Pages 94-105, ISSN 0950-0618, <https://doi.org/10.1016/j.conbuildmat.2019.07.180>. [Journal Impact Factor (JIF): 4.086]
2. **Swathy Manohar**, Karpagam Bala, Manu Santhanam and Arun Menon (2020) “Characteristics and deterioration mechanisms in coral stones used in a historical monument in a saline environment”, Construction and Building Materials, Volume 241, 118102, ISSN 0950-0618, <https://doi.org/10.1016/j.conbuildmat.2020.118102>. [Journal Impact Factor (JIF): 4.086]

International Conference Papers

* Indicates presenter

1. **Swathy Manohar*** and Manu Santhanam (2018), “Salt crystallization in building materials in the marine environment”, 3rd R.N.Raikar Memorial International

Conference & Gettu-Kodur International symposium on Advances in science and technology of concrete, Mumbai, India, 14 – 15 December, 2018.

2. **Swathy Manohar*** and Manu Santhanam (2018), “Microstructural assessment of fire damaged granite”, International Conference on Urban Conservation, Kolkata, India. 26-28 November, 2018.
3. **Swathy Manohar*** and Manu Santhanam (2019), “Characterization and durability analysis of coral stones in a marine environment”, Historic Mortars Conference, University of Navarra, Spain, June 2019.
4. **Swathy Manohar*** and Manu Santhanam (2020), “A methodology to select an efficient protective treatment for brick structures”, 3rd International Conference on Innovative Technologies for Clean and Sustainable Development, Chandigarh, India, 19-21 February 2020.

DOCTORAL COMMITTEE

CHAIRPERSON

Dr. Ramamurthy K.
Professor
Department of Civil Engineering

GUIDE

Dr. Manu Santhanam
Professor and Head
Department of Civil Engineering

MEMBERS

Dr. Arun Menon
Associate Professor
Department of Civil Engineering

Dr. Dhamodharan R.
Professor
Department of Chemistry

Dr. Sivakumar Palaniappan
Associate Professor
Department of Civil Engineering

CURRICULUM VITAE

Name	Swathy Manohar
Date of birth	November 06, 1991
Educational qualifications	
2013	Bachelor of Technology (B.Tech.)
Institution	T.K.M. College of Engineering, Kollam, Kerala, India
Specialization	Civil Engineering
2015	Master of Technology (M.Tech.)
Institution	Indian Institute of Technology Roorkee, Uttarakhand, India
Specialization	Building Science and Technology
2020	Doctor of Philosophy (Ph.D.)
Institution	Indian Institute of Technology Madras Chennai, Tamilnadu, India
Specialization	Study of characteristics, deterioration mechanisms and protection of historic masonry units Civil Engineering